UNIVERSITÀ DEGLI STUDI DI TRIESTE

UNIVERSITÀ DEGLI STUDI DI TRIESTE

XXXVIII CICLO DEL DOTTORATO DI RICERCA IN BIOMEDICINA MOLECOLARE

PERSONALIZED APPROACHES TO LIVER DISEASE: DEVELOPMENT OF NOVEL RESEARCH TOOLS

Settore scientifico-disciplinare: MED/12

DOTTORANDA
BENEDETTA BLARASIN

COORDINATORE
PROF. ALESSANDRO TOSSI

SUPERVISORE DI TESI
PROF. CLAUDIO TIRIBELLI

SUPERVISORE DI TESI
DOTT.SSA CRISTINA BELLAROSA

ANNO ACCADEMICO 2024/2025

INDEX

List of Abbreviations

18S	18S ribosomal RNA
2D	Two - Dimensional
3D	Three - Dimensional
A83	Selective Inhibitor of TGF - β type I receptor (ALK5)
ABCB4	ATP Binding Cassette Subfamily B Member 4
ABCB11	ATP Binding Cassette Subfamily B Member 11
ABCD3	ATP Binding Cassette Subfamily D Member 3
AFP	Alpha - Fetoprotein
ALB	Albumin
ALD	Alcohol Related Liver Disease
ANIT	α - Naphthyl isothiocyanate
APOF	Apolipoprotein F
ASBT	Apical Sodium - Dependent Bile Acid Transporter
ASC	Ascorbic Acid
ASCs	Adult Stem Cells
ASGR2	Asialoglycoprotein receptor 2
ATP8B1	ATPase Phospholipid Transporting 8N1
BIL	Bilirubin
BLD	Blood
BMP4	Bone Morphogenetic Protein 4
BSA	Bovine Serum Albumin
BSL – 2	Biosafety Level 2
BSEP	Bile Salt Export Pump
CDFDA	5 - (and - 6) - carboxy - 2',7' - dichlorofluorescein diacetate
cDNA	Complementary DNA
CHIR	Selective inhibitor of GSK - 3α/β (activator of Wnt/β - catenin signalling pathway)
CHOP	C/EBP Homologous Protein
CI	Confidence Interval
c - MYC	Cellular Myelocytomatosis Oncogene
CNV	Copy Number Variations
CO_2	Carbon Dioxide
CRISPR	Clustered Regularly Interspaced Short Palindromic Repeats
CsA	Cyclosporine A
Ct	Cycle Threshold
CYP3A11	Cytochrome3A11
DAPI	4',6 - diamidino - 2 - phenylindole
DCA	Deoxycholic acid
DE	Definitive Endoderm
DILI	Drug - induced Liver Injury
DMEM	Dulbecco's Modified Eagle Medium
DMSO	Dimethyl Sulfoxide
DNA	Deoxyribonucleic Acid
DPBS	Dulbecco's Phosphate - buffered Saline
ECM	Extracellular Matrix

EDTA	Ethylenediaminetetraacetic acid
EdU	5’ - Ethynyl - 2’ - deoxyuridine
EFLM	European Federation of Clinical Chemistry and Laboratory Medicine
EGF	Epidermal Growth Factor
ELISA	Enzyme - Linked Immunosorbent Assay
EHS	Engelbreth - Holm - Swarm
ER	Endoplasmic Reticulum
ERN	European Reference Network
FBS	Fetal Bovine Serum
FGF2	Fibroblast Growth Factor 2
FIC1	Familial Intrahepatic Cholestasis 1 Protein
FOXA2	Forkhead box A2
FRT	Flippase Recognition Target
FXR	Farnesoid X Receptor
GAPDH	Glyceraldehyde - 3 - phosphate dehydrogenase
gDNA	Genomic DNA
GFP	Green Fluorescent Protein
GLP	Good Laboratory Practice
GLU	Glucose
GMP	Good Manufacturing Practices
GRP78	Glucose - regulated Protein 78
H_2O	Water
H_3PO_4	Phosphoric Acid
HBSS	Hank’s Balanced Salt Solution
HBV	Hepatitis B Virus
HCM	Hepatocyte Culture Medium
HCV	Hepatitis C Virus
HEK	Human Embryonic Kidney
HEPES	4 - (2 - hydroxyethyl) - 1 - piperazineethanesulfonic acid
HepG2	Human hepatocellular carcinoma, clone G2
Hep - Orgs	Hepatic Organoids
hESC	Human Embryonic Stem Cells
HGF	Hepatocyte Growth Factor
HH	Henderson - Hasselbalch
hiPSC	Human Induced Pluripotent Stem Cells
HIV	Human Immunodeficiency Virus
HLC	Hepatocyte - like Cells
HNF4α	Hepatocyte Nuclear Factor 4
HP	Hepatic Progenitors
HPRT	Hypoxanthine phosphoribosyltranferase 1
hPSC	Human Pluripotent Stem Cells
HSC	Hepatic Stellate Cells
IBAT	Ileal Bile Acid Transporter
ICP	Intrahepatic Cholestasis of Pregnancy
IEBAM	Inborn Errors of Bile Acid Metabolism
iPSC	Induced Pluripotent Stem Cells
IRCCS	Istituto di Ricovero e Cura a Carattere Scientifico
ISCBI	International Stem Cell Banking Initiative

ISSCR	International Society for Stem Cell Research
IVC	Inferior Vena Cava
KET	Ketones
KLF4	Kruppel - like Factor 4
KRT18	Keratin 18
L – Glut	L - Glutamine
L1CAM	L1 Cell Adhesion Molecule
LEU	Leukocytes
Lgr5	Leucine - rich repeat - containing G protein - coupled receptor 5
LTR	Long Terminal Repeats
MASLD	Metabolic Dysfunction Associated Steatotic Liver Disease
MET	Mesenchimal - to - Epithelial Transition
MHO1	MHO1 Homolog
MOI	Multiplicity of Infection
MRP2	Multidrug Resistance - associated Protein 2
MSC	Mesenchymal Stem Cells
MYO5B	Myosin 5b
NaH_2PO_4	Monosodium Phosphate
$NaHPO_4$	Disodium Phosphate
NANOG	Nanog homeobox
NaOH	Sodium Hydroxide
NEAA	Non - Essential Amino Acids
NGS	Next Generation Sequencing
NIT	Nitrites
NIH	National Institutes of Health
NR3C2	Nuclear Receptor Subfamily 3 Group C Member 2
NRF2	Nuclear Factor Erythroid 2 - Related Factor
NTSCs	Nuclear Transfer Stem Cells
O_2	Oxygen
OCT3/4	POU class 5 homeobox 1
OLT	Orthotopic Liver Transplantation
OP	Optical Density/Mean Absorbance
OSM	Oncostatin M
PBS	Phosphate - Buffered Saline
PBC	Primary Biliary Cholangitis
PCK1	Phosphoenolpyruvate carboxykinase 1
PCR	Polymerase Chain Reaction
Pen - Strep	Penicillin - Streptomycin
PFA	Paraformaldehyde
PFIC	Progressive Familial Intrahepatic Cholestasis
PHs	Primary Hepatocytes
PHHs	Primary Human Hepatocytes
PMX	Plasmid Maxiprep
PPAR	Peroxisome Proliferator - Activated Receptor
PPE	Personal Protective Equipment
PRO	Protein
PSC	Pluripotent Stem Cells
PTEC	Proximal Tubular Epithelial Cells

PV	Portal Vein
qPCR	Quantitative Polymerase Chain Reaction
RCL	Replication - Competent Lentivirus
Rcmdr	R Commander
REBM	Renal Epithelial Cell Growth Basal Medium
REGM	Renal Epithelial Cell Growth Medium
RH	Relative Humidity
RNA	Ribonucleic Acid
ROI	Regions of Interest
RPMI	Rosewell Park Memorial Institute (cell culture medium)
RSCs	Reprogrammed Stem Cells
RT	Reverse Transcription
RT – PCR	Reverse Transcription Polymerase Chain Reaction
SBD	Surgical Biliary Diversion
SCNT	Somatic Cell Nuclear Transfer
SD	Standard Deviation
SeV	Sendai Virus
SG	Specific Gravity
SLUG	Snail family transcriptional repressor 2
SOD2	Superoxide Dismutase 2
SOX2	SRY - box transcription factor 2
SOX17	SRY – box transcription factor 17
TDO2	Tryptophan 2,3 - Dioxygenase
TJP2	Tight Junction Protein 2
TNFα	Tumor Necrosis Factor Alpha
TTR	Transthyretin
UBG	Urobilinogen
UDCA	Ursodeoxycholic Acid
UGTA1	UDP glucuronosyltransferase family 1 member A1
UNC45A	Unc - 45 Myosin Chaperone A
UPR	Unfolded Protein Response
UV	Ultraviolet
VSELs	Very Small Embryonic – like Stem Cells
VSV – G	Vesicular Stomatitis Virus Glycoprotein
WES	Whole Exome Sequencing
WNT3A	Wnt Family Member 3A
ZO – 1	Zonula Occludens 1

SUMMARY

Liver diseases profoundly disrupt hepatic homeostasis and remain a global health burden. Conventional *in vitro* and *in vivo* models frequently lack reproducibility, stability, and translational relevance. Recent advances in human induced pluripotent stem cells (hiPSCs) and organoid biology offer new opportunities to recapitulate individual genetic backgrounds and model disease mechanisms in personalized settings. Within this context, the present thesis developed two research tools designed to support precision hepatology: a 2D patient - specific platform derived from urinary proximal tubular epithelial cells (PTEC) reprogrammed into hiPSC and differentiated into hepatocyte - like cells (HLCs), and a 3D murine hepatic organoid model (Hep - Orgs).

A robust workflow was first established for non - invasive isolation and expansion of PTEC from urine. Optimization identified major variables affecting cellular yield and viability, including donor - and gender - specific factors, urine pH, and squamous cells contamination. Protocol refinements – such as cell straining, phosphate - buffer supplementation, and reduced storage time – significantly improved reproducibility across donors.
Subsequently, PTEC were reprogrammed into hiPSCs using lentiviral delivery of pluripotency factors. While validated pluripotent hiPSC colonies were successfully obtained, residual transgene expression was detected, posing a known limitation for downstream hepatic differentiation.
Directed differentiation into HLCs was then investigated using multiple protocols. Comparative analysis demonstrated that final maturation states were influenced not only by biochemical cues but also by practical aspects of cell handling – coating substrates, seeding approaches, and culture format – highlighting the need for rigorous standardization in personalized HLC models.

A 3D hepatic organoid strategy (Hep - Orgs) was also pursued. Rat - derived organoids proved suboptimal, displaying instability and insufficient hepatic phenotype. In contrast, mouse - derived hepatic organoids exhibited strong reproducibility and long - term maintenance of hepatic architecture and cell diversity, supporting their utility as an intermediate platform between simplified cell culture and *in vivo* physiology. Importantly, this model was also validated in a translational context, as Hep - Orgs successfully recapitulated features of drug - induced cholestasis, demonstrating their suitability for toxicity and therapeutic testing.

Despite remaining challenges, the methodologies developed here advance the field toward reliable frameworks for disease modelling and therapeutic testing in liver diseases, particularly cholestatic

diseases. These platforms represent important steps in translating personalized cellular models into future precision medicine applications.

1. INTRODUCTION

1.1. Relevance of Liver Disease

Liver diseases encompass a broad spectrum of pathological conditions that impair hepatic homeostasis and normal physiological functions. These disorders may present in acute or chronic forms and can arise from both communicable and non - communicable aetiologies. Viral agents, including hepatitis viruses A - E, cytomegalovirus, and Epstein - Barr virus, are among the primary causes of viral hepatitis.

Non - viral liver diseases are typically attributed to metabolic, immunologic, toxic, genetic, or parasitic factors. Globally, liver diseases are responsible for over 2 million deaths annually, representing approximately 4% of total mortality worldwide (1).

Moreover, liver diseases are associated with a wide range of extrahepatic comorbidities, which substantially contribute to increased mortality and diminished quality of life. In addition, liver diseases represent a substantial economic burden on the global healthcare system. Among the different diseases, metabolic dysfunction - associated steatotic liver disease (MASLD) is associated with higher healthcare costs.

Among the most clinically significant categories of liver diseases are alcohol - related liver disease (ALD), Hepatitis B Virus (HBV), Hepatitis C Virus (HCV), liver cancer, MASLD, and other conditions.

Figure 1.1 presents the age - standardized mortality rates for individual liver diseases, based on data collected from 2000 to 2019, showing that liver cancer was the leading cause of liver - related mortality, accounting for approximately 484.25 thousand deaths globally. This was followed by HCV (399.49 thousand deaths), ALD (370.56 thousand deaths), HBV (365.24 thousand deaths), other chronic liver diseases with 279.46 thousand deaths, and MASLD with 134.95 thousand deaths (2).

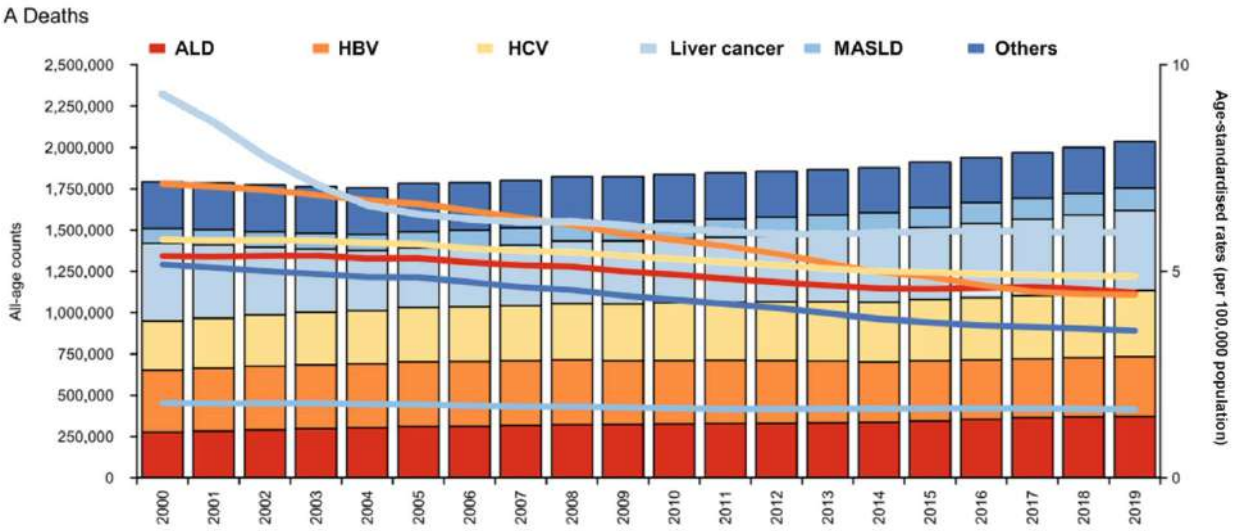

Figure 1.1. Age - standardized mortality rates for individual liver diseases. The figure presents the total number of deaths and corresponding age - standardized mortality rates at the global level for six major liver disease categories from 2000 to 2019 (2).

From a pathogenetic perspective, rare liver diseases are highly heterogeneous and result from multiple, largely uncharacterized mechanisms, making their classification challenging. According to the European Reference Network (ERN) for rare liver diseases, these disorders can be categorized as autoimmune, infectious (viral, bacterial, or parasitic), genetic/hereditary (metabolic, cholestatic, and structural phenotypes are encompassed), vascular, neoplastic, of unknown aetiology.

Rare liver diseases are frequently attributable to the production of defective or non - functional proteins that are essential for key functions of hepatic epithelial cells, including differentiation, secretion, and proliferation.

Despite the difficulty of studying these conditions, due to the limited availability of large patient cohorts and biological specimens, they hold significant translational research potential. In particular, of interest are diseases like genetic metabolic disorders, genetic cholestatic liver diseases, immune - mediated and inflammatory liver diseases, and rare liver cancers (3).

In this context, the group of drug - induced liver injuries (DILI) also constitutes a significant challenge in the field of hepatology. Between 1953 and 2013, drug - induced liver injury was the most frequent reason for drug withdrawal, accounting for 18% of cases. The estimated incidence of DILI ranges from 1 in 10,000 to 1 in 1,000,000 patients, depending on several factors like the definition of DILI employed, the frequency and sensitivity of liver function monitoring, and population demographics (1).

Among the various clinical manifestations of drug - induced liver injury, drug - induced cholestasis represents a notable and clinically relevant subtype, warranting further discussion alongside genetically determined forms of cholestasis.

1.2. Drug - induced and Genetic Cholestasis

Cholestasis is defined as an impairment of bile flow due to biliary tract obstruction or impairment of bile acid uptake, conjugation, or excretion by hepatocytes or cholangiocytes to canaliculi. It results in cholestatic jaundice, clay - coloured or pale stools, dark urine, inability to digest certain foods, and itching. It is classified as intrahepatic and extrahepatic, the former type involving the bile canaliculi and the latter intrahepatic bile ducts. Cholestasis is generally clinically defined as a conjugated or direct serum bilirubin level >17 μmol/L (1 mg/dL) when the total bilirubin is <85.5 μmol/L (5 mg/dL) or >20% of the total bilirubin if the total bilirubin is >85.5 μmol/L (4). Jaundice develops when the serum bilirubin level rises above 3 mg/dL (51.3 μmol/L). Considering the causes of conjugated hyperbilirubinemia, and focusing on the intrahepatic form of cholestasis, drug–induced liver cholestasis and genetic hepatic diseases are noted (5).

Neonatal cholestasis affects about 1 in 2,500 live births. Among the different causes of neonatal jaundice, which is the main symptom, there are biliary atresia (1/3 of the cases), inborn errors of metabolism, and congenital infections (20% and 5% of the cases), alpha - 1 - antitrypsin deficiency (5% - 15%), and other inherited forms of cholestasis (10% - 20%) (6).

Among the inherited forms of intrahepatic cholestasis, Progressive Familial Intrahepatic Cholestasis (PFIC) should be mentioned. PFIC is a heterogeneous group of genetic cholestatic liver diseases. The exact prevalence remains unknown but the estimated incidence ranges between 1/50,000 and 1/100,000 births. Regarding the most known PFIC genetic types, PFIC1 is due to genetic defects in ATPase phospholipid transporting 8B1 gene (ATP8B1), which encodes for familial intrahepatic cholestasis 1 protein (FIC1). PFIC2 is due to a defect in ATP binding cassette subfamily B member 11 (ABCB11) gene, which encodes for the main transporter of bile acids from hepatocytes to bile canaliculi (BSEP, Bile Salt Export Pump). PFIC3 is caused by defects in the ATP binding cassette subfamily B member 4 (ABCB4) gene, which encodes for ABCB4 protein. PFIC4 is due to a defect in the tight junction protein 2 gene (TJP2). Genetic defects in Farnesoid X Receptor (FXR) lead to PFIC5, while PFIC6 is due to different mutations on Myosin 5b gene (MYO5B) (7).

Indeed, new genetic abnormalities continue to be described in the literature, e.g., a novel UNC45A - related syndrome of cholestasis (8). Among the main complications of PFIC, intractable pruritus, end

- stage liver disease, and hepatocellular carcinoma are the most common. Current treatments for PFIC include non - invasive methods using ursodeoxycholic acid (UDCA), rifampicin or apical sodium - dependent bile acid transporter (ASBT) inhibitors, and invasive approaches with several kinds of surgical biliary diversion (SBD) techniques.

At the moment, there are still clinically diagnosed forms of cholestasis that remain without a molecular pathology definition or where the mechanism is controversial. It is noteworthy that a significant number of drugs commonly used in medicine can cause intrahepatic cholestasis. Among these are, for instance, nonsteroidal anti - inflammatory drugs, anti - infective drugs, anti - cancer drugs, sedatives, neuropsychiatric drugs, checkpoint inhibitors, oral contraceptives, anabolic - androgenic steroids, herbal and dietary supplements, and antibiotics (9) (10).

1.3. Strategies for the Discovery of Novel Therapeutics for the Treatment of Liver Diseases

Liver transplantation, whether orthotopic (OLT) or auxiliary, remains the only definitive therapeutic option for end - stage liver diseases and various inherited liver - based metabolic disorders, serving as a vital intervention for patients with acute and chronic liver failure (11). Despite its clinical efficacy, this approach faces a significant limitation: it is contingent upon the availability of suitable donor organs and necessitates substantial technical expertise and healthcare resources. The persistent shortage of donor livers further exacerbates this challenge, often delaying timely transplantation for many patients. As a result, this organ scarcity has prompted intensive research into alternative therapeutic strategies aimed at reducing reliance on donor organs and addressing the urgent unmet need for liver transplantation (12).

One of the primary challenges in the development of novel therapies for liver diseases is the absence of reliable *in vitro* models that faithfully recapitulate the liver's complex physiological functions. This limitation significantly impedes the investigation of hepatic pathophysiology and the preclinical evaluation of therapeutic candidates under conditions that closely resemble the human *in vivo* environment (13).

1.4. Personalized Medicine in Liver Diseases

Personalized medicine, also referred to as precision medicine, represents a paradigm shift in healthcare by tailoring medical care to the individual characteristic of each patient. This approach leverages genomic, proteomic, metabolomic, and other molecular data to improve disease prevention, diagnosis, and treatment. Rather than relying on generalized treatment protocols, personalized medicine enables clinicians to select therapies that are more likely to be effective based on a patient's unique biological profile.

Personalized medicine aims to enhance treatment outcomes by aligning therapeutic strategies with the patient's genetic makeup, environmental exposures, and lifestyle factors. This stratification helps to reduce adverse drug reactions, improve therapeutic efficacy, and promote a more rational use of healthcare resources (14).

Precision medicine in liver diseases represents a transformative approach that stratifies patients based on the molecular, genetic, metabolic, and clinical features in order to tailor diagnosis, monitoring, and therapies.

As previously discussed, cholestasis represents one of the hepatic disorders of major clinical interest, particularly because its inherited forms can, and should, benefit from advances in personalized medicine. In this context, earlier diagnosis, accurate risk stratification, and the selection of optimal therapeutic strategies based on specific genetic variants exemplify how personalized medicine holds substantial promise for improving patient outcomes (15).

Personalized medicine in the context of cholestatic disorders encompasses multiple dimensions. First, it is essential to determine whether cholestasis is of hereditary origin and, if so, to identify the specific genetic variants driving disease pathogenesis. In this regard, genetic and molecular diagnostics play a pivotal role, leveraging next - generation sequencing (NGS) and whole - exome sequencing (WES), as well as detailed profiling of bile acid metabolites to guide clinical decision - making (16).

Second, the assessment of molecular biomarkers capable of predicting therapeutic response or disease progression, potentially supported by metabolomics approaches, further refines patient stratification and management strategies (17). Consequently, treatment paradigms are increasingly targeted and mechanism - based, addressing the molecular pathways responsible for cholestatic injury. For example, novel ileal bile acid transporter (IBAT) inhibitors provide a rational therapeutic option for

cholestatic pruritus, a hallmark symptom resulting from elevated bile acid levels in various forms of cholestasis (18).

Among the types of cholestasis that can benefit most substantially from personalized medicine, inherited paediatric and young - adult cholestatic disorders such as PFIC and Alagille Syndrome are particularly notable. As these diseases result from inborn errors of bile acid metabolism (IEBAM), targeted therapeutic approaches, including cholic acid supplementation, IBAT inhibitors, and selected surgical interventions, can be implemented based on the underlying molecular defect (19). Furthermore, personalized strategies are increasingly relevant in primary biliary cholangitis (PBC), where validated risk - stratification scoring systems enable the prediction of transplant - free survival in patients treated with ursodeoxycholic acid, thus guiding tailored clinical decision – making (20).

More recently, in the context of intrahepatic cholestasis of pregnancy (ICP), genetic contributions of ATP Binding Cassette Subfamily B Member 4 (ABCB4) and ATP Binding Cassette Subfamily B Member 11 (ABCB11) variants have been investigated to clarify variant - specific phenotypic expression and potential therapeutic implications, further reinforcing the value of precision approaches in cholestatic disorders (21).

Among the tools and strategies increasingly applied in cholestatic liver disease, genetic profiling in children with advanced cholestasis enables screening for pathogenic variants in established disease - related genes, thereby facilitating aetiologic diagnosis and guiding individualized therapeutic decision – making (15). Multi - omics approaches, including genomics, transcriptomics, proteomics, and metabolomics, further provide predictive insights into biomarkers discovery for treatment response and disease progression (17).

Building on these advances, novel therapeutics are being developed to specifically target the underlying molecular pathways. For instance, Farnesoid X Receptor (FXR) agonists such as obeticholic acid have been approved for clinical use in patients who are intolerant of, or non - responsive to, ursodeoxycholic acid. Peroxisome proliferator - activated receptor (PPAR) agonists – including Seladelpar (PPAR - δ) and Elafibranor (PPAR - α/δ), alongside conventional fibrates – increase bile acid clearance, diminish bile - acid - induced toxicity, and mitigate fibrogenesis, particularly benefiting individuals with PBC who fail to respond adequately to ursodeoxycholic acid therapy (22). Meanwhile, inhibitors of the ileal bile acid transporter, such as Odevixibat and Maralixibat, reduce enterohepatic bile acid recirculation, lowering the systemic bile acid burden and effectively alleviating refractory pruritus in inherited cholestatic disorders including PFIC and Alagille Syndrome (23).

Collectively, these molecularly targeted therapeutic strategies demonstrate how prognostic and pharmacogenomic profiling can refine treatment selection and improve clinical outcomes in cholestatic liver diseases. In summary, advances in NGS have substantially accelerated the diagnosis of inherited cholestatic disorders and facilitated the identification of novel mutations affecting bile acid transport. Emerging therapeutic strategies increasingly focus on molecular targets regulating hepatocellular bile acid export and intestinal reuptake. In parallel, innovative approaches aimed at correcting the underlying genetic defects – such as hepatocyte transplantation using induced pluripotent stem cells (iPSC), gene therapy, and more recently, hepatocyte - to - cholangiocyte transdifferentiation to restore intrahepatic bile ducts – are under active investigation.

Importantly, continued innovation also depends on the development of robust and physiologically relevant research models to study diseases mechanisms and evaluate target therapies. Ideally, such models should be generated through minimally invasive or non - invasive approaches, ensuring both feasibility and wider clinical applicability.

1.5. Traditional Models and Related Issues

Several experimental models have been developed to enhance our understanding of the pathophysiological mechanisms underlying liver diseases, as well as to evaluate pharmacological therapies - particularly in cases involving known genetic mutations (24).
However, progress in the field remains limited by the scarcity of appropriate animal models and physiologically relevant cell culture systems (25). *In vitro* disease modelling is critically dependent on the availability of disease - relevant cell types that not only are the primary targets of liver pathology, but also faithfully recapitulate disease - specific phenotypes.
Considering genetic liver diseases, patient - derived biopsies represent a valuable model for assessing the steady - state distribution of mutant proteins; however, they do not provide insight into the dynamic regulatory processes involving these specific proteins, such as their polarized intracellular trafficking (7).

Primary Human Hepatocytes (PHHs) are widely regarded as the gold standard for *in vitro* liver disease modelling and drug development, due to their strong morphological and biochemical resemblance to hepatocytes *in vivo*. They retain key functional properties, including drug - metabolizing enzyme activity, making them highly valuable for studying hepatic metabolism,

toxicity, and genetic disorders (25). PHHs are typically isolated from human liver biopsies or surgical resections; however, their use is limited by several critical challenges, including the invasive method of collection. Procurement of high - quality tissue is difficult, especially from patients with rare liver diseases, and donor - to - donor variability can lead to inconsistencies in experimental outcomes (25) (26).
Furthermore, PHHs rapidly lose their functional phenotype in standard culture conditions - often within a few days - thereby restricting their utility for long - term studies or high - throughput applications. This limited viability necessitates a constant supply of fresh donor tissue, significantly constraining their broader applicability in translational liver research.

Tumor - derived human hepatocytes and immortalized hepatocyte cell lines (e.g. HepG2, HuH7, HepaRG cells) are constrained by several inherent limitations that significantly reduce their utility across a range of research and therapeutic applications. In particular, their tumorigenic origin contributes to further drawbacks, including cellular immaturity and dysfunctional apoptotic signalling pathways, which confer resistance to toxic insults and render them suboptimal for drug toxicity screening (27).
Moreover, as these cell lines are generally derived from a single hepatocellular carcinoma, they lack the genotypic heterogeneity required to accurately model the diverse genetic landscape of human populations. As a result, their relevance for disease modelling and pharmacological testing is considerably restricted.

Another approach for studying liver diseases involves the use of animal models (e.g. knockout mice). However, the use of non - human species may result in phenotypes that are less severe than those observed in humans (24) or may lead to embryonic lethality at early developmental stages. Furthermore, the use of animal models should be minimized in accordance with the 3Rs principles (Replacement, Reduction, and Refinement), which promote strategies to reduce the number of animals used in biomedical research whenever possible.

1.6. Innovative Emerging Liver Models

1.6.1. Human - induced Hepatocytes (hiHeps)

Among existing iPSC - derived models, human induced - Hepatocytes (hiHeps, also known as Hepatocyte - like cells or HLCs) are of particular interest for the study of genetic rare liver diseases.

Human induced hepatocytes are functional hepatocyte - like cells generated by the direct conversion (transdifferentiation) of somatic cells – such as fibroblasts – into a hepatocyte fate by ectopic expression of liver - enriched transcription factors (and/or small molecules), thereby circumventing a pluripotent stem cell intermediate (28).

Current *in vitro* hepatic differentiation protocols aim to recapitulate the *in vivo* developmental process of liver embryogenesis. Most protocols for generating hiHeps from human iPSC use a stepwise administration of specific growth factors and small molecules to mimic the sequential stages of liver development. This process progresses from pluripotent blastula - stage cells through definitive endoderm, hepatic progenitors, and hepatocyte - like cells (13).
Substantial research has focused on the differentiation of iPSC into HLCs, aiming to recapitulate the functional characteristics of native hepatocytes through the application of various cytokines, growth factors, and small molecules, including Hepatocyte Growth Factor (HGF), Oncostatin M (OSM), Dexamethasone (DEX), and Fibroblast Growth Factor (FGF), administered according to a well - defined temporal protocol (29).

The generation of hiHeps typically involves three sequential stages (shown in Figure 1.2):

- Definitive Endoderm stage: this process is predominantly orchestrated by exposure to key members of the transforming growth factor - β (TGF - β) family, notably activin A and bone morphogenetic protein 4 (BMP4). WNT3A, acting with activin A, can enhance the efficiency of definitive endoderm induction. The combined action of FGFs and BMP4 reinforces commitment to the definitive endoderm lineage. During this stage, the expression of specific marker genes, including SRY - box (SOX17), and forkhead box A2 (FOXA2), indicates the formation of foregut endoderm, which subsequently gives rise to pancreatic and hepatic lineages (12).
- Hepatic Progenitors stage: the subsequent pivotal stage toward the hepatocyte lineage involves the induction of hepatic progenitor cells, or hepatoblasts, *In vitro*, a combination of growth factors is used, among which HGF plays a central role. In addition, the transition of definitive endoderm cells toward hepatic progenitors is highlighted by the upregulation of Hepatocyte Nuclear Factor 4 alpha (HNF4α), which during embryogenesis is initially expressed in the hepatic diverticulum and progressively increases throughout liver development. Another key marker at this stage is the expression of alpha - fetoprotein (AFP), indicative of primitive hepatocytes (12).

- Hepatocyte - like cells / Induced Hepatocytes stage: in this final stage, hepatic progenitors cells are induced to differentiate into hiHeps/HLCs through exposure to OSM, a cytokine of the interleukin - 6 family, in combination with glucocorticoids such as dexamethasone (DEX). OSM plays a pivotal role in fetal liver development and has been shown to promote hepatic progenitor maturation. When combined with DEX, it markedly upregulates key hepatocyte maturation genes, thereby enhancing cellular functionality and protein synthesis capacity (12).

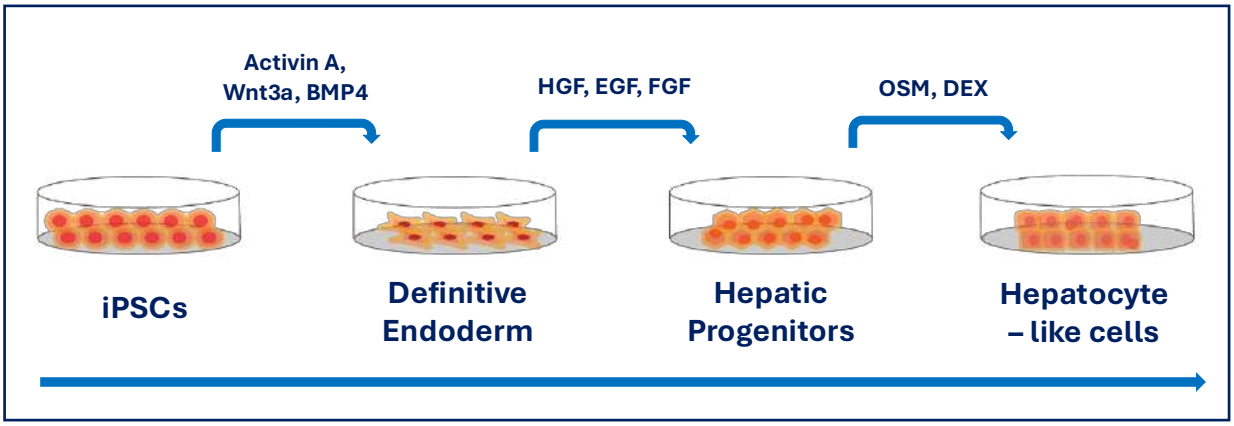

Figure 1.2. Schematic representation of the three main differentiation stages for the generation of Hepatocyte – like cells from pluripotent stem cells. The first step involves the formation of definitive endoderm cells from iPSC using Activin A, Wnt3A and BMP4 as growth factors. The second step involves the formation of hepatic progenitors by supplying cells with HGF, EGF, and FGF. The last step allows the formation of Hepatocyte - like cells by using specific factors such as Oncostatin M (OSM) and Dexamethasone (DEX). Figure adapted from Xie et al. (30).

Differentiating iPSCs into HLCs is a lengthy and complex process, often hindered by limitations of conventional 2D culture systems, which fail to replicate the liver's native microenvironment. The adoption of defined extracellular matrix components and advanced 3D scaffolds has improved cell polarization, maturation, and functionality.

hiHeps represent a versatile platform for disease modelling, drug discovery, personalized and regenerative medicine. They enable patient - specific models of inherited and infectious liver diseases, support hepatotoxicity assessment and pharmacological screening, and offer a renewable cell source for transplantation and bioartificial liver systems. When combined with genetic engineering, hiHeps hold promise for personalized therapies targeting metabolic disorders, while advanced culture systems aim to enhance their maturation and functional fidelity, facilitating their translation into clinical and biotechnological applications (12). Furthermore, they represent a suitable model to investigate mechanisms involved in cholestasis of unknown origin.

Despite significant progress in generating HLC from pluripotent stem cells, several limitations remain. Current differentiation protocols do not achieve the maturity of adult primary hepatocytes, and iPSC – derived HLC often display a fetal - or neonatal - like phenotype (31) (32). While some liver - specific genes are expressed, many hepatocyte - preferred genes are present at much lower levels than in primary hepatocytes, and certain genes, such as UGTA1 and SERPINA1, may even exceed the levels observed in neonatal hepatocytes. This incomplete maturation can limit the utility of HLCs in pharmacological testing, disease modelling, and cell - based liver regeneration. In addition, like primary hepatocytes, HLC rapidly lose liver - specific gene expression during *in vitro* culture. Standardization and reproducibility across laboratories remain critical challenges, as differentiation protocols, culture conditions, and functional readouts vary widely. Moreover, current iPSC - derived liver models are generally not produced under GLP conditions, which limits their direct applicability in regulatory or pharmaceutical contexts. Finally, multi - centre validation and regulatory acceptance of these models are still lacking, and their translation into robust, high – throughput platforms require further optimization of maturation, functional assessment, and quality control standards (12) (33).

Stem Cells - derived Models

Stem cells represent a powerful tool for *in vitro* modelling due to their exceptional capacity for self - renewal and their potential to differentiate into specific cell types. This makes them particularly valuable for generating mature, functional hepatic cells with reproducible quality for experimental and therapeutic applications. The use of stem cell - derived hepatocyte - like cells allows the development of human - relevant models, enhancing disease modelling, drug testing, and personalized medicine.

Stem cells are broadly categorized into two major groups based on their origin and differentiation potential: adult stem cells (ASCs) and pluripotent stem cells (PSCs). ASCs are tissue - specific progenitors found in adult organs, such as the liver, or obtained from other sources like mesenchymal stem cells (MSCs). PSCs, in contrast, include both human embryonic stem cells (hESCs), derived from the inner cell mass of blastocysts, and human induced pluripotent stem cells (hiPSCs), generated through somatic cell reprogramming.

Each stem cell type possesses distinct advantages and limitations depending on its proliferation capacity, differentiation efficiency, ethical considerations, and technical accessibility. A

comprehensive understanding of these differences is critical for optimizing their application in both research and regenerative medicine (31).

Currently, five major categories of stem cells are recognized based on their origin and method of derivation: embryonic stem cells (ESCs), very small embryonic - like stem cells (VSELs), nuclear transfer stem cells (NTSCs), reprogrammed stem cells (RSCs, such as iPSCs), and adult stem cells (ASCs).

It is important to note that hepatology has recently evolved towards more integrated approaches, incorporating novel *omics* technologies (i.e., genomics, proteomics, metabolomics) to gain deeper insights into molecular events within biological systems. Considering the characteristics and limitations of models previously employed in the study of rare liver diseases, and with the aim of identifying specific molecular targets associated with these conditions, induced pluripotent stem cells (iPSCs) and tissue - derived organoids represent significant advances in disease modelling (34).

iPSC - derived cells can be used to generate a wide range of cellular models with varying degrees of complexity, including both 2D monolayer cultures and 3D organoid systems. In 2D models, specific cell types can be studied in isolation to investigate cell - mechanisms, perform high - throughput drug or CRISPR/Cas9 - based genetic screens, and analyze cellular responses to perturbations. While these models offer simplicity and scalability, they lack structural complexity of native tissues. For these reasons, it is important to consider that, under appropriate differentiation conditions, iPSCs can self - organize into 3D organoids, which contain multiple cell types and better mimic tissue architecture and function. These 3D models enable the study of developmental processes, context - dependent cell behaviour, and organ - specific diseases in a more physiologically relevant environment (35).

The historical progression of stem cell science has been marked by several seminal milestones. In 1961, Till and McCulloch first identified stem cells in mouse bone marrow with the potential to differentiate into multiple cell types. In 1996, the cloning of Dolly the sheep via somatic cell nuclear transfer (SCNT) demonstrated the feasibility of reprogramming differentiated cells. In 1998, James Thomson successfully isolated hESCs from human embryos. Later, iPSCs were derived from reprogrammed adult somatic cells with just four basic transcription factors. In 2012, Shinya Yamanaka and John Gurdon were jointly awarded the Nobel Prize in Physiology or Medicine for their discovery that fully differentiated somatic cells can be reprogrammed into a pluripotent state (Figure 1.3) (36).

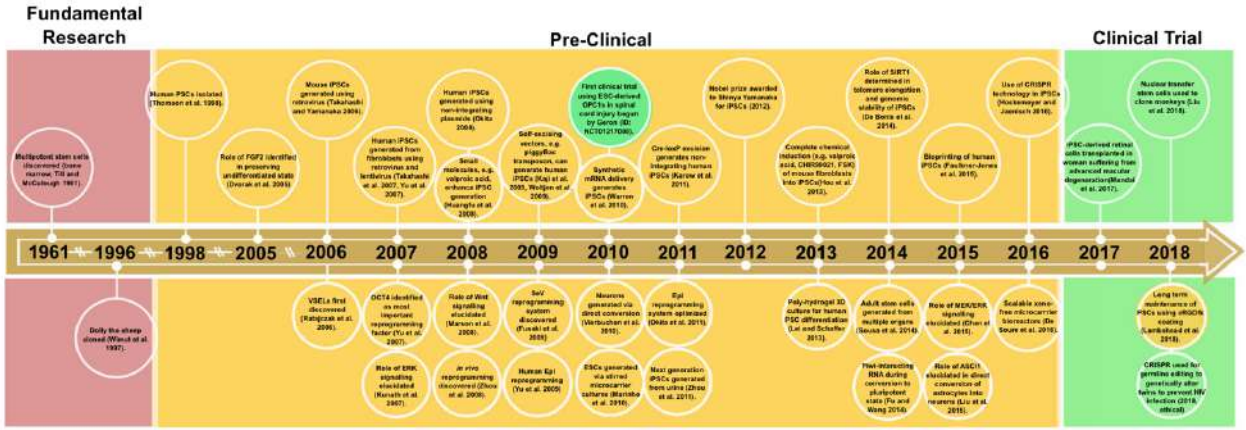

Figure 1.3. Schematic representation of the timeline of major scientific advances during the history of stem cell research. Multipotent stem cells were firstly discovered in 1961, and Dolly the sheep was cloned in 1997. The progression from fundamental research to preclinical investigation and ultimately to clinical trials is propelled by numerous discoveries and key milestones. Recent advances in the identification of optimal reprogramming factor combinations, the refinement of experimental methodologies, and the elucidation of critical signalling pathways have collectively enabled the initiation of the first clinical trials involving retinal and spinal cord cell transplantation. Figure taken from Liu et al. (36).

iPSC represent a promising and versatile source of pluripotent stem cells that offer a valuable platform for regenerative medicine and cell - based therapies. Since their discovery, the number of studies utilizing iPSCs or seeking to improve reprogramming efficiency has continued to grow, reflecting the expanding interest in their therapeutic applications. iPSC have demonstrated potential in treating a wide spectrum of diseases, including retinal disorders, cardiovascular conditions, neurodegenerative diseases, and various form of cancer. Donor - derived iPSC lines are typically stored in dedicated stem cell banks, the number of which is increasing in parallel with the demand for iPSC - based therapeutics products (37).

iPSC potential

Given their numerous advantages, iPSCs can be derived from patients affected by specific diseases and subsequently differentiated into relevant cell types to investigate pathological molecular mechanisms *in vitro*. These patient - specific iPSC - derived models are highly valuable for the development of personalized therapies, as they enable the direct assessment of individual responses to specific drugs or treatments. Moreover, iPSCs serve as a powerful platform for evaluating drug efficacy and safety, contributing to a significant reduction in the use of animal models in preclinical research. A key strength of iPSCs lies in their ability to differentiate into virtually any cell type, which opens avenues for the replacement of damaged tissues and the development of autologous cell - based therapies. Furthermore, advanced genome editing technologies such as CRISPR/Cas9 can be applied

to iPSCs to introduce, correct, or delete diseases - associated mutations, thereby enhancing their utility for both disease modelling and potential therapeutic applications (35).

iPSC challenges

Unlike conventional small or large molecule drugs, which exhibit well - defined pharmacological properties and can be produced with high reproducibility, iPSC - derived therapies are associated with a number of complex and unique challenges. These include concerns regarding safety, potency, genetic stability, immunogenicity, tumorigenic potential, cellular reproducibility, and scalability. One of the most critical issues lies in the reprogramming process itself and the subsequent long - term *in vitro* expansion of iPSCs, which are frequently associated with the accumulation of genomic alterations. These may include chromosomal aneuploidies, sub - chromosomal copy number variations (CNVs), and point mutations - some of which may confer selective growth advantages in culture, interfere with the accurate modelling of disease phenotypes, and compromise the safety and efficacy of regenerative therapies. In addition to genetic instability, the reprogramming process must successfully reset the somatic cell's epigenetic landscape to silence lineage - specific transcriptional programs and activate pluripotency - associated genes. However, incomplete or aberrant reprogramming can result in epigenetic abnormalities, leading to heterogeneous gene expression and variable biological behaviour among different iPSC lines. Moreover, residual epigenetic memory from the donor cell of origin can significantly influence the efficiency and fidelity of directed differentiation into specific lineages. The variability poses substantial limitations for the use of iPSCs in disease modelling, drug screening, and especially in clinical applications such as cell replacement therapy, where consistency and predictability are paramount (38).

iPSC sources

Since the work by Takahashi and Yamanaka, a wide range of somatic cell types have been reprogrammed into iPSCs, with efficiencies generally below 4%, depending on the cell type, differentiation state, and reprogramming method. Over the last 18 years, to address safety concerns and improve reprogramming efficiency, various delivery methods have been developed beyond traditional integrative vectors (lenti - or retroviral - mediated) that are used to obtain iPSCs from somatic cells. Non - integrative approaches include Sendai virus (SeV), episomal plasmids, synthetic mRNA, and mini - circle DNA vectors (38).

As shown in Figure 1.4, common sources include skin fibroblasts, peripheral blood cells, hair keratinocytes, urine - derived epithelial cells, bone marrow cells, mesenchymal stem cells. More unconventional sources, including cells from biological waste such as adipose tissue, dental pulp, liver, stomach, neural progenitors, and even fetal tissues.

Despite the versatility, reprogramming remains inefficient and stochastic, with only a small fraction of donor cells reaching pluripotency. Factors such as donor cell age and proliferation capacity critically influence reprogramming success (39).

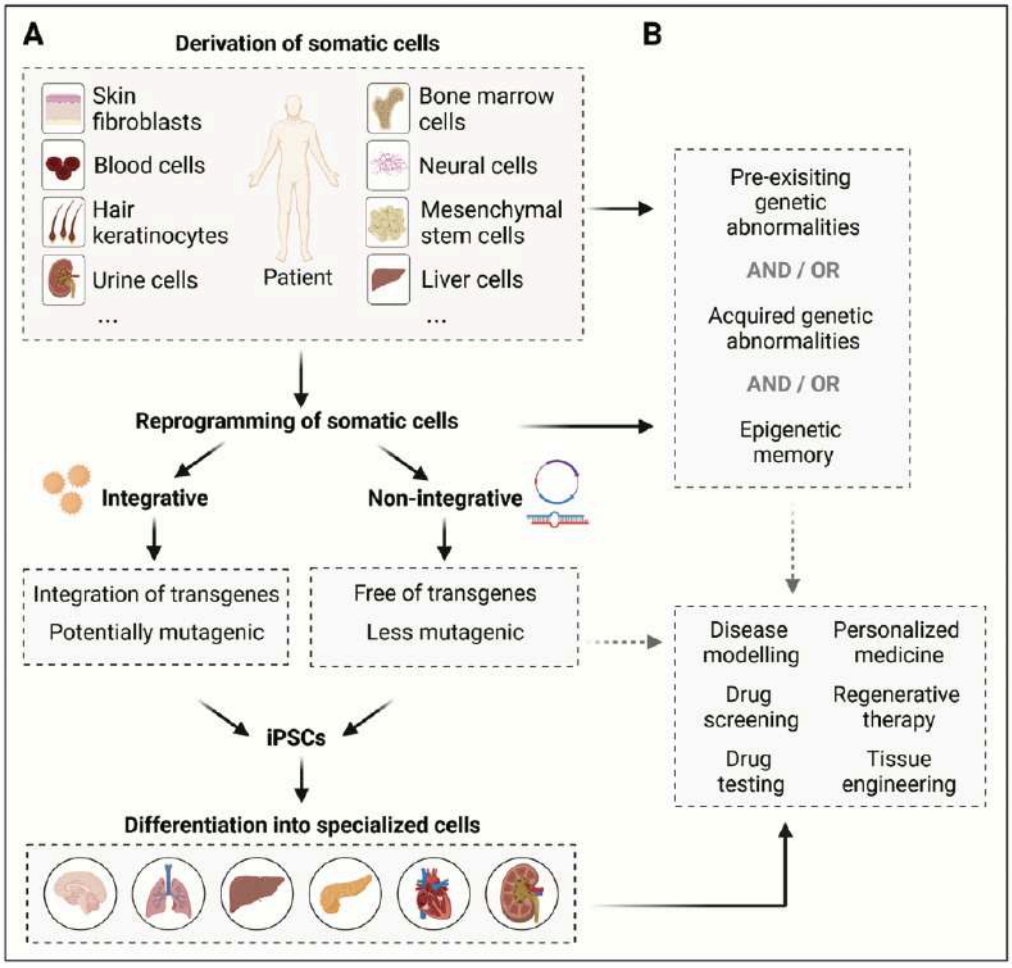

Figure 1.4. (A) iPSC generation from a variety of somatic cell types using integrative or non - integrative approaches. (B) Pre - existing genetic abnormalities of somatic cells can limit their utility and safety for clinical or regenerative therapy. Figure taken from Poetsch et al (38).

Currently, skin fibroblasts and blood cells are the most widely used due to their accessibility, well - established culture protocols, and compatibility with iPSC biobanking (38).

However, fibroblasts present several limitations. Their collection typically requires invasive skin punch biopsies, which are painful, can cause bleeding, scarring, and carry risks of infection and

allergic reactions, necessitating medical supervision. A key challenge is their mesenchymal identity, which requires a mesenchymal - to - epithelial transition (MET) during reprogramming. In addition, they must be used at early passages (≤5) to avoid reduced efficiency and genomic instability. Considering blood cells, and in particular peripheral blood cells, the method of collection is less invasive if compared with skin biopsies, but several important limitations exist concerning low reprogramming efficiency (10 - 50 times lower than that of fibroblasts), technical complexity, donor limitations, and practical challenges in both collection and culture. Blood - derived cells often lack long - term culture stability, limiting their scalability and use in extended protocols. A high volume of cells is usually required for these techniques, and although recent advances show promise using small volumes, these methods are not yet widely standardized.
For these reasons, new sources have been considered, including urine.

iPSC from Proximal Tubular Epithelial Cells (PTEC)

Specifically, urine provides a non-invasive, easily accessible source of proximal exfoliated renal epithelial cells, typically collected from 50 - 200 mL of midstream urine. These cells can be cultured and reprogrammed into iPSC that display comparable pluripotency and gene expression profiles to embryonic stem cells. Urine - derived cells are a promising somatic source for iPSC generation due to their high accessibility, non - invasive nature, and relatively high efficiency (higher than that of fibroblasts and blood cells), though their use is best limited to early - passage cultures (39)(40).
To identify the cellular composition of urine, it is first necessary to consider the structure of the urinary tract. The system comprises two kidneys, with numerous nephrons containing renal corpuscles and tubules, along with the ureters, bladder, and urethra (Figure 1.5) (41) (42). Owing the extensive tubular network and mechanical stress from glomerular filtrate flow, approximately 2000 - 7000 viable and non - viable cells are shed daily into urine (43) (44). These exfoliated epithelial cells represent a heterogenous population originating from different regions of the urinary tract, including renal tubular cells from the nephron, urothelial cells from downstream areas such as the renal pelvis, ureters, and bladder, and squamous cells from the distal urethra or female genital tract. Additionally, blood - derived cells (erythrocytes, leukocytes, macrophages) are commonly present, with their abundance increasing with age or in pathological conditions (42).

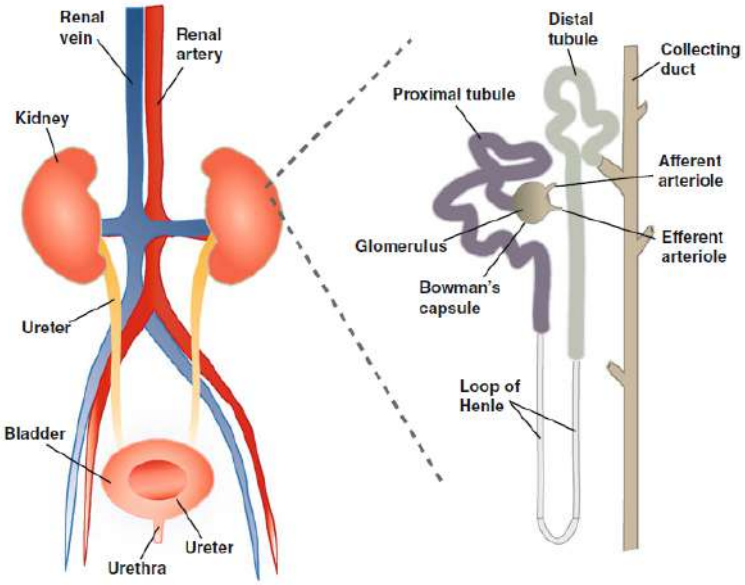

Figure 1.5. The left panel illustrates the anatomical organization of the urinary tract, whereas the right panel provides a detailed representation of the nephron, the functional unit of the kidney. Each nephron comprises two principal components: the renal corpuscle, which includes the glomerulus and Bowman's capsule, and the renal tubule, consisting of the proximal convoluted tubule, the loop of Henle, and the distal convoluted tubule. Figure adapted from Benda et al. (42).

As noted above, epithelial cells exfoliated in human urine may originate from any region of the urinary tract, including the kidneys. The two main renal cell types commonly identified are podocytes and proximal tubular epithelial cells (PTEC) (34).

- Podocytes are specialized epithelial cells forming a key component of the glomerular filtration barrier. Their interdigitating foot processes create slit diaphragms that, together with the glomerular basement membrane, ensure selective permeability during blood filtration (34).
- Proximal Tubular Epithelial Cells (PTEC) play a central role in reabsorbing water and solutes from the glomerular filtrate via specialized channels and transporters (45). *In vivo,* they exhibit a cuboidal morphology with basolateral invaginations and an apical brush border, while in culture they lose polarity and therefore present a spindle - shape orientation (46) (47). These cells represent the main target for isolation in this thesis.

1.6.2. Liver Organoids

Conventional 2D hepatocyte culture systems suffer from well – recognized functional limitations, including the rapid dedifferentiation of primary hepatocytes and the loss of key polarized features required for directional metabolite transport. The disruption of hepatocyte polarity has been associated with impaired physiological functions, such as reduced low – density lipoprotein internalization, ultimately limiting the predictive value of these models for metabolic and toxicological studies. Advanced 2D configurations, such as sandwich cultures, partially address these shortcomings by promoting hepatocyte polarization and canaliculi - like network formation, thereby extending culture longevity and enhancing drug sensitivity. Nevertheless, despite these improvements, hepatocytes cultured in sandwich systems still undergo progressive dedifferentiation over prolonged culture periods, underscoring the intrinsic limitations of these culture formats in sustaining mature hepatic function (48) (49).

In this context, 3D polarized tissue models, including hepatic organoids, have emerged as promising alternatives capable of better preserving liver - specific architecture and functionality. Organoids have been shown to achieve functional states approaching those of adult hepatocytes following appropriate maturation protocols, as evidenced by enhanced albumin secretion, cytochrome P450 activity, and transcriptomic profiles. Importantly, hepatic organoids display superior metabolic competence compared to 2D counterparts, including improved glucose and lipid metabolism, heightened insulin responsiveness, and increased glycogen synthesis. Beyond metabolic maturation, 3D systems enable the inducible establishment of liver zonation - like features, allowing spatially resolved modelling of adult liver functions (49).

For these reasons, three - dimensional (3D*) in vitro* culture systems have recently emerged as innovative platforms for investigating tissue morphogenesis, organ development, and stem cell behaviour. Their potential lies on the establishment of a multidimensional network of biochemical and mechanical cues that overcomes the structural and functional limitations inherent to 2D cultures (50).

In 2015, Meritxell Huch and Bon - Kyoung Koo (51) defined organoids as follows:

"We define an "organoid" as a 3D structure derived from either PSCs (pluripotent stem cells), neonatal tissue stem cells or AdSCs (adult stem cells)/adult progenitors, in which cells spontaneously self - organize into properly differentiated functional cell types and progenitors, and which resemble their in vivo counterpart and recapitulate at least some function of the organ."

Organoids offer a unique platform for modelling liver physiology and pathology, as they closely recapitulate the microarchitecture of native hepatic tissue. Lumen formation enables the distinction between intraluminal and extraluminal compartments, facilitating active molecular transfer between these domains. The extracellular matrix can be precisely manipulated to investigate cellular responses to specific mechanical cues in their microenvironment. Compared to conventional two - dimensional cultures, organoids exhibit enhanced functionality, likely due to their ability to mimic the physiological niche and promote a higher degree of cellular maturity. Their three-dimensional organization allows faithful reproduction of the spatial relationships between different hepatic cell types, supporting self - organization processes and enabling advanced studies in morphogenesis. Furthermore, they are highly suitable for multicellular co - cultures and for exploring cell - cell signalling and interactions. The long - term culture and expansion of primary cells within organoids, achieved with minimal manipulation, reduces barriers to clinical translation and underscores their potential in regenerative medicine and bioengineering. Taken together, these features establish organoids as an optimal system for fundamental and translational liver research.

Despite their numerous advantages, organoids also present several limitations that currently restrict their broader application. Sampling distinct compartments, such as the organoid lumen and the extraluminal space, remains technically challenging. Furthermore, the complex extracellular matrices typically used are often chemically undefined, not compliant with good manufacturing practices (GMP), and thus incompatible with certain regenerative medicine applications. Organoid cultures are generally costly, time - and labour - intensive. These systems are also less amenable to large - scale expansion and manufacturing, and their inherent heterogeneity complicates quality control and standardization. From a technical standpoint, culturing, maintaining, and extracting cells from organoids requires advanced expertise, while characterization of their multicellular complexity often demands high - resolution methodologies such as single - cell RNA sequencing. Addressing these

challenges will be essential to fully harness the potential of organoids in both research and clinical settings (52).

Liver organoids are specifically defined as 3D structures originating from pluripotent stem cells, progenitor cells, and/or differentiated cells, as well as from primary or metastatic tumour tissue, which self - organize through coordinated cell - cell and cell - extracellular matrix interactions to reproduce key architectural and functional characteristics of the liver tissue of origin (53).

As defined by Huch et al., organoids can be generated from pluripotent stem cells, including embryonic stem cells (ESCs), induced - pluripotent stem cells (iPSCs), and adult pluripotent stem cells (ASCs), as well from differentiated primary cells of adult origin (51).

iPSC - Derived Organoids

During early development, the totipotent zygote gives rise to both embryonic and extraembryonic tissues. As the blastocyst forms, outer cells commit to extraembryonic lineages, while the inner cell mass retains pluripotency. As described previously, several protocols have been established to differentiate iPSCs into HCLs by mimicking embryonic development. A major advantage of iPSC - based models is the non - invasive accessibility of patient - derived samples – such as urine, blood, or skin – avoiding limitations linked to biopsies (54). This enables the generation of patient - specific organoids that preserve the original genotype, allowing the modelling of genetic diseases or the use of genetic engineering to introduce desired phenotypes. To produce multicellular organoid models, iPSCs can also be co - cultured with other cell types, with the aim to better reproduce *in vivo* cellular heterogeneity and to study complex diseases such as fibrosis and cancer (55).
However, limitations remain. iPSC - derived organoids often display mixed fetal/adult characteristics, as reprogramming can introduce genetic and functional discrepancies compared with the original cells. Moreover, the requirement for recombinant growth factors makes large - scale applications costly (56).

Hepatoblast - Derived Organoids

Hepatoblast – derived organoids originate from hepatoblasts, bipotent fetal liver progenitors that give rise to both hepatocytes and cholangiocytes during liver development. These organoids exhibit high

proliferative capacity, long - term expandability, and stable bipotency, while retaining the ability to differentiate into more mature and polarized hepatocyte - like structure. As such, hepatoblast - derived organoids represent a promising platform for large - scale production of hepatic tissue, disease modelling, drug development, and the study of liver polarization and viral infection mechanisms (57) (58). However, when these organoids are derived from embryonic stem cells (ESCs), their derivation and use are not permitted in certain countries, such as Italy (59).

Adult Pluripotent Stem Cells - Derived Organoids

Adult - tissue resident stem cells, known as oval cells, are characterized by oval - shaped nuclei, small cytoplasm, and surface expression of the Leucine - rich repeat - containing G protein - coupled receptor 5 (Lgr5). Localized within the terminal branches of the bile duct, they can undergo the oval cell reaction, known as ductal reaction (60).
Huch et al. (54) established liver organoid cultures from $Lgr5^{+}$ hepatic stem cells, mimicking the pericentral hepatocyte niche, characterized by high Wnt activity. These organoids were able to maintain a normal karyotype and express mature hepatocyte markers (25).

Organoids Obtained from Adult Hepatocytes (Hep - Orgs)

The liver exhibits a heterogeneous cellular composition, consisting of approximately 65% hepatocytes, 10% tissue - resident macrophages (Kupffer cells), 5% hepatic stellate cells (HSCs), 15% liver sinusoidal endothelial cells, 5% cholangiocytes, and smaller population of other immune and adult stem cells, which cooperate spatially and temporally coordinated manner to establish and maintain liver function (53).

Following partial hepatectomy, hepatocytes are the primary parenchymal cells driving liver regeneration. Primary hepatocytes (PHs) can be expanded *in vitro* and used to generate hepatocyte – derived organoids, known as Hep - Orgs (61).
In 2018, two independent groups led by Clevers and Nusse established two models that require the activation of mitogenic signalling via epidermal growth factor (EGF), HGF, FGF, and potentiation of the Wnt pathway to sustain long - term culture (62) (63).
The main difference between the two protocols is based on the inclusion of tumour necrosis factor α (TNFα) in the culture medium by Peng et al. (63).

Primary hepatocytes cultured with EGF, HGF, and TNFα formed organoids within two weeks; TNFα supplementation enabled expansion of Hep - Orgs for over six months. Given its known role in injury - induced liver regeneration, TNFα was hypothesized to promote Hep - Orgs proliferation. In particular, the medium proposed by Peng et al. supported robust murine primary hepatocytes proliferation, containing TNFα, EGF, HGF, CHIR99021, A83 - 01, and Y27632, giving rise to grape - shape Hep - Orgs of up to 100 μm (64).
Hep - Orgs retain stable characteristics, including albumin expression at levels only two - to fourfold lower than PHs, and demonstrate functional maturity, making them valuable for disease modelling from patient - specific hepatocytes. Their genetic stability at both sequence and chromosomal levels supports their use in modelling monogenic disorders such as α1 - antitrypsin deficiency (A1AT) and Alagille syndrome (ALGS) (55).
Compared with iPSC - derived organoids, Hep - Orgs offer a longer functional window for experimental testing and sustained activity over extended culture periods (52).

After considering the various sources from which hepatic organoids can be obtained, it is important to note that other liver - related organoid systems have been developed and are increasingly being used to model specific aspects of hepatic and biliary biology.

Biliary Organoids

Biliary organoids are generated from biliary epithelial cells, liver progenitor cells, or pluripotent stem cells, and exploit the intrinsic stem/progenitor capacity of these cell types to form three – dimensional structures that closely recapitulate bile duct architecture and function. These organoids provide a valuable platform for studying biliary development, disease pathogenesis, and regenerative mechanisms, as well as for drug screening, and have been generated using a variety of culture approaches ranging from conventional matrix embedding to advanced technologies such as organ - on - a – chip systems and 3D printing (65) (66).

Hepatic Lineage Organoids

Hepatic lineage organoids are defined by the integration of multiple liver – relevant cell populations within a unified three - dimensional architecture, typically derived from pluripotent stem cells or lineage – specified progenitors. By incorporating hepatocyte – like populations, these organoids more

closely recapitulate the cellular complexity of the native liver. This multicellular composition enables the study of dynamic parenchymal – non – parenchymal interactions that are central to liver maturation, homeostasis, and disease progression, particularly in conditions such as fibrosis where stromal activation and extracellular matrix remodelling play pivotal roles. As such, multi – lineage organoids provide an advanced platform for modelling human - specific liver pathophysiology and evaluating therapeutic interventions in a context that extends beyond hepatocyte - centric systems (67) (48).

Table 1.1 provides a summary of the advantages and disadvantages of the hepatic organoid types discussed above.

Organoid model	Advantages	Disadvantages
iPSC - derived organoids	(a) Easy and non invasive access to patient's sample. (b) iPSC can derive from a donor (specific genotype) or be modified by genetic engineering. (c) Multiple cell types can be co - cultured.	(a) Mixed fetal and adult features. (b) Shorter functional windows compared to Hep - Orgs. (c) Genetic abnormalities from reprogramming can be present. (d) The growth factors needed are very expensive.
Hepatoblast - derived organoids	(a) Expandable and genetically stable. (b) Enable generation of polarized and relative mature hepatocyte organoids. (c) Suitable for large - scale production, disease modelling, and drug development.	(a) Developmentally immature origin (fetal - like). (b) Incomplete functional maturation compared with adult hepatocytes. (c) Differentiation outcomes are protocol - dependent.
ASCs - derived organoids	(a) Long - term expansion. (b) They exhibit mature hepatocyte functions and express - specific markers. (c) Therapeutic potential. (d) Versatility.	(a) Incomplete maturation. (b) Culture complexity to sustain growth and Wnt activation, with increase costs and variability. (c) Donor variability.
Hep - Orgs from adult hepatocytes	(a) PHs can be grown for long - term with functional maturity. (b) Genomic stability. (c) PHs can be derived from patients. (d) The starting material can match the desired phenotype, reducing animal use.	(a) Difficult access to primary tissue. (b) Lack of heterogeneity in the starting population.
Organoid type	**Advantages**	**Disadvantages**
Biliary organoids	(a) High physiological relevance for biliary development and disease modelling. (b) Suitable for studying cholangiopathies and biliary regeneration. (c) Compatible with advanced culture platforms.	(a) Limited hepatocyte representation. (b) Not suitable for modelling hepatocyte - specific metabolism. (c) Variability depending on cell source and culture protocol. (d) Complex culture requirements.
Hepatic lineage organoids	(a) Enable modelling of complex liver diseases (e.g. fibrosis). (b) Capture interactions beteween parenchymal and non - parenchymal cells. (c) Amenable to genome editing.	(a) High complexity and heterogeneity. (b) Limited standardization and reproducibility. (c) Reduced stability for high - throughput screening. (d) Maturation and functionsl consistency remain challenging.

Table 1.1. Advantages and disadvantages of iPSC - derived organoids, ASCs - derived organoids, and Hep - Orgs obtained from adult hepatocytes.

2. AIM OF THE THESIS

The overall aim of this thesis is to develop and optimize advanced *in vitro* liver models to investigate the molecular and cellular mechanisms underlying cholestasis and liver diseases in general. Current *in vivo* and *in vitro* systems often fail to reproduce the structural complexity, functional polarization, and dynamic processes characteristic of hepatocytes, thereby limiting the possibility to elucidate the molecular pathways responsible for hepatobiliary dysfunctions of either genetic or pharmacological origin. For this reason, from a personalized - medicine perspective, it is evident that there is a need to have patient - specific models, possibly obtained in a non - invasive way.

To address these limitations, this work focuses on the establishment of two - and three - dimensional experimental systems that are based on induced pluripotent stem cells (iPSC) and adult hepatocyte - derived organoids. The iPSC - based approach relies in the reprogramming of renal epithelial cells obtained non - invasively from urine samples, followed by their differentiation into hepatocyte - like cells. This strategy enables the generation of donor - specific cellular models that preserve the donor's genetic background, are amenable to precise genome editing, and can be used to explore the pathophysiological mechanisms of human liver diseases.

In parallel, three - dimensional organoids derived from primary adult hepatocytes (Hep - Orgs) have been developed and characterized to assess hepatocyte function in a physiologically relevant context. These organoids reproduce key architectural features of the native liver tissue, allowing the evaluation of responses to pharmacological agents within a controlled microenvironment.

Despite the intrinsic limitations of both experimental systems, the project aims to establish a versatile and reproducible platform capable of dissecting the complex molecular interactions occurring during cholestasis. The use of the donor - derived model and adult hepatocyte - based organoids is expected to provide a robust tool for studying gene - function relationships, investigating the effects of pharmacological compounds, and ultimately contributing to the development of targeted therapeutic strategies.

In a broader perspective, the thesis seeks to validate innovative, ethically sustainable, and highly translational *in vitro* models that can be applied not only to genetically determined or drug - induced hepatic dysfunctions but also to a wider spectrum of liver pathophysiology where conventional approaches remain insufficient.

3. MATERIALS AND METHODS

General description of the project

The first part of this chapter will describe the materials and methods used to first obtain PTEC from urine samples (Step 1, Methods 3.1), then iPSCs from PTEC (Step 2, Methods 3.2), and finally hepatocyte -like cells from iPSC (Step 3, Methods 3.3) (Figure 3.1).

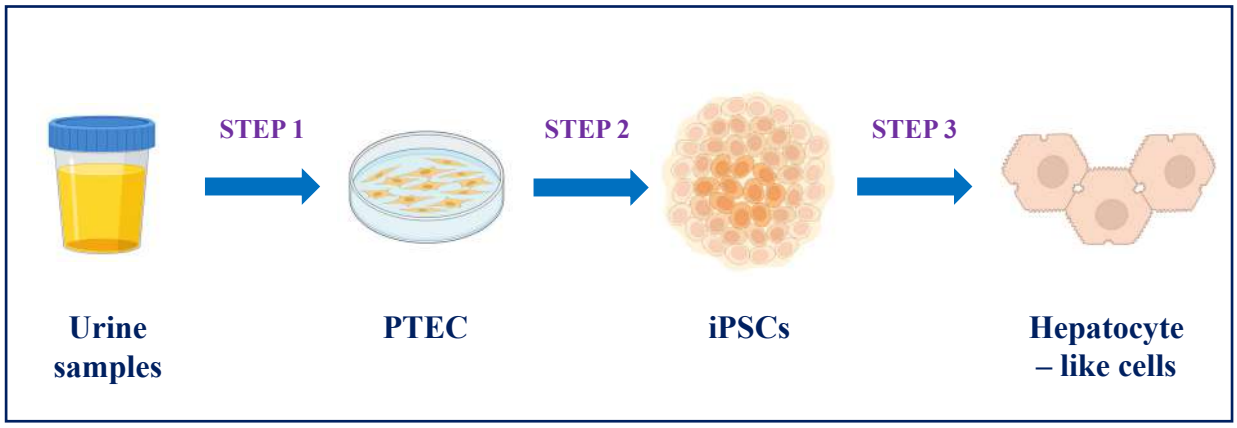

Figure 3.1. General description of the protocol to obtain urinary cells (PTEC) from urine samples (STEP 1), iPSC from PTEC (STEP 2), and finally Hepatocyte - like cells from iPSC (STEP 3). This image was created using BioRender.com.

Subsequently, the protocols used to generate Hep - Orgs from primary rat (Methods 3.4) and mouse (Methods 3.5) hepatocytes will be outlined (Figure 3.2.).

Figure 3.2. General description of the protocol to obtain primary hepatocytes and then hepatic organoids from rat and mouse livers. This image was created using BioRender.com.

3.1. PTEC Isolation and Culture from Urine: Protocol Improvements (Step 1)

Chosen Donors and Informed Consent

Urine samples were obtained from healthy voluntary donors of both sexes, aged between 25 and 49 years, and of different ethnic backgrounds, including Asian and European origins. Donors were instructed to collect 100 mL of urine six times a day. All samples were maintained at 4°C; however, the storage duration and number of samples collected varied depending on the specific analysis to be performed. Informed consent was obtained from each donor after they received a detailed explanation of the study rationale (Figure 3.3).

Prior to sample collection, donors received direct and individual oral instructions regarding the procedures required for proper urine collection, with particular emphasis on adherence to hygienic practices to minimize the risk of sample contamination and on the immediate addition of a phosphate - buffered solution containing antibiotics following collection. For this purpose, donors were provided with serological pipettes to facilitate the accurate addition of the buffer and antibiotics to the urine samples and to ensure thorough mixing.

Fondazione Italiana Fegato
ONLUS

INFORMATION SHEET AND INFORMED CONSENT FORM
FOR THE DONATION OF SAMPLES FOR INTERNAL USE TO THE FIF

TITLE OF THE PROJECT: Development of the protocol for obtaining induced hepatocytes from urine samples
PROMOTER: Italian Liver Foundation
STRUCTURE IN WHICH THE STUDY WILL BE CARRIED OUT: Italian Liver Foundation
RESPONSIBLE EXPERIMENTATOR: Cristina Bellarosa
CONTACTS OF THE RESPONSIBLE EXPERIMENTATOR: Tel: 0039 [illegible] E-mail: cristina.bellarosa@fegato.it

Objective and characteristics of the project

The project aims to develop, for basic research purposes only, the experimental procedure for obtaining hepatocytes in 2D culture starting from urine samples. Renal epithelial cells will be isolated from donated urine, which will then be de-differentiated into pluripotent cells (iPSC). Kidney epithelial cells and iPSCs can be frozen and used later. The iPSCs will then be differentiated into hepatocytes (the main liver cells) by culture with suitable growth factors. In the end, if the whole process is successful, cultured hepatocytes with the characteristics of the donor will be obtained.

The characteristics of the project, in this phase, provide for the collection of urine from a dozen volunteers. Participation in the study does not involve any type of drug treatment or preparation (e.g. fasting). Each donor is provided with 6 urine collection containers, 6 antibiotic tubes and 6 antifungal tubes. Each donor is required to collect 1 sample of approximately 100 ml of urine 6 times a day (excluding the first urination in the morning). After each collection, the donor must add the antibiotic and antifungal supplied to the sample collected and must place the jar in a special space indicated at + 4°C. The investigator will start processing 24 hours after collection.

FONDAZIONE ITALIANA FEGATO - ONLUS

Fondazione Italiana Fegato
ONLUS

INFORMED CONSENT FORM FOR PARTICIPATION IN THE STUDY

DONOR _____ _____ (Name and Surname in capital letters)

I, the undersigned (Name and Surname in capital letters) _____ _____

born in_____ the: ___/___/____

I declare that I have received, through personal interview with the investigator informing _____ detailed and understandable information, written and verbal, on the nature, significance, expected benefits, risks, and implications of the study. Furthermore, I have read and understood the text of the patient information.
I discussed the conduct of the study with the investigator and had the opportunity to ask questions about the study. All my questions were answered satisfactorily regarding the unclear points.

I declare:

- to have had the necessary time to reflect on the information received and to freely make a decision and to have had the opportunity to discuss it with the investigator;
- I understand the purpose of this study and the procedures to which I will be subjected;
- to be free to refuse to participate in the proposed project, without giving a reason and without my medical care or my legal rights being compromised;
- to voluntarily give my consent to participate in the project, as it has been described to me in this document, without having been coerced and to be aware of the possibility of revoking my consent to participate in the study at any time without giving any reason (orally or in writing), without losing any right or benefit, without prejudice to my medical care or my legal rights and without this choice affecting in any way my relationship with the medical and health personnel of the facility;
- to be aware that the results of the study will be disclosed to the scientific community and that my identity will not be mentioned in any study report and that all information obtained during the trial will be treated as strictly confidential;

I further understand that I will receive a copy of this document signed by me. The original will remain at the trial center. This consent is valid unless and until I revoke it.

FONDAZIONE ITALIANA FEGATO - ONLUS

Fondazione Italiana Fegato
ONLUS

☐ I AGREE - I DISAGREE to participate in the above study.

☐ I AGREE - I DISAGREE to be informed by the investigator about the results of this study.

Possible statements of the patient, additional questions or other aspects of informed consent:

_____

Full name and surname of the patient or of the legal representative / support administrator in capital letters:

_____

Date: _____

Signature of the patient or the legal representative / support manager:

_____

Fondazione Italiana Fegato
ONLUS

DECLARATION OF THE INFORMATION OF THE INVESTIGATOR WHO PRESENT THE INFORMATION TO THE DONOR

I, the undersigned (name and surname of the informing investigator in capital letters) _____ declare that the purposes and methods of the study have been correctly explained to the donor and that the donor has freely consented to participate.
I have ascertained that the donor is able to read and understand this form written in Italian, that he has understood all the information contained therein and that he has been fully informed on the conduct and impact of the this study, as well as the nature and revocability of your consent to participate in the study.
I also declare that I have provided a copy of this information and that I have obtained the consent of the donor
Date: _____

Signature of the Lead Investigator: _____
(readable)

Signature of the informing investigator (the one who administered and collected the informed consent, if different from the responsible investigator):

_____
(readable)

DRAWN UP IN TWO COPIES, THE ORIGINAL TO BE KEEPED BY THE STUDY INVESTIGATOR, AND THE COPY TO BE DELIVERED TO THE DONOR.

FONDAZIONE ITALIANA FEGATO - ONLUS

Figure 3.3. Template of informed consent obtained from healthy voluntary donors for urine sample collection.

3.1.1. Original Protocols

PTEC Isolation and Culture from Urine

Urinary cell isolation was performed following the protocol described by Zhou et al. (40).
Each 100 mL urine sample was transferred into two 50 mL conical tubes and centrifuged at 400 xg for 15 minutes at room temperature. Following centrifugation, the supernatant was discarded, and the resulting pellet was gently resuspended in 5 mL of Washing Buffer composed of Dulbecco's

phosphate - buffered saline (DPBS) supplemented with 1% penicillin/streptomycin and 0.2% amphotericin B. The pellets from the two tubes of the same sample were then combined into a single 50 mL tube and subjected to a second centrifugation at 200 xg for 15 minutes at room temperature. After discarding the supernatant, the final cell pellet was resuspended in 1.5 mL of Primary Medium consisting of a 1:1 mixture of DMEM/High glucose and Ham's F12, supplemented with 1% penicillin/streptomycin, 1% amphotericin B, and the REGM® SingleQuots kit supplements (Lonza). Each sample was then seeded into a single well of a 24 - well plate pre - coated with Embryomax Gelatin (300 µL/well, Sigma - Aldrich), which facilitates initial cell attachment. Cultures were incubated at 37°C, 5% CO_2 and 95% RH (Relative Humidity). During the first three days, the Primary Medium was partially changed daily (removing and replacing 700 µL) to promote cell adhesion while not removing specific factors released by the cells. After three days, the Primary Medium was gradually replaced with Proliferation Medium consisting of REBM medium supplemented with 1% penicillin/streptomycin, 1% amphotericin B, and REGM SingleQuot kit supplements (Lonza). The Primary Medium, containing a higher concentration of fetal bovine serum (FBS), supports initial cell adhesion, while the Proliferation Medium selectively promotes the expansion of the renal tubular epithelial cells.

In the case of bacterial contamination, penicillin and streptomycin were added to the medium at a concentration of 10 µL/mL. In the presence of mold or fungal contamination, amphotericin B was added at the same concentration as an antifungal agent.

Once the PTEC reached confluence, they were passaged using Trypsin - EDTA (EuroClone) for further expansion or cryopreserved in liquid nitrogen for future use.

3.1.1.1. PTEC Preparation within 4h of Sample Storage

Donors were instructed to collect two 100 mL urine samples per day, at different time points during the day, over a period of three consecutive days. A total of 36 samples were collected: 18 from female donors and 18 from male donors. All urine samples were subsequently stored at 4°C for 4 hours prior to processing (Table 3.1).

	Daily urine samples
Total number of donors	6
Female	3
Male	3
N° sample/donor/day	2
N° days	3
Total of samples	36
Storage temperature	4°C
Storage time	4 hours

Table 3.1. Schematic representation of the total number of donors, the number of samples provided per donor per day, the number of donation days per donor, the overall number of samples collected, the storage temperature of urine samples post - collection, and the duration of storage at the specified temperature.

3.1.1.2. PTEC Preparation after 24h of Sample Storage

Urine Preparation from Morning Urine Collection

Donors were instructed to collect one 100 mL sample of first morning urine per day for three consecutive days. A total of 18 samples were collected: 6 from female donors and 6 from male donors. All urine samples were subsequently stored at 4°C for 24 hours prior to processing.

	Morning urine samples
Total number of donors	6
Female	3
Male	3
N° sample/donor/day	1
N° days	3
Total of samples	18
Storage temperature	4°C
Storage time	24 hours

Table 3.2. Schematic representation of the total number of donors, the number of samples provided per donor per day, the number of donation days per donor, the overall number of samples collected, the storage temperature of urine samples post - collection, and the duration of storage at the specified temperature.

PTEC Preparation from Urine Collected During the Day

Donors were instructed to collect six 100 mL urine samples at different time points throughout the day, over a period of three consecutive days. A total of 108 samples were collected: 54 from female

donors and 54 from male donors. All urine samples were stored at 4°C for 24 hours prior to processing.

	Daily urine samples
Total number of donors	6
Female	3
Male	3
N° sample/donor/day	6
N° days	3
Total of samples	108
Storage temperature	4°C
Storage time	24 hours

Table 3.3. Schematic representation of the total number of donors, the number of samples provided per donor per day, the number of donation days per donor, the overall number of samples collected, the storage temperature of urine samples post - collection, and the duration of storage at the specified temperature.

3.1.2. Challenges in PTEC Isolation and Plating, and Strategies for Their Resolution

3.1.2.1. Urine Test Strip Analysis

Following the designated storage period at 4°C, urine samples were equilibrated to room temperature (15 - 25°C) for subsequent test strip analysis using the COMBI SCREEN® 11 SYS PLUS system. This analytical step represents a novel addition to the standard isolation protocol.

COMBI SCREEN® 11 SYS PLUS test strips serve as semi - quantitative diagnostic tools for detecting various analytes in urine. The test strip enables the simultaneous evaluation of 11 parameters: ascorbic acid, bilirubin, blood, glucose, ketones, leukocytes, nitrite, pH, protein, specific gravity, and urobilinogen (Table 3.4). Each parameter provides between 4 and 7 measurable levels, indicated by colorimetric changes on the reagent pads.

Strips were briefly immersed in the urine sample (~ 2 seconds) to ensure complete saturation of all reagent pads. Excess urine was removed by gently wiping the strip against the edge of the collection container or blotting on absorbent paper. To avoid cross - reactivity between adjacent reagent areas, the strips were incubated in a horizontal position. Colour development was evaluated after 60 seconds of incubation (60 - 120 seconds for the leukocyte pad) by visually comparing the colour of each reagent area with the reference scale provided on the container. Colour changes appearing only at the rim of the pad or beyond 2 minutes post - immersion were considered artefactual and excluded from

interpretation. All readings were performed under diffuse daylight or a standardized daylight lamp to ensure consistency.

Parameter	Acronym	Time	Reading						
Bilirubin	BIL	60 sec	neg	1 mg/dL	2 mg/dL	4 mg/dL			
Urobilinogen	UBG	60 sec	norm	2 mg/dL	4 mg/dL	8 mg/dL	12 mg/dL		
Ketones	KET	60 sec	neg	trace	25 mg/dL	100 mg/dL	300 mg/dL		
Ascorbic acid	ASC	60 sec	neg	5 mg/dL	10 mg/dL				
Glucose	GLU	60 sec	norm	50 mg/dL	100 mg/dL	250 mg/dL	500 mg/dL	> 1000 mg/dL	
Protein	PRO	60 sec	neg	trace	30 mg/dL	100 mg/dL	500 mg/dL		
Blood	BLD	60 sec	neg	5 - 10 ery/**µ**L	~50 ery/**µ**L	~300 ery/**µ**L			
pH	pH	60 sec	5	6	6.5	7	8	9	
Nitrite	NIT	60 sec	neg	0.05 mg/dL	0.1 mg/dL				
Leukocytes	LEU	60 - 120 sec	neg	~25 leu/**µ**L	~75 leu/**µ**L	~500 leu/**µ**L			
Specific gravity	SG	60 sec	1000	1005	1010	1015	1020	1025	1030

Table 3.4. The table summarizes the eleven parameters assessed using the Urine Strips COMBI SCREEN® 11 SYS PLUS. The first and second columns report the parameter acronym and its corresponding analyte, respectively. The third column specifies the time interval after immersion at which the reagent areas can be read. The remaining seven columns present the range of possible results obtainable for each parameter.

3.1.2.2. Use of a Buffer for the Stabilization of Urine Samples

Use of PBS to Buffer Urine Samples

Donors were instructed to collect a single 25 mL urine sample during the day. In total, urine samples were obtained from eight individual donors. Each sample was processed immediately upon collection. Initially, 2.5 mL of 10X PBS was added to each 25 mL urine sample to achieve a final PBS concentration of around 1X. Subsequently, an additional 5 mL of 10X PBS was added, bringing the total volume to 30 mL and the final PBS concentration to around 2X. Finally, 20 mL of 10X PBS was added to reach a final volume of 50 mL, corresponding to a PBS concentration of 5X. The pH of each sample was measured using a pH meter after each addition of 10X PBS.

Final concentration	PBS 1X	PBS 2X	PBS 5X
Volume of 10X PBS added to 25 mL of urine	2.5 mL	5 mL	25 mL

Table 3.5. Volume of 10X PBS added to 25 mL of urine to achieve the desired pH range.

Use of Phosphate Buffer for the Stabilization of Urine Samples

Prior to preparing the buffer solution, the desired pH, final volume, and target molarity were defined. Phosphoric acid has three pKa values: 2.16, 7.21, and 12.32. To prepare a buffer with a final pH of 7.4, the pKa value closest to the desired pH was selected (pKa = 7.21), using monosodium phosphate (NaH_2PO_4), and its conjugate base disodium phosphate (Na_2HPO_4). The appropriate acid - to - base ratio required to achieve the target pH was determined using the Henderson - Hasselbalch (HH) equation:

$$pH = pHa + log_{10}\frac{[Base]}{[Acid]}$$

Separate solutions of monosodium phosphate and disodium phosphate were prepared at the desired initial concentrations and subsequently mixed to obtain a stock phosphate buffer at the final concentration reported in Table 3.7. The pH of the resulting solution was adjusted to 7.4, if necessary, using phosphoric acid (H_3PO_4) or sodium hydroxide (NaOH). Finally, distilled water was added to bring the solution to the required final volume.

Stock buffer solution **Cf**	pH	pKa	NaH2PO4 **Ci**	Na_2HPO_4 $\mathbf{C_i}$
5 M	7.4	7.2	1.92 M	3.08 M
2.5 M	7.4	7.2	0.96 M	1.54 M
1 M	7.4	7.2	0.38 M	0.62 M
0.5 M	7.4	7.2	0.18 M	0.32 M

Table 3.6. The first column of the table reports the concentration of the phosphate buffer stock solution to be prepared. The second column specifies the target pH of the resulting buffer solution. The third column lists the pKa value of phosphoric acid employed in the HH equation, selected as the value closest to the desired pH. The fourth and fifth columns present the calculated concentrations of monosodium phosphate and disodium phosphate, respectively, as determined using the HH equation.

Stock solution concentration	Volume added in 100 mL of urine	Phosphate buffer final concentration
5 M	2 mL	0.1 M
2.5 M	4 mL	0.1 M
1 M	10 mL	0.1 M
0.5 M	10 mL	0.05 M

Table 3.7. Volume of phosphate buffer stock solution added to urine samples to achieve a neutral pH. The first column reports the initial concentration of the phosphate buffer stock solution, the second column indicates the volume of buffer added to 100 mL of urine, and the third column presents the final concentration of the diluted phosphate buffer within the urine sample.

In this experiment, donors were asked to collect a single 25 mL urine sample over the course of the day. A total of eight samples were obtained from eight individual donors. The initial pH of each sample was measured. To increase the variability of urine pH and assess the buffering capacity under alkaline conditions, sodium hydroxide (NaOH) was added to selected samples. Urine samples were processed immediately upon collection. To each sample, 250 µL of 5 M phosphate buffer was added to achieve a final concentration of 0.05 M. Subsequently, an additional 250 µL of 5 M phosphate buffer was added, for a total of 500 µL, corresponding to a final phosphate buffer concentration of 0.1 M. The pH of each sample was measured using a pH meter following each addition of the phosphate buffer.

Final concentration	Phosphate buffer 0.05 M	Phosphate buffer 0.1 M
Volume of phosphate buffer 5M added to 25 mL of urine	250 **µ**L	500 **µ**L

Table 3.8. Volume of phosphate buffer 5 M added to 25 mL of urine to reach the desired pH range.

1 M Phosphate Buffer addition

Donors were asked to collect a single 100 mL urine sample over the course of the day. A total of 36 samples were collected, comprising 18 from female and 18 from male donors (Table 3.9). The samples were stored at 4°C for 24 hours prior to processing. Before further analysis, all samples were visually inspected to exclude those exhibiting salt precipitation.

	Daily urine samples
Total number of donors	3
Female	2
Male	1
N° sample/donor/day	2
N° days	1
Total of samples	6
(a) total buffered samples	3
(b) total internal control samples	3
Storage temperature	4°C
Storage time	24 hours

Table 3.9. Schematic representation of donor sampling parameters, including the total number of donors, the number of samples provided per donor per day, the number of donation days per donor, the total number of samples collected, the storage temperature of urine samples following collection, and the duration of storage at the specified temperature.

0.5 M Phosphate Buffer addition

Donors were instructed to collect two 100 mL urine samples per day over a period of three consecutive days. A total of 36 samples were obtained, comprising 18 from female and 18 from male donors (Table 3.10). Following collection, all samples were stored at 4°C for 24 hours. Prior to processing, samples were inspected to exclude those exhibiting visible salt precipitation.

	Daily urine samples
Total number of donors	6
Female	3
Male	3
N° sample/donor/day	2
N° days	3
Total of samples	36
(a) total buffered samples	18
(b) total internal control	18
Storage temperature	4°C
Storage time	24 hours

Table 3.10. Schematic representation of donor sampling parameters, including the total number of donors, the number of samples provided per donor per day, the number of donation days per donor, the total number of samples collected, the storage temperature of urine samples following collection, and the duration of storage at the specified temperature.

3.1.2.3. Optimization of PTEC Isolation and Culture Using Cell Strainers

Evaluation of various cell strainer sizes for female samples processing

Urinary cell isolation was performed following the protocol described by Zhou et al. (40), as mentioned previously. Each donor was instructed to collect two 100 mL urine samples, to which antibiotics and antifungal agents were immediately added to ensure proper preservation at 4°C for up to 4 hours. After the storage period, the two samples from each donor were pooled to obtain a homogeneous 200 mL sample. A urine test strip analysis was then performed using the COMBI SCREEN® 11 SYS PLUS system, as detailed previously (subchapter 3.1.3.1).

The pooled sample was divided into four 50 mL conical tubes and centrifuged at 400 xg for 15 minutes. The resulting pellet was resuspended in Washing Buffer and subjected to a second centrifugation at 200 xg for 15 minutes. The supernatant was discarded, and the pellet was resuspended in 2 mL of Primary Medium. At this stage, 1 mL of the suspension was directly seeded into a 24 - well plate previously coated with EmbryoMax Gelatin. The remaining 1 mL was filtered using pluriStrainers (PluriSelect, Germany) with mesh sizes of 15, 20, and 30 μm, and then plated under identical conditions.
Cell cultures were maintained at 37°C, 5% CO_2, 95% RH. During the first three days, the Primary Medium was partially changed daily by removing 700 μL and replacing it with an equal volume of fresh medium to promote cell adhesion. Following this initial phase, the Primary Medium was gradually replaced with Proliferation Medium. Phase - contrast images of cells were acquired at day 1 and day 8 with a Nikon ECLIPSE - TS 100 Microscope (Nikon Corporation, Tokyo, Japan).

Isolation of PTEC from female donors using a 20 μm cell strainers

Female donors were instructed to collect two 100 mL urine samples per day over a period of six consecutive days. A total of 36 samples were obtained, corresponding to 12 samples per donor. Following collection, all samples were stored at 4°C for 4 hours prior to processing.

	Daily urine samples
Total number of donors	3
Female	3
N° sample/donor/day	2
N° days	6
Total of samples	36
(a) total buffered samples	18
(b) total internal control	18
Storage temperature	4°C
Storage time	4 hours

Table 3.11. Schematic representation of donor sampling parameters, including the total number of donors, the number of samples provided per donor per day, the number of donation days per donor, the total number of samples collected, the storage temperature of urine samples following collection, and the duration of storage at the specified temperature.

3.1.3. Improved and Definitive Protocols: Integrated Use of Test Strips, 0.5 M Phosphate Buffer, and 20 µm Cell Strainer

Urinary cell isolation was carried out following the protocol described by Zhou et al (40). Each donor was instructed to collect a single 100 mL urine sample and immediately supplemented with a solution containing 10 mL of 0.5 M phosphate buffer and a mixture of antibiotics and antifungal agents. Samples were then stored at 4°C for 24 hours (subchapter 3.1.3.1) and 4 hours (subchapter 3.1.2.2).

3.1.3.1 Preparation of PTEC by Combined Application of Test Strips, 0.5 M Phosphate Buffer and 20 µm Cell Strainer (After 24 Hours)

Following the storage period (see details in Table 3.12), samples were equilibrated to room temperature for urine test strip analysis, as described previously. Each sample was subsequently divided into two 50 mL conical tubes and centrifuged at 400 xg for 15 minutes. The resulting pellet was resuspended in Washing Buffer and centrifuged again at 200 xg for 15 minutes. After discarding the supernatant, the final pellet was resuspended in 1 mL of Primary Medium. The cell suspension was then filtered using a 20 µm pluriStrainer (PluriSelect, Germany) and plated in culture. Cultures were maintained in the incubator (37°C, 5% CO_2, 95% RH). During the first three days, the Primary Medium was partially replaced daily by removing 700 µL and adding an equal volume of fresh medium to facilitate cell attachment. Thereafter, the Primary Medium was gradually replaced with Proliferation Medium. Throughout the three - week culture period, PTEC adhered to the substrate and progressively expanded.

	Daily urine samples
Total number of donors	6
Female	3
Male	3
N° sample/donor/day	6
N° days	3
Total of samples	108
(a) total buffered samples	108
(b) total filtered samples	108
Storage temperature	4°C
Storage time	24 hours

Table 3.12. Schematic representation of donor sampling parameters, including the total number of donors, the number of samples provided per donor per day, the number of donation days per donor, the total number of samples collected (buffered and filtered), the storage temperature of urine samples following collection, and the duration of storage at the specified temperature.

3.1.3.2 Preparation of PTEC by Combined Application of Test Strips, 0.5 M Phosphate Buffer and 20 µm Cell Strainer Only for Female Samples (After 4 Hours)

Following the storage period (see details in Table 3.13), samples were equilibrated to room temperature for urine test strip analysis, as described previously. Each sample was subsequently divided into two 50 mL conical tubes and centrifuged at 400 xg for 15 minutes. The resulting pellet was resuspended in Washing Buffer and centrifuged again at 200 xg for 15 minutes. After discarding the supernatant, the final pellet was resuspended in 1 mL of Primary Medium. The cell suspension, only for female samples, was then filtered using a 20 µm pluriStrainer (PluriSelect, Germany) and plated in culture. Cultures were maintained in the incubator (37°C, 5% CO_2, 95% RH). During the first three days, the Primary Medium was partially replaced daily by removing 700 µL and adding an equal volume of fresh medium to facilitate cell attachment. Thereafter, the Primary Medium was gradually replaced with Proliferation Medium. Throughout the three - week culture period, PTEC adhered to the substrate and progressively expanded.

	Daily urine samples
Total number of donors	4
Female	2
Male	2
Total of samples	99
(a) total buffered samples	99
(b) total filtered samples	66
Storage temperature	4°C
Storage time	4 hours

Table 3.13. Schematic representation of donor sampling parameters, including the total number of donors, the total number of samples collected (buffered and filtered), the storage temperature of urine samples following collection, and the duration of storage at the specified temperature.

The final chosen protocol is illustrated in Figure 3.4.

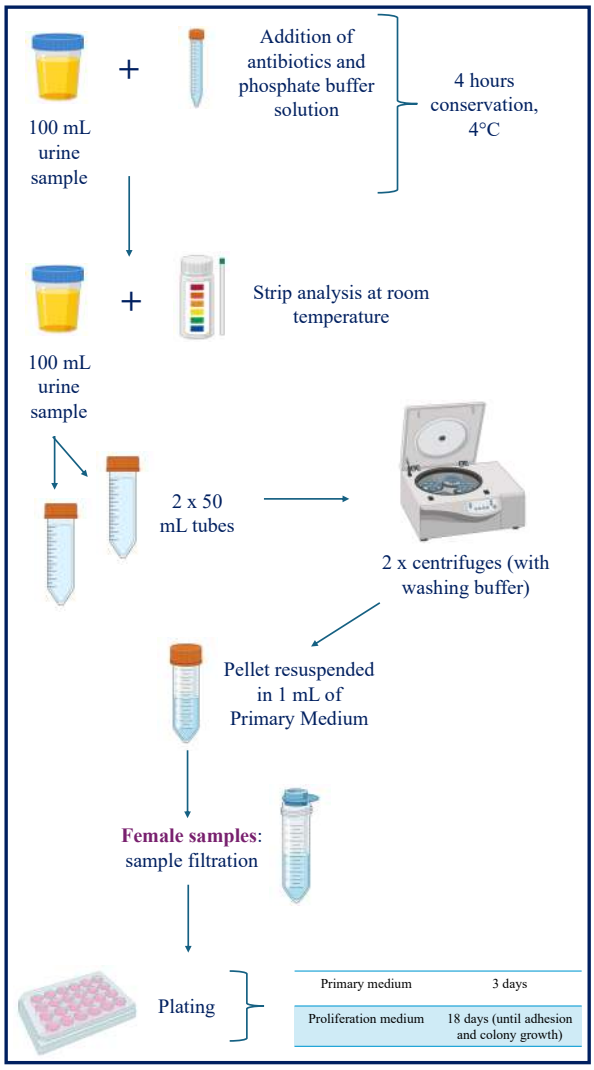

Figure 3.4. Graphical representation of the PTEC isolation process from urine samples. The figure illustrates the specific stages at which buffer solution was added, and sample filtration was performed. This image was created using BioRender.com

3.1.4. Statistical Analysis

Statistical analysis was performed for the last two experiments (described in Sections 3.1.3.1. and 3.1.3.2. of the Materials and Methods), whereas all preceding experiments were considered pilot studies. The minimum sample size was determined according to Rcmdr (R Commander).

Data for the various parameters were obtained from the urine strip analysis. For each parameter, the percentage of samples in which urinary cell adhesion occurred and the percentage in which adhesion did not occur were calculated. A 95% confidence interval (CI) was then computed for each group using Rcmdr.. In this context, the confidence interval for a population proportion was used to estimate the likelihood of a specific characteristic - namely, urinary cell adhesion or non - adhesion - occurring within the population.

To evaluate whether urine pH influences urinary cell adhesion, a Chi - Square test for independence was performed using Rcmdr. The null hypothesis (H_0) stated that *urine pH is independent of urinary cell adhesion*, whereas the alternative hypothesis (H_1) posited that *urinary cell adhesion is dependent on urine pH*.

Degrees of freedom were calculated by multiplying the number of categories for each variable minus one. In this case, urine pH was categorized into two groups: $pH < 7$ and $pH \geq 7$, while the second variable corresponded to the presence or absence of urinary cell adhesion. The significance level (α) was set at 0.05, representing a 5% risk of committing a Type I error - that is, rejecting a true null hypothesis. Results were then reported in the following format:

$$\chi^2 \text{ (degrees of freedom, } N = \text{sample size)} = \text{test statistic, } p = p \text{ value}$$

It should be noted that the Chi - Square test for independence identifies associations between variables but does not imply causality.

3.2. iPSC Generation from PTEC and Their Subsequent Culture (Step 2)

3.2.1. Lentiviral Vector Production and PTEC Transduction

Lentiviral vector production was carried out according to the protocols described by Zhou et al. and Overeem et al. (40) (68).

To induce the reprogramming of PTEC into induced pluripotent stem cells (iPSC), a second - generation lentiviral vector system was employed. This approach enabled efficient transduction of PTEC and facilitated their reprogramming through the expression of the four Yamanaka factors – **OCT4, SOX2, KLF4, and c - MYC** – as originally described by Takahashi and Yamanaka (69).
The lentiviral system was generated using a three - plasmid transfection method, consisting of:

- A packaging plasmid (**psPAX2**) (Figure 3.5 - A)
- A reprogramming plasmid (**pRRL.PPT.SF.hOct34co.hKlf4co.hSox2co.hmyc.itdTomato.pre.FRT**) encoding codon - optimized versions of the Yamanaka factors along with a fluorescent reporter (Figure 3.5 - B), and
- A plasmid encoding the vesicular stomatitis virus glycoprotein (pMD2.G) for envelope formation (Figure 3.5 - C)

The reprogramming plasmid was kindly provided by Prof. C. Baum and Prof. A. Schambach from the Institute of Experimental Haematology, Hannover, Germany. The psPAX2 and pMD2.G plasmids were generously provided by Prof. Serena Zacchigna from the Department of Medical, Surgical and Health Sciences, University of Trieste. All three plasmids were subsequently amplified by Dr. Luisa Napolitano and Dr. Antonio Longo at the Structural Biology Laboratory, Elettra - Sincrotrone, Trieste, Italy.

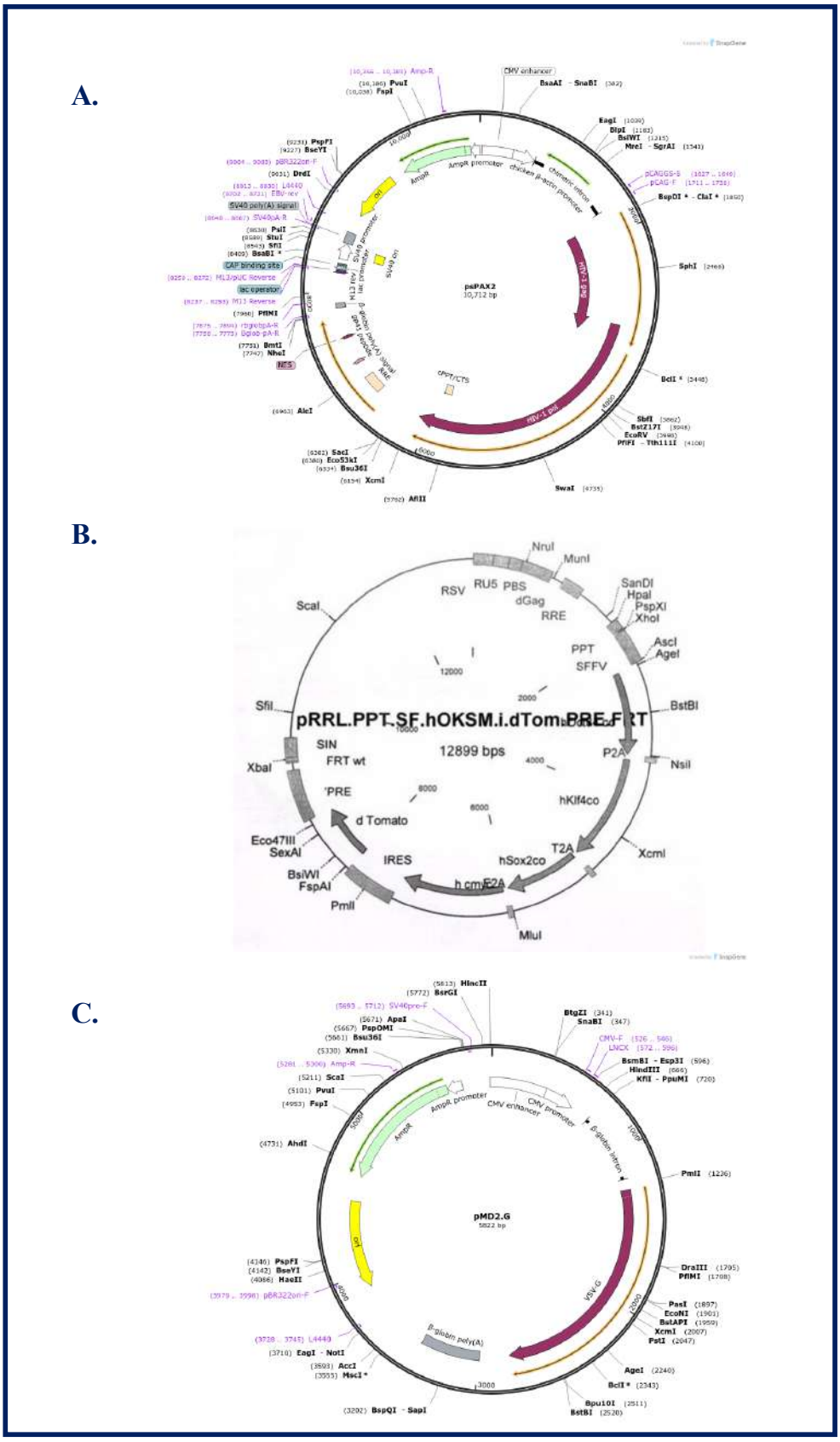

Figure 3.5. Schematic representation of the three plasmids encoding the lentiviral vector. The figure illustrates the structure of the plasmids used for HEK293T transfection. (A) the packaging plasmid psPAX2 (AddGene plasmid #12260); (B) the transfer plasmid pRRL.PPT.SF.hOct34co.hKlf4co.hSox2co.hmyc.itdTomato.pre.FRT; and (C) the envelope plasmid pMD2.G (AddGene plasmid #12259).

The HIV - based lentiviral vector system employed in this study is designed with enhanced - biosafety features to minimize the risk of generating replication - competent viruses. Key safety modifications include:

- Self - inactivating design: a deletion in the enhancer region of the U3 segment within the 3'ΔLTR ensures self - inactivation of the vector following transduction and integration into the host cell genome
- Tat - independent transcription: the presence of an RSV promoter upstream of the 5'LTR allows efficient transcription of the viral RNA in the absence of the HIV - 1 Tat protein, thereby reducing the number of HIV - 1 genes utilized in the system
- Minimal packaging components: only three HIV - 1 genes (gag, pol, and rev) are required for viral packaging, replication, and transduction. These genes are supplied in trans from separate helper plasmids that lack packaging signals and do not share significant sequence homology with the expression vector or with the pVSV - G envelope plasmid, thus minimizing the risk of homologous recombination leading to the formation of replication - competent lentivirus (RCL).
- Replication incompetence: the gag, pol, and rev genes are not present in the packaged viral genome, as they are expressed from helper plasmids lacking packaging sequences. Consequently, the resulting lentiviral particles are replication - deficient.
- Cargo specificity. The pseudotyped viral particles carry only the expression cassette of interest, ensuring that no viral coding sequences are transferred to the target cells.

Despite the aforementioned safety features, the use of HIV - based lentiviral vectors is classified under NIH Biosafety Level 2 (BSL - 2) guidelines (see: https://www.izsmportici.it/wp-content/uploads/2025/02/Normativa-rischio-biologico-Inail.pdf) due to the potential biological risks associated with recombination events involving endogenous viral sequences, which could generate replication - competent viruses, or the possibility of insertional mutagenesis.

All procedures involving lentiviral particle preparation and handling were conducted following BSL - 2 biosafety protocols. Work was performed in a designated cell culture room using a Class II (P2) laminar flow cabinet. During incubation, culture plates were placed within secondary containment to prevent accidental spills. Appropriate personal protective equipment (PPE), including laboratory coat and gloves, was always worn. Open tubes were handled exclusively within the laminar flow hood; when removed, tubes were tightly closed and externally disinfected with 75% ethanol. All laboratory

materials that came into contact with viral particles were treated as biohazardous waste. Liquid waste was aspirated into a dedicated container containing freshly added concentrated bleach and replenished whenever the solution lost its yellow coloration. Once the container was full and following a minimum 10 - minute contact time for decontamination, the liquid waste was transferred to a designated biohazardous liquid waste disposal system. Solid waste, including consumables and plasticware, was collected in a waste bag placed under the laminar flow cabinet. Once filled, the bags were sealed within the cabinet and subsequently transferred to certified biohazard disposal containers.

To enable the transduction of PTEC, lentiviral vector production was first carried out. Human Embryonic Kidney 293T (HEK293T) cells were seeded at a density of 600,000 cells per well in a 6 - well plate and maintained in HEK medium composed of High - glucose DMEM (Gibco), supplemented with 5% FBS, 1% L - Glut, and 1% penicillin - streptomycin. Upon reaching approximately 80% confluency, cells were transfected with equimolar amounts (1:1:1 ratio) of the three required plasmids using Lipofectamine 2000 (Life Technologies) in Opti - MEM reduced serum medium (Gibco). The lipid - based nature of Lipofectamine facilitated the fusion of adjacent cell membranes, leading to the formation of multicellular aggregates within the HEK293T culture.
16 hours post - transfection, the medium was replaced with fresh HEK medium. After 36 hours, the lentiviral particles assembled and secreted into the supernatant by the HEK293T cells were harvested for use in the transduction of PTEC. Prior to transduction, the viral supernatant was passed through a 0.45 μm filter to remove any residual HEK cells or cellular debris. Polybrene (final concentration: 8 μg/mL) was added to the filtered medium to enhance viral entry into PTEC. The lentiviral suspension was then applied to the target cells dropwise to facilitate efficient transduction. Following the first collection, fresh medium was added to the HEK293T cells, and a second round of viral supernatant was collected 24 hours later, processed in the same manner. After this second harvest, the HEK293T cells were discarded.

Assessment of Lentiviral Transduction Efficiency in PTEC

Cell segmentation and counting were performed in Fiji (RRID:SCR_002285) using TrackMate - Cellpose plugin. Brightfield images were analyzed with the cyto2 model to identify all cells, while tdTomato fluorescence images were processed separately to detect transduced (tdTomato - positive) cells. The resulting Regions of Interest (ROIs) data and counts were exported from Fiji to compute transduction efficiency as the percentage of tdTomato - positive cells relative to the total cell population.

3.2.2. iPSC Generation and Their Culture

Induced pluripotent stem cells (iPSCs) were generated from PTEC through lentiviral vector - mediated reprogramming. PTEC were seeded several days prior to transduction to reach approximately 75% confluency on the day of the first lentiviral exposure (2,000,000 cells per well in 6 - well plates). Two consecutive transductions were carried out 24 hours apart using the culture supernatant collected from HEK293T cells containing the lentiviral vector. Between transductions, the culture medium was replaced with fresh Proliferation Medium for 8 - 12 hours to allow for cellular recovery.

To verify the insertion of the plasmid carrying the tdTomato fluorescent signal in the cells, PTEC were examined under a ZEISS Axiovert 200 Fluorescence Microscope.

Two days after the second transduction, cells were transferred to vitronectin - coated wells (0.5 $\mu g/cm^2$) and cultured in Essential 6 Medium (Thermo Fisher) supplemented with fibroblast growth factor (FGF; 100 ng/µL) and 0.5% penicillin - streptomycin.

Emerging iPSC colonies typically appeared between days 7 and 12 post - transduction. At this point, the culture medium was switched to Essential 8 Medium (Thermo Fisher) supplemented with 0.5% penicillin - streptomycin to support colony maintenance and expansion. iPSC colonies were passaged using 0.5 mM EDTA in PBS for over 10 passages and cryopreserved in liquid nitrogen for future use. For each passage, colonies were replated onto freshly vitronectin - coated culture dishes in the presence of 1% RevitaCell Supplement (Thermo Fisher) to enhance post - passaging cell survival. Medium was refreshed daily. The generation of iPSC colonies was typically complete within two weeks of culture.

Verification of Transgene Integration in Lentivirus - Generated iPSC cDNA through Qualitative PCR

Transgene integration was assessed on cDNA obtained from iPSC generated using lentiviral vectors. Primer pairs specific for the transgene were employed (Table 3.14). PCR amplification was performed on samples subjected to reverse transcriptase (+RT) and on negative controls lacking reverse transcriptase (-RT). PX459, gDNA, and PMX were included as expression controls.

Two primer pairs were designed on the reprogramming plasmid (pRRL.PPT.SF.hOct34co.hKlf4co.hSox2co.hmyc.itdTomato.pre.FRT) to specifically amplify the endogenous genes.

Figure 3.6 presents the map of the plasmid employed, while Table 3.14 provides the specific sequences corresponding to each primer.

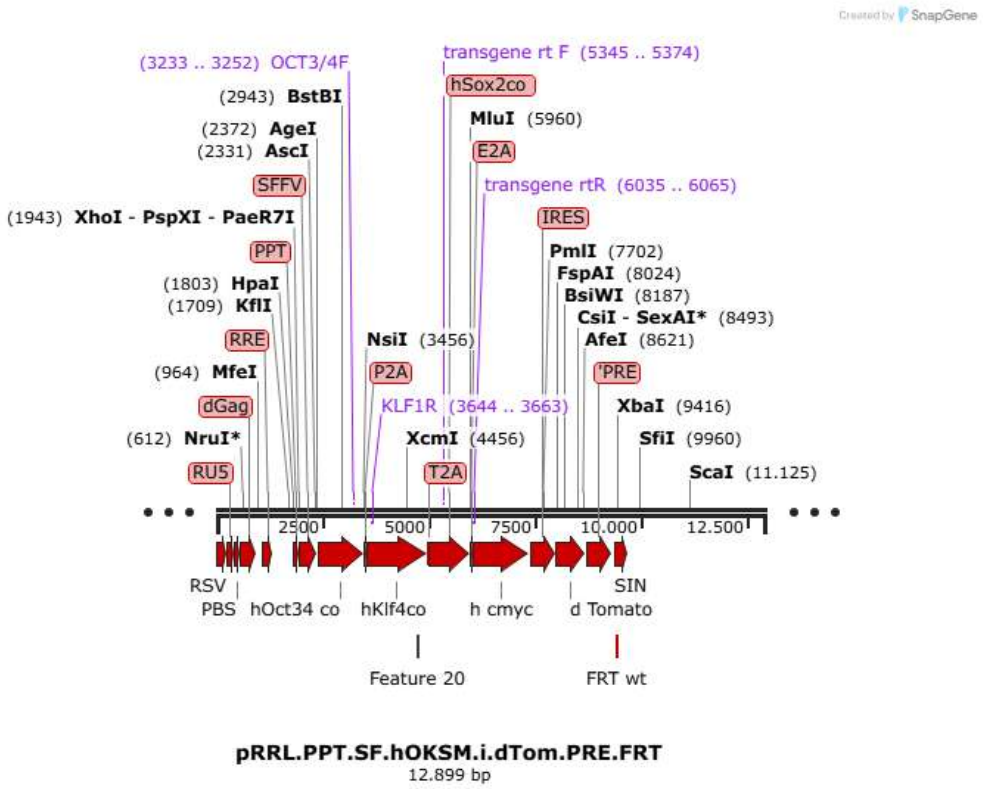

Figure 3.6. Map representing the reprogramming plasmid and position of the two primer pairs. Image was created with SnapGene.

Primer	Sequence
OCT3/4 F	AAGGGCAAGAGAAGCAGCAG
KLF1 R	CGCTTCATGTGGCTCAGTTC
Transgene rt F	AGAAGAAAGACCAAGACCCTGATGAAGAAG
Transgene rt R	CATAGTTCCTGTTGGTGAAGCTAACGTTGAG

Table 3.14. Sequences of the two primer pairs used.

3.3. iPSC Differentiation into Hepatocytes - Protocol Comparison (Step 3)

Four different protocols [(68); (70); (71); (72)] were compared, as listed below.

Overeem's Protocol (68)

This differentiation protocol consists of 4 stages and has a total duration of 19 days.

150.000 iPSCs were plated as single cells in vitronectin - coated 12 multi - well plate, cultured in Essential 8™ medium with RevitaCell supplement. The day after, PSC Definitive - Endoderm Induction Kit was used to differentiate them into definitive endoderm. After 2 days, RPMI - 1640 supplemented with 20 ng/mL BMP4, 10 ng/mL FGF2, 0.5% DMSO (Sigma-Aldrich) and B-27™ supplement (Thermo Fisher) was added for 5 days. Then, cells were detached as single cells using Accutase (StemPro™ Accutase™ Cell Dissociation Reagent, Gibco™, Life Technologies Corporation, 3175 Staley Rd., Grand Island, NY 14072, USA) and then transferred to Matrigel - coated wells in RPMI - 1640 with 20 ng/mL HGF, 0.5% DMSO, and B - 27 supplement with 1% RevitaCell supplement on the first day. After 5 days, cells were cultured in Hepatocyte Culture Medium Bulletkit™ medium (Lonza, Walkersville, MD USA) with 20 ng/mL Oncostatin M and overlaid with Matrigel (at a concentration of 0.25 mg/mL). The medium was changed daily for all stages of differentiation.

Matakovic's Protocol (70)

This differentiation protocol consists of 4 stages and has a total duration of 19 days.
At day 0, 150.000 iPSC were plated into a Matrigel - coated (Corning ® Matrigel ® hESC - qualified Matrix, 354277, Stem Cell Technologies, Discovery Labware, Inc, Two Oak Park, Bedford, MA 01730 USA) 12 multi - well plate and cultured for 24 hours in the cell culture incubator. To prevent and contain bacterial contamination, we added to each media 1% Pen - Strep and 0.5% Gentamicin (Euroclone S.p.A., Pero (MI), Italy).
On day 1, the medium was replaced with PSC DE - Induction Medium A (Gibco™, Life Technologies Corporation, Grand Island, NY 14072, USA) and the cells were left for 24 hours in the cell culture incubator. On day 2, the medium was replaced with PSC DE - Induction Medium B (Gibco™, Life Technologies Corporation, Grand Island, NY 14072, USA). On day 3, Medium B was replaced with RPMI - 1640 medium (Euroclone S.p.A., Pero (MI), Italy), supplemented with B - 27 Supplement - 50x (1:50) serum free (Gibco™, Life Technologies Corporation, Grand Island, NY 14072, USA), 10 ng/mL Fibroblast Growth Factor 2 (FGF2) (PeproTech, Thermo Fisher , Waltham, Massachusetts, USA), 20 ng/mL Bone Morphogenetic Protein (BMP) 4 (PeproTech, Thermo Fisher , Waltham, Massachusetts, USA), 0,5% (v/v) dimethyl sulfoxide (DMSO, Sigma - Aldrich, Co., 3050 Spruce Street, St. Louis, MO 63103 USA). From day 4 to day 7, daily, this medium was aspirated and replaced with an equal volume of the same fresh medium. On day 8, the medium was switched to RPMI - 1640 medium, supplemented with B - 27 supplement, 20 ng/mL Hepatocyte Growth Factor (HGF) (PeproTech, Thermo Fisher, Waltham, Massachusetts, USA) and 0.5% (v/v) DMSO. From

day 9 to day 12, on a daily basis, this medium was aspirated and replaced with an equal volume of the same fresh medium. On day 13, the medium was switched to William's E medium (without phenol red, Gibco™, Life Technologies Corporation, 3175 Staley Rd., Grand Island, NY 14072, USA) supplemented with Primary Hepatocyte Maintenance Supplements (Gibco™, Life Technologies Corporation, 3175 Staley Rd., Grand Island, NY 14072, USA), 20 ng/mL Oncostatin M (PeproTech, Thermo Fisher , Waltham, Massachusetts, USA) and embryonic stem cell - qualified Matrigel, at a concentration of 0.25 mg/mL. On a daily basis, from day 14 to day 19, this medium was aspirated and replaced with an equal amount of the same fresh Matrigel supplemented medium.

Mallanna's Protocol (71)

This experimental part of the project was carried out, inside a multicentric study, by the research group of the Medical Genetics Laboratory, led by Professor Adamo Pio d'Adamo, at the IRCCS Materno Infantile "Burlo Garofolo" Hospital in Trieste, Italy.

This differentiation protocol consists of 3 stages and has a total duration of 20 days.
iPSCs were seeded onto 100 mm tissue culture dishes pre - coated with either E - Cadherin - Fc (StemAdhere) or Matrigel. Upon reaching a confluency of no more than 50%, cells were transferred to an appropriate number of 35 mm dishes in a 6 - well tissue culture plate, also coated with Matrigel, and incubated overnight at 37°C, 4% O_2, 5% CO_2. On differentiation days 1 and 2, the culture medium was replaced with RPMI 1640 medium (pre - warmed to 37°C) supplemented with 2% B27 supplement lacking insulin, 100 ng/mL Activin A, 10 ng/mL BMP4, and 20 ng/mL FGF2. From days 3 to 5 of differentiation, the medium was switched to RPMI with 2% B27 (without insulin) supplemented with 100 ng/mL Activin A. From days 6 to 10, the cells were cultured in RPMI with 2% B27 (without insulin) containing 20 ng/mL BMP4 and 10 ng/mL FGF2. During days 11 to 15, hepatic progenitor cells were maintained in RPMI medium supplemented with 2% B27 (with insulin) and 20 ng/mL hepatocyte growth factor (HGF). From days 16 to 20, differentiation was continued in Clonetics® Hepatocyte Culture Medium (HCM™) supplemented with the provided "SingleQuots" (excluding EGF) and 20 ng/mL Oncostatin M.

STEMdiff™ Hepatocyte Kit (72)

This experimental part of the project was carried out, inside a multicentric study, by the research group of the Medical Genetics Laboratory, led by Professor Adamo Pio d'Adamo, at the IRCCS Materno Infantile "Burlo Garofolo" Hospital in Trieste, Italy.

This differentiation protocol consists of 3 stages and has a total duration of 21 days.
One day prior to cell seeding, 24 - well or 96 - well tissue culture - treated plates were coated with Matrigel according to the manufacturer's instructions. iPSCs were seeded at a density of 4 x 10^5 cells per well (24 - well plate) or 7 x 10^4 cells per well (96 - well plate) in mTeSR™1 medium and incubated at 37°C and 5% CO_2 incubator for 24 hours. On day 1 of differentiation, the medium was replaced with STEMdiff ™ Basal Medium (Hepatic) supplemented with STEMdiff ™ Definitive Endoderm Supplement MR and STEMdiff ™ Definitive Endoderm Supplement CJ, which was maintained through days 3 and 4 with daily medium changes. On day 5, cells received a full medium change with STEMdiff™ Hepatic Progenitor Medium. On days 6 and 7, fresh STEMdiff™ Hepatic Progenitor Medium was added with full medium changes performed daily. A subsequent medium change with the same formulation was conducted on day 9. On day 10, the medium was replaced with STEMdiff™ Hepatocyte Medium, and cells were incubated at 37°C for 48 hours. Beginning on day 12 and continuing every other day until day 21, a complete medium change with fresh STEMdiff ™ Hepatocyte Medium was performed.

3.3.1. Phase - Contrast Microscopy

Phase - contrast photos were captured with a Nikon ECLIPSE - TS 100 Microscope (Nikon Corporation, Tokyo, Japan) at the magnification of 10X and 20X.
Photos were taken at the main three stages of differentiation for each protocol (Definitive Endoderm, Hepatic Progenitors, Hepatocyte - like Cells).

3.3.2. ELISA - Albumin Release in the Medium

The release of albumin in the medium was evaluated through the Human Albumin ELISA kit (RayBio ®, RayBiotech Life, Inc., GA 30092, USA) according to the manufacturer instructions, using Multimode Plate Reader (Perkin Elmer - EnSpire®, Perkin - Elmer, Inc., Waltham, Massachusetts,

USA). Cell culture media were collected and centrifuged at 1500 rpm for 10 minutes at 4°C to remove debris.
For each protocol, the media of the two key steps of hepatic differentiation (Hepatic Progenitors and Hepatocyte - like Cells) were collected. The media of HepG2 cell line and Upcyte® hepatocytes were used as a control.

For a detailed description of the molecular analysis methods and immunofluorescence experiments, please refer to subchapters 3.6 and 3.7 of this chapter.

3.4. 2D and 3D Cultures from Rat Primary Adult Hepatocytes

3.4.1. Rat Liver Perfusion and Digestion

To establish the liver perfusion protocol in rodents, rats were selected as the model organism. This procedure was adapted from the method described by Shen et al. (73). All procedures and animal housing were conducted at the Animal Facility of the University of Trieste, according to the guidelines of the Italian Law and European Community directive. The experimental protocol was approved by the local Animal Care Committee and by the Italian Health Ministry (permit n° 321/2022-PR) according to art.31 of decree 26/2014. The animals used were Wistar rats, maintained on a standard chow diet with *ad libitum* access to water.

Preparation for Surgical Procedure

Prior to initiating the surgical procedure, all tubing was flushed with 70% ethanol, then thoroughly dried at 37°C. Surgical instruments, including tweezers, surgical scissors, and Klemmer forceps, were similarly disinfected and dried at 37°C. All equipment was subsequently exposed to UV light for 15 minutes under a biological safety cabinet to ensure sterility. Following UV treatment, materials were wrapped in aluminium foil to prevent contamination during transport to the animal facility. A water bath was pre - warmed to 42°C, and both the Perfusion Buffer and 1X PBS were incubated in the bath for approximately 20 minutes prior to use. Due to the heat sensitivity of the enzymes, the Digestion Buffer was warmed only immediately before use, after perfusion had begun. William's Complete Medium and PBS supplemented with 3% penicillin/streptomycin were kept on ice throughout the procedure. The peristaltic pump was connected to the tubing system, which included

a glass reservoir bottle and a bubble trap, both pre - filled with warm Perfusion Buffer. To prime the system, the tubing was filled with the buffer at low pump speed to remove air bubbles and to eliminate residual ethanol from the tubes.

Initial Procedure and Anaesthesia

Adult Wistar rats (10 - 12 weeks old, body weight 250 - 350 g) were anesthetized via intraperitoneal injection of an anaesthesia cocktail consisting of xylazine (22.5 mg/kg) and ketamine (112.5 mg/kg). Depth of anaesthesia was assessed using the toe - pinch reflex, and surgery was initiated only after the animal failed to respond to noxious stimuli, typically within 3 - 5 minutes. The abdominal area was shaved and disinfected with 70% ethanol to reduce the risk of bacterial contamination. The animal was placed in the centre of a dissection tray, and its limbs were secured using sterile pins. A U - shaped incision was made through both the skin and abdominal muscle, extending from the lower abdomen to the rib cage. The skin was retracted and held in place using clamps near the thoracic region. Special care was taken throughout the surgical procedure to avoid damaging large blood vessels, as bleeding can obscure the surgical field and hinder access to critical anatomical structures necessary for liver perfusion. In the event of bleeding, gentle pressure was applied to promote clot formation and minimize blood loss. The intestines were carefully displaced to the right, exposing the portal vein (PV) and inferior vena cava (IVC). Using forceps, a cotton thread was passed underneath the portal vein, and a loose ligature was prepared without tightening it at this stage. To prevent intravascular coagulation, 250 units of heparin diluted in 300 µL of 1X PBS were injected into the inferior vena cava. Immediately prior to cannulation, the pre - positioned cotton thread beneath the PV was prepared for ligation. After insertion of the cannula (angiocath) into the portal vein, the ligature was securely tightened to stabilize the cannula and prevent displacement during perfusion.

Cannulation and Liver Perfusion

The peristaltic pump was initially set to a flow rate below 1 mL/min. An 18 - gauge angiocath was inserted into the PV at the site of the pre - positioned ligature, maintaining a shallow insertion angle relative to the vein to minimize vessel damage. After insertion, the inner stylet of the angiocath was removed, leaving the plastic cannula in place. Liver Perfusion Medium (Gibco) was used as the initial perfusate. While the perfusion buffer was running through the tubing, the cannula was connected to the outlet line using a Luer - lock connector. The ligature around the PV was then securely tightened to fix the cannula in place. Subsequently, the IVC was cut to allow blood to exit, establishing an open

circulatory system. The perfusion was initiated at 1 mL/min. Within 2 - 3 seconds, the liver began to swell and blanch, indicating correct buffer flow through the vasculature. The pump speed was gradually increased to 10 ml/min and maintained for a minimum of 10 minutes to effectively flush out residual blood from the liver. A slow initial flow rate was used to validate proper cannulation of the portal vein. In cases where surrounding extrahepatic tissues began to swell, cannulation was considered suboptimal. Minor adjustments – either advancing or slightly retracting the cannula – were made to correct positioning and restore efficient perfusion. To ensure full perfusate outflow, the IVC was severed, confirming an open, unidirectional flow from the PV to the cut IVC. Correct liver perfusion was further supported by gentle manual pressure on the IVC using a cotton swab to enhance distribution of the buffer throughout all liver lobes. Since liver swelling is a critical determinant of successful cell isolation, alternating cycles of pressure and release were performed throughout the perfusion process. Specifically, intermittent pressure was applied to the IVC using a cotton swab for 10 - second intervals, followed by relaxation. These cycles were repeated 5 - 10 times, promoting visible liver swelling during clamping and relaxation during release, thus facilitating enhanced dissociation and improved cell yield.

Liver Digestion

Following the initial perfusion, the system was seamlessly switched to the pre - warmed Liver Digestion Medium (Gibco) without interrupting flow and ensuring no air bubbles entered the tubing. The peristaltic pump speed was increased to 20 mL/min, and intermittent pressure was again applied to the IVC using a cotton swab to promote alternating liver swelling and relaxation. As the digestion buffer circulated (for approximately 15 minutes), the liver began to appear soft and friable, indicating adequate enzymatic digestion. At this point, the cannula was carefully removed, and the pump was turned off. The liver was then gently excised. Using forceps, the central connective tissue between the lobes was grasped, and all attachments to adjacent organs were carefully severed. The liver was immediately briefly immersed in pre - chilled PBS supplemented with 3% penicillin/streptomycin (P/S) for a few seconds to remove residual buffer and then transferred to a tube containing pre - chilled Williams' Complete Medium for subsequent processing.

3.4.2. Hepatocytes Isolation

Under a biological hood, the liver was transferred into a sterile 100 mm Petri dish containing 15 mL of ice - cold William's E Complete Medium (Thermo Fisher). The dish was placed on an ice - filled

tray to maintain low temperature throughout the procedure. The intact liver tissue was mechanically dissociated using a cell scraper to release parenchymal hepatocytes into the medium. The Glisson's capsule was gently disrupted by vigorous scraping to promote the release of single hepatocytes. This process was continued until only residual capsular collagen fibres remained visible. The resulting cell suspension was collected and passed through a 100 μm cell strainer into a sterile 450 mL Falcon tube to remove connective tissue and undigested fragments. To further maximize cell release, the remaining liver remnants in the Petri dish were washed with an additional 15 mL of cold William's Complete Medium supplemented with 100 nM dexamethasone (Sigma - Aldrich), 1X penicillin/streptomycin, L - glutamine, 1X Insulin - Transferrin - Selenium supplement (Life Technologies), and 5% FBS. This solution was used to rinse the Petri dish and added to the filtered cell suspension. The pooled filtrate was centrifuged at 50 xg for 3 minutes at 4°C using a low brake setting. The supernatant was carefully discarded, and the resulting pellet was resuspended in 40 mL of ice - cold Williams' Complete Medium. A second identical centrifugation step was performed, followed by resuspension in 25 mL of the same medium. To purify viable hepatocytes, 25 mL of 90% Percoll solution (Santa Cruz) was added to the cell suspension and gently mixed. This density gradient centrifugation step enables separation of live (higher density) from dead (lower density) cells. The suspension was centrifuged at 200 xg for 10 minutes at 4°C. Following centrifugation, a visible pellet of a viable hepatocytes was observed at the bottom of the tube, while a layer of dead cells formed near the top of the gradient. The dead cell layer was carefully aspirated, leaving approximately 1 - 2 mL of medium above the viable cell pellet. The hepatocytes pellet was resuspended in 30 - 40 mL of ice - cold William's E Complete Medium, followed by a final centrifugation at 200 xg for 10 minutes at 4°C. The supernatant was removed, and the final pellet containing primary hepatocytes (PHs) was plated in collagen type VI (Sigma - Aldrich) precoated multiwell plates. The cells were then used for further analyses, including phase - contrast microscopy, Trypan Blue exclusion assay to assess cell viability, and RNA extraction.

3.4.3. Primary Hepatocyte Culture

Each well of a 6 - well plate was coated with 8 μg/cm^2 of collagen solution (Sigma - Aldrich) and incubated overnight at 4°C to allow protein binding. The following day, excess collagen was removed, and the wells were air - dried at 37°C for approximately 2 hours. PHs were seeded at a density of 50,000 cells per 10 cm^2 well and cultured in Williams' E complete medium (Thermo Fisher), which was replaced daily. Cells were harvested at defined time points (day 0, 1, 2, 3, 4, and 5) for viability

assessment via Trypan Blue exclusion assay, morphological evaluation using phase - contrast microscopy, and RNA extraction.

3.4.4. Primary Hepatocytes - derived Organoids (Hep - Orgs) Culture

For the establishment of 3D long - term hepatocyte culture, cells were resuspended in cold, undiluted matrix at a concentration of 1,000 - 10,000 cells per 20 μL, carefully avoiding the formation of air bubbles. Using pre - chilled pipette tips, droplets containing the cell - matrix suspension were dispensed into pre - warmed cell culture plates. The plates were then inverted and incubated for 20 - 30 minutes to allow proper gelation. Subsequently, the plates were returned to their upright position, and pre - warmed 3D long - term hepatocyte medium, supplemented with the specific culture medium described by Kluiver et al. (74), was added. Cultures were maintained under standard incubator conditions, and the medium was replaced every 2 - 3 days. After a minimum of 14 days in culture, the Hep - Orgs were dissociated from the matrix, and their viability was assessed using Trypan Blue exclusion and EdU incorporation assays. The viable organoids were subsequently passaged following the protocol described by Peng et al. (63).

For a detailed description of the molecular analysis methods and immunofluorescence experiments, please refer to subchapters 3.6 and 3.7 of this chapter.

3.5. 3D Culture from Mouse Primary Adult Hepatocytes

3.5.1. Mouse Liver Perfusion and Digestion

The liver perfusion technique in the mouse was adapted from the protocol described by Charni - Natan and Goldstein (75), and was established based on prior experience with the rat model (76).
Due to their larger size, rats are more amenable to surgical procedures, facilitating the initial optimization of the technique. All procedures and animal housing were conducted at the Animal Facility of the University of Trieste, according to the guidelines of the Italian Law and European Community directive. The experimental protocol was approved by the local Animal Care Committee and by the Italian Health Ministry (permit n° 321/2022-PR) according to art. 31 of Decree 26/2014.

Surgical Procedure

Liver perfusion was performed on 10 - week - old mice with an average body weight of 28 g.
Mice were anesthetized via intraperitoneal injection of a xylazine/zolazepam - tiletamine (Zoletil®) solution in PBS (final concentrations: xylazine 2.5 mg/kg; ketamine 11.25 mg/kg). Following anaesthesia, the abdominal area was shaved and disinfected with 70% ethanol to minimize bacterial contamination. Once full anaesthesia was confirmed, a midline laparotomy was performed to expose the abdominal cavity. The IVC was visualized by gently displacing the intestines to the left. A 24G angiocath was then inserted into the IVC and secured with a wire to ensure stable cannulation. Peristaltic pump tubing was initially disinfected with 70% ethanol, followed by thorough rinsing with PBS to remove any residual disinfectant. The liver was perfused with 35 mL of Hank's Balanced Salt Solution (HBSS) supplemented with 0.5 mM EDTA and 25 mM HEPES (Sigma - Aldrich), adjusted to a final pH of 7.4 (referred to as Perfusion buffer). The flow rate of the peristaltic pump was slowly raised to a final rate of 4 mL/min. Following cannulation, the PV was severed to establish an open system, allowing for efficient blood outflow from the circulatory system. The second perfusion was performed without interrupting the flow of the Perfusion buffer to prevent air bubble formation. A total of 15 mL of HBSS supplemented with Ca^{2+}, Mg^{2+}, Phenol red, 25 mM HEPES, and 1 mg/mL Liberase (Sigma - Aldrich) was used. Following adequate liver swelling during both the washing and digestion phases, always maintaining the same flow rate, the liver was detached from its ligaments, the gallbladder was removed, and the tissue was rinsed with PBS. The liver was then washed into ice - cold PBS and then transferred to ice - cold HBSS containing Ca^{2+}, Mg^{2+}, Phenol red, and 25 mM HEPES for subsequent processing.

3.5.2. Hepatocytes Isolation

One Petri dish, one beaker, one scraper (size M), one pair of forceps, two 70 μm cell strainers, and two 50 mL Falcon tubes were sterilized under UV light for 15 minutes. Under the biological hood and working on ice, the liver and medium were transferred to the Petri dish. The liver was gently manipulated with forceps to facilitate the release of hepatocytes from the Glisson's capsule. Using a medium cell scraper, the liver tissue was gently compressed until the parenchymal components were fully released into the medium. At this stage, only the fibrotic capsule should remain intact.
The cell suspension was then filtered through two 70 μm cell strainers using a 25 mL pipette and collected into two 50 mL Falcon tubes. To isolate primary hepatocytes (PHs) from other parenchymal and non - parenchymal liver cells, the suspension underwent differential centrifugation at 50 xg for 2

minutes with a slow brake setting. Subsequently, viable cells were separated from dead cells by density gradient centrifugation. Hepatocytes were resuspended in 10 mL of Percoll solution (90% Percoll, Santa Cruz; 10% NaCl) and centrifuged at 300 xg for 10 minutes 4°C with slow braking. This step resulted in viable cells forming a pellet at the bottom of the tube, while dead cells formed a pellet at the top. The supernatant, including dead cell pellet, was discarded, and the viable cells were resuspended in an appropriate volume of Williams E medium (Gibco).
Cell viability was assessed using Trypan Blue exclusion. Briefly, 10 μL of the cell suspension was mixed with 90 μL of Trypan Blue (Sigma - Aldrich) in a 250 μL tube before microscopic evaluation.

3.5.3. Primary Hepatocytes - derived Organoids (Hep - Orgs) Culture

The procedures following the isolation of hepatocytes from both rat and mouse livers were identical for both rodent species and were carried out according to the protocol described by Peng et al. (63) (2018).

Medium Preparation

William's E Medium (GIBCO) was supplemented with 1% (v/v) L - glutamine, 1% (v/v) Non - Essential Amino Acids (NEAA), 1% (v/v) Penicillin/Streptomycin, 0.2% (v/v) Normocin, 2% B27, 1% N2 supplement, 10 mM nicotinamide, 1.25 nM N - acetylcysteine, 10 mM Y - 27632, 1 mM A83 – 01, 3 mM CHIR99021, 25 ng/mL Epidermal Growth Factor (EGF), 50 ng/mL Hepatocyte Growth Factor (HGF), and 100 ng/mL Tumour Necrosis Factor - alpha (TNFα).

Medium was replaced every 2 - 3 days of culture.

Hep - Orgs Plating

PHs isolated from mouse were centrifuged at 200 xg for 2 minutes and resuspended in Geltrex (Gibco) at a typical concentration of 10,000 cells per 20 μL. Ten 20 - μL droplets were dispensed onto a single well of a 6 - well plate (Corning). The plates were then incubated inverted at 37°C for 30 minutes to allow droplet polymerization. Following gelation, 2 mL of William's Peng medium were added to each well.

Hep - Orgs Passaging

Between days 14 and 20, Hep - Orgs were passaged to prevent over - confluence and degradation of the extracellular matrix. The culture medium was completely aspirated, and 1 mL of 5 U/mL Dispase (STEMCELL Technologies) was added to each well. During Dispase addition, matrix droplets were mechanically disrupted by repeated pipetting with a P1000 micropipette to enhance matrix digestion, by cutting the tip of the pipette to avoid disrupting the organoids, followed by incubation at 37°C for 20 minutes.

The solution of Dispase and Organoids of at least 3 wells was pooled together in a 15 mL Falcon tube. Hep - Orgs were washed with PBS 10% FBS and pelleted by centrifugation at 300 xg for 3 minutes at 4°C with low brake. The supernatant was discarded, and the centrifugation step was repeated at least three times to ensure complete removal of Dispase, as residual enzyme may compromise matrix integrity during subsequent culture.

At the first passage, Hep - Orgs were collected and replated following the procedure previously described. For second - passage Hep - Orgs, dissociation into single cells was achieved by incubating the organoids with 0.5 mL of TrypLE Select (Gibco) at 37°C for 5 minutes. Following enzymatic dissociation, samples were centrifuged at 300 xg for 2 minutes at 4°C. The supernatant was then removed, and the cell pellet was resuspended in Geltrex at a concentration of approximately 5,000 cells per 20 μL. To prevent nonspecific adhesion of Hep - Orgs to plastic surfaces, all plasticware was pre - treated at least once with PBS containing 10% (v/v) FBS to saturate potential binding sites.

3.5.4. Phase - Contrast Microscopy

Morphological changes and growth of both PHs and Hep - Orgs were monitored using a Nikon Eclipse TS100 inverted microscope. Image acquisition and size measurements of Hep - Orgs were performed using the Digital Sight DS - L1 imaging software.

3.5.5. EdU Proliferation Assay

This experimental part of the project was carried out thanks to Dr. Davide Selvestrel of the Advanced Disease Models Group, led by Professor Giovanni Sorrentino, at the International Centre for Genetic Engineering and Biotechnology (ICGEB) in Trieste, Italy.

The assay was conducted using the Click - iT® EdU Imaging Kit (Life Technologies), following the manufacturer's protocol for 2D cultures and adapting it to 3D organoids based on the indications provided by Dr. Davide Selvestrel (Advanced Disease Models Group, International Centre for Genetic Engineering and Biotechnology (ICGEB), Trieste). EdU (5 - ethynyl - 2' - deoxyuridine) is a thymidine analog that is actively incorporated into DNA during replication. It exhibits an excitation maximum at 495 nm and an emission maximum at 519 nm, allowing detection via fluorescence microscopy. Cells that have incorporated EdU are green - stained.

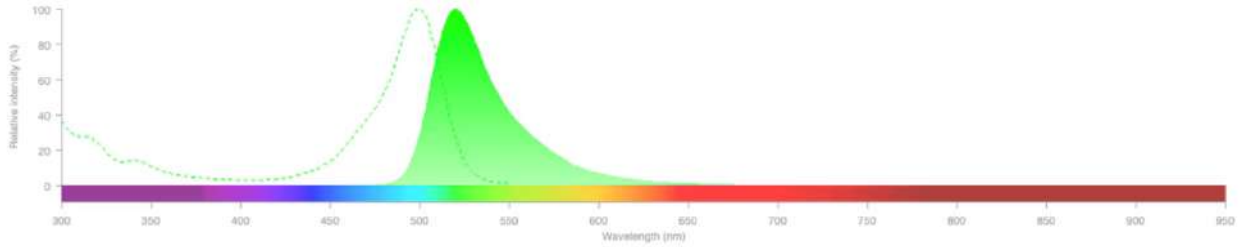

Figure 3.7. Fluorescent spectra of EdU (Thermo Fisher). In green, the emission spectrum is underlined.

EdU was added to the culture medium at 1:1000 dilution, and Hep - Orgs were incubated at 37°C overnight to allow EdU incorporation into newly synthesized DNA. To improve the recovery and yield of Hep - Orgs at the end of the procedure, pre - conditioning of tubes and pipette tips with FBS or BSA were recommended to reduce sample loss due to adhesion.

Following EdU incubation, under sterile conditions in a biological safety cabinet, the supernatant containing residual EdU was carefully aspirated from the wells. The wells were washed once with phosphate - buffered saline (PBS), followed by the addition of 2 mL of 4% paraformaldehyde (PFA). Repeated pipetting was performed to facilitate detachment of the organoids and ensure effective fixation. Notably, PFA alone was sufficient to disrupt the matrix droplets, eliminating the need for enzymatic digestion with Dispase. The PFA - cell suspension was transferred to a 15 mL conical tube preconditioned with FBS to minimize sample loss. Fixation was carried out for 20 - 30 minutes at room temperature while gently agitated on a stirrer. Subsequently, 7 mL of PBS were added to dilute the fixative, and the sample was centrifuged at 300 xg for 5 minutes at 15°C. After centrifugation, the supernatant was discarded, and the Hep - Orgs pellet was washed once with PBS. The organoids were then transferred to a 1.5 mL microcentrifuge tube, and a second centrifugation was performed (300 xg for 3 minutes at 15°C). The pellet was resuspended in an appropriate volume of nuclease - free water, depending on the pellet size, and finally adjusted to 30 µL total volume. The resuspended Hep - Orgs were spotted in a circular pattern into a Superfrost™ Plus microscope slide, avoiding the

edges to prevent spreading. The slides were left to air dry under the chemical hood for at least 30 minutes. If PBS is used instead of water, precipitated crystals can be found on the top of the Superfrost™ glass. Once dried, the region containing the Hep - Orgs was outlined using a hydrophobic barrier pen (Liquid Blocker Super PAP Pen, Sigma - Aldrich). The enclosed area was rehydrated dropwise with water, which was removed after a few minutes. To permeabilize the cellular membranes, 0.5% Triton X - 100 in PBS was added and incubated for 20 - 30 minutes at room temperature. This step was followed by two washes with PBS containing 3% BSA to reduce background staining. The Click - iT® reaction cocktail was prepared according to the manufacturer's instructions, scaled to the number of slides. After removing the BSA solution, the reaction mixture was added to the slide and incubated for 30 minutes at room temperature, in the dark. Subsequently, the slides were stained with Hoechst 33342 (1:100 dilution in PBS) for 15 minutes to label cell nuclei. Excess Hoechst was removed by two PBS washes. Hoechst binds DNA, with excitation at 350 nm and emission at 461 nm. After the final wash, the slide was allowed to air dry and ProLong ™ Gold Antifade Mountant (Thermo Fisher) was applied. A coverslip was gently placed over the sample, and the slide was stored at room temperature overnight. The following day, fluorescence images were acquired using a Leica DFC490 fluorescence microscope.

3.5.6. Mouse Albumin ELISA

Mouse albumin concentration was measured using the AssayMax™ Mouse Albumin ELISA Kit (AssayPro), following the manufacturer's instructions. Cell culture supernatants were collected, gently mixed, and centrifuged at 1500 rpm for 10 minutes at 4°C to remove cellular debris. The clarified supernatants were then aliquoted and stored at -80°C until analysis. All reagents provided in the kit, including Mix Diluent Concentrate, Mouse Albumin Standard, Biotinylated Mouse Albumin Antibody, Wash Buffer, SP Conjugate, Chromogen Substrate, and Stop Solution, were prepared immediately prior to use, as per the manufacturer's guidelines. The entire assay was performed at room temperature. A total of 50 µL of either Mouse Albumin Standard or sample was added to each well of the pre - coated ELISA microplate, which contains immobilized polyclonal antibodies specific to mouse albumin. The plate was gently tapped to ensure proper liquid distribution, bubbles were removed, and the plate was sealed with adhesive film and incubated for 2 hours. Following incubation, the wells were washed thoroughly: the plate was inverted and tapped 4 - 5 times on absorbent paper to eliminate residual liquid. Then, 50 µL of Biotinylated Mouse Albumin Antibody was added to each well, the plate was resealed and incubated for 1 hour. After washing, 50 µL of SP Conjugate was added to each well and incubated for 30 minutes. Another washing step was performed

as previously described. Next, 50 µL of Chromogen Substrate was added to each well and incubated for 20 minutes in ambient light, allowing development of a blue colour. The reaction was stopped by adding 50 µL of Stop Solution, resulting in a yellow colour, and absorbance was measured immediately at 450 nm using a PerkinElmer EnSpire ™ Multimode Plate Reader. Each standard and sample was assayed in duplicate, and the mean absorbance (OD) values were calculated. A standard curve was generated by plotting the known concentrations of albumin (x - axis) against their corresponding mean OD values at 450 nm (y - axis). Albumin concentrations in unknown samples were determined by interpolation from the standard curve and normalized to the number of organoids droplets used in the culture.

3.5.7. CsA Treatment and CDFDA Assay

Hep - Orgs were treated with 10 µM Cyclosporine A (CsA) for 24 hours and with 50 µM CsA for 4 hours. Following treatment, biliary excretory function was assessed using 5 - (and - 6) - carboxy - 2',7' - dichlorofluorescein diacetate (CDFDA) at a concentration of 0,5 µM for 2 hours. CDFDA clearance was evaluated using a Nikon A1 MP confocal microscope.

For a detailed description of the molecular analysis methods and immunofluorescence experiments, please refer to subchapters 3.6 and 3.7 of this chapter.

3.6. Detailed Protocols for Quantitative and Qualitative PCR Analyses

This section describes the molecular analysis methodologies applied to the different experimental steps and to both models (2D and 3D) presented in this thesis.

RNA Extraction and Quantification

RNA was collected using TRI - Reagent™ RNA Isolation Reagent (Sigma - Aldrich, Co., 3050 Spruce Street, St. Louis, MO 63103 USA) and extracted following the manufacturer's instructions. cDNA was obtained from 1 µg of purified RNA using the High - Capacity cDNA Reverse Transcription Kit (Applied BiosystemsTM, Waltham, Massachusetts, USA). The reaction was run in a T-100 Thermal Cycler (Bio Rad, Hercules, California, USA) according to the reaction protocol proposed by the manufacturer.

For RNA extraction from Hep - Orgs, the Quick - DNA/RNA Miniprep Plus Kit (Zymo Research) was employed following the manufacturer's instructions. Hep - Orgs were collected in DNA/RNA Shield, mixed with an equal volume of DNA/RNA Lysis Buffer, and thoroughly homogenized. The lysate was transferred to a Spin - Away Filter placed in a collection tube and centrifuged at 14,000 xg for 30 seconds. The resulting flow - through was retained, mixed with 300 µL of 100% ethanol, and loaded into a Zymo - Spin IIICG Column. After centrifugation, the flow - through was discarded, and the column was washed with 400 µL of DNA/RNA Prep Buffer, followed by two washes with DNA/RNA Wash Buffer. Finally, RNA was eluted in 15 µL of DNase/RNase - free water.

RNA was quantified and its quality assessed using a NanoDrop 2000 spectrophotometer (Thermo Fisher). RNA concentration and purity were determined by measuring absorbance at 230 nm, 260 nm, and 280 nm. The A260/A280 ratio was calculated for each sample to evaluate RNA purity and confirm its suitability for downstream applications.

Retrotranscription

RNA was collected using TRI - Reagent™ RNA Isolation Reagent (Sigma - Aldrich, Co., 3050 Spruce Street, St. Louis, MO 63103 USA) and extracted following the manufacturer's instructions. cDNA was obtained from 1 µg of purified RNA using the High - Capacity cDNA Reverse Transcription Kit (Applied BiosystemsTM, Waltham, Massachusetts, USA). The reaction was run in a T - 100 Thermal Cycler (Bio Rad, Hercules, California, USA) according to the reaction protocol proposed by the manufacturer.

Real - Time qPCR

Gene expression levels were measured by Real – Time Quantitative PCR (RT - qPCR) according to the iQ5 SYBR Green Supermix (Bio Rad Laboratories, Hercules, California, USA) using CFX Connect Real - Time System (Bio Rad, Hercules, California, USA).

The sequences of the primers were designed with the Beacon Designer 8 software (PREMIER Biosoft International, Palo Alto, CA, USA).
For Step 1, 10 different PTEC samples were analyzed, and fibroblasts were used as a control (mRNA expression = 1) (Table 3.15).

RNA was collected from each step of differentiation of the four protocols (Step 3). The RNA from the HepG2 cells and from the Upcyte® hepatocytes was collected to be used as a control (Table 3.16).

Genes and Primers Real Time PCR - PTEC Characterization (Step 1) - Human			
Gene name	**Accession number**	**Forward primer**	**Reverse primer**
Housekeeping genes			
18S	NR_003286.4	5' - TAACCCGTTGAACCCCATT - 3'	3' - CCATCCAATCGGTAGTAGCG - 5'
HPRT1	NM_000194	5' - ACATCTGGAGTCCTATTGACATCG - 3'	3' - CCGCCCAAAGGGAACTGATAG - 5'
Epithelial Markers			
CLAUDIN1	NM_021101	5' - AGCAAGATGATGTAATGGA - 3'	3' - ACAGACGGTGATTGATAG - 5'
E - CADHERIN	NM_004360.5	5' - CTATATTCTTCTGTGAGAGGAA - 3'	3' - GTGTTAGTTCTGCTGTGA - 5'
Renal Tubular Markers			
NR3C2	NM_000901.5	5' - CACTCGTTAGCGTCCATT - 3'	3' - GTAAAGCCAACACAATAGATACT - 5'
L1CAM	NM_001278116	5' - ACAACCACTCAGACTACAT - 3'	3' - GGTCAATGGGTTCCTTCT - 5'
Fibroblasts			
SLUG	NM_003068.5	5' - CGCAATCAATGTTTACTC - 3'	3' - CATATTATTTGGTTGGTCAG - 5'

Table 3.15. Primer sequences used for RT - PCR, including epithelial markers, renal tubular markers, and fibroblast markers.

Genes and Primers Real Time PCR (Step 3) - Human			
Gene name	**Accession number**	**Forward primer**	**Reverse primer**
Housekeeping genes			
18S	NR_003286.4	5' - TAACCCGTTGAACCCCATT - 3'	3' - CCATCCAATCGGTAGTAGCG - 5'
HPRT1	NM_000194	5' - ACATCTGGAGTCCTATTGACATCG - 3'	3' - CCGCCCAAAGGGAACTGATAG - 5'
iPSC Markers			
SOX2	NM_003106.4	5' - TAGTCTCCAAGCGACGAA - 3'	3' - AGCAAGAAGCCTCTCCTT - 5'
OCT3/4	NM_001173531.3	5' - GGATTAAGTTCTTCATTCA - 3'	3' - GTGTCTATCTACTGTGTC - 5'
NANOG	NM_024865.4	5' - TTCCGTGTATGAATCTGTAATTG - 3'	3' - CTGCGTAGCTGCTCTTAA - 5'
Hepatic Markers			
ALB	NM_000477	5' - GGCATCCTGATTACTCTGTCG - 3'	3' - AATTCTGAGGCTCTTCCACAAG - 5'
AFP	NM_001134	5' - GCGGCTGACATTATTATCG - 3'	3' - TTGGCACAGATCCTTATGG - 5'
HNF4α	NM_000457.6	5' - AAACCCATTCCACCTTAATAAC - 3'	3' - AGGACCACAACTCAAGTAG - 5'
SERPINA1	NM_000295	5' - ATTCAGTCTAATCAATGGATACC - 3'	3' - AGGCTGTCAGTGAGTAAG - 5'
TTR	NM_000371.4	5 ' - ACGAGGGATGGGATTTCA - 3'	3' - TCTGCCTGGACTTCTAACA - 5'
ASGR2	NM_001181.4	5' - TTTGAGGAAAGGAAGAAACA - 3'	3' - TGAAGAAGGGCTGACGATTA - 5'
APOF	NM_001638.4	5' - ATCCAGTATTACCAAGAT - 3'	3' - AACTTACTACTTCTGATATG - 5'

Table 3.16. Primer sequences used for RT - PCR, including housekeeping genes, iPSC markers, and hepatic markers.

The primers used for the analysis of primary hepatocytes and Hep - Orgs derived from rat and mouse were listed in 3.17 and 3.18.

Genes and Primers Real Time PCR - Rat			
Gene name	Accession number	Forward primer	Reverse primer
Housekeeping genes			
ACT	NM_031144.3	5' - CTCTCTGCTCCTCCCTGTTC - 3'	5' - CACCGACCTTCACCATCTTG - 3'
GAPDH	NM_017008.4	5' - GGTGTGATGGTGGGTATG - 3'	5' - CAATGCCGTGTTCAATGG - 3'
Hepatic genes			
ALB	NM_134326	5' - ATCTCCAGAAATGCCCATAT - 3'	5' - TTCTCATCAGCGACACAT - 3'
PCK1	NM_198780	5' - CCTGTCTGTCTCATTGTCT - 3'	5' - GGTAAGAAAGGGCAGTGTA - 3'
ABCD3	NM_012804	5' - TATTGCTGTTATGCTGGTA - 3'	5' - GCGATGAAGTTGAATAAGTAT -3'
KRT18	NM_053976	5' - GTCTCTCGCTTCGTTCTC - 3'	5' - CGGTAGTTGGTGGAGAAG -3'
SERPINA1	NM_022519	5' - TTCGACCACCCTTTCATT - 3'	5' - GTGACTTCTGAGGACAGT -3'
TDO2	NM_022403	5' - AAGGAGGACTTATCTATGG - 3'	5' - CTCACGAACAGAATCAAG -3'

Table 3.17. Primer sequences used for RT - qPCR, including housekeeping genes and hepatic markers (rat).

Genes and Primers Real Time PCR - Mouse			
Gene name	Accession number	Forward primer	Reverse primer
Housekeeping genes			
ACT	NM_007393	5'- AATAAGTGGTTACAGGAAGTC - 3'	5' - ATGAAGTATTAAGGCGGAAG - 3'
GAPDH	NM_008084	5'- CCAGTATGACTCCACTCACG - 3'	5' - CTCGCTCCTGGAAGATGGTG - 3'
Hepatic genes			
ALBUMIN	NM_009654.4	5' - GTAGAAGAGCCTAAGAACT - 3'	5' - GGTGTAGCGAACTAGAAT - 3'
HNF4α	NM_001312906.1	5' - TGATAACCACGCTACTTG - 3'	5' - GCCTACTTCTGAATGTTTG - 3'
AFP	NM_007423.4	5' - CTCATCCTCCTGCTACAT - 3'	5' - CACATTCTTCTCCGTCAC - 3'
SERPINA1	NM_001252569.1	5' - TTGTTGTGGACTTGAGAT - 3'	5' -TTAGAGCAGATGGTTCTT - 3'
CYP3A11	NM_007818.3	5' - GTGCTGAATTATTACAAGG - 3'	5' -CACATTCTTAATCGTCTCT - 3'
Oxidative stress genes			
MHO1	NM_010442	5' - TGTGAACTCTGTCCAATG - 3'	5' - CTTAGAGGCCCAAGAGAA - 3'
MSOD2F	NM_013671	5' - TGAATTGCTTGGATGCTA - 3'	5' - GTAGAACAGGATTACAGACT - 3'
MNRF2	NM_010902.3	5' - GATGACCATGAGTCGCTTG - 3'	5' - CGGTATTAAGACACTGTAATTCG - 3'
GRP78	NM_014339	5' - GTATTCTCCGAGTGACAG - 3'	5' -AGCATCATTAACCATCCTT - 3'
CHOP	NM_000014	5' - AAACCTTCACTACTCTTG - 3'	5' -TAGAACTCTGACTGGAAT - 3'

Table 3.18. Primer sequences used for RT - qPCR, including housekeeping genes and hepatic markers (mouse).

The cyclical parameters were determined, and the results analyzed using the comparative Ct method as the means of relative quantification, normalized to two references genes, and expressed as 2-ΔΔCT. Melting curve analysis was performed to assess product specificity. In each experiment a housekeeping gene was used to normalize the expression level of the analyzed genes. To determine the relative expression of the mRNA for the same sample (Sample or Control), the Ct of the target gene has been normalized on the Ct of the housekeeping gene (reference). The expression of the gene of interest in the sample is reported as relative to that of the control that is always considered one. The formula used for computing the relative expression (Figure 3.8) also considers the amplification efficiency of the primers: Etarget for the gene of interest and Eref for housekeeping gene. To evaluate the efficiency of primers for each gene, it is necessary to construct a standard curve that is generated by scalar dilutions of a sample cDNA that expresses the gene of interest. Various sample dilutions will be associated with Ct values that are represented according to the concentration in a graph Ct / log (concentration). Experiments were accepted if the correlation coefficient of the straight lines obtained was ≥ 0.99. The slope of the straight line is directly related to the efficiency of the reaction by the formula:

Efficiency = [10(-1/slope)] – 1.

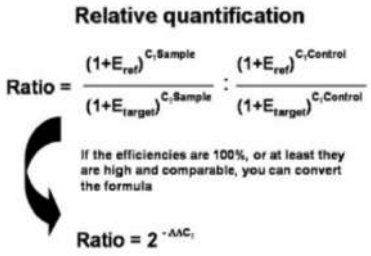

Figure 3.8. Formula to calculate the relative expression of the mRNA of one sample in analogy with a sample selected as a control. Eref is the efficiency of the housekeeping gene; It targets the efficiency of the gene of interest; C_T sample is the Ct value of the sample in question; C_T Control is the Ct value of the sample chosen as a control.

Qualitative PCR

Gene expression levels were measured by qualitative PCR according to KAPA2G Fast HotStart ReadyMix PCR Kit protocol.

In Table 3.19 the sequences of the primers are listed.

Genes and Primers Qualitative PCR (Step 3)			
Gene name	**Accession number**	**Forward primer**	**Reverse primer**
Housekeeping genes			
ACT*β*	NM_00101.5	5' - CACCTTCTACAATGAGCTGC - 3'	3' - CACAGCCTGGATAGCAACG - 5'
iPSC Markers			
SOX2	NM_003106.4	5' - GTGAACCAGCGCATGGACAGCTACGCGC - 3'	3' - TCGTAGCGGTGCATCGGTTGCATCTGTGC - 5'
OCT3/4	NM_001173531	5' - GACAACAATGAGAACCTTCAGGAGATATGC - 3'	3' - CCAAGCTGATTGGCGATGTGAGTGATCTGC - 5'
Hepatic Markers			
ALB	NM_000477.7	5' - CCTTTGGCACAATGAAGTGGGTAACC - 3'	3' - CAGCAGTCAGCCATTTCACCATAGG - 5'
AFP	NM_001134.3	5' - AGAACCTGTCACAAGCTGTG - 3'	3' - GACAGCAAGCTGAGGATGTC - 5'
HNF4**α**	NM_178849.3	5' - CTGCTCGGAGCCACCAAGAGATCCATG - 3'	3' - ATCATCTGCCACGTGATGCTCTGCA - 5'
SERPINA1	NM_000295.5	5' - CCGAAGAGGCCAAGAAACAG - 3'	3' - GGTCTCTCCCATTTGCCTTT- 5'
TTR	NM_000371.4	5' - GCCGTGCATGTGTTCAGAAAG - 3'	3' - GACAGCCGTGGTGGAATAGGA - 5'
ASGR2	NM_001181.4	5' - CGTGGGTGACAAGATCACAT - 3'	3' - GGGAAGTGCTTCAGATGGAA - 5'
APOF	NM_001638.4	5' - GGAAGCGATCAAACCTACCA - 3'	3' - ATCAGCCTGACAACCAGCTT - 5'

Table 3.19. Primer sequences used for qualitative PCR, including housekeeping genes, iPSC markers, and hepatic markers.

3.7. Detailed Protocols for Immunofluorescence Experiments

This section details the immunofluorescence methodologies employed across the various experimental procedures and applied to both the 2D and 3D models investigated in this thesis.

2D model - PTEC (Step 1)

The characterization of PTEC for specific epithelial markers was performed using an immunofluorescence protocol provided by ibidi®, the manufacturer of the substrates employed for this staining.

Both µ - slide 4 Well and µ - slide 8 Well were utilized. The culture medium was aspirated and PTEC were washed with PBS. Cells were fixed with 4% PFA (paraformaldehyde, 36.5 - 38% in H_2O, Sigma - Aldrich) for 10 minutes. PFA was then removed, and cells were washed three times with PBS. Then, cells were incubated for 10 minutes in Perforation Buffer (0.5% Triton - X - 100 in PBS). The Perforation Buffer was then removed and PTEC were washed with PBS. Cells were then blocked with Blocking Buffer (1% BSA + 0.2% Triton - X - 100 in PBS) for 30 minutes. Primary Antibodies (Table 3.20) were diluted in Antibody Dilution Buffer (1% BSA + 0.05% Triton - X - 100 in PBS). Blocking Buffer was removed and then PTEC were incubated in Primary Antibodies overnight at 4°C, protected from light. On the following day, cells were washed twice with Blocking Buffer and incubated with Secondary Antibodies (Table 3.21) and the phalloidin (ActiGreen™ 488 ReadyProbes™ reagent, Invitrogen) for two hours at room temperature, protected from light. After 2 hours, cells were washed twice with Blocking Buffer and then incubated with Hoechst 33258 (Sigma Aldrich) for 10 minutes. Hoechst was then removed, and all wells were emptied and drops of ibidi® Mounting Medium were added. Samples were stored in the dark at 4°C and then observed under a ZEISS Axiovert 200 Fluorescence Microscope microscope (Olympus XM - 10 Camera, X - Cite120Q excitation light source) and a Leica Stellaris 5 confocal microscope.

Primary Antibodies					
Recognized Antigen	Type	Dilution	Species of origin	Production	Product number
ZO - 1	monoclonal	1:50	mouse	Invitrogen	339100

Table 3.20. Primary antibodies used in immunofluorescence experiments.

Secondary Antibodies					
Name	Type	Dilution	Species of origin	Production	Product number
Alexa Fluor 546 anti - mouse	polyclonal	1:500	donkey	Invitrogen	A10036

Table 3.21. Secondary antibodies used in immunofluorescence experiments.

2D model - Hepatocyte - like Cells (Step 3)

Immunofluorescence experiments were performed on HLC stages for each protocol, and Upcyte® hepatocytes were used as a positive control. Cells were plated on µ-Slide 8 Well ibiTreat® chamberslides (ibidi GmbH, 82166 Gräfelfing, Germany).

At the stage of Hepatocyte - like Cells, samples were washed three times with PBS, then fixed with 4% PFA (paraformaldehyde, 36.5 - 38% in H_2O, Sigma - Aldrich) in PBS for 30 minutes at room temperature. Then, samples were washed again for three times with PBS. Cells were then permeabilized with a solution of PBS supplemented with 0.2% (v/v) Triton - X - 100 at 37°C for 10 minutes. Then, cells were washed three times with PBS to remove the Triton - X - 100 and non - specific binding sites were blocked by incubating the cell in PBS supplemented with 1% (v/v) bovine serum albumin (BSA) at 37°C for 60 minutes. Subsequently, cells were incubated with primary antibodies (see Table 3.22), diluted in PBS with 1% (w/v) BSA, at the concentrations suggested by provider, at 4°C for 18 hours. The next day, cells were washed three times with HBSS and incubated with appropriate fluorescently labelled secondary antibodies (Table 3.23), diluted in PBS with 1% (w/v) BSA, at the concentrations suggested by the provider, at 37°C for 30 minutes. A DNA - staining agent (DAPI) was also included. Finally, cells were washed three times with PBS, and the coverslip was mounted on a microscopy slide for microscopy analyses. Samples were analyzed using a ZEISS LSM 900 Confocal laser scanning microscope.

Primary Antibodies					
Recognized Antigen	Type	Dilution	Species of origin	Production	Product number
OCT3/4	monoclonal	1:300	mouse	Santa Cruz	sc5379
HNF4α	monoclonal	1:200	mouse	Santa Cruz	sc374229
ALB	monoclonal	1:100	mouse	R&D System	MAB1455
BSEP	polyclonal	1:500	rabbit	Atlas Antibodies	HPA019035
MRP2	polyclonal	1:100	rabbit	Sigma - Aldrich	M8316
ZO - 1	monoclonal	1:100	mouse	Invitrogen	339100
E - cadherin	polyclonal	1:100	goat	R&D System	AF648

Table 3.22. Primary antibodies used in immunofluorescence experiments.

Secondary Antibodies					
Name	Type	Dilution	Species of origin	Production	Product number
Alexa Fluor 488 anti - mouse	polyclonal	1:2000	goat	Invitrogen	A - 11001
Alexa Fluor 488 anti - rabbit	polyclonal	1:1000	goat	Invitrogen	A - 11008
Alexa Fluor 488 anti - goat	polyclonal	1:1000	donkey	Invitrogen	A - 11055

Table 3.23: Secondary antibodies used in immunofluorescence experiments.

3D model - Hep - Orgs

Hep - Orgs cultured in a 6 - well plate were fixed with 4% paraformaldehyde (PFA) and pipetted thoroughly to facilitate matrix dissolution. The fixed organoids where then transferred to 15 mL Falcon tubes (e.g., organoids from 3 wells per tube), previously preconditioned with fetal bovine serum (FBS) to prevent sample adhesion. An additional 2 mL of 4% PFA was added to each tube, which was then placed on a shaker and incubated for 20 - 40 minutes at room temperature. To avoid centrifugation, the tubes were allowed to stand upright to enable passive sedimentation of the organoids. If sedimentation was incomplete, organoids were washed with phosphate – buffered saline (PBS) and centrifuged at 200 xg for 5 minutes at 4°C. After centrifugation, the supernatant was aspirated, and 1 mL of PBS was added to resuspend the pellet. Organoids were then transferred to 1.5 mL Eppendorf tubes, also preconditioned with FBS, washed once with PBS, and centrifuged again at 200 xg for 4 minutes at 4°C. The supernatant was removed, and 1 mL of Permeabilization buffer (0,5% Triton X - 100 in PBS) was added. The sample was divided equally into two tubes to generate experimental and control conditions. Three rounds of permeabilization were performed, each consisting of 10 minutes of incubation with gentle shaking, followed by removal and replacement of the buffer. After permeabilization, the buffer was removed and replaced with Blocking Buffer (1% bovine serum albumin (BSA) and 0,5% Triton X - 100 in PBS). Samples were incubated for 1 hour at room temperature with gentle agitation. Following blocking, the buffer was removed from the experimental tube, and primary antibody solution was added (Table 3.24). The control tube received fresh Blocking Buffer. Samples were incubated overnight at 4°C. The next day, the primary antibody solution was removed, and samples were washed three times for 10 minutes each with Washing Buffer (0,2% Triton X - 100 in PBS). After washing, the experimental sample was incubated with the secondary antibody (Table 3.25) and phalloidin (ActiGreen™ 488 ReadyProbes™ reagent, Invitrogen), while the control sample received only the secondary antibody. Samples were incubated for 2 hours at room temperature, protected from light, with gentle agitation. Following incubation, the secondary antibody solution was removed. A final series of washes was performed: first with PBS, then with distilled water to prevent salt crystal formation during drying. Water was removed, and the organoids were carefully spotted onto Superfrost™ glass slides using pre - cut and FBS - functionalized pipette tips. Slides were left to air dry under a chemical hood. Finally, mounting medium (Prolong™ Gold antifade reagent with DAPI, Thermo Fisher) was applied, a coverslip was placed, and the slides were allowed to dry in a closed cardboard box, protected from light and dust, until analysis. Confocal imaging was performed using ZEISS - LSM -

880 with Airyscan Confocal microscope, a ZEISS Apotome 3, and a Leica Stellaris 5 confocal microscope.

Primary Antibodies					
Recognized Antigen	Type	Dilution	Species of origin	Production	Product number
ZO - 1	monoclonal	1:50	mouse	Invitrogen	339100
HNF4**α**	monoclonal	1:100	rabbit	Abcam	ab199431

Table 3.24: Primary antibodies used in immunofluorescence experiments.

Secondary Antibodies					
Name	Type	Dilution	Species of origin	Production	Product number
Alexa Fluor 546 anti - mouse	polyclonal	1:500	donkey	Invitrogen	A10036
Alexa Fluor 546 anti - rabbit	polyclonal	1:500	donkey	Invitrogen	A10040

Table 3.25: Secondary antibodies used in immunofluorescence experiments.

Note

Immunofluorescence images were acquired using the microscopes specified in the figure legends, with magnifications indicated for each image. Exposure settings varied depending on the sample, the specific experimental conditions, and the type of microscope. For each immunofluorescence result presented in the Results section, individual images corresponding to DAPI or Hoechst staining, as well as images for the marker of interest, are shown, along with a merged figure combining these channels. Adjustments of brightness and contrast using Fiji (Image J, version 2.3.0/1.53f) were applied uniformly only to the individual source images, ensuring consistent representation across comparable images.

4. RESULTS

Within the Results section, subchapters 4.1 - 4.3 pertain to the 2D model concerning the derivation of Hepatocyte - like Cells (HLCs) from iPSC obtained starting from proximal tubular epithelial cells (PTEC), while subchapters 4.4. - 4.5 address the 3D liver organoid model and its characterization.

4.1 PTEC Isolation and Culture from Urine: Protocol Improvements (STEP 1)

This first section is dedicated to the isolation of Proximal Tubular Epithelial Cells (PTEC) from urine samples collected from 6 healthy donors.

The original protocol of Zhou (40) was improved by us to obtain the final one reported in subchapter 3.1.3. Urine samples were plated primarily after 4 hours of storage at 4°C or, alternatively, after 24 hours of storage at 4°C.

4.1.1. Original Protocols

4.1.1.1. PTEC Preparation within 4h of Sample Storage

The procedure for urine sample collection from volunteers has been previously described in subchapter 3.1.1.1 of the Materials and Methods.

This experiment aimed to assess the adhesion efficiency of PTEC in samples stored at 4°C and processed within 4 hours of collection. The results are shown in Table 4.1.
As an initial analysis, the yield was evaluated in terms of percentage of samples in which urinary cell adhesion and proliferation occurred. 53% of the total collected and plated samples exhibited adherent PTEC after 3 weeks of culture.
As a second analysis, yields were evaluated separately for male and female donors. A marked difference was observed: the percentage of samples with adherent PTEC was 94% ± 10% in males and 11% ± 19% in females. The standard deviation was acceptable for male - derived samples whereas

it was considerably higher for female - derived samples and, consequently, for the overall dataset. These findings clearly indicate that gender differences may play an important role in urinary cell colony formation.

As a third analysis, yields were assessed at the level of individual donors. Table 4.1 shows that adherent PTEC were obtained from all donors except for two females (A and L). Among female donors, adhesion was observed only in donor B (33%), even if this yield was consistently lower than the yields of male donors H, I, and M. This further supports the hypothesis of a correlation between urinary cell adhesion and donor gender.

Identity code	Collected samples	Plated samples	Samples with urinary cells adhesion	% samples with urinary cells adhesion	% samples with urinary cells adhesion by gender	Total % of samples with urinary cells adhesion
A	6	6	0	0%	11% ± 19%	53% ± 48%
B	6	6	2	33%		
L	6	6	0	0%		
H	6	6	6	100%	94% ± 10%	
I	6	6	5	83%		
M	6	6	6	100%		
TOTAL	36	36	19			

Table 4.1. The columns of the table report the following information: donor identification code; donor sex (indicated in pink for females and blue for males); total number of samples collected from each donor; number of samples processed and plated after 4 hours of storage at 4°C; number of samples exhibiting urinary cell adhesion; percentage of samples showing urinary cell adhesion relative to the number of plated samples for each donor; percentage of samples ± SD with urinary cell adhesion stratified by donor gender; and the overall percentage of samples ± SD with urinary cell adhesion relative to the number of plated samples.

4.1.1.2. PTEC Preparation after 24h of Sample Storage

The volunteers described in subchapter 3.1.1.1 of the Materials and Methods collected urine samples in the laboratory where sample preparation was performed. Nevertheless, considering future scenarios in which patient may collect urine samples at home or at sites distant from the processing laboratory, it was evaluated the yield after extending the storage period at 4°C from 4 hours to 24 hours (considering the potential transport time, which may extend up to 24 hours).

PTEC Preparation from Morning Urine Collection

The procedure for urine sample collection from volunteers has been previously described in subchapter 3.1.1.2 of the Materials and Methods.
As shown in Table 4.2, no adhesion of PTEC was observed in any of the donor samples. One possible explanation is that urine, being a waste product, does not provide an environment suitable to cell survival.

Identity code	Collected samples	Plated samples	Samples with urinary cells adhesion	% samples with urinary cells adhesion	% samples with urinary cells adhesion by gender	Total % of samples with urinary cells adhesion
A	3	3	0	0%	0% ± 0%	0% ± 0%
B	3	2	0	0%		
L	3	3	0	0%		
H	3	3	0	0%	0% ± 0%	
I	3	3	0	0%		
M	3	1	0	0%		
TOTAL	18	15	0			

Table 4.2. The columns of the table report the following information: donor identification code; donor sex (indicated in pink for females and blue for males); total number of samples collected from each donor; number of samples processed and plated after 24 hours of storage at 4°C; number of samples exhibiting urinary cell adhesion; percentage of samples showing urinary cell adhesion relative to the number of plated samples for each donor; percentage ± SD of samples with urinary cell adhesion stratified by donor gender; and the overall percentage ± SD of samples with urinary cell adhesion relative to the number of plated samples.

Given these results with the aforementioned procedure, it was decided to adopt an alternative approach.

PTEC Preparation from Urine Collected During the Day

The procedure for urine sample collection from volunteers has been described in subchapter 3.1.1.2 of the Materials and Methods.

As an initial analysis, the yield was assessed by determining the percentage of samples in which urinary cell adhesion and proliferation was observed. As shown in Table 4.3, the percentage yield of plated samples exhibiting urinary cell adhesion after 3 weeks of culture, relative to the total number of collected and plated samples, was 21% ± 27%. Comparison with the data reported in subchapter

4.1.1.1. indicates that increasing the storage time of urine samples resulted in a decrease in yield from 53% to 21%. In both cases, the standard deviation remained high.

As second analysis, yields were evaluated separately for male and female donors. As illustrated in Table 4.3, a clear difference between sexes was observed, in line with previous results. Specifically, the percentage of samples with urinary cell adhesion was higher in males (37% ± 30%) than in females (6% ± 10%).

As third analysis, yields were assessed at the level of individual donors. As previously reported in Section ("PTEC Preparation from Morning Urine Collection"), no adherent PTEC were obtained from donors A and L. Furthermore, Table 4.3 shows that donors B, H, I and M displayed different yields of urinary cell adhesion and proliferation, confirming the variability in adhesion capacity across donors.

Identity code	Collected samples	Plated samples	Samples with urinary cells adhesion	% samples with urinary cells adhesion	% samples with urinary cells adhesion by gender	Total % of samples with urinary cells adhesion
A	18	18	0	0%	6% ± 10%	21% ± 27%
B	18	18	3	17%		
L	18	18	0	0%		
H	18	18	12	67%	37% ± 30%	
I	18	18	7	39%		
M	18	17	1	6%		
TOTAL	108	107	23			

Table 4.3. The columns of the table report the following information: donor identification code; donor sex (indicated in pink for females and blue for males); total number of samples collected from each donor; number of samples processed and plated after 24 hours of storage at 4°C; number of samples exhibiting urinary cell adhesion; percentage of samples showing urinary cell adhesion relative to the number of plated samples for each donor; percentage ± SD of samples with urinary cell adhesion stratified by donor gender; and the overall percentage ± SD of samples with urinary cell adhesion relative to the number of plated samples.

4.1.1.3. PTEC Culture, Morphology, and Heterogeneous Components

Following collection and processing of urine samples, as outlined in subchapter 3.1, the samples were plated. As shown in Figure 4.1-A, the plated samples contained heterogeneous cells populations and additional components. Adhesion of PTEC and the formation of colonies were observed approximately 3 - 10 days post - plating (Figure 4.1-B). Subsequent proliferation of PTEC resulted in progressive colony expansion (Figure 4.1-C). Once a confluence of 70 - 80% was achieved (Figure 4.1-D), cells were either passaged for further expansion or cryopreserved for future applications.

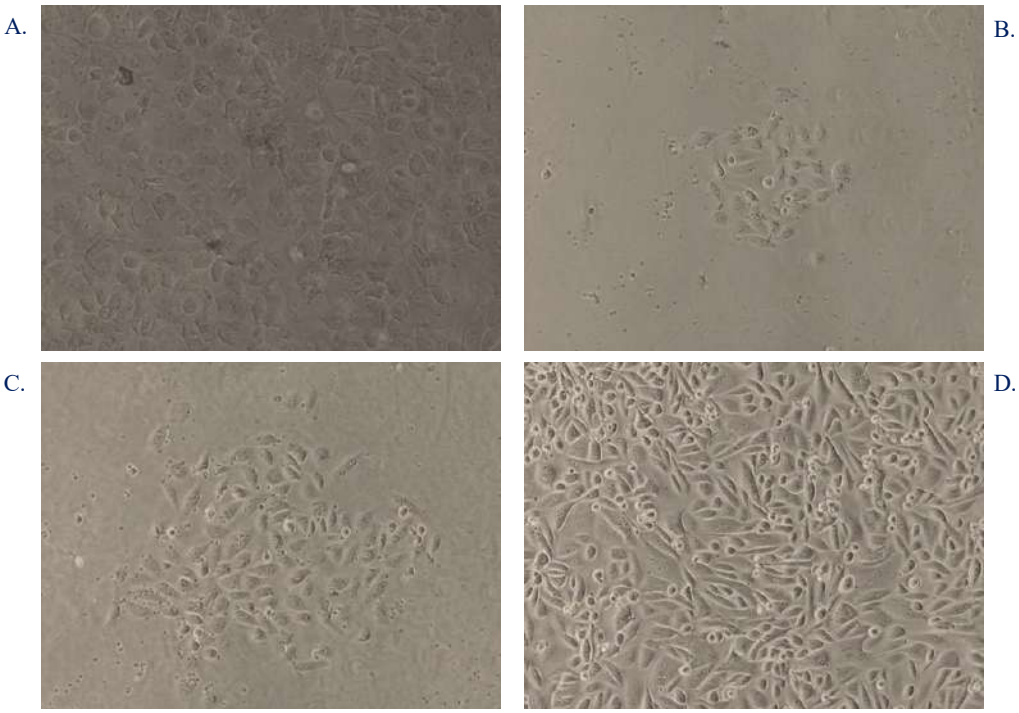

Figure 4.1. Representative phase - contrast images (magnification 10X) illustrating the sequential stages of urinary cell culture following sample collection. (A) Female donor sample at day 1 post - plating, showing the presence of multiple cell types and components. (B) Adhesion of PTEC at day 7 of culture (10X). (C) Formation of urinary cell colonies at day 8 of culture (10X). (D) Proliferation of PTEC leading to colony expansion at day 12 of culture (10X).

Proliferating PTEC gave rise to colonies exhibiting distinct morphologies. Two main cellular phenotypes were identified. Type I cells displayed a rounded morphology, growing in close contact with neighbouring cells and forming well - organized colonies. In contrast, type II cells exhibited an elongated shape, proliferating in a more dispersed and irregular arrangement, as illustrated in Figure 4.2. Both phenotypes are regarded as suitable for reprogramming into iPSC.

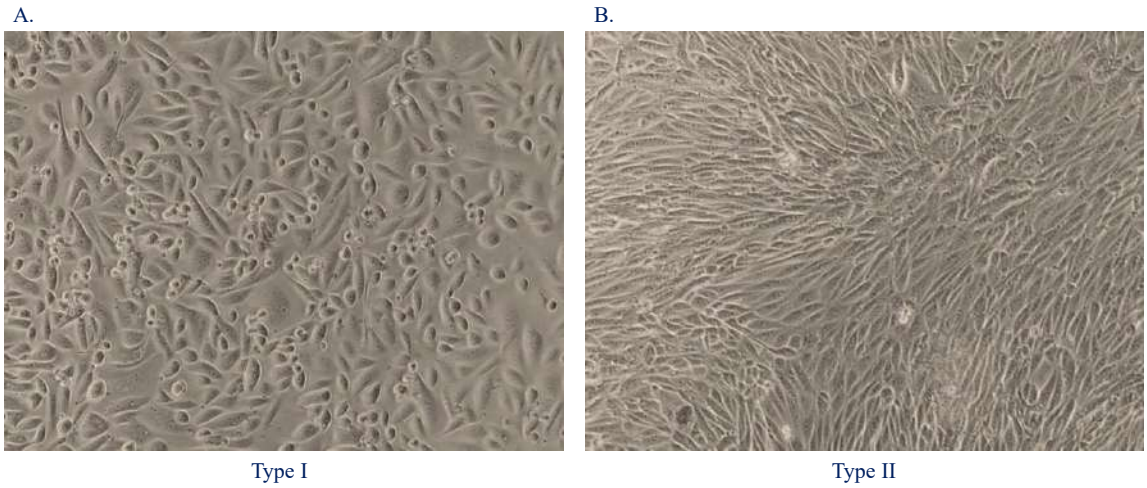

Figure 4.2. Representative images illustrating distinct PTEC colony morphologies (magnification 10X). (A) Type I urinary cells. (B) Type II urinary cells.

Heterogeneous Components Detected in Urinary Cell Samples

As illustrated in Figure 4.3, plating of urine samples did not exclusively yield urinary cells but also revealed the presence of multiple additional components in varying amounts. Despite washing steps performed after the initial centrifugation, it was not possible to isolate PTEC derived from the renal tubular epithelium in a completely pure form, given that urine is a complex biological fluid containing a heterogeneous mixture of components.

These included cellular and non - cellular elements such as bacteria, both cocci (Figure 4.3-B) and rods (Figure 4.3-A), debris (Figure 4.3-B), mold (Figure 4.3-C), different types of exfoliated fiber (more frequently observed in female samples) (Figure 4.3-D), and uric acid crystals (Figure 4.3-E).

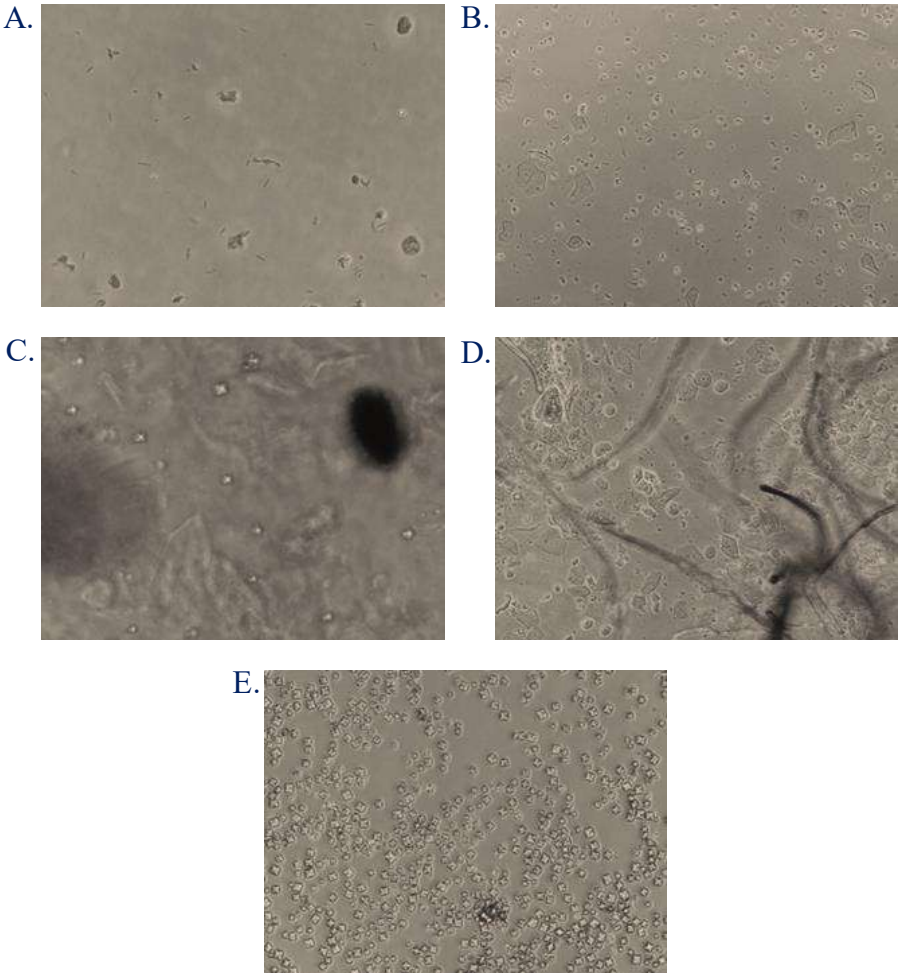

Figure 4.3. Phase - contrast images of representative components observed in urine samples. (A) Rods; (B) Cocci and debris; (C) Mold; (D) Fibers; (E) Uric acid crystals. Magnification 10X.

Both male and female samples contained all components previously identified in Figure 4.4. Cells exhibiting a rounded morphology correspond to PTEC, whereas those displaying a more polygonal, irregular, and flattened shape correspond to squamous cells. A clear distinction between male and female samples, however, was observed in the abundance of squamous cells: male urine samples generally contained very few squamous cells (Figure 4.4-A), whereas female samples consistently displayed a markedly higher number, often forming a continuous “cell carpet” within the well after plating (Figure 4.4-B).

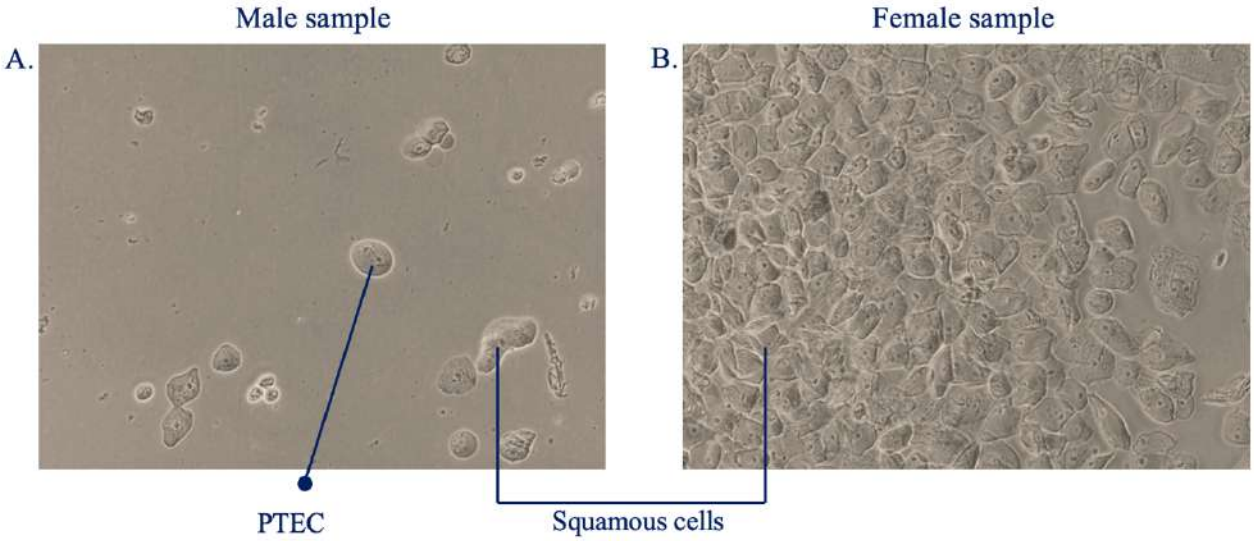

Figure 4.4. Phase - contrast representative images of the differences between male (A) and female (B) samples. Magnification 20X.

The presence of a high number of squamous cells in female - derived samples represent an obstacle to the adhesion of PTEC to the well surface. For this reason, as described in subchapter 3.1.2, procedural modifications were introduced to address this issue.

4.1.2. Challenges in PTEC Isolation and Plating, and Strategies for Their Resolution

Considering the results obtained, it was evident that two sources of variability could be identified:

- Variability associated with the individual donor (called “donor - specificity”)
- Variability related to donor sex (called “gender - specificity”).

For both types of variability, strategies were developed to improve the procedure for isolation and plating of PTEC. In this section, donor - specificity will be addressed first, followed by gender - specificity analysis.

4.1.2.1. Addressing Donor - Specificity

The next objective was to assess whether urine samples derived from donors in which PTEC adhesion failed to occur after three weeks in culture exhibited distinctive characteristics. To address this, urine test strips (COMBI SCREEN® SYS PLUS Urine Strips) were used, as described in subchapter

3.1.2.1 of the Materials and Methods. The rationale for employing these strips was to evaluate whether any urinary parameter could influence cell adhesion independently of the donor source.

Identification of the parameters affecting cell adhesion

Table 4.4 reports the values obtained using test strips for the collected and plated urine samples (n = 107) from the experiment described in subchapter 3.1.2.1 of Materials and Methods. It should be noted that all urine samples were obtained from healthy volunteers. For each of the 11 parameters assessed, the corresponding values were recorded and highlighted. All measured parameters fell within the normal reference range, thereby confirming the absence of pathological conditions in the donors.

PARAMETER	ACRONYM	READING						
Bilirubin	BIL	neg	1 mg/dL	2 mg/dL	4 mg/dL			
	BIL n. strip	107	0	0	0			
Urobilinogen	UBG	norm	2 mg/dL	4 mg/dL	8 mg/dL	12 mg/dL		
	UBG n. strip	107	0	0	0	0		
Ketones	KET	neg	trace	25 mg/dL	100 mg/dL	300 mg/dL		
	KET n. strip	107	0	0	0	0		
Ascorbic acid	ASC	neg	5 mg/dL	10 mg/dL				
	ASC n. strip	97	10	0				
Glucose	GLU	norm	50 mg/dL	100 mg/dL	250 mg/dL	500 mg/dL	> 1000 mg/dL	
	GLU n. strip	107	0	0	0	0	0	
Protein	PRO	neg	trace	30 mg/dL	100 mg/dL	500 mg/dL		
	PRO n. strip	85	22	0	0	0		
Blood	BLD	neg	5 - 10 Eri/µL	~50 Eri/µL	~300 Eri/µL			
	BLD n. strip	82	20	5	0			
pH	pH	5	6	6.5	7	8	9	
	pH n. strip	38	28	15	17	12	0	
Nitrite	NIT	neg	0.05 mg/µL	0.1 mg/µL				
	NIT n. strip	106	1	0				
Leukocytes	LEU	neg	~25 Leu/µL	~75 Leu/µL	~500 Leu/µL			
	LEU n. strip	91	14	2	0			
Specific gravity	SG	1000	1005	1010	1015	1020	1025	1030
	SG n. strip	36	23	23	18	6	1	0

Table 4.4. The table summarizes the 11 parameters assessed using the COMBI SCREEN® 11 SYS PLUS urine strips. The first and second columns report the parameter acronym and its corresponding full name. The last seven columns list the possible outcomes detectable for each parameter. The values recorded during the experiments (n = 107) are highlighted, with the frequency of occurrence for each specific parameter also indicated numerically.

Then, a more detailed analysis of the data presented in Table 4.4 was performed. For each of the 11 parameters assessed the total number of samples exhibiting a given value was determined. Subsequently, for each value, the number of samples in which PTEC adhesion was either present or absent was examined. The aim of this analysis was to evaluate whether any of the parameters could exert a positive or negative influence on PTEC adhesion. To this end, the percentage of samples in which adhesion occurred (or did not occur), together with the corresponding confidence interval for each parameter, was measured.

As reported in Table 4.5, the parameters Bilirubin (BIL), Urobilinogen (UBG), Ketones (KET) and Glucose (GLU) showed only one value across all samples analyzed (n = 107). In each case, the proportion of samples with (21.5%) or without (78.5%) PTEC adhesion was identical, indicating that these values are independent of adhesion outcomes.
Ascorbic acid (ASC), Protein (PRO), and Nitrites (NIT) displayed two distinct values, while Blood (BLD) and Leukocytes (LEU) exhibited three. In all instances, negative values predominated, and no correlation with adhesion capacity was observed. These findings are consistent with the healthy status of the donors. The only parameters demonstrating notable variability were Specific Gravity (SG) and pH.

The effect of pH was first examined by categorizing values into acidic (5 - 6.5) and neutral to mildly basic (7 - 8) ranges. The proportion of samples in which adhesion occurred was 15.4% for $pH < 7$ and 37.9% for $pH \geq 7$, with 95% confidence intervals showing only partial overlap.

Subsequently, specific gravity (SG), a measure of urine density influenced by hydration status and certain pathological conditions, was analysed. Values were grouped into two categories: $SG < 1020$, indicative of diluted urine and adequate hydration, and $SG \geq 1020$, indicative of concentrated urine and reduced fluid intake or dehydration. A higher tendency toward cell adhesion (23%) was observed in samples with $SG < 1020$, whereas adhesion was not observed in samples with higher SG values. However, the 95% confidence intervals overlapped, suggesting that the difference may not be statistically significant.

Parameter	Value	N. samples	samples with urinary cells adhesion	samples without urinary cells adhesion	% adhered cells	Lower bound (95% CI)	Upper bound (95% CI)	% non - adhered cells	Lower bound (95% CI)	Upper bound (95% CI)
BIL	neg	107	23	84	21.5	14.1	30.5	78.5	69.5	85.9
UBG	norm	107	23	84	21.5	14.1	30.5	78.5	69.5	85.9
KET	neg	107	23	84	21.5	14.1	30.5	78.5	69.5	85.9
GLU	norm	107	23	84	21.5	14.1	30.5	78.5	69.5	85.9
ASC	neg	97	19	78	19.59	12.22	28.89	80.41	71.11	87.78
ASC	+	10	4	6	40.0	12.16	73.76	60.0	26.24	87.84
PRO	neg	85	20	65	23.53	15.0	33.97	76.47	66.03	85.0
PRO	trace	22	3	19	13.64	2.91	34.91	83.36	65.09	97.09
NIT	neg	106	22	84	20.75	13.49	29.72	79.25	70.28	86.51
NIT	pos	1	1	0	100.0	2.5	100.0	0.0	0.0	97.5
BLD	neg	82	11	71	13.41	6.89	22.74	86.59	77.26	93.11
BLD	5	20	10	10	50.0	27.2	72.8	50.0	27.2	72.8
BLD	50	5	2	3	40.0	5.27	85.34	60.0	14.66	94.73
LEU	neg	91	23	68	25.27	16.75	35.47	74.73	64.53	83.25
LEU	25	14	0	14	0.0	0.0	23.16	100.0	76.84	100.0
LEU	75	2	0	2	0.0	0.0	84.19	100.0	15.81	100.0
pH	5	38	3	35	7.89	1.66	21.38	92.11	78.62	98.34
pH	6	25	7	18	28.0	12.07	49.39	72.0	50.61	87.93
pH	6.5	15	2	13	13.33	1.66	40.46	86.67	59.54	98.34
pH	7	17	7	10	41.18	18.44	67.08	58.82	32.92	81.56
pH	8	12	4	8	33.33	9.92	65.11	66.67	34.89	90.08
SG	1000	36	8	28	22.22	10.12	39.15	77.78	60.85	89.88
SG	1005	23	6	17	26.09	10.23	48.41	73.91	51.59	89.77
SG	1010	23	6	17	26.09	10.23	48.41	73.91	51.59	89.77
SG	1015	18	3	15	16.67	3.58	41.42	83.33	58.58	96.42
SG	1020	6	0	6	0.0	0.0	45.93	100.0	54.07	100.0
SG	1025	1	0	1	0.0	0.0	97.5	100.0	2.5	100.0
pH	< 7	78	12	66	15.4	8.2	24.3	85.0	74.0	91.0
pH	≥ 7	29	11	18	37.9	20.7	57.7	62.0	42.0	79.0
SG	< 1020	100	23	77	23.0	15.17	32.49	77.0	67.51	84.33
SG	≥1020	7	0	7	0	0	40.96	100.0	59.04	100.0

Table 4.5. The table reports the 11 parameters measured using the COMBI SCREEN® 11 SYS PLUS urine strips. The first and second columns present the parameter acronym and the corresponding value measured by the strip. The third column shows the number of samples corresponding to that specific parameter, followed by the number of samples with or without urinary cell adhesion (fourth and fifth column). The final columns present the percentage of samples showing urinary cell adhesion or non - adhesion within three weeks, along with the corresponding 95% confidence intervals (upper and lower limits).

The distribution of pH values across the 107 urine samples was represented, together with the percentage of samples exhibiting urinary cell adhesion according to pH (Figure 4.5). As shown in Figure 4.5 - A, the majority of urine samples (73%) displayed an acidic pH, whereas Figure 4.5 - B indicates that most of the samples in which urinary cell adhesion occurred (38%) were characterized by a neutral to mildly basic pH (≥ 7). Further stratification by sex revealed that, at pH ≥ 7, urinary cell adhesion was observed in 82% of male samples and 11% of female samples.

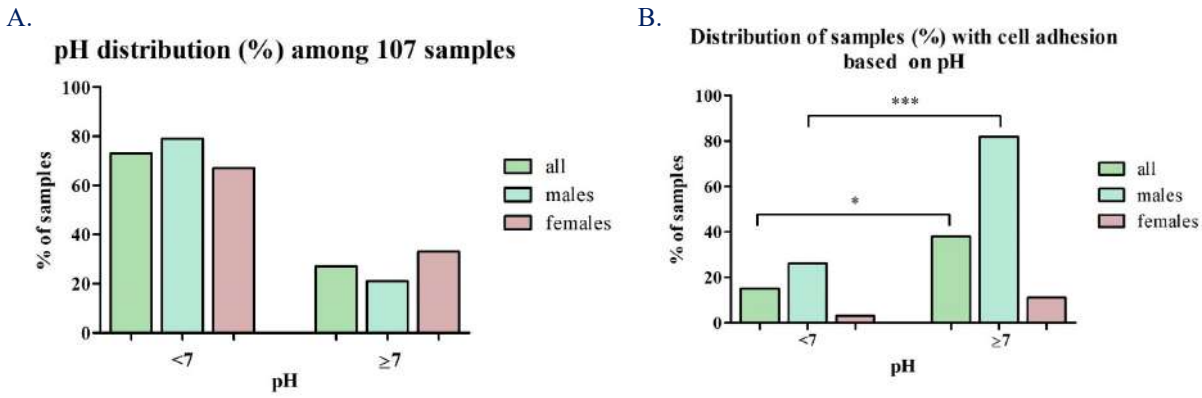

Figure 4.5. (A)Percentage distribution of urine samples according to pH. Each urine sample (n = 107), collected and processed after 24 h of storage at 4°C, was classified based on the measured pH as acidic (< 7) or neutral to mildly basic (≥ 7). Green columns indicate the percentage distribution of all samples, blue columns represent male samples, and pink columns represent female samples.
(B) Percentage distribution of urine samples exhibiting urinary cell adhesion according to pH, classified as acidic (< 7) or neutral to mildly basic (≥ 7). Green columns indicate the percentage distribution of all samples, blue columns represent male samples, and pink columns represent female samples.
p – values were calculated by Chi - Square test; * = $p < 0.05$; *** = $p < 0.001$.

To assess the potential effect of pH on PTEC adhesion, a Chi - Square test was performed. As reported in Table 4.6, samples were classified into two categories: pH < 7 and pH ≥ 7. Within each category, samples were further distinguished based on the presence or absence of PTEC adhesion. The null hypothesis assumed that PTEC adhesion is independent of pH. This hypothesis was rejected, as the test yielded the following result:

$$\chi^2 (1, N = 107) = 6.36, p = 0.0116$$

Since the p - value was lower than the alpha level, the analysis indicated a significant association between pH and urinary cell adhesion, with a higher frequency of adhesion observed in samples with pH ≥ 7.

	Samples with urinary cell adhesion	Samples without urinary cell adhesion	Marginal Row Totals	p - value
pH < 7	12 (16.77)	66 (61.23)	78	0.0116
pH ≥ 7	11 (6.239	18 (22.77)	29	
Marginal Column Totals	23	84	107	

Table 4.6. Representation of the values used in the Chi – Square test. Sample were stratified into two groups: pH < 7 and pH ≥ 7. For each group, the number of samples exhibiting urinary cell adhesion and those without adhesion are reported. The tables display the observed frequencies, with the expected frequencies shown in parentheses. Row and column totals of the observed values are provided, along with the overall total (n = 107). The last column reports the corresponding p - value.

Subsequently, the same analysis was performed after stratifying the subjects by gender, as reported in Table 4.7. In the male subgroup (in blue), the Chi - Square test yielded the following result:

$$\chi^2 (1, N = 53) = 11.48, p = 0.000703$$

Since the p - value was below the 0.05 threshold, a statistically significant association between pH and urinary cell adhesion was observed. Conversely, in the female subgroup (in pink), the Chi - Square test produced the following result:

$$\chi^2 (1, N = 54) = 1.59, p = 0.207578$$

In this case, the p – value exceeded the alpha level, indicating that PTEC adhesion did not appear to be associated with pH and that other variables could interfere with cell adhesion.

MALES	Samples with urinary cell adhesion	Samples without urinary cell adhesion	Marginal Row Totals	p - value
pH < 7	11 (15.85)	31 (26.159)	42	0.000703
pH ≥ 7	9 (4.15)	2 (6.85)	11	
Marginal Column Totals	20	33	53	
FEMALES	**Samples with urinary cell adhesion**	**Samples without urinary cell adhesion**	**Marginal Row Totals**	**p - value**
pH < 7	1 (2)	35 (34)	36	0.207578
pH ≥ 7	2 (1)	16 (17)	18	
Marginal Column Totals	3	51	54	

Table 4.7. Representation of the values used in the Chi - Square test for male (blue) and female (pink) samples. Samples were classified into two categories: pH < 7 and pH ≥ 7. Within each category, the number of samples with and without PTEC adhesion is reported. Row and column totals of the observed values are provided, along with the overall total. The last column reports the corresponding p - value. The tables display the observed frequencies, with the expected frequencies shown in parentheses, for male subjects only (blue) and female subjects only (pink).

Overall, these results suggested that samples with a neutral to slightly basic pH exhibit greater urinary cell adhesion. Consequently, 24 - hour storage at these pH levels may exert a less adverse effect on cell survival and adhesion.

A similar analysis was conducted for specific gravity (SG). To assess whether SG influenced PTEC adhesion, a Chi - Square test was performed. The resulting p - value (0.491839) indicated no significant association between SG and urinary cell adhesion. Nevertheless, it may still be advisable to recommend adequate hydration prior to urine collection, particularly to minimize bacterial accumulation in urine samples.

Use of Phosphate Buffer for the Stabilization of Urine Samples

To address the issue of the 24 - hour storage of cells in an acidic environment, as observed in the majority of urine samples, a buffer solution was added at the time of collection to adjust the urine to a neutral pH and thereby promote PTEC viability. Phosphate - buffered saline (PBS) was initially employed to prepare a highly concentrated stock solution. This approach was designed to require only

a minimal proportion of buffer relative to the total urine volume, with the aim of adjusting the final pH as close as possible to 7.4. The pH of each urine sample was measured, and the PBS solution was prepared. The main limitation encountered was the solubility of PBS, which did not allow the preparation of stock solution at concentrations higher than 10X. As a result, achieving a final concentration of 5X required the addition of an excessive volume of buffer (1:1 ratio), corresponding to 25 ml of buffer for 25 mL of urine. This requirement rendered the procedure impractical, highlighting the need to identify an alternative approach not involving PBS.

A 5 M phosphate buffer stock solution was prepared. As shown in Figure 4.6, starting from an initial pH range of 5.3 - 8.9, the addition of phosphate buffer to a final concentration of 0.05 M resulted in a pH range of 6.3 - 8.0. In contrast, a final concentration of 0.1 M produced a narrowed pH range of 6.6 - 7.7, which can be regarded as optimal. The urine samples were subsequently stored at 4°C, and pH stability was maintained after both 72 and 120 hours.

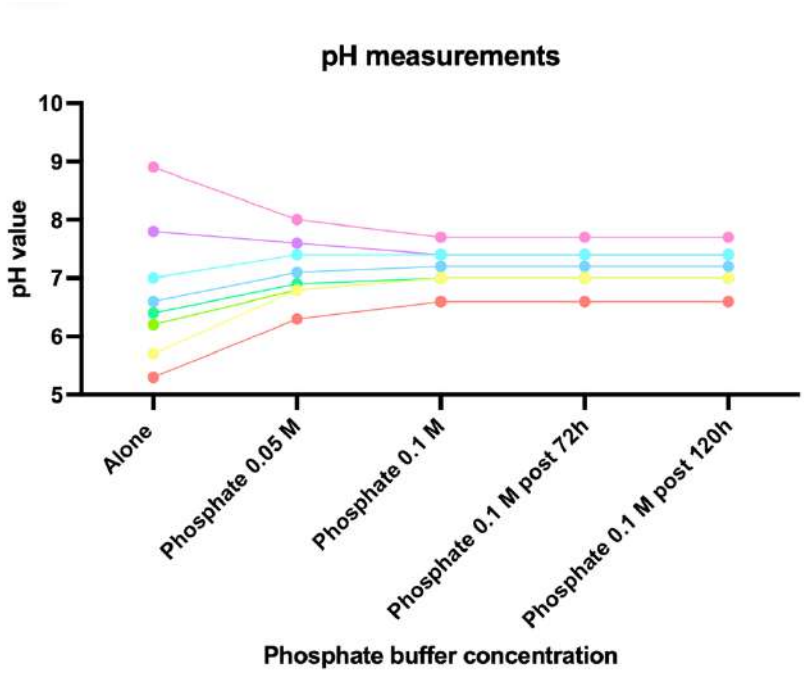

Figure 4.6. Graphical representation of pH measurements in urine samples following the addition of 5 M phosphate buffer. The y - axis reports the measured pH values, while the x - axis indicates the final phosphate buffer concentration obtained by adding increasing volumes of 5 M buffer to the urine samples. The last two data points represent pH values measured after 72 and 120 hours of storage at 4°C.

Since 1 M results as a good mother buffer concentration to maintain a pH as close as possible to neutral values, it was decided to start from a 1 M solution and a dilution ratio of 1:10 was maintained between the mother stock solution and the buffer added to the urine samples.

1 M Mother Phosphate Buffer Addition

Then, a 1 M phosphate buffer was employed to adjust the pH of urine samples toward neutrality, as described in the Materials and Methods. However, the addition of the buffer led to salt precipitation in most of the samples. During centrifugation, the precipitates pelleted together with the cells, preventing their proper separation. Consequently, salts were co - plated with the cells, forming a dense layer in the wells that impaired cell survival in culture (Figure 4.7).

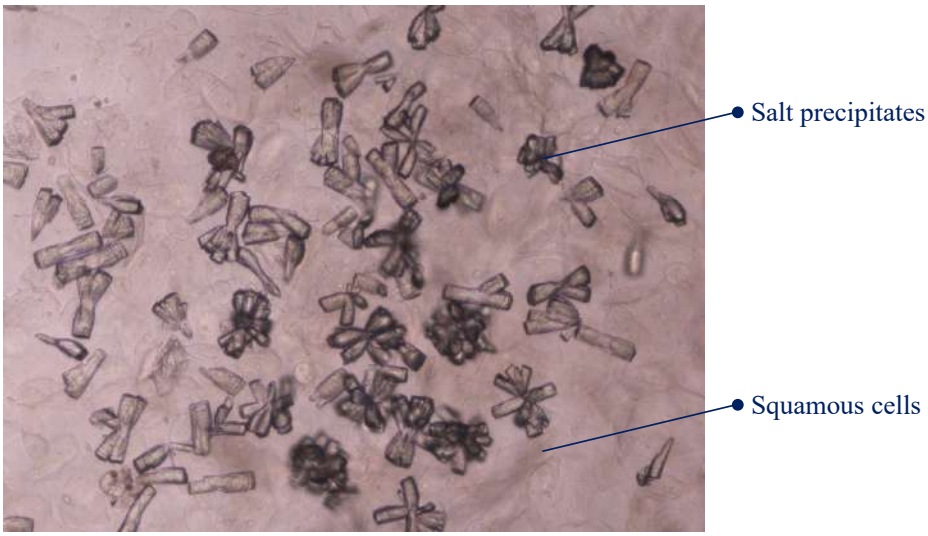

Figure 4.7. Phase - contrast image (magnification 10X) of salt precipitates in plated urine samples. These precipitates are clearly recognizable and distinguishable from the squamous cells present within the well.

0.5 M Mother Phosphate Buffer Addition

To minimize salt precipitation in urine samples, a 0.05 M final concentration of phosphate buffer was employed. A 0.5 M phosphate buffer stock solution was prepared to achieve a final concentration of 0.05 M, instead of 0.1 M. The objective was to find the best mediation between adjusting the pH of urine collected from volunteers toward neutrality in order to enhance urinary cell survival and avoiding salt precipitation.

Phosphate buffer was added to one of each pair of samples. Salt precipitation was not observed in 16 out of 18 samples, while it occurred in only 2 of the total urine samples collected. The frequency of salt formation was therefore markedly reduced compared with the previous experiment. Based on these findings, a final concentration of 0.05 M phosphate buffer was considered the most suitable for subsequent analyses.

4.1.2.2. Addressing Gender - Specificity

Considering the differences observed in urine samples, specifically the higher number of squamous cells in female - derived samples, the quantitative differences in the yield of adherent PTEC obtained from female compared to male samples, as well as the different impact of neutral - mildly basic pH on PTEC adhesion, the use of cell strainers was introduced into the original protocol.

Preliminary Analysis Using Different Strainer Sizes

A preliminary analysis was performed to test three different strainer sizes (30 μm, 20 μm, and 15 μm). In this experiment, only female urine samples were considered, given their high content of squamous cells that could interfere with process yield. The aim of this analysis was to identify the strainer size capable of reducing the number of squamous cells in female samples while still permitting the passage of urinary cells.

As shown in Figure 4.8, one day after plating, all filtered samples exhibited a marked qualitative improvement. In contrast, unfiltered samples (A, D, G in Figure 4.8) contained mucus, debris, and exfoliated fibres, which were absent in the filtered samples (B, E, H in Figure 4.8). The most notable improvement in all filtered conditions was a substantial reduction in the number of squamous cells. Our goal was to identify the smallest strainer size that would allow PTEC to pass while retaining squamous cells. As shown in Figure 4.8 (C, F, I), at day 8 post - plating, urinary cell adhesion and proliferation occurred only in samples filtered with the 30 μm and 20 μm strainers. The 15 μm strainer likely prevented the passage of urinary cells, resulting in the absence of adhered cells at day 8.

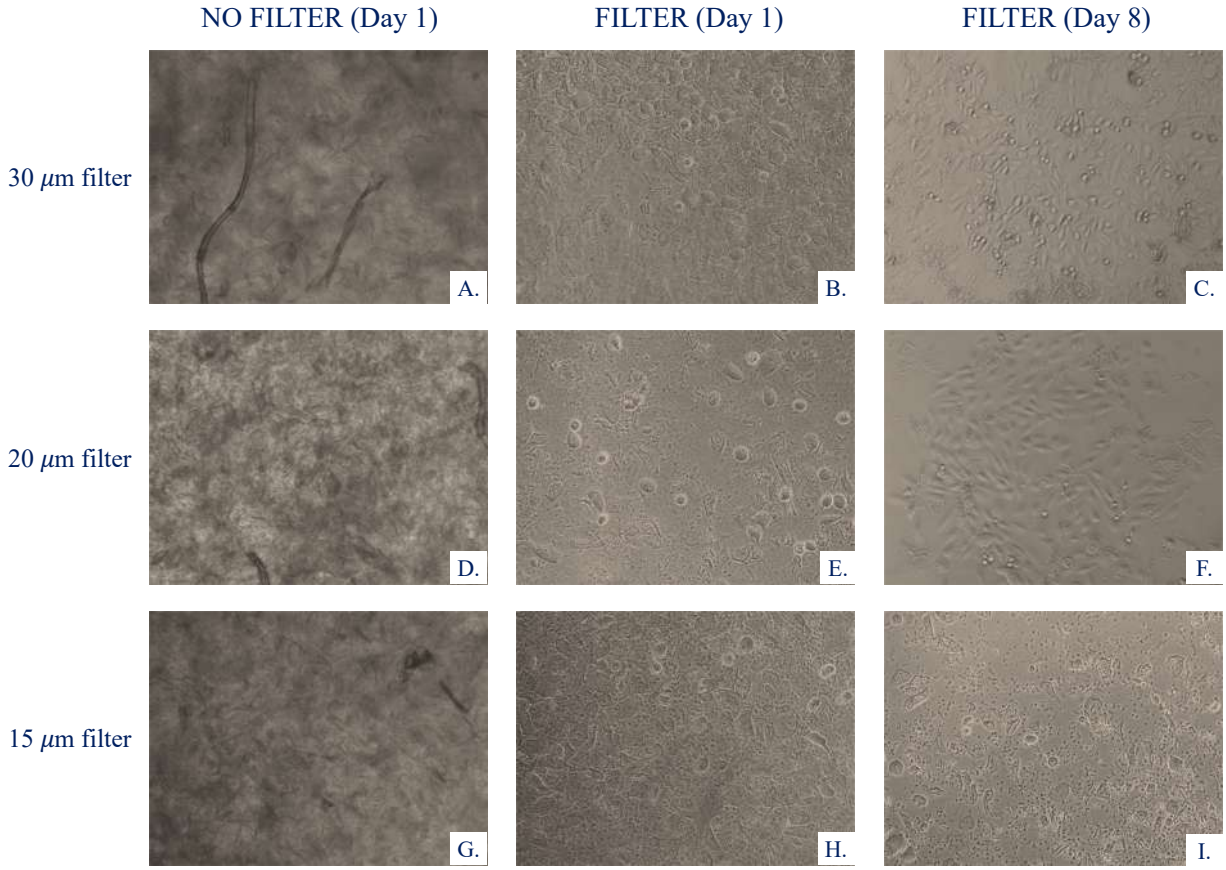

Figure 4.8. Phase – contrast images at 10X magnification of a female urine sample plated using three different strainer sizes: 30 μm, 20 μm, and 15 μm. The first column (images A, D, and G) shows the cells at day one, plated without using the filter. The second column (images B, E, H) shows the cells at day 1, following the use of the strainer. The last column (images C, F, I) show the samples on day 8 post - plating using strainers, underlying the presence or absence of adhered PTEC.

Based on these results, the 20 μm strainer was identified as the smallest size that both permitted PTEC passage and qualitatively improved female urine samples and was therefore selected for subsequent analyses.

Application of a 20 μm Strainer for Urinary Cell Preparation from Female Donors

The aim of the subsequent analysis was to assess whether the use of strainers could improve the yield of PTEC adhesion in female samples by separating them from squamous cells and by removing sediment and mucus that might negatively affect cell adhesion.

Also for this experiment, samples were processed within 4 hours of collection to ensure optimal yield conditions and to allow comparison with the previous experiments.

As described in the previous Section, the 20 μm strainer was selected, as it permitted the passage of PTEC in female samples. The samples taken in considerations were obtained from female donors A, B, and L. A qualitative improvement was evident in all three samples as early as day 1 with a marked reduction in the number of squamous cells, mucus, debris, and fibres. The use of the strainer enabled the passage and adhesion of PTEC in samples from donor B and L, whereas no adhesion occurred in sample A. Notably, in contrast to previous experiments, in which no urinary cell adhesion was ever observed in donor L, the use of strainers allowed adhesion to occur. By contrast, donor A consistently failed to yield PTEC, even with the use of strainers, confirming the relevance of donor - specificity in PTEC adhesion.

The results were subsequently analyzed from a quantitative perspective.
The use of strainers enabled the adhesion of PTEC from donor L. As previously reported, no urinary cell adhesion had ever been detected in samples obtained from this donor. This finding was noteworthy, as it markedly enhanced the yield of these samples, achieving 100% PTEC adhesion (Table 4.8). In contrast, no adherent PTEC were obtained from donor A under the same experimental conditions.
The overall yield was then evaluated by calculating the percentage of female donor samples in which urinary cell adhesion and proliferation were observed. As presented in Table 4.8, the proportion of plated samples (post - filtration) exhibiting adherent PTEC after three weeks of culture, relative to the total number of collected and plated samples, was 44% ± 51%. When compared with the data reported in subchapter 4.1.1.1, it became evident that the use of 20 μm strainers increased the process yield by approximately fourfold (from 11% to 44%). The standard deviation, however, remained substantial, reflecting inter - donor variability.

Identity code	Collected samples	Plated samples without strainers	Plated samples with strainers	Samples with urinary cells adhesion with strainers	% samples with urinary cells adhesion with strainers	% samples with urinary cells adhesion with strainers
A	12	6	6	0	0%	44% ± 51%
B	12	6	6	2	33%	
L	12	6	6	6	100%	

Table 4.8. The table reports the following information: donor identification codes; the total number of samples collected from each donor; the number of samples processed and plated with 20 μm strainers after 4 hours of storage at 4°C; the number of samples processed and plated without strainers after 4 hours of storage at 4°C; the number of samples exhibiting urinary cell adhesion; the percentage of samples with urinary cell adhesion relative to the plated samples (processed with 20 μm strainers) for each donor; and the overall percentage ± SD of samples with urinary cell adhesion among those plated using 20 μm strainers.

Based on this analysis, it could be concluded that pre - filtration of urine samples from female donors with 20 μm strainers enhanced the overall process yield.

4.1.3. Improved and Definitive Protocols

4.1.3.1. Preparation of PTEC by Combined Application of Test Strips, 0.5 M Phosphate Buffer, and a 20 μm Strainer (After 24h)

The preparation of urine samples is described in subchapter 3.1.3.1 of the Materials and Methods.

As initial analysis, the effect of 0.5 M phosphate buffer on pH adjustment was assessed. This evaluation was carried out after 24 hours of storage at 4°C. Figure 4.9 shows the pH distribution of the 108 samples analyzed. The majority of urine samples (87%) exhibited a neutral to slightly basic pH (pH ≥ 7), thereby confirming the expected buffering effect.

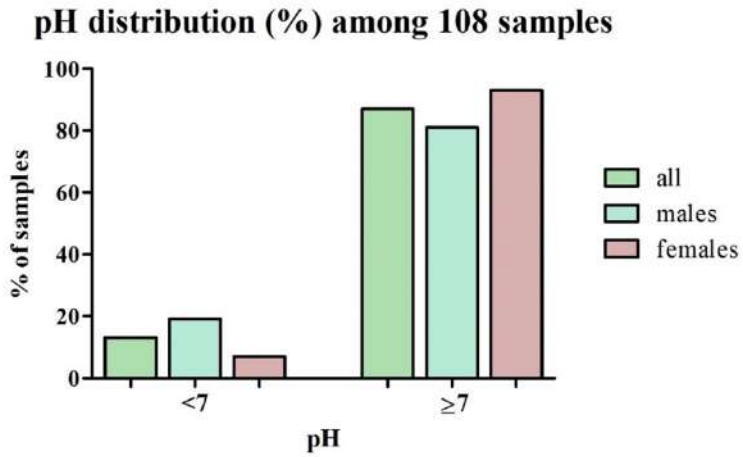

Figure 4.9. Percentage distribution of urine samples by pH value. Each urine sample (n = 108), collected and analyzed after 24h of storage at 4°C, was classified according to the measured pH as acidic (< 7) or neutral - slightly basic (≥ 7). Green bars represent the percentage distribution of all samples, blue bars represent male samples only, and pink bars represent female samples only.

The purpose of this analysis was to determine whether the introduction of the buffer combined with the use of strainers in the original protocol could improve the yield of PTEC isolation.

As a first evaluation, yield was expressed in percentage terms based on PTEC adhesion. As shown in Table 4.9, the percentage yield of plated samples exhibiting PTEC adhesion after three weeks of culture was 25% ± 14%. When compared with the result reported in subchapter 4.1.1.2. (21% ± 27%), a modest increase in yield and a reduction in standard deviation were observed.

Then, the yield of the samples was evaluated according to donor gender. As shown in Table 4.9, a marked increase in yield was observed in female samples following the combined use of buffer and strainers. The percentage of samples with PTEC adhesion increased from 6% ± 10% (subchapter 4.1.1.2.) to 26 ± 20%. This protocol modification also allowed PTEC adhesion in all female donors, including donors A and L, from whom adherent PTEC had not been obtained in previous analyses. In male donors, the yield decreased from 37% ± 30% to 25% ± 8%. However, a reduction in the standard deviation was noted. Overall, the results appeared more homogeneous and less variable than in the previous analysis, thereby increasing their reliability. Notably, the final yield was comparable between male and female samples.

Identity code	Collected samples	Plated samples	Samples with salt precipitation	% samples eliminated due to salt precipitation	Samples with urinary cells adhesion	% samples with urianry cells adhesion	% samples with urinary cells adhesion by gender	Total % of samples with urinary cells adhesion
A	18	18	0	0%	1	6%	26% ± 20%	25% ± 14%
B	18	13	5	28%	6	46%		
L	18	12	6	33%	3	25%		
H	18	12	6	33%	3	25%	25% ± 8%	
I	18	18	0	0%	6	33%		
M	18	18	0	0%	3	17%		
TOTAL	108	91	17		22			

Table 4.9. The table reports the following information: donor identification codes; the total number of samples collected from each donor; the number of samples processed and plated after 24 hours of storage at 4°C; the number of samples in which salt precipitation occurred; the percentage of samples excluded due to salt precipitation occurred; the percentage of samples excluded due to salt precipitation relative to the total collected per donor; the number of samples exhibiting urinary cell adhesion; the percentage of plated samples showing urinary cell adhesion for each donor; the percentage ± SD of samples with urinary cell adhesion stratified by donor gender (male or female); and the overall percentage ± SD of samples with urinary cell adhesion relative to the total number of plated samples.

One of the most relevant findings of this experiment concerns the persistence of donor - specific variability, even after the combined use of buffers and filters. Another parameter of interest is the occurrence of salt precipitation following buffer addition. As shown in Table 4.9, salt precipitation displayed marked inter - individual variability, being detected only in donor B, L, and H, and affecting approximately 30% of their samples.

4.1.3.2. Preparation of PTEC by Combined Application of Test Strips, 0.5 M Phosphate Buffer, and a 20 μm Strainer Only for Female Samples (After 4h)

The preparation of urine samples is described in subchapter 3.1.3.2 of the Materials and Methods.

Considering the results of the previous experiment, a decrease was observed in the percentage of male samples yielding adherent PTEC, from 35% ± 30% to 25% ± 8%. In addition, plating within 4 hours of collection resulted in a high proportion of samples successfully yielding PTEC (94% ± 10%). On this basis, a new analysis was conducted, collecting a total of 99 samples (66 samples from females, 33 from males). Filters were subsequently applied only to female samples, while urine samples were plated within 4 hours of collection. The use of buffer immediately after collection was maintained to ensure appropriate pH stabilization.
Table 4.10 shows the result of this last experiment. Samples from donor B (female) and donor H (male) were not available for collection.

Identity code	Collected samples	Plated samples	Samples with salt precipitation	% samples eliminated due to salt precipitation	Samples with urinary cells adhesion	% samples with urianry cells adhesion	% samples with urinary cells adhesion by gender	Total % of samples with urinary cells adhesion
A	42	42	0	0%	7	17%	31% ± 21%	40% ± 20%
L	24	24	0	0%	11	46%		
I	14	14	0	0%	9	64%	48% ± 23%	
M	19	19	0	0%	6	32%		
TOTAL	99	99	0		33			

Table 4.10. For female samples plated after the use of 20 μm strainer and for male samples plated without the use of the filter, the table presents the following information: the total number of samples plated, the number of samples with PTEC adhesion and the percentage ± SD of cell adhesion calculated on the number of wells plated.

By applying filters only to female samples, and by plating all samples after buffer addition and within 4 hours of collection with storage at 4°C, the percentages of PTEC adhesion, compared with 24 - hour storage and the use of filters for all samples, changed as follows:

- Female samples: from 31% to 21%
- Male samples: from 48% to 23%

4.1.4. PTEC Characterization

After optimizing the protocol for PTEC isolation, the cells were characterized both molecularly and through immunofluorescence assays.

Specifically, the molecular markers analyzed included the following genes: Claudin - 1 and E - cadherin (epithelial markers), L1CAM (L1 cell adhesion molecule) and NR3C2 (nuclear receptor subfamily 3 group C member 2) (renal markers), and SLUG (Snail family transcriptional repressor 2) (fibroblast marker). These markers were specifically selected to confirm the renal epithelial identity of the PTEC cells: Claudin – 1 and E – cadherin to verify the epithelial characteristics, L1CAM and NR3C2 to verify renal – specific features, and SLUG as a fibroblast marker to exclude mesenchymal contamination. Fibroblasts were used as a positive control. Figure 4.10 shows the results of this molecular characterization.

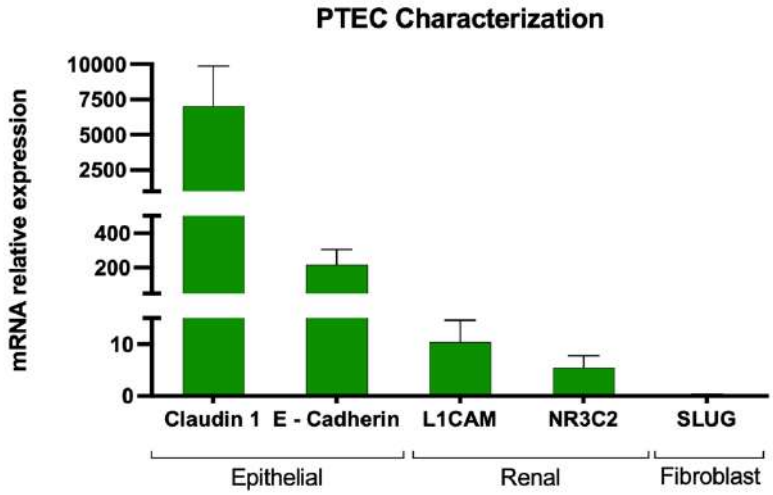

Figure 4.10. Analysis of genes by qRT - PCR. The figure displays the expression of epithelial genes (Claudin - 1; E - cadherin), renal genes (L1CAM; NR3C2), and SLUG gene. Gene expressions were normalized on 18S and HPRT as housekeeping. mRNA expression is relative to fibroblasts (expression value = 1). Data are reported as average ± SD of 10 biological samples.

The analyzed PTEC (n = 10) exhibited high expression levels of the Claudin - 1 gene, as well as substantial expression of E - cadherin, the second epithelial marker evaluated. Regarding renal markers, their expression levels were lower than those of epithelial genes but remained approximately tenfold higher than in the positive control. Conversely, the SLUG gene, typically expressed by fibroblasts, was not detected in the PTEC.

In addition to the molecular characterization, immunofluorescence experiments were performed to investigate the expression of structural markers such as F - actin and ZO - 1. Figure 4.11 shows the results of this analysis, revealing a strong signal for F - actin and a weaker signal for the tight junction protein ZO - 1.

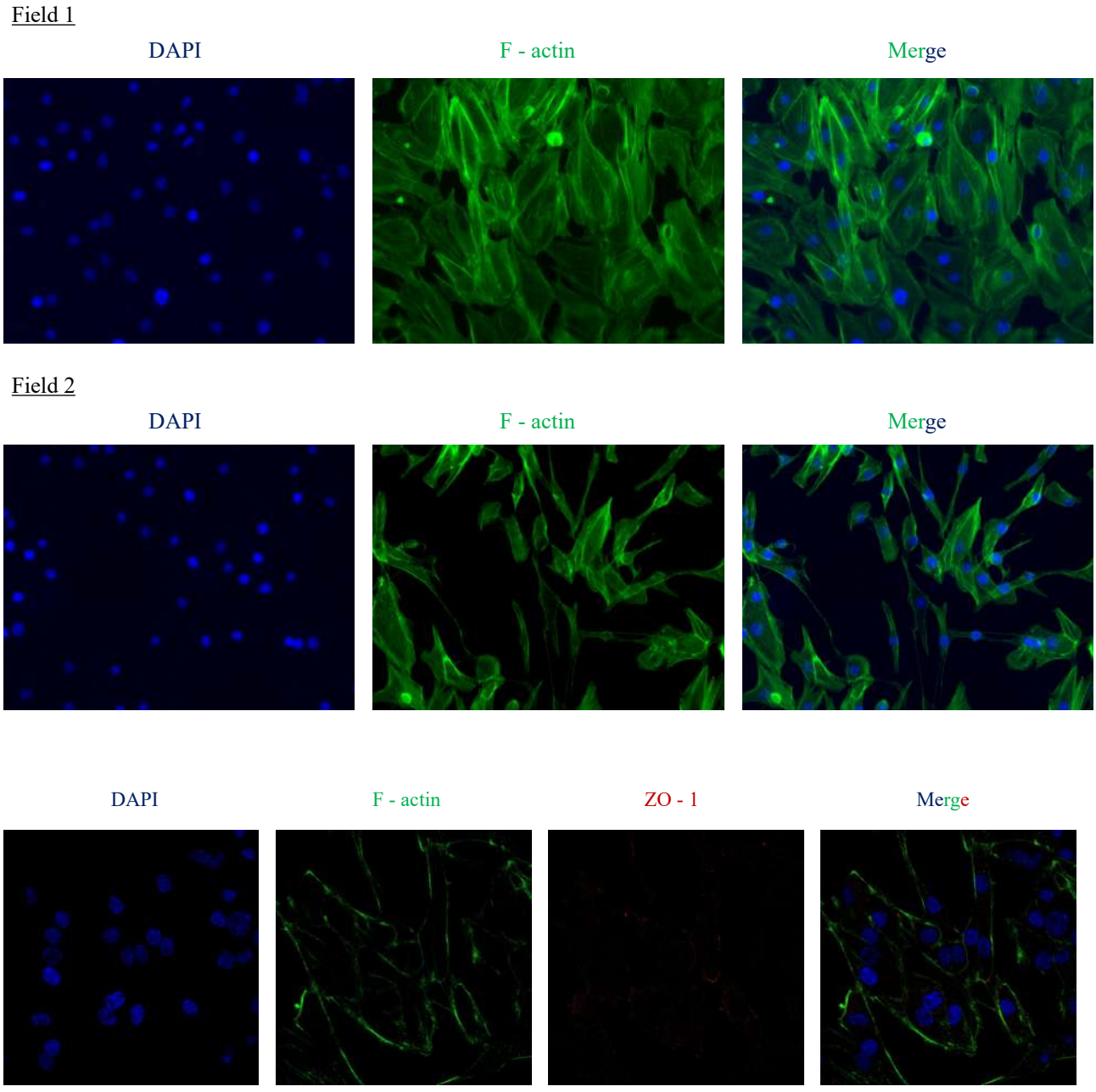

Figure 4.11. The two first rows show the staining for DAPI and F - actin (2 different fields), images acquired with a ZEISS Axiovert 200 Fluorescence Microscope (Magnification 20X). The third row presents the staining for DAPI, Phalloidin and ZO - 1. Images were acquired with a Leica Stellaris 5 confocal microscope (magnification 20X).

4.2. iPSC Generation from PTEC and Their Subsequent Culture (Step 2)

Following the isolation and establishment of PTEC colonies, these cells were dedifferentiated into iPSC through standardized procedures that have been previously detailed in the Materials and Methods section.

4.2.1. PTEC Transduction Efficiency

Plasmid transfection efficiency and production in HEK 293T cells was evaluated by fluorescence microscopy (data not shown), exploiting the expression of the tdTomato reporter encoded in the retro - transforming plasmid (pRRL.PPT.SF.hOct34co.hKlf4co.hSox2co.hmyc.itdTomato.pre.FRT), which emits in the orange - red spectrum (data not shown).

In addition, viral integration into the genome of PTEC cells was verified by fluorescence microscopy (Figure 4.12).

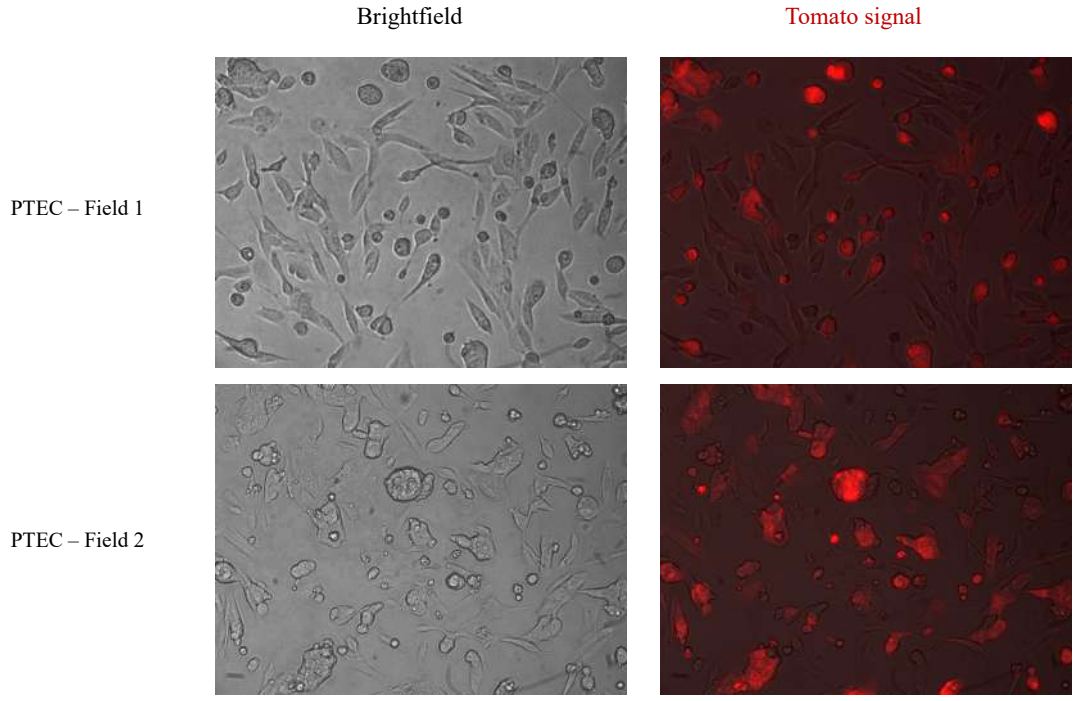

Figure 4.12. Representative images of infected PTEC cells from two different donors acquired using brightfield microscopy and TRITC filter settings. The TRITC filter allows visualization of the Tomato fluorescent signal, encoded by one of the plasmids employed for viral production and subsequent infection. Images were captured at 20X magnification with a ZEISS Axiovert 200 Fluorescence Microscope.

Subsequently, based on images acquired from multiple fields of lentivirus - treated cells, transduction efficiency was calculated as the percentage of infected cells exhibiting a detectable Tomato signal, yielding a value of around 45 %.

4.2.2. iPSC Generation and Their Culture

Following transduction of the urinary cells, the first morphological changes became evident after approximately 3 - 4 days (Figure 4.13). Subsequently, the transformed cells appeared smaller and more compact, displaying a high nuclear density, whereas the differentiated (non - transformed) cells retained the elongated morphology characteristic of PTEC.

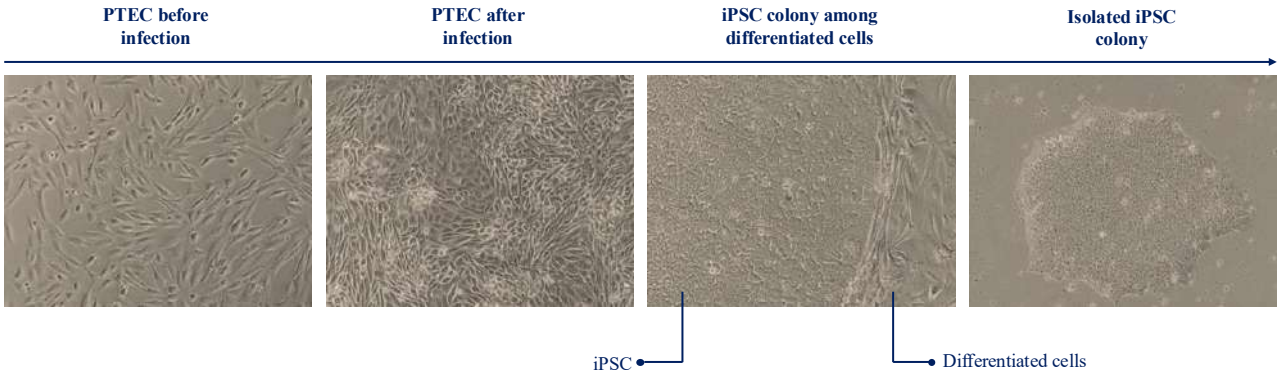

Figure 4.13. Phase - contrast images acquired during the sequential steps of morphological transition from PTEC to iPSC. The third panel shows the emergence of an iPSC colony and, on the right, non - reprogrammed cells that have undergone differentiation. Magnification 10X.

PTEC at early passages are preferably used to facilitate the bypass of the senescence barrier that may rise following infection. No significant differences were observed between the use of type I or type II colonies in the infection procedure.

Once generated, iPSC colonies were serially passaged until acquiring a well - rounded morphology (Figure 4.14, panel A), after which they were either passaged, directed toward hepatocyte differentiation or cryopreserved in liquid nitrogen. Following colony passaging, it was observed, particularly at higher passage numbers, the coexistence of colonies that retained morphological features consistent with iPSC, alongside others that had already undergone differentiation after passaging, displaying a more flattened morphology and increased cytoplasmic content (Figure 4.14, panel B). Similarly, even in the presence of differentiated cells, the growth of new iPSC colonies was

still observed after passaging; these colonies were subsequently isolated and individually expanded to prevent differentiation (Figure 4.14, panel C).

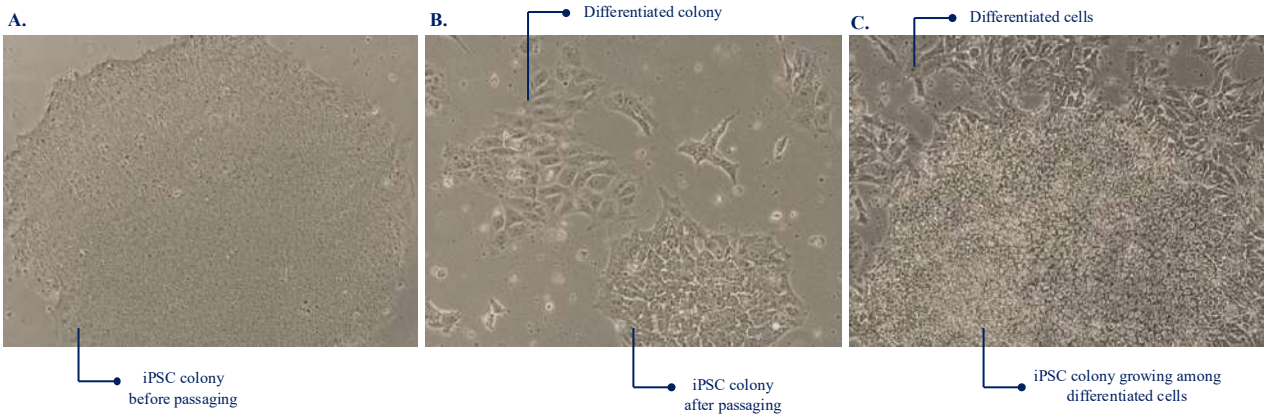

Figure 4.14. Morphological analysis by phase - contrast imaging (magnification 10X) of iPSC colonies before passaging (panel A) and after passaging (panels B and C).

Cells that underwent differentiation during the various passages were neither retained nor employed for subsequent induction into hepatocytes.

Verification of Transgene Integration in Lentivirus - Generated iPSC cDNA through Qualitative PCR

A qualitative PCR was carried out to assess the presence of the transgene in newly derived iPSC colonies originating from PTEC cells. The results (Figure 4.15) clearly demonstrate and confirm the detection of the target genes within the iPSC.

Figure 4.15. Results of the qualitative PCR (upper panel: OCT3/4 F/KLF4 R; lower panel: transgene F/transgene R). PCR amplification was performed on samples subjected to reverse transcriptase (+RT) and on negative controls lacking reverse transcriptase (-RT) PX459, gDNA (genomic DNA), and PMX were included as expression controls.

4.3. iPSC Differentiation into Hepatocytes - Protocol Comparison (Step 3)

4.3.1. General Comparison

Considering a general comparison among the four protocols under investigation, as described in the Materials and Methods section 3.3, differences can be observed mainly in the coating employed, the characteristics of the starting cells, the media and factors used, and the duration of the different induction steps. Figure 4.16 provides a schematic summary of the four protocols, which facilitates their comparison.

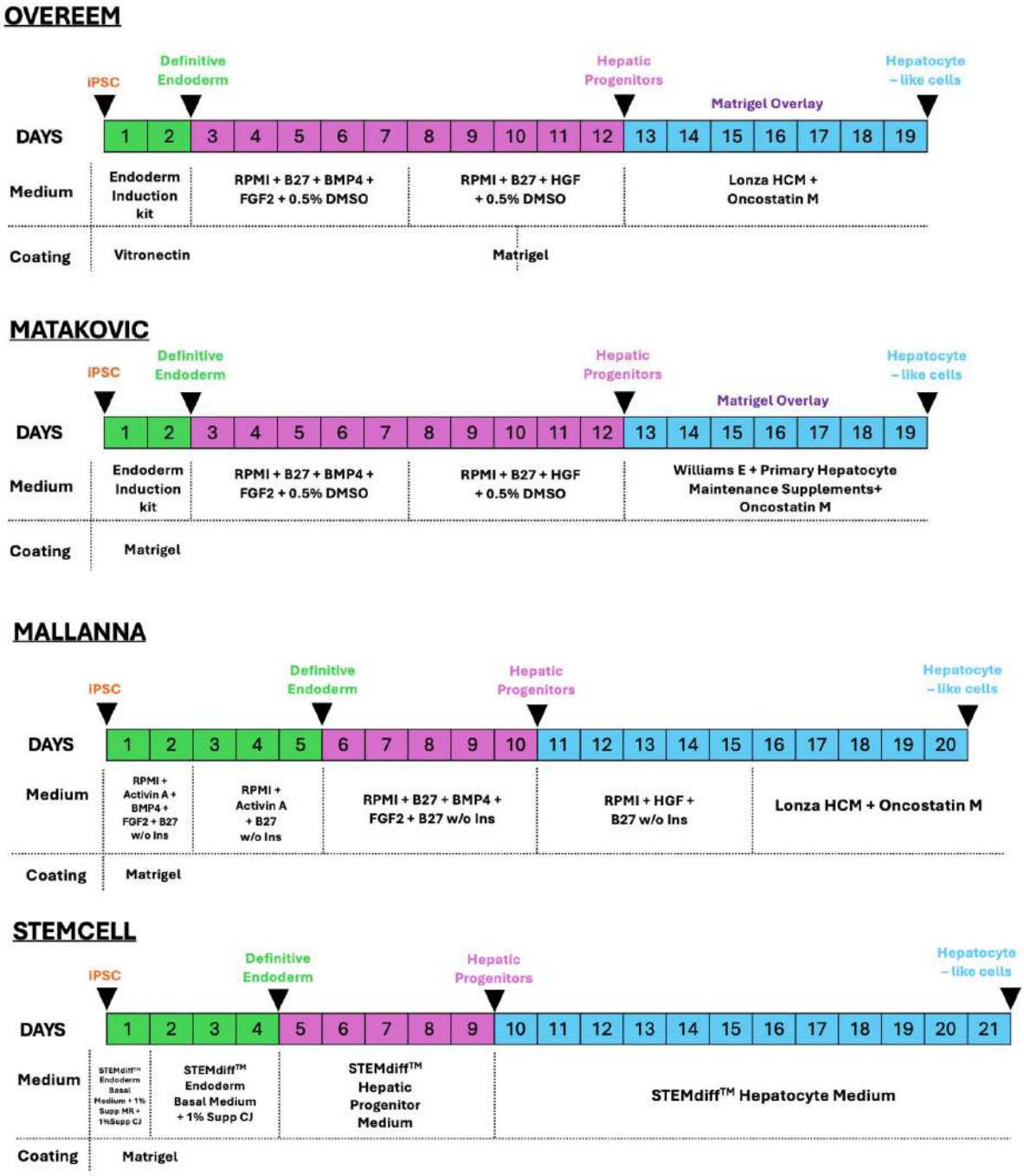

Figure 4.16. General comparison of the four different protocols under analysis. The figure illustrates a timeline for each protocol, with different colours used to highlight the attainment of the various stages. In addition, the media employed at each stage and the specific coating associated with each protocol are indicated.

With regard to the four protocols under analysis, the Matakovic's, Mallanna's, and STEMCELL protocols employ Matrigel coating from day 0, whereas the Overeem's protocol makes use of vitronectin for the first 7 days, followed by cell transfer into Matrigel - coated wells after passaging with Accutase enzyme. Considering Overeem's protocol, vitronectin is a recombinant human protein that offers a defined and xeno - free substrate for the feeder - free maintenance of iPSC, by

maintaining pluripotency and normal growth characteristics, supporting the attachment of the cells and reducing variability in iPSC cultures. Accutase facilitates the detachment of iPSC as single cells, thereby enhancing subsequent proliferation of these cells on Matrigel - coated surfaces.
Matrigel is a solubilized basement membrane preparation derived from Engelbreth - Holm - Swarm (EHS) mouse sarcoma, a tumor abundant in extracellular matrix (ECM) protein such as laminin, collagen IV, heparan sulphate proteoglycans, entactin/nidogen, as well as various growth factors that help the iPSC growth during the induction into hepatocyte - like cells.

A key distinction among the protocols, with respect to the characteristics of the starting cells, concerns the use of single - cell suspensions plated after Accutase passaging (Overeem's and Matakovic's protocol) as opposed to confluent monolayer covering the entire well (Mallanna's and STEMCELL protocols). This distinction translates into differences in the number of cells plated, with the Overeem's and Matakovic's protocols employing lower cell densities, whereas the Mallanna's and STEMCELL protocols require higher cell numbers.

The distinct media formulations and supplementary factors employed lead to different durations for each differentiation step and for the total protocol duration (19 days for the first two protocols, 20 days for the third, and 21 days for the last one). In the first two protocols, the initial medium employed is a commercially available formulation that allows efficient induction of iPSCs to definitive endoderm in only two days. The Mallanna's protocol employs a basal medium supplemented with factors such as Bone Morphogenetic Protein 4 (BMP4), Fibroblast Growth Factor 2 (FGF2), B27, and Activin A, to achieve the definitive endoderm stage within 5 days. In contrast, the STEMCELL protocol attains this stage after 4 days of culture through the use of commercial media in combination with their respective supplements. Notably, in the transition from definitive endoderm to hepatic progenitors, the first two protocols diverge in the choice of medium, with one supplemented with BMP4 and FGF2, and the other with B27 and Hepatocyte Growth Factor (HGF). Both protocols maintain a duration of 10 days for this step. By contrast, the Mallanna's protocol achieves the same stage in only 5 days through the combined use of BMP4, FGF2, and B27. The STEMCELL protocol differs further, relying exclusively on commercial medium throughout this phase.
The first two protocols allocate 7 days to reach the final stage (HLC), employing two distinct basal media and two different commercial kits. In both protocols, the commercial kit provides reagents that formulate a highly reproducible maintenance medium for primary hepatocytes. The Mallanna's protocol, by contrast, involves the use of two distinct media to achieve the final stage within 10 days: the first supplemented with HGF and B27, and the second identical to the medium described by

Overeem. As in the previous stage, the STEMCELL kit provides a commercial medium which is added to the cultured cells for the final 12 days.
The presence of Oncostatin M is evident in the first three protocols, where it has been reported to promote the development of hepatocyte polarity. By contrast, this cannot be ascertained for the commercial STEMCELL kit, as its exact composition is not disclosed. With the aim of promoting cellular polarity in the final stage, the first two protocols also incorporate a Matrigel overlay, which is absent in the latter two protocols.

For this part of the project, the following experimental activities were carried out, inside a multicentric study, by the research group of the Medical Genetics Laboratory, led by Professor Adamo Pio d'Adamo, at the IRCSS Materno Infantile "Burlo Garofolo" Hospital in Trieste, Italy: development of Mallanna's and STEMCELL differentiation protocols; acquisition of phase - contrast images for the Mallanna's and STEMCELL differentiation protocols; qualitative PCR for all four protocols; immunofluorescence experiments on HLCs for all four protocols under analysis and subsequent image acquisition.

4.3.2. Morphological Comparison

For all four protocols, the successive stages of differentiation were successfully obtained and subsequently compared on a morphological basis. The results are presented in Figure 4.17.

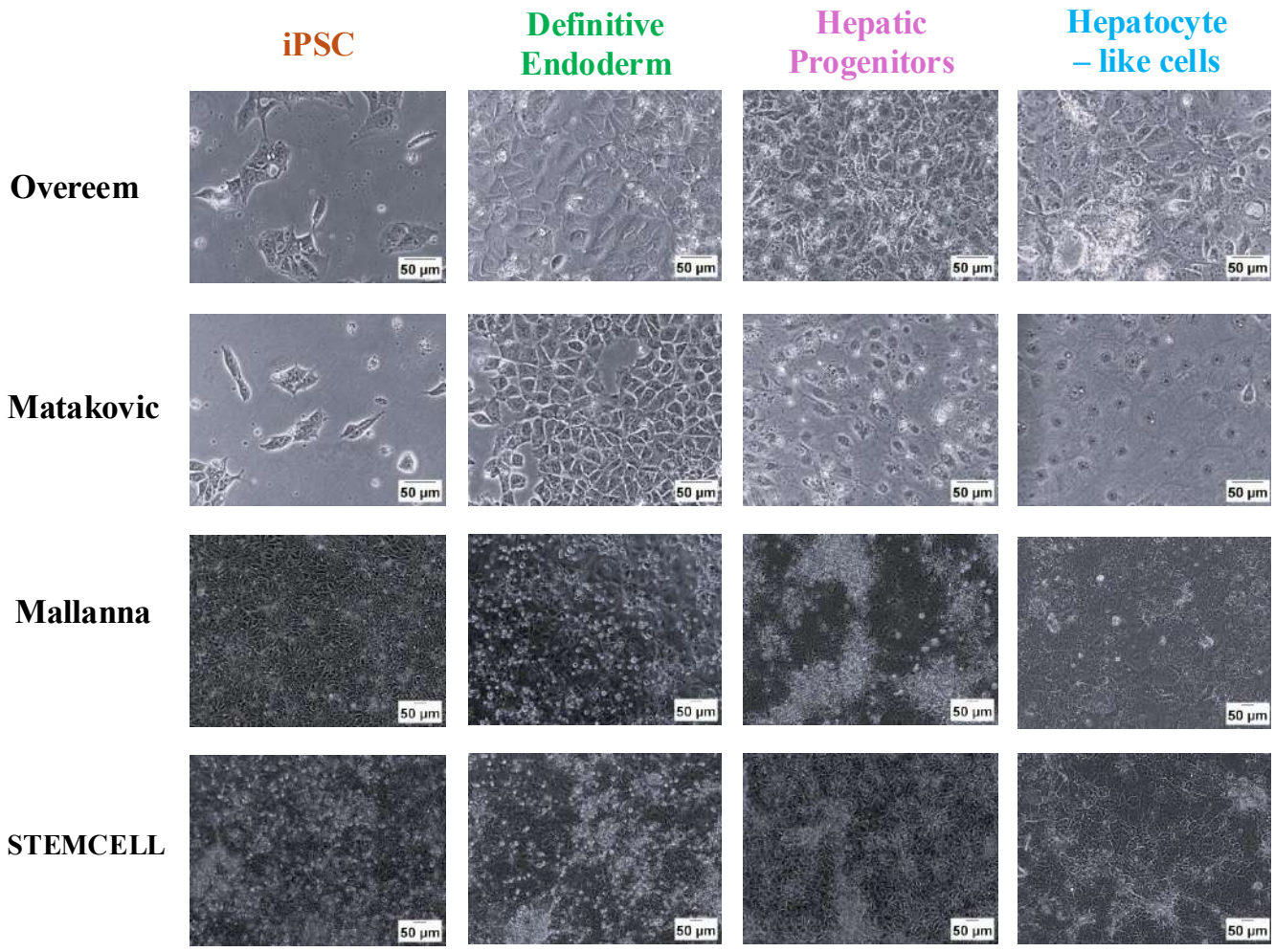

Figure 4.17. Morphological comparison among the four protocols. Phase - contrast images (magnification 20X, scalebar: 50 µm) display, for each protocol, the four principal stages of differentiation: iPSCs, definitive endoderm, hepatic progenitors, and hepatocyte - like cells. Phase - contrast images for both the Overeem's and Matakovic's protocol were acquired at Fondazione Italiana Fegato ONLUS, while for both the Mallanna's and STEMCELL protocols images were acquired at the Medical Genetics Laboratory at the IRCCS Materno Infantile "Burlo Garofolo" Hospital in Trieste, Italy.

As can be observed, the first major difference between the initial two protocols and the latter two concerns the number of starting cells. Specifically. Overeem's and Matakovic's protocols display single cells, whereas the other two protocols exhibit a monolayer of cells. This difference in initial cell number evidently results in a greater amount of cell death in the latter two protocols, visible at the different stages of differentiation as "white" cells overlying the monolayer.

In the definitive endoderm stage, cells derived from all four protocols display a polygonal morphology, which is markedly different from that observed in the iPSC stage. It is also evident that, although not confluent at the initial stage, the cells derived from the first two protocols begin to form a monolayer and to spread across the surface. Notably, differences in adhesion can be observed in the Overeem's protocol, where the cells are attached to a vitronectin coating rather than to Matrigel.
Distinct variations were evident at the hepatic progenitor stage across the four protocols. The Matakovic's protocol was characterized by a pronounced difference in the nuclear - to - cytoplasmic ratio, a feature less apparent in the remaining protocols. In those derived from confluent monolayers, cellular over proliferation was observed; however, the overall morphology remained largely comparable.
At the final differentiation stage, Mallanna's and STEMCELL protocols display a similar morphology, characterized by a monolayer of polygonal cells. In contrast, Matakovic's protocol yields cells with a larger cytoplasmic volume compared to the other protocols, and additionally reveals the presence of binucleated cells, a hallmark of hepatocytes. The Overeem's protocol, however, exhibits a distinct morphology at this stage, with regions where cells appear to have grown in multiple layers, one above the other.

4.3.3. Pluripotency Markers Expression

For each protocol, pluripotency markers were analyzed at the four differentiation stages, as described in the Materials and Methods section of this thesis. In addition, immunofluorescence analyses were performed. Specifically, the expression of the pluripotency marker OCT3/4, expected to be absent at the final stage of differentiation, was assessed.

The pluripotency markers analyzed – SOX2 (SRY - box transcription factor 2), OCT3/4 (POU class 5 homeobox 1), and NANOG (Nanog homeobox) – were specifically selected to assess the stem - like properties of the cells. SOX2, a member of the SRY - related HMG - box transcription factor family, is required for stem - cell maintenance and regulation of gene expression during development. OCT3/4 is a POU homeodomain transcription factor critical for embryonic development and the maintenance of stem cell pluripotency, while NANOG is a homeobox transcription factor involved in embryonic stem cell proliferation, self - renewal, and the inhibition of differentiation. Together, these markers provide a comprehensive assessment of the pluripotent state.

Figure 4.18 presents the results of the analysis for the three pluripotency - associated genes (SOX2, OCT374, NANOG), showing the comparative outcomes between the qualitative and quantitative PCR, which were performed for a subset of the analyzed genes.

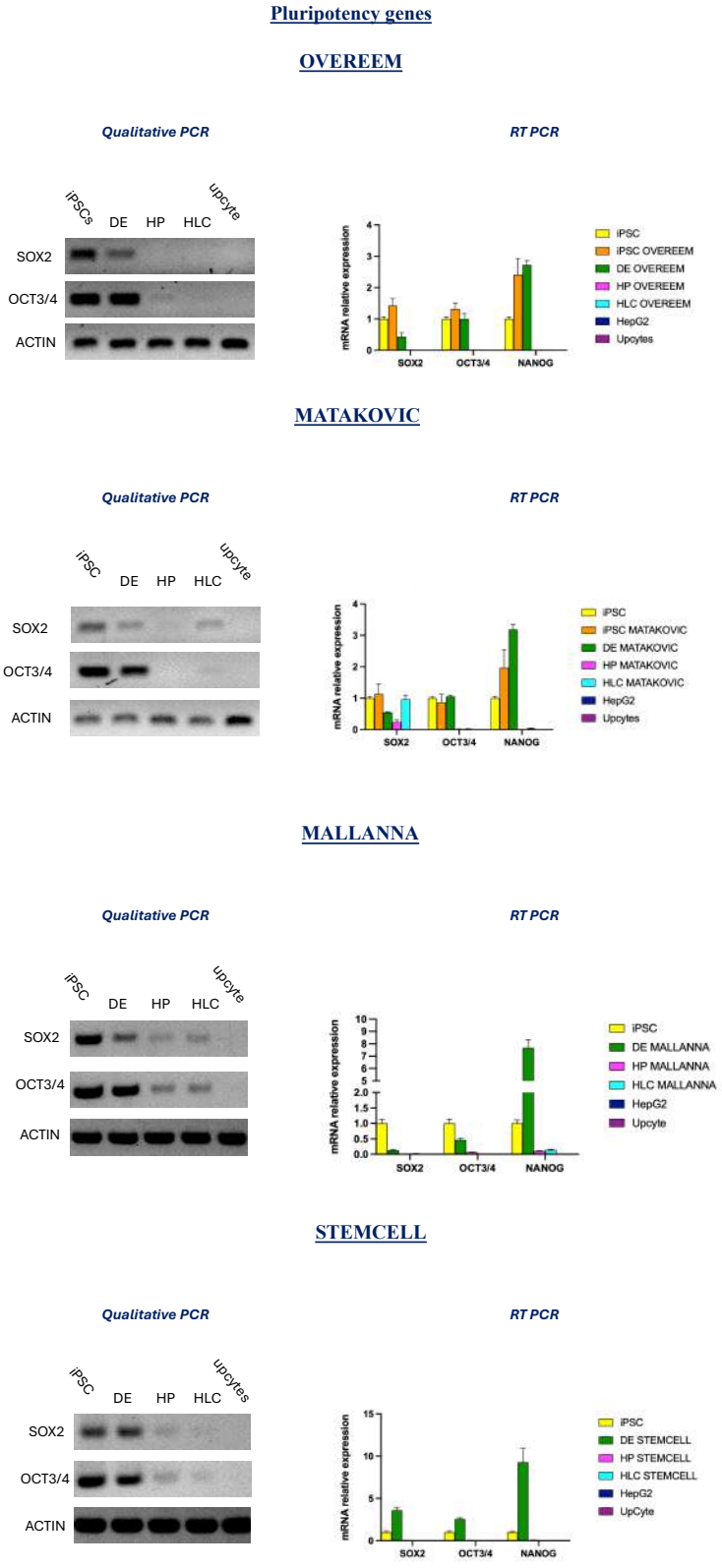

Figure 4.18. Analysis of pluripotency - associated genes by qualitative PCR and RT - PCR. The figure displays, for each protocol, the results of the qualitative PCR and the relative mRNA expression levels of SOX2, OCT3/4, and NANOG (RT - PCR). For the qualitative PCR, ACTIN was used as an internal control. For RT - PCR, differentiation stages are indicated by distinct colours (orange = iPSC, green = definitive endoderm [DE], pink = hepatic progenitors [HP], light blue = hepatocyte - like cells [HLC]). Gene expressions were normalized on 18S and HPRT as housekeeping. Yellow denotes the reference iPSCs, whose expression level is set to 1 (positive control). Purple corresponds to the expression of HepG2 cells, and dark blue to that of UpCyte cells, both used as negative controls. Data are reported as average ± SD of at least 3 biological samples.

For RT - PCR, for the STEMCELL and Mallanna's protocols, data corresponding to iPSC (orange) are not shown, as RNA was not collected at this stage.

Considering RT PCR, as expected, SOX2, OCT3/4, and NANOG were not expressed in the HepG2 and UpCyte cell line (negative controls).
In all four protocols, the three genes exhibited a progressive decrease in expression from the iPSC stage to the HLC stage, although with varying extent.
In Overeem's protocol, SOX2, OCT3/4, and NANOG were still expressed in the DE step, while they were unexpressed in the HP and HLC steps. For SOX2 and OCT3/4 it is possible to underline a decrease from the iPSC step to the DE step, while for NANOG the expression in DE was higher than the one in iPSC.
In Matakovic's protocol, OCT3/4 and NANOG were still expressed in the DE step, with an expression that was still higher than the one in the iPSC step, but they were not expressed in the next two steps (HP and HLC). SOX2 was expressed at all four differentiation stages, showing an initial decrease in expression up to the HP stage, followed by an increase at the HLC stage.
In Mallana's protocol, all three genes remained expressed at the DE stage; however, NANOG was the only gene expressed at a level higher than that of the reference iPSC. For NANOG, very low expression levels (approximately tenfold lower) were also detected at the HP and HLC stages.
In the STEMCELL protocol, the DE stage exhibited expression levels of all three genes higher than those of the reference iPSC. However, gene expression was completely silenced at the subsequent stages.
Considering the comparison with the qualitative PCR results for the SOX2 gene, a slight expression also detected by RT - PCR was observed in the Overeem's protocol at the DE stage. In the Matakovic's protocol, the expression pattern identified by RT - PCR was confirmed by the qualitative assay, showing an increase in gene expression at the HLC stage. In the Mallanna's protocol, although qualitative PCR indicated a decreasing SOX2 expression at the HP and HLC stages, no corresponding expression was detected by RT - PCR for these stages. In the STEMCELL protocol, SOX2 expression was observed qualitatively at the DE stage (and slightly at HP and HLC), which was consistent with the quantitative results, although expression levels at HP and HLC were not detectable by RT – PCR.
For the OCT3/4 gene, in the Overeem's protocol, expression persisted at the DE differentiation stage but was no longer detectable in the subsequent stages. A similar trend was observed for the Matakovic's protocol. In the Mallanna's protocol, the qualitative PCR showed a faint expression of OCT3/4 at the HP and HLC stages, while the quantitative analysis revealed only a slight expression

at the HP stage. In the STEMCELL protocol, the qualitative results indicated a residual SOX2 expression at HP and HLC stages, which was not detectable in the quantitative PCR analysis.

Taken together, these findings indicate that, apart from the persistence of SOX2 expression in the Matakovic's protocol, the three pluripotency - associated genes displayed a consistent downregulation trend across the differentiation protocols.

Considering OCT3/4 expression, none of the four protocols showed a significant signal at the final stage of differentiation. A faint nuclear signal was observed in the Overeem's and Matakovic's protocols, while for Mallanna's and STEMCELL protocols the absence of a signal was confirmed (Figure 4.19).

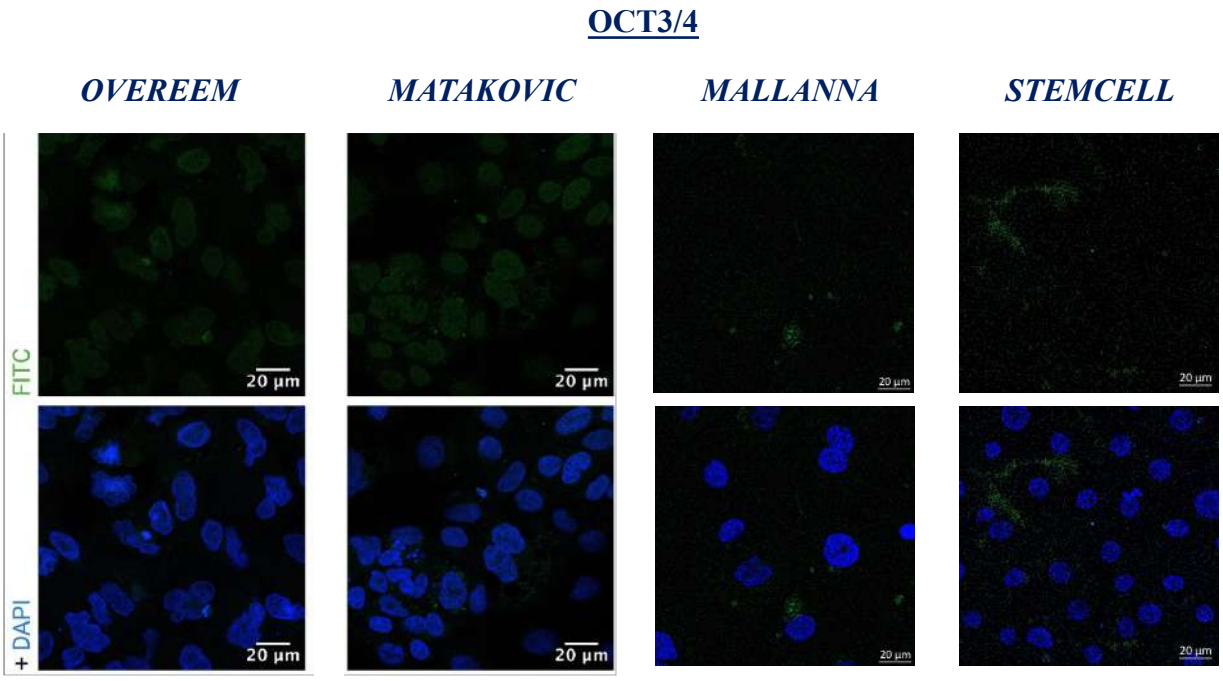

Figure 4.19. Representative immunofluorescence images showing OCT3/4 expression across the four differentiation protocols. The first row displays OCT3/4 (green) for each protocol, while the second row shows the merged signal with nuclear counterstaining (DAPI, blue). Images were acquired using a 3 Microscope (magnification 40X) a ZEISS LSM 900 Confocal laser scanning microscope thanks to the research group of the Medical Genetics Laboratory, led by Professor Adamo Pio d'Adamo, at the IRCCS Materno Infantile "Burlo Garofolo" Hospital in Trieste, Italy.

4.3.4. Hepatic Markers Expression

For each protocol, hepatic markers were analyzed at the four differentiation stages, as described in the Materials and Methods section of this thesis. In addition, immunofluorescence analyses were performed. Specifically, the expression of the HNF4α and ALB genes was assessed.

The analysis of hepatic genes was subdivided into two main groups: the first comprising genes Asialoglycoprotein receptor 2 (ASGR2), Serpina.1 (SERPINA1), Apolipoprotein F (APOF), and Albumin (ALB), the second one comprising genes Transthyretin (TTR), Hepatocyte Nuclear Factor 4α (HNF4α), and Alpha - fetoprotein (AFP).

Regarding the first group, the hepatic markers analyzed – ALB, SERPINA1, APOF, and ASGR2 – were specifically selected to assess the liver - specific characteristics of the cells. ALB encodes albumin, the most abundant plasma protein, predominantly produced by the liver. SERPINA1 encodes a serine protease inhibitor with a key role in liver function and protein homeostasis. APOF encodes a minor apolipoprotein involved in lipoprotein complex formation and cholesterol transport, with high hepatic expression. ASGR2 encodes a subunit of the asialoglycoprotein receptor, a liver - specific transmembrane protein critical for glycoprotein clearance and a target for liver - specific viral infection and drug delivery.
The additional hepatic markers analyzed – HNF4α, TTR, and AFP – were selected to further characterize the liver - specific properties of the cells. HNF4α encodes a nuclear transcription factor that regulates the expression of multiple hepatic genes and plays a role in liver development. TTR encodes transthyretin, a tetrameric carrier protein involved in the transport of thyroid hormones and retinol, and participates in various intracellular processes including proteolysis, autophagy, and glucose homeostasis. AFP encodes α - fetoprotein, a major fetal plasma protein produced by the liver and yolk sac, whose expression in adults is associated with hepatocarcinoma and teratoma. Collectively, these markers provide a comprehensive evaluation of the hepatic identity of the cells.

Regarding the RT - PCR results, considering the first group of genes (Figure 4.20), HepG2 cells exhibit higher expression of all genes when compared with the positive control (UpCyte, expression = 1). No expression of ASGR2, SERPINA1, or ALB was detected in the Overeem's protocol. By contrast, APOF expression increased from the iPSC stage to the HP stage, followed by a decrease at the HLC stage, with expression levels remaining lower than those observed in the HepG2 cell line.

The Matakovic's protocol exhibited the same expression pattern for ASGR2, SERPINA1, and ALB. APOF expression levels were higher than those of the positive control but remained lower than those detected in HepG2 cells.

In the Mallanna's protocol, ASGR2 and SERPINA1 were expressed at the HP and HLC stages, whereas ALB expression was detected only at the final differentiation stage. Expression levels of ASGR2, SERPINA1, and ALB were higher than those of the positive control, with SERPINA1 being the only gene expressed at levels exceeding those of HepG2 cells. For APOF, the highest expression was detected at the DE stage, while at the HLC stage its expression level remained above that of the positive control but below that of the HepG2 cells.

In the commercial STEMCELL protocol, ASGR2 and SERPINA1 expression was detected at both the HP and HLC stages, with SERPINA1 levels at the HLC stage exceeding those of HepG2 cells. ALB expression, on the other hand, was higher than in UpCyte cells but remained lower than in HepG2 cells. As observed in the other protocols, APOF expression was detected across all four stages, with the last three differentiation stages displaying levels higher than the positive control but lower than those of HepG2 cells.

In summary, APOF was the only gene to exhibit expression levels comparable to or higher than the positive control across all four protocols. In contrast, the other three genes analyzed showed higher expression than the positive control only in the Mallanna and STEMCELL protocols.

Considering the comparison with the qualitative PCR results for the ASGR2 gene, the outcomes of the two PCR analyses were consistent for the Overeem's and Matakovic's protocols, with no detectable expression in either case. In contrast, in the Mallanna and STEMCELL protocols, ASGR2 expression was detected at both the HP and HLC stages in both qualitative and quantitative assays.

For SERPINA1, a similar pattern was observed in the Overeem's and Matakovic's protocols, with no detectable expression in either PCR approach. In the Mallanna's and STEMCELL protocols, however, qualitative PCR confirmed the quantitative findings, showing evident expression levels in the last two differentiation stages.

Regarding ALB (albumin), no expression was detected by either qualitative or quantitative PCR in the Overeem's and Matakovic's protocols. In the Mallanna's and STEMCELL protocols, qualitative PCR results were consistent with the quantitative data, showing ALB expression in the HP (slight) and HLC stages for Mallanna, and at the HP stage for STEMCELL.

Finally, APOF expression was not detected by qualitative PCR in any of the protocols. In the Mallanna's and STEMCELL protocols, despite clear expression observed in RT - PCR, no corresponding expression was identified in the qualitative assay.

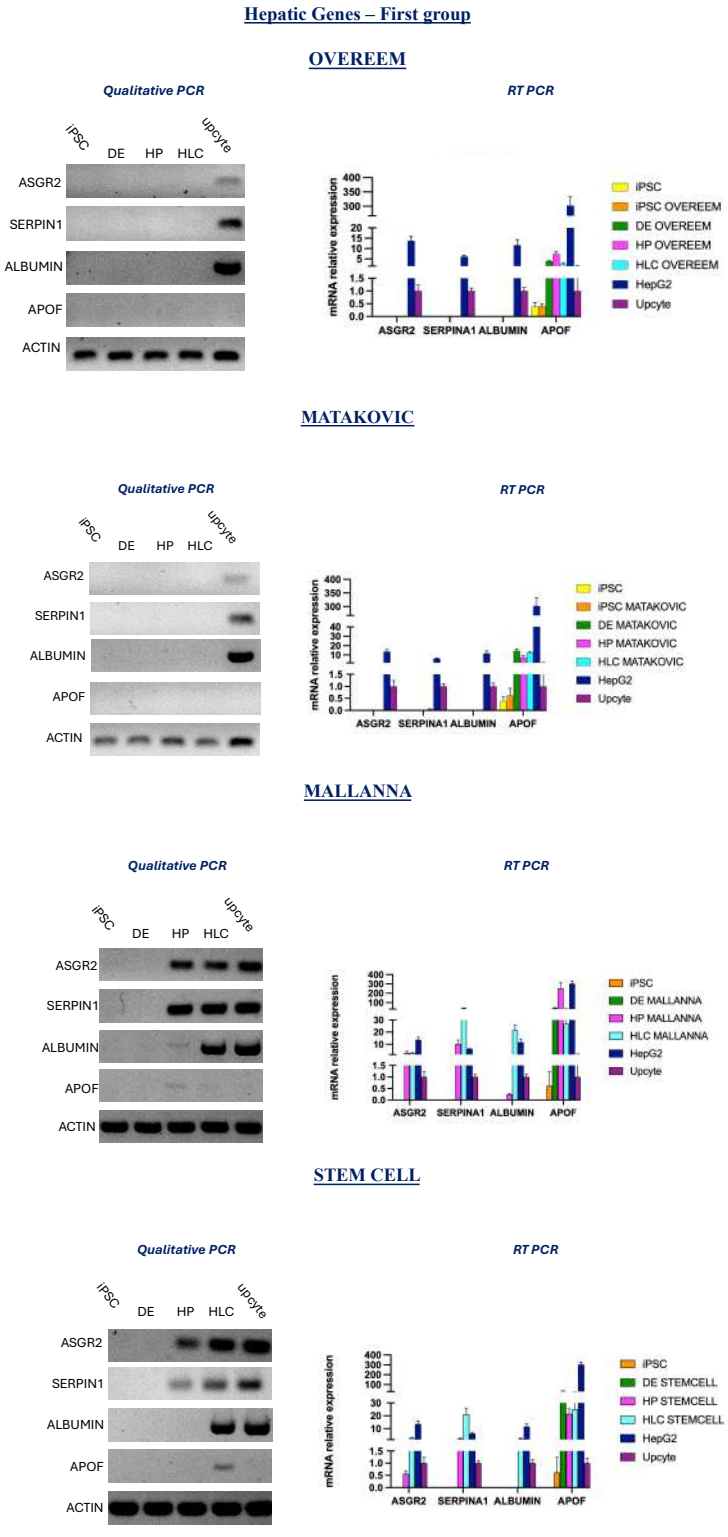

Figure 4.20. Analysis of hepatic genes by qualitative PCR and RT – PCR. The figure displays, for each protocol, the results of the qualitative PCR and the relative mRNA expression levels of ASGR2, SERPINA 1, ALBUMIN, and APOF. For the qualitative PCR, ACTIN was used as an internal control. For RT – PCR, differentiation stages are indicated by distinct colors (orange = iPSC, green = definitive endoderm [DE], pink = hepatic progenitors [HP], light blue = hepatocyte – like cells [HLC]). Gene expressions were normalized on 18S and HPRT as housekeeping. Purple denotes the reference UpCyte, whose expression level is set to 1 (positive control). Dark blue corresponds to the expression of HepG2 cells. Yellow corresponds to iPSC, used as negative control. Data are reported as average ± SD of at least 3 biological samples.

Considering the staining for albumin (Figure 4.21), it was diffused and included also a nuclear component in the Overeem's protocol. A faint cytoplasmic, but not nuclear, signal was detected for the Matakovic's protocol, while clearer signals were detected in the Mallanna's and STEMCELL protocol, showing no staining at the nuclear level. The staining pattern appeared more appropriate in the last two protocols, as no overlap with the nucleus was observed.

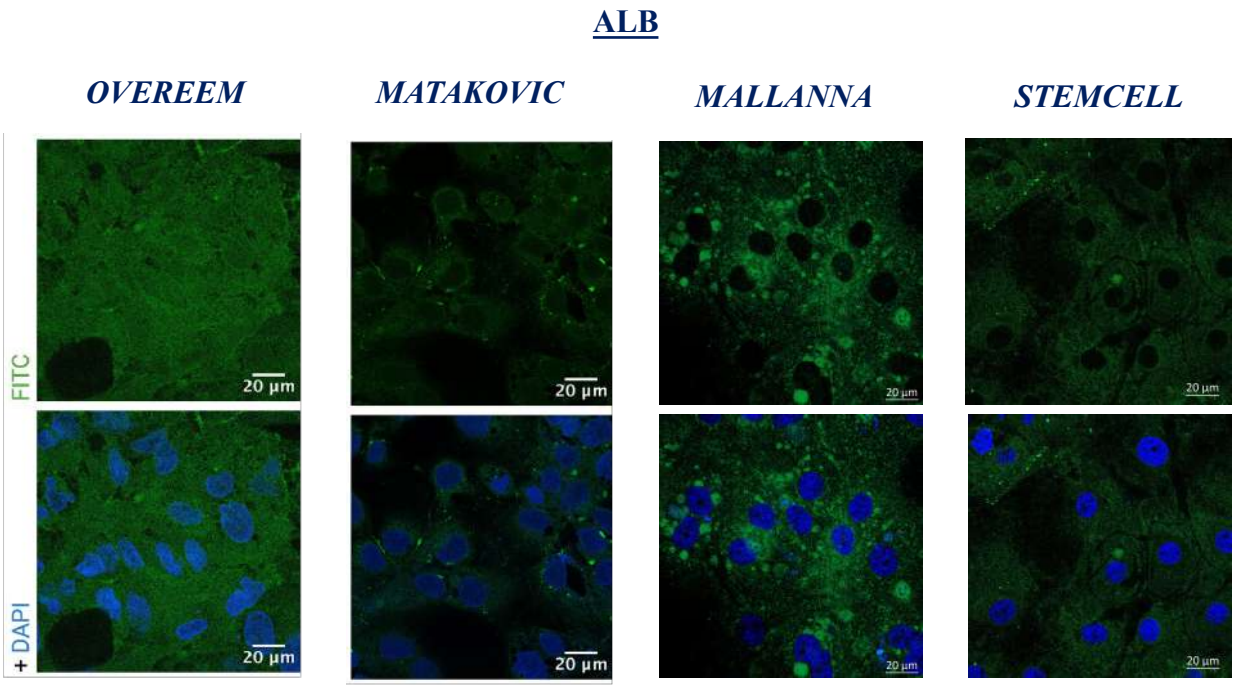

Figure 4.21. Representative immunofluorescence images showing ALB expression across the four differentiation protocols. The first row displays ALB (green) for each protocol, while the second row shows the merged signal with nuclear counterstaining (DAPI, blue). Images were acquired using a 3 Microscope (magnification 40X) a ZEISS LSM 900 Confocal laser scanning microscope thanks to the research group of the Medical Genetics Laboratory, led by Professor Adamo Pio d'Adamo, at the IRCCS Materno Infantile "Burlo Garofolo" Hospital in Trieste, Italy.

Regarding RT - PCR, considering the second group of genes (Figure 4.22), HepG2 cells exhibit higher expression of all genes when compared with the positive control (UpCyte, expression = 1).

The HepG2 cell line exhibited markedly higher expression levels of TTR, HNF4α, and, most prominently, AFP (approximately 1000 - fold), compared with the positive control (UpCyte). According to the Overeem's protocol, TTR expression was detected at both the HP stage and, at lower levels, the HLC stage, although in both cases it remained below the levels observed in HepG2. HNF4α expression was restricted to the DE stage, where it was present only at very low levels compared with both HepG2 and the positive control. In contrast, AFP was most highly expressed at the iPSC stage, but its expression persisted, even if at reduced levels, in the HLC stage.

The Matakovic's protocol showed higher TTR expression levels compared with both the positive control and HepG2 cells at the HP and HLC differentiation stages. HNF4α expression was significant

only at the DE stage, whereas AFP was expressed at higher levels than the positive control but much lower than HepG2 cells at the HLC stage.
With the Mallanna's protocol, all three genes displayed higher expression levels at the HP and HLC stages compared with both the positive control and HepG2 cells. In particular, a decreasing trend was observed from HP to HLC for TTR and HNF4α, whereas AFP showed an increasing trend.
In the STEMCELL protocol, TTR expression was comparable between the HP and HLC stages, while HNF4α was more strongly expressed at the HP stage. AFP, which was also expressed at the DE stage similarly to HNF4α, showed an increasing trend, reaching levels higher than HepG2 and becoming particularly elevated at the HLC stage.

Considering the comparison with the qualitative PCR results for the TTR gene, in the Overeem's protocol, the qualitative PCR confirmed the quantitative findings, showing higher expression at the HP stage compared to HLC. In the Matakovic's protocol, expression was confirmed at both the HP and HLC stages. For the Mallanna's and STEMCELL protocols, the results of the two PCR analyses were also consistent.
For the HNF4α gene, the expression detected at the DE stage by quantitative PCR corresponded to that observed in the qualitative assay for both the Overeem's and Matakovic's protocol. In the Mallanna's and STEMCELL protocols, HNF4α expression at the DE, HP and, HLC stages was confirmed by qualitative PCR.
Regarding AFP, for the Overeem's and Matakovic's protocols, the qualitative PCR results did not correspond to those obtained from quantitative analysis. In contrast, for the Mallanna's and STEMCELL protocols, qualitative PCR did not detect expression at the DE stage but confirmed expression at the HP and HLC stages.

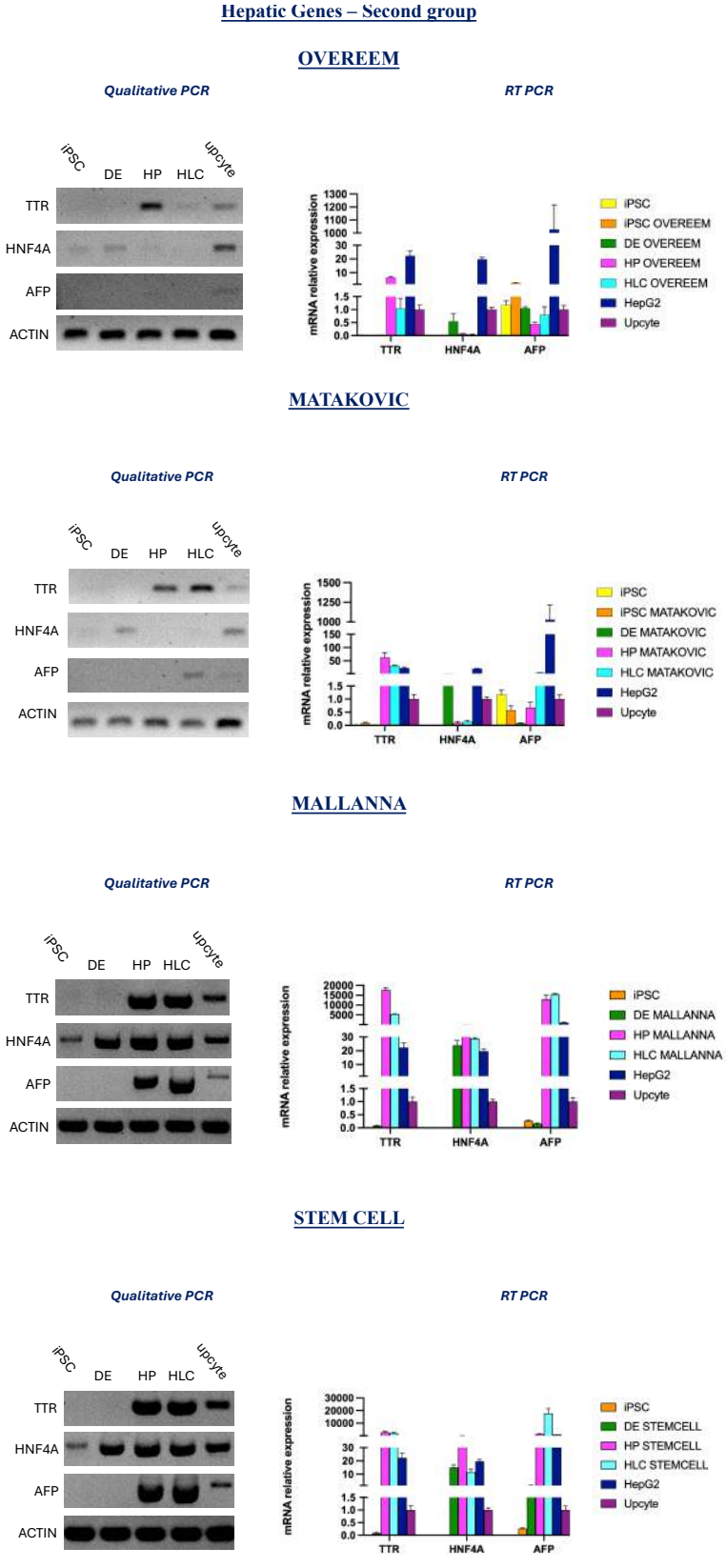

Figure 4.22. Analysis of hepatic genes by qualitative PCR and RT - PCR. The figure displays, for each protocol, the results of the qualitative PCR and the relative mRNA expression levels of TTR, HNF4α, AFP. For the qualitative PCR, ACTIN was used as an internal control. For RT - PCR, differentiation stages are indicated by distinct colors (orange = iPSC, green = definitive endoderm [DE], pink = hepatic progenitors [HP], light blue = hepatocyte - like cells [HLC]). Gene expressions were normalized on 18S and HPRT as housekeeping. Purple denotes the reference UpCyte, whose expression level is set to 1 (positive control). Dark blue corresponds to the expression of HepG2 cells. Yellow corresponds to iPSC, used as negative control. Data are reported as average ± SD of at least 3 biological samples.

Regarding HNF4α expression, in the final stage of differentiation, only the STEMCELL protocol showed a clear nuclear signal, while the other three protocols showed a faint signal, clearly nuclear but not as well defined as in the STEMCELL protocol (Figure 4.23).

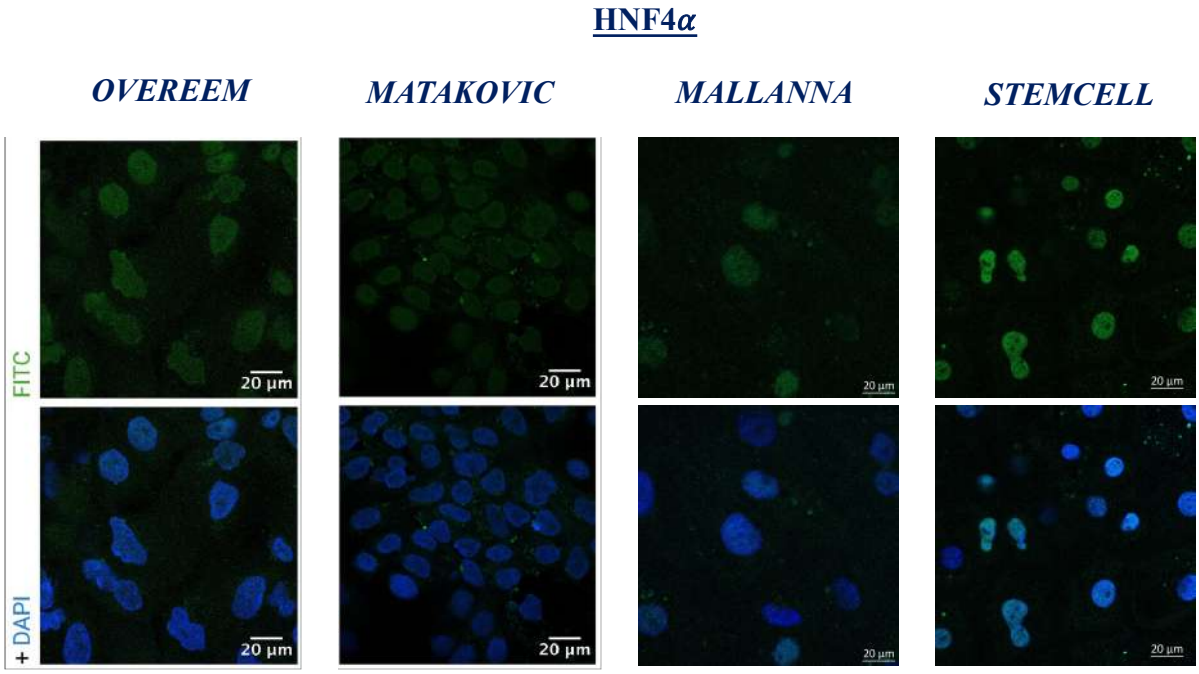

Figure 4.23. Representative immunofluorescence images showing HNF4α expression across the four differentiation protocols. The first row displays HNF4α (green) for each protocol, while the second row shows the merged signal with nuclear counterstaining (DAPI, blue). Images were acquired using a 3 Microscope (magnification 40X) a ZEISS LSM 900 Confocal laser scanning microscope thanks to the research group of the Medical Genetics Laboratory, led by Professor Adamo Pio d'Adamo, at the IRCCS Materno Infantile "Burlo Garofolo" Hospital in Trieste, Italy.

In addition, the expression levels of two bile acid transporters (BSEP and MRP2), as well as structural proteins of interest such as E - cadherin and ZO - 1, were also evaluated on the last stage of differentiation for all the four protocols.

Figure 4.24 represents the results for the Overeem's protocol. Canalicular transporter BSEP localized to the plasma membrane, even if a background signal can be observed in the cytoplasm. MRP2 displayed a diffuse intracellular pattern. The tight - junction marker ZO - 1 was confined to cell borders, even if a background signal can be noted also for this marker. E - cadherin was likewise restricted to the membrane.

OVEREEM

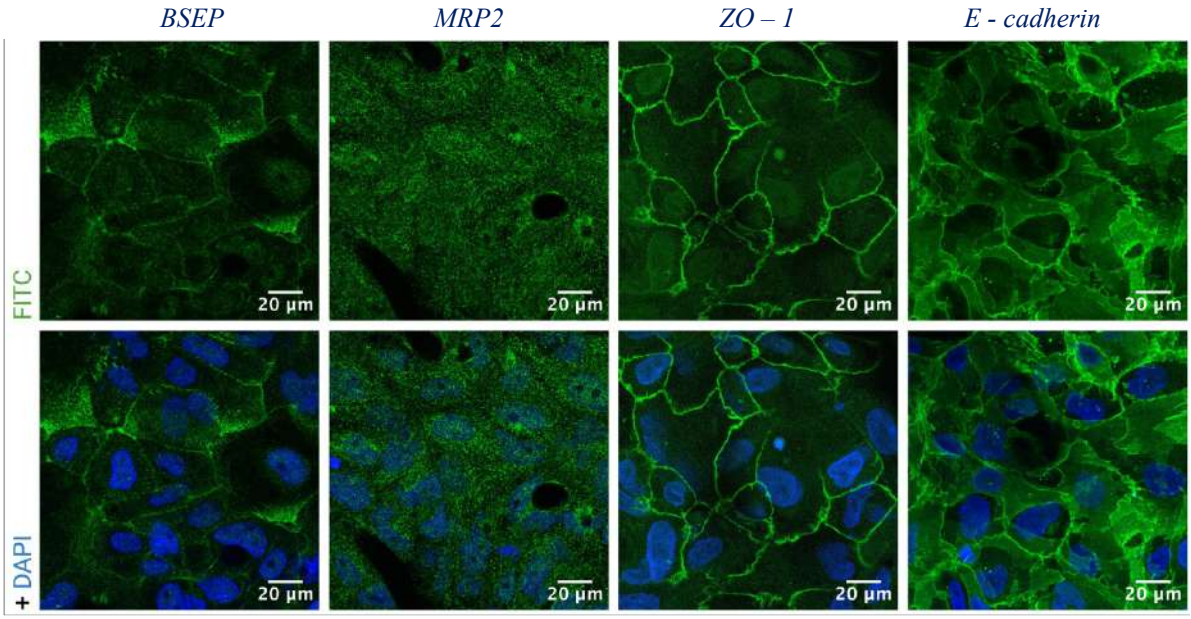

Figure 4.24. Representative pictures of BSEP, MRP2, ZO - 1 and E - cadherin staining for the Overeem's protocol. The first row displays the green signal for each marker, while the second row shows the merged signal with nuclear counterstaining (DAPI, blue). Images were acquired using a 3 Microscope (magnification 40X) a ZEISS LSM 900 Confocal laser scanning microscope thanks to the research group of the Medical Genetics Laboratory, led by Professor Adamo Pio d'Adamo, at the IRCCS Materno Infantile "Burlo Garofolo" Hospital in Trieste, Italy.

In Matakovic's protocol (Figure 4.25), BSEP localized to the membrane, while MRP2 exhibited a diffuse and nonspecific distribution. ZO - 1 delineated intercellular border, and E - cadherin likewise restricted to the membrane.

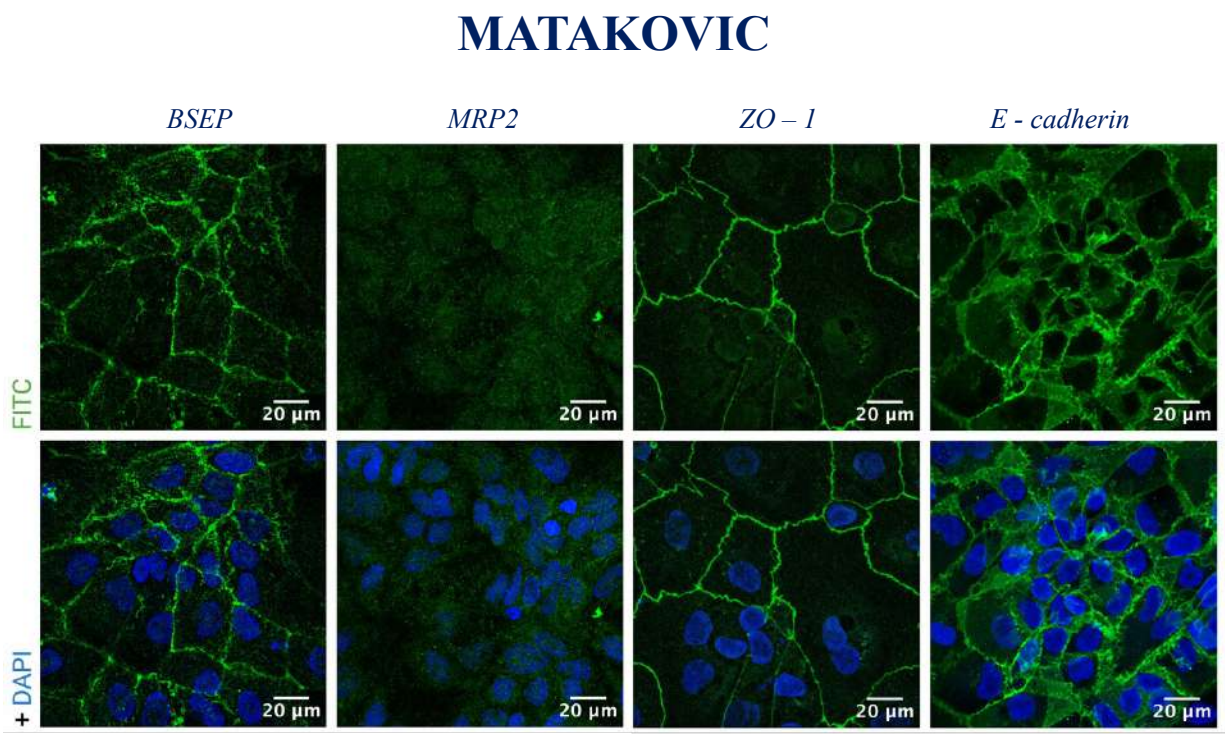

Figure 4.25. Representative pictures of BSEP, MRP2, ZO - 1 and E - cadherin staining for the Matakovic's protocol. The first row displays the green signal for each marker, while the second row shows the merged signal with nuclear counterstaining (DAPI, blue). Images were acquired using a 3 Microscope (magnification 40X) a ZEISS LSM 900 Confocal laser scanning microscope thanks to the research group of the Medical Genetics Laboratory, led by Professor Adamo Pio d'Adamo, at the IRCCS Materno Infantile "Burlo Garofolo" Hospital in Trieste, Italy.

Figure 4.26 represents the results for the Mallanna's protocol. BSEP localized both to the membrane and to the nuclei, with a clear nonspecific signal. MRP2 showed a diffuse, nonspecific, intracellular pattern. ZO - 1 was clearly membrane - associated at junctions, while E - cadherin was detected at the membrane with additional cytoplasmic signal.

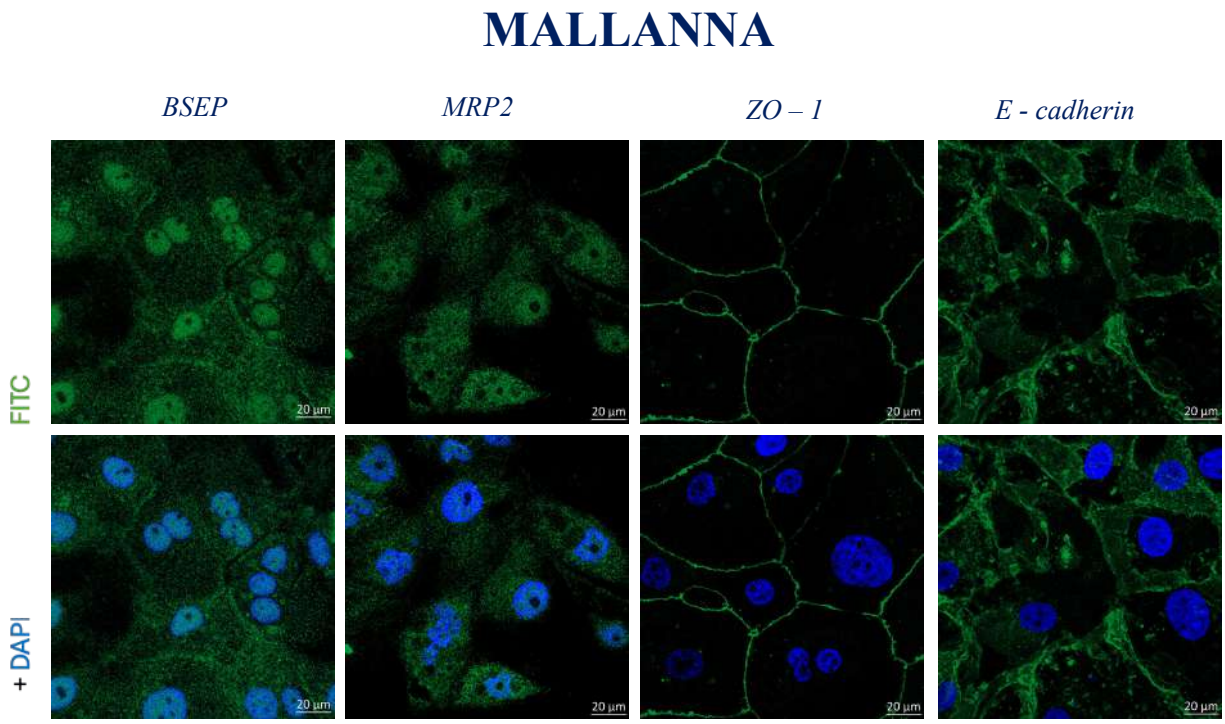

Figure 4.26. Representative pictures of BSEP, MRP2, ZO - 1 and E - cadherin staining for the Mallanna's protocol. The first row displays the green signal for each marker, while the second row shows the merged signal with nuclear counterstaining (DAPI, blue). Images were acquired using a 3 Microscope (magnification 40X) a ZEISS LSM 900 Confocal laser scanning microscope thanks to the research group of the Medical Genetics Laboratory, led by Professor Adamo Pio d'Adamo, at the IRCCS Materno Infantile "Burlo Garofolo" Hospital in Trieste, Italy.

In STEMCELL protocol (Figure 4.27), BSEP showed a widespread punctate pattern, with clear overlap with the nuclei. MRP2 staining was diffuse. ZO - 1 localized to the membrane, and E - cadherin was also membrane - restricted.

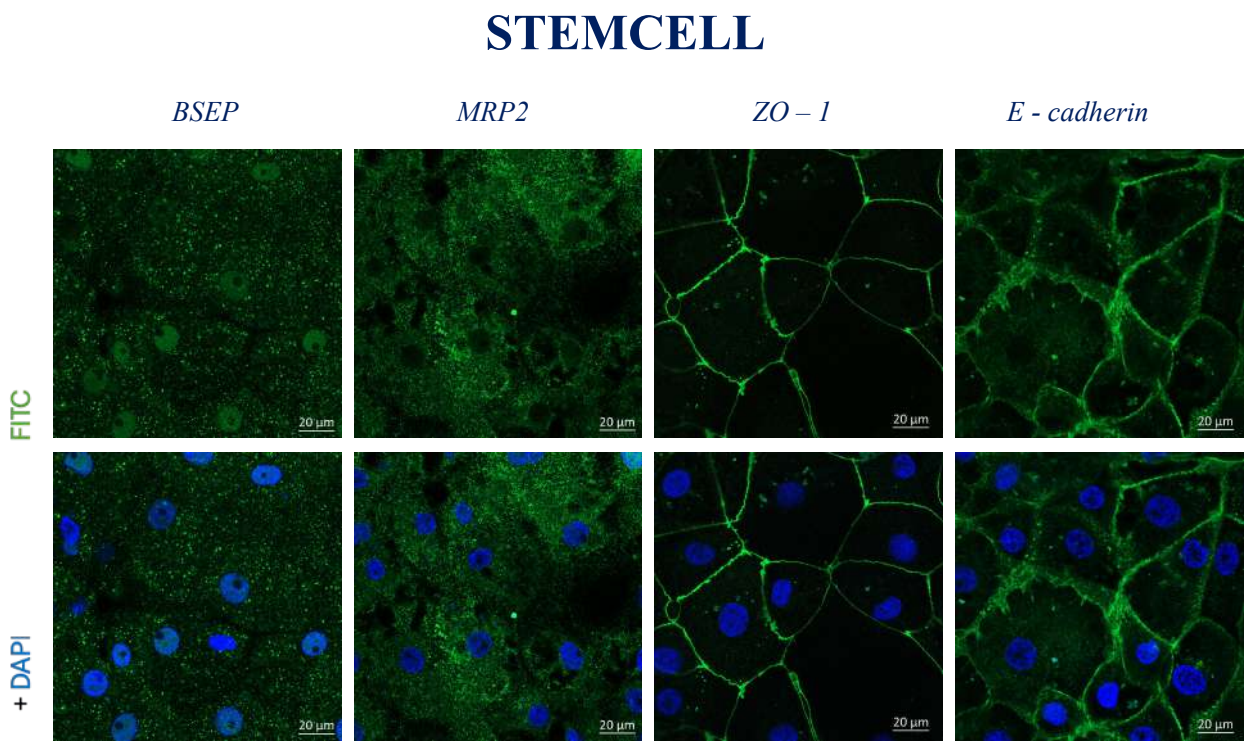

Figure 4.27. Representative pictures of BSEP, MRP2, ZO - 1 and E - cadherin staining for the STEMCELL protocol. The first row displays the green signal for each marker, while the second row shows the merged signal with nuclear counterstaining (DAPI, blue). Images were acquired using a 3 Microscope (magnification 40X) a ZEISS LSM 900 Confocal laser scanning microscope thanks to the research group of the Medical Genetics Laboratory, led by Professor Adamo Pio d'Adamo, at the IRCCS Materno Infantile "Burlo Garofolo" Hospital in Trieste, Italy.

Considering the other markers analzyed in the final differentiation stage, the strongest expression of BSEP marker was observed in the Overeem's and Matakovic's protocols. In contrast, for the MRP2 marker, the Mallanna's and STEMCELL protocols showed no overlap with the nuclei. The membrane markers ZO - 1 and E - cadherin were correctly expressed in all four protocols, although a slight background signal was detected in the Overeem's and Matakovic's HLCs.

4.3.5. Albumin Release

The culture media collected from the final two differentiation stages (HP and HLC), as well as from HepG2 and UpCyte cells, were analyzed using ELISA kit to assess the release, and consequently the production, of albumin, a key functional marker of hepatocytes. Results are shown in Figure 4.28.

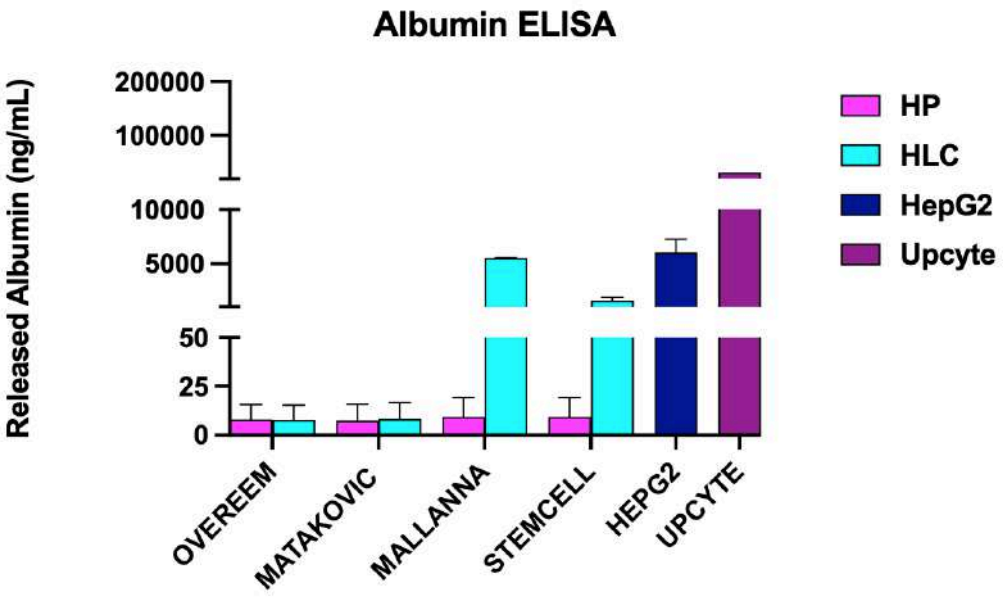

Figure 4.28. Albumin concentration (ng/mL) released into the culture medium by HP (pink) and HLC (light – blue) cells across all four protocols. For comparison, albumin release is also reported for the HepG2 cell line (blue) and the UpCyte cell line (purple). Data are reported as average ± SD of at least 3 biological samples.

Albumin release by the HepG2 cell line exceeded 6 500 ng/mL, whereas UpCyte cells exhibited a fivefold higher release, surpassing 32 000 ng/mL. Among the differentiation protocols, the HLC stage of both the Mallanna protocol (> 5 500 ng/mL) and the STEMCELL protocol (> 1 500 ng/mL) displayed substantial albumin release, approaching the levels observed in HepG2 cells. In contrast, both the HP and HLC stages of the Overeem's and Matakovic's protocols yielded markedly lower albumin release compared with the other two protocols and with the HepG2 and UpCyte cell lines.

A comparative analysis of albumin release into the culture medium and ALB gene expression revealed several marked discrepancies. First, despite the minimal albumin release observed in the Matakovic's and Overeem's protocols (both at the HP and HLC stages), no detectable ALB gene expression was measured. In the Mallanna's protocol, ALB expression was lower at the HP stage compared with the HLC stage, a trend consistent with the corresponding albumin release (Figure 4.28). Although UpCyte cells exhibited a higher albumin release compared with HepG2 cells, their ALB mRNA expression levels were lower than those observed in HepG2 cells.

4.4. 2D and 3D Cultures from Rat Primary Adult Hepatocytes

4.4.1. Liver Perfusion and Hepatocytes Isolation

The points we identified as crucial for achieving good efficiency, along with the main improvements introduced, are:

- age and weight of the animal
- cannulation
- perfusion and digestion solutions
- swelling
- centrifugation and hepatocytes isolation

The age and body weight of the animals (250 - 300 g, corresponding to 10 - 12 weeks) are critical determinants of surgical efficiency, since in older animals increased adiposity hampers the exposures of the inferior vena cava due to the excessive accumulation of abdominal fat tissue.

The accumulation of solutions in extrahepatic vessels can result in suboptimal liver perfusion. This issue may arise from the cannulation step and can be exacerbated by excessive flow velocity within the blood vessels. Furthermore, when the PV is cannulated upstream of the splenic vein branching, part of the perfusion solution may be diverted to the pancreatic region, leading to fluid accumulation.

The prepared in - house perfusion and digestion solutions proved to be suboptimal if compared with the commercial products. In particular, collagenase type IV displayed high instability and poor efficiency during the procedure, resulting in a low yield of viable hepatocyte. The reduced enzymatic activity was confirmed by insufficient liver digestion, as the organ remained structurally intact and lacked the expected “mushy” consistency. The use of the Liver Perfusion and Digestion solutions markedly improved solution stability and procedural efficiency compared to the homemade preparation. Accurate control of the two perfusion steps is critical. The initial perfusion step is essential to remove residual blood, clots, and soluble molecules, while also chelating Ca^{2+} ions involved in cell - cell and cell - matrix junctions, thereby promoting their dissociation. The subsequent digestion step, employing collagenase, is required to degrade the extracellular matrix (ECM) collagen and facilitate hepatocytes release.

Adequate tissue swelling facilitates the distribution of solutions throughout the hepatic vasculature, thereby enhancing collagen digestion and promoting efficient hepatocytes release.

Centrifugation speed and duration were optimized in accordance with established protocols. During the first differential centrifugation step, hepatocytes sedimented to the bottom of the tube, whereas other cell populations (stellate cells, Kupffer cells, and others) remained in the supernatant. This separation relies on differences in cell density, which enables hepatocytes to pellet while non - parenchymal cells remain suspended. Using this approach, an average yield of approximately 50 million viable hepatocytes was obtained. The procedure requires high precision and accuracy, particularly during the cannulation step. Moreover, the large volumes of solutions perfused necessitate an extended perfusion time.

4.4.2. 2D Primary Hepatocytes Culture and Characterization

Following primary hepatocytes isolation (see Methods, subchapter 3.5.2.), cells were seeded onto collagen type VI pre - coated multi - well plates.
Three key features were assessed at different time points during culture:

- morphological changes monitored by phase - contrast microscopy
- cell viability determined by Trypan Blue exclusion
- expression of hepatocyte - specific genes analyzed by qRT - PCR.

It is well established that primary hepatocytes progressively lose their characteristic morphology and hepatic functions and cannot be maintained in culture for extended periods.

As shown in Figure 4.29, morphological alterations became particularly evident after day 2 of culture, with a complete change from an initial cuboidal shape at day 0, to a hexagonal shape at day 1, finally to a fibroblast - like morphology at day 2.

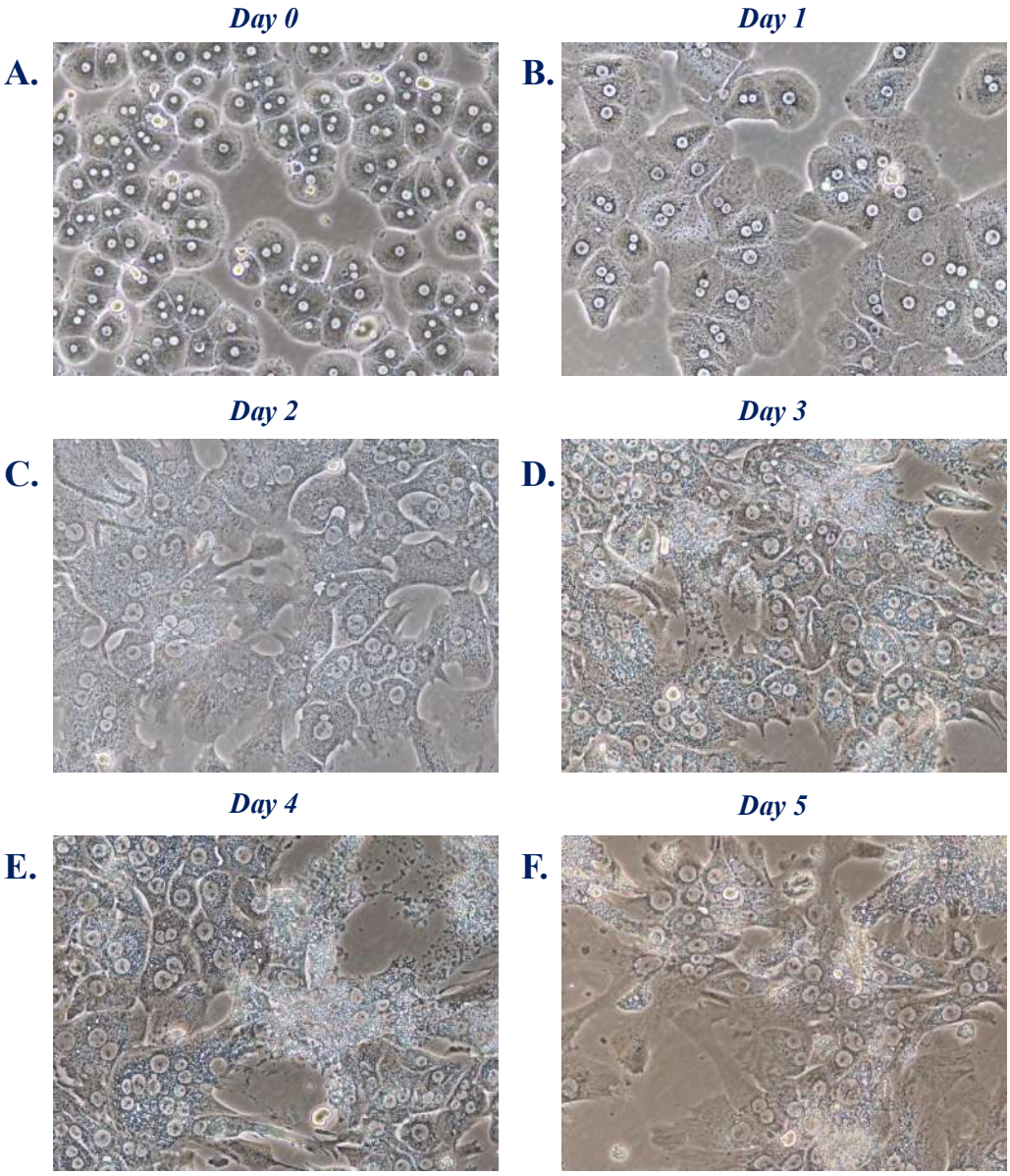

Figure 4.29. Hepatocyte morphology at day 0 (A), day 1 (B), day 2 (C), day 3 (D), day 4 (E), day 5 (F). Picture magnification: 20X.

Cell viability was assessed by Trypan Blue testing in hepatocytes collected from day 0 to day 5 (Figure 4.30). Viability was 94% immediately after isolation (day 0) but declined dramatically to 49.5% on day 1 (SD ± 12.7), to 45.2% (SD ± 18.2) on day 2, and 33.5% (SD ± 0.77) on day 3. Viability further declined to 16.9% (SD ± 5.4) on day 4 and reached 9.1% (SD ± 0.38) by day 5. This trend was consistent with the observed loss of typical morphology (Figure 4.29).

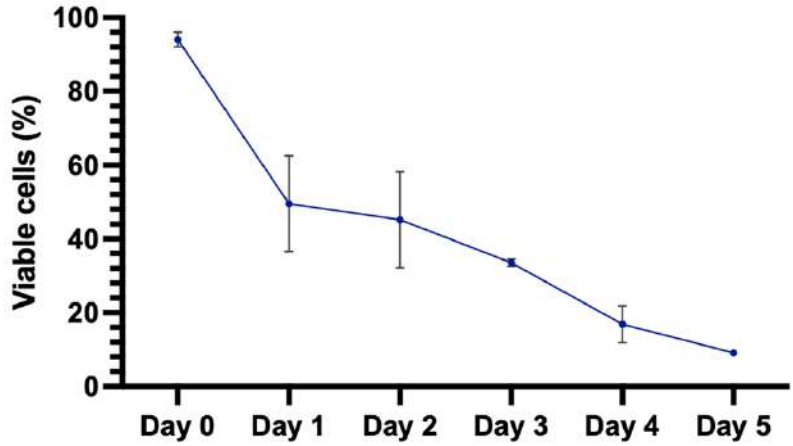

Figure 4.30. Percentage of hepatocyte viability shown at day 0, 1, 2, 3, 4, and 5 of *in vitro* culture. Day 0 is considered as 100%. Results are reported as average ± SD of 3 different experiments.

Primary Hepatocytes Characterization

Based on the progressive loss of morphology and viability, RNA was extracted at days 0, 1, 2, and 3 of *in vitro* culture to evaluate the mRNA expression of hepatocyte - specific genes. Isolated hepatocytes prior to plating (day 0) exhibited high mRNA expression of hepatic marker genes, as assessed by RT - qPCR (Albumin - 1 [ALB - 1]; Phosphoenolpyruvate carboxykinase 1 [PCK1]; Keratin 18 [KRT18]; ATP Binding Cassette Subfamily D Member3 [ABCD3]; Serpin [SERPIN]; Tryptophan 2,3 - dioxygenase [TDO2]). These markers were selected to further assess hepatocyte functionality and liver – specific processes. PCK1 encodes phosphoenolpyruvate carboxykinase 1, the rate – limiting enzyme in gluconeogenesis, converting oxaloacetate to phosphoenolpyruvate. KRT18 encodes keratin 18, a marker of epithelial cell death, with serum levels reflecting hepatocyte damage. ABCD3 mediates the transport of dicarboxylic acids into peroxisomes, contributing to lipid metabolism. TDO2 encodes tryptophan 2,3 - dioxygenase, a liver - enriched enzyme that regulates energy homeostasis and tryptophan metabolism. Together, these markers provide complementary information on hepatic identity, metabolic functionality, and liver - specific physiological processes.

All analyzed genes displayed a time - dependent decrease in expression, with a marked reduction already evident at day 1 of culture. These expression profiles reflect the progressive loss of function and viability of primary hepatocytes over time (Figure 4.31).

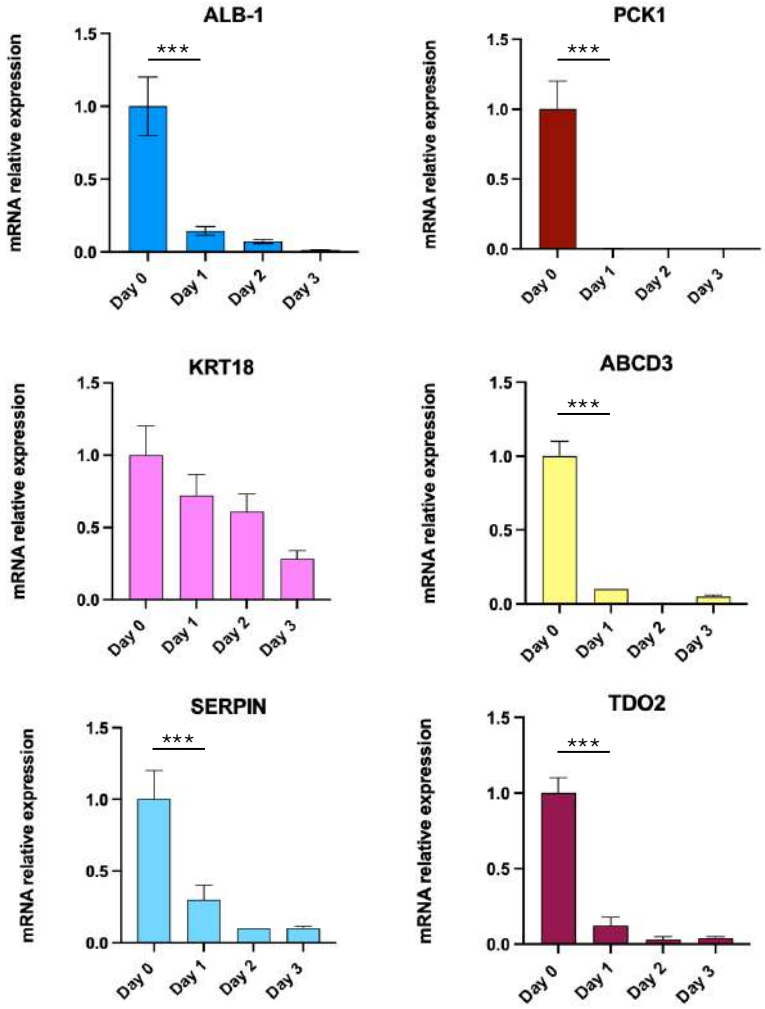

Figure 4.31. mRNA expression of hepatic markers measured by RT - qPCR in primary hepatocytes. Data were normalized to β - actin and GAPDH (housekeeping genes) and are expressed relative to primary hepatocytes collected prior to plating (day 0, set as 1). Values are presented as mean ± SD from at least three independent experiments (*** p - value ≤ 0.001).

The inability to maintain primary hepatocytes in culture beyond two days prompted the search for an alternative long - term culture system capable of sustaining hepatocytes for extended periods. A suitable model for this purpose is represented by adult Hep - Orgs.

4.4.3. 3D Culture from Rat Primary Adult Hepatocytes (Hep - Orgs)

Rat hepatocytes were embedded in Matrigel to promote Hep - Orgs formation and cultured in optimized medium supplemented with cytokines to stimulate hepatocyte proliferation and prevent apoptosis, as detailed in the Methods. Cell density was intentionally kept low to provide hepatocytes with sufficient space for growth, and to enable direct visualization of organoid development. Primary

hepatocytes underwent cell division during the first days of culture (Figure 4.32). At day 0, Hep - Orgs measured approximately 30 μm; by day 2, their size had nearly doubled, highlighting a growth trend that persisted until day 15 (33.08 μm at day 1; 64,86 μm at day 2; 45.06 μm at day 5; 55.19 μm at day 7; 51.93 μm at day 10; and 62.90 μm at day 15). In terms of morphology, Hep - Orgs were spherical at day 1 but progressively acquired the characteristic "bunch - of - grapes" shape, typical of hepatic organoids, in the subsequent days.

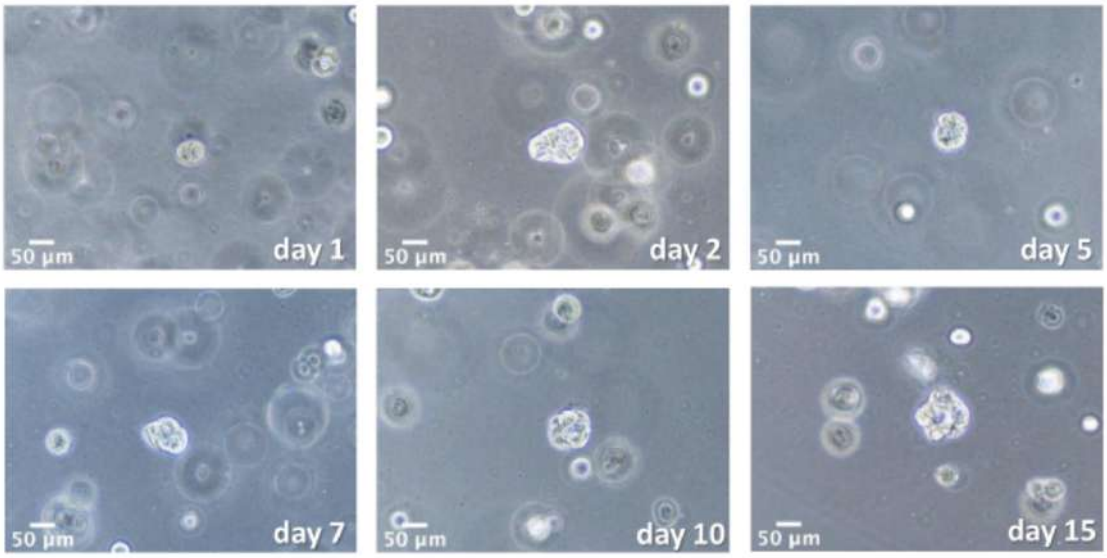

Figure 4.32. Phase - contrast images of rat hepatic organoids at different culture time points: day1, 2, 5, 7, 10, and 15. Images acquired at 20X magnification. Scale bar in μm (76).

To assess the proliferative capacity of rat hepatic organoids, an EdU assay was performed at day 15 (Figure 4.33). Hoechst staining, however, revealed a predominance of single cells rather than organized Hep - Orgs. Despite the relatively low EdU incorporation, proliferative hepatocytes (green cells) were still detected. In contrast to 2D - cultured hepatocytes, Hep - Orgs remained viable and exhibited proliferative activity at day 15, highlighting their potential for long - term culture.

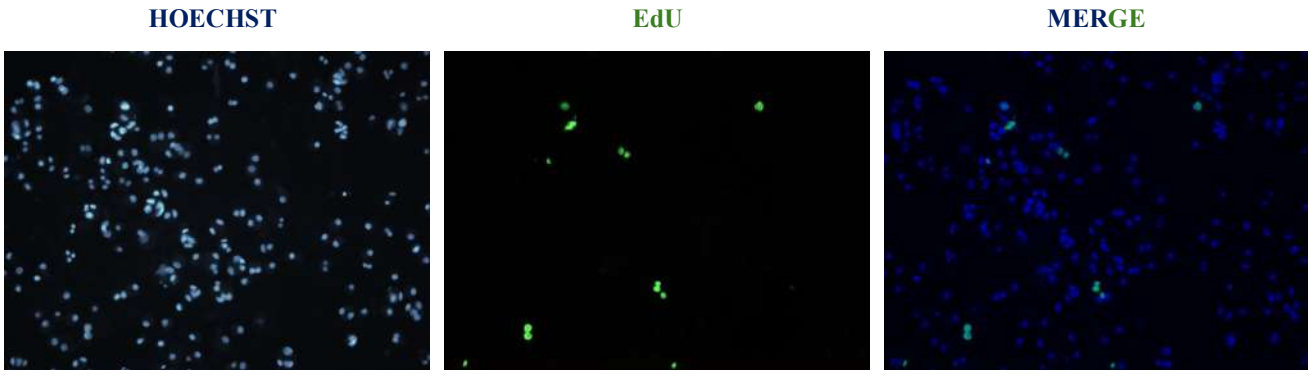

Figure 4.33. EdU incorporation assay of rat hepatic organoids at day 15 (Hoechst, EdU, Merge). Images were acquired at 20X magnification using a Leica DFC490 fluorescence microscope.

4.5. 3D Culture from Mouse Primary Adult Hepatocytes

4.5.1. Liver Perfusion and Primary Hepatocytes Isolation

Once the procedure was well established in the rat model, it was then adapted for use in mice. Preliminary observations suggested that mice possess a greater potential for Hep - Orgs formation compared to rats. However, the surgical procedure in mice presents considerable challenges due to the animal's smaller size. Although the overall surgical approach was similar, several modifications were implemented to account for the differences in size and anatomy.

The first major adjustment involved cannulation of the inferior vena cava (IVC). Despite its small diameter, the IVC in mice is comparatively larger and more accessible than the portal vein. In this adaptation, the PV was clamped to induce hepatic swelling. Given the reduced vessel dimension in mice, the perfusion flow rate was adjusted, with the pump's maximum speed set at 4 mL/min. Additionally, the volumes of both perfusion and digestion solutions were decreased, resulting in a shorter overall procedure time.

Based on our experience, the critical factors determining the success of the procedure are the achievement of adequate hepatic swelling, essential for proper liver perfusion and optimal yield, and the strict adherence to perfusion and digestion timings, which must be precisely followed to obtain reliable results.

The average hepatocyte yield obtained from the liver of a mouse weighing approximately 25 - 30 g was in the range of 20 to 58 million cells.

4.5.2. Mouse Hep - Orgs Culture

Phase - contrast microscopy

Hep - Orgs growth was monitored over time, and organoid dimensions were measured microscopically. During the initial days of culture, primary hepatocytes exhibited a spherical morphology with diameters of approximately 40 - 50 μm (Figure 4.34, panel A). As culture progressed, Hep - Orgs typically underwent a morphological transition from a simple spherical form to a characteristic "grape - like" structure. Notably, by day 21, Hep - Orgs reached diameters of approximately 125 μm, and by day 38, they attained ~ 175 μm, displaying the typical "bunch - of - grapes" morphology. Hep - Orgs were maintained in culture for 63 days.

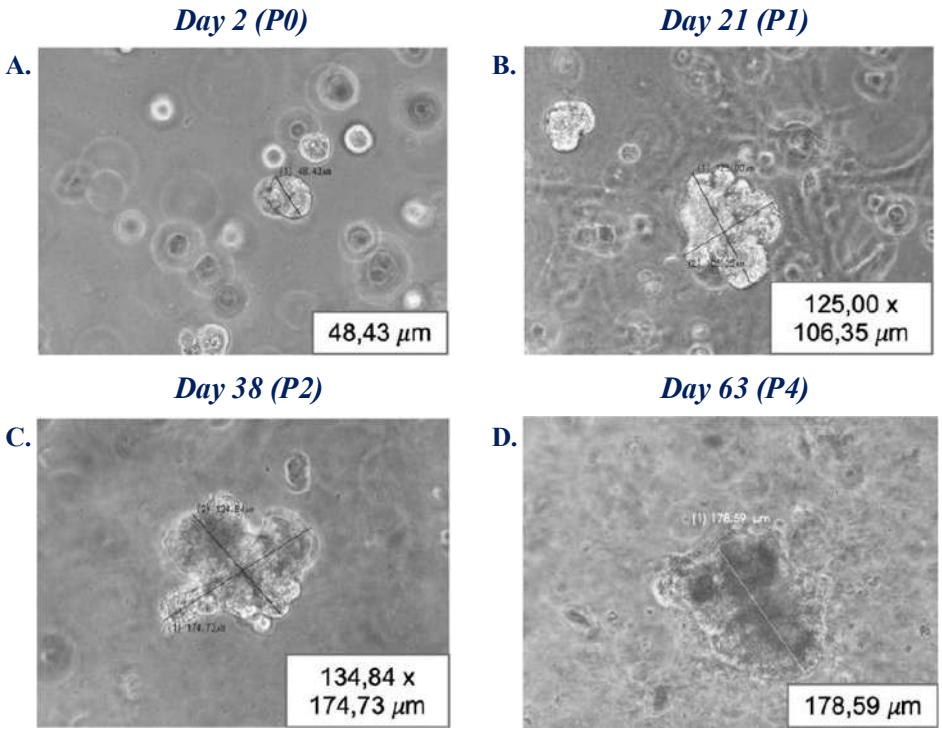

Figure 4.34. Phase - contrast images of Hep - Orgs growth over time (images acquired at 20X magnification; dimension indicated in μm). Hep - Orgs were passaged at 14 - 20 days of culture without complete disaggregation, and after 28 - 30 days following disaggregation into single hepatocytes.

The first passage was typically performed after 14 - 20 days in culture, without complete disaggregation of the organoids. By contrast, at the second passage (28 - 30 days), organoids were enzymatically dissociated into single hepatocytes. This step was essential, as cells located within the organoid core have reduced exposure to both the culture medium and intercellular interactions, leading to accumulation of dead cells; dissociation helps to remove these cells and restore optimal

growth conditions. In addition, it is also important to replace the matrix composing the droplets, as its instability may contribute to suboptimal organoid growth.
Considering Figure 4.34, it should be noted that the growth analysis represents a general trend, as no automated system was available to track the growth of individual organoids over time.

Hep - Orgs Passaging

As underlined before, Hep - Orgs passaging is critical because after approximately 14 days, cells typically reach confluence, and the extracellular matrix may become compromised. It is essential to maintain Hep - Orgs within an intact matrix droplet, free of cell debris and dead cells, which tend to accumulate within the droplet, thereby compromising the stability of the droplet itself. Since the matrix appeared heavily contaminated, displaying abundant dead cells, cellular debris, and aggregates of residual matrix, to enhance passaging efficiency, it was crucial to disrupt the matrix droplets immediately after enzyme addition. This was achieved by repeated pipetting, which facilitated enzyme accessibility and droplet dissociation. In addition, it was clear that shorter centrifugation times improved cell viability, increased Hep - Orgs recovery, and promoted the removal of debris and dead cells. Another important factor to consider is the residual presence of Dispase following passaging, which can induce further matrix degradation. For this reason, it is important to wash in the correct way the Hep - Orgs during passaging.

4.5.3. Mouse Hep - Orgs Characterization

EdU Proliferation Assay

This assay was conducted to assess the replicative activity of Hep - Orgs after 34 days of culture. This approach enables the evaluation of the proliferation rate of organoid - forming cells that are actively engaged in the replicative phase, and it allows also to observe the typical grape - like morphology of Hep - Orgs.

The obtained results demonstrated that the Hep - Orgs are capable of maintaining both their morphological characteristics and their proliferative capacity for over one month.

Due to the differential accessibility of organoid - forming cells to the culture medium, cells located at the periphery of the organoids exhibited higher incorporation of EdU and Hoechst, as shown in Figure 4.35.

It is well known that the lumen of organoids predominantly contains dead cells that accumulate and cannot be cleared, except through mechanical disruption and reseeding of the organoids.

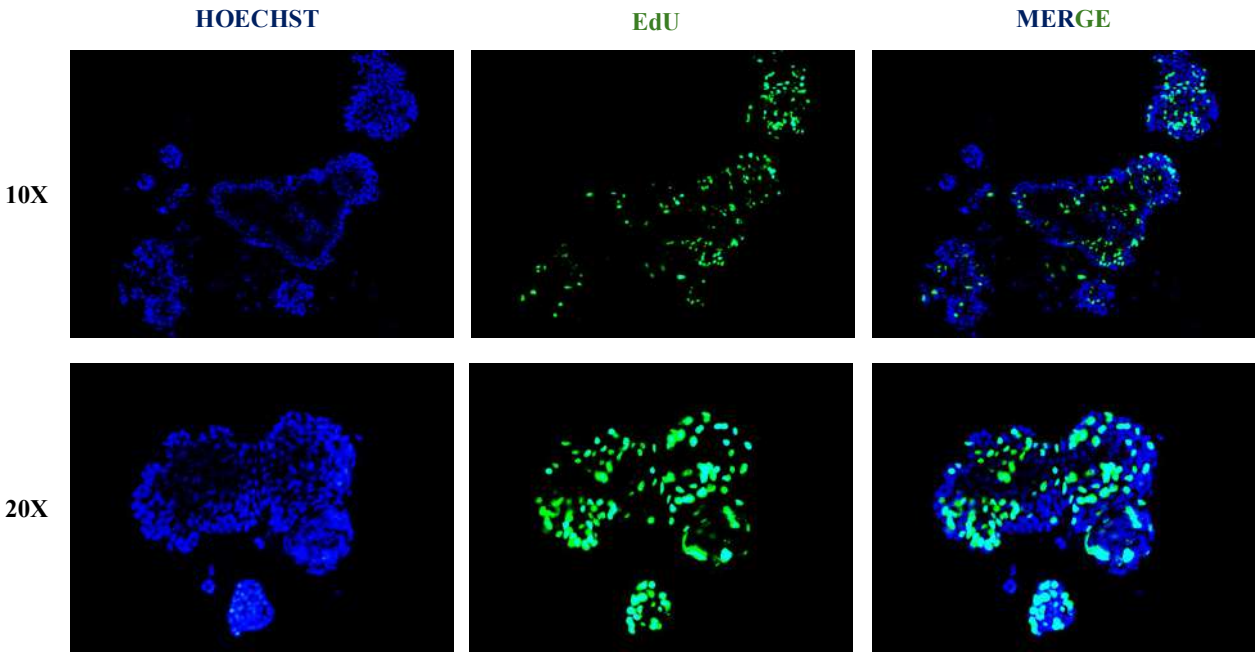

Figure 4.35. EdU cell proliferation assay at day 34 of Hep-Orgs culture. The first column shows the Hoechst staining, the second column shows the proliferating cells in green (EdU incorporation), and the last column shows the merged images. Picture magnification 10X (first row) and 20X (second row). Images acquired using a Leica DFC490 fluorescent microscope. This experimental part of the project was carried out by Dr. Davide Selvestrel of the Advanced Disease Models Group, led by Professor Giovanni Sorrentino, at the International Centre for Genetic Engineering and Biotechnology (ICGEB) in Trieste, Italy.

Mouse Albumin ELISA Assay

Among their diverse functions, hepatocytes are specifically responsible for albumin production. Albumin is a carrier protein involved in the transport of lipophilic molecules, such as bilirubin, fatty acids, and hormones, into the bloodstream. Hepatocytes secrete albumin into the culture medium, where it can be detected by immunoassays.

According to literature, Hep - Orgs are able to preserve the mature functional activities of primary hepatocytes. To evaluate the functional activity of the model, an ELISA albumin assay was performed. Culture medium was collected on days 15, 30, 45, and 55 of Hep - Orgs growth to quantify albumin secretion.

As shown in Figure 4.36, the overall trend revealed a progressive increase in albumin production over time, followed by a plateau phase between days 45 and 55. At day 15, albumin secretion was relatively

low, but it increased substantially by day 30 and continued to increase until day 45, after which it stabilized. This albumin production pattern was consistent with the growth dynamics observed in Hep - Orgs.

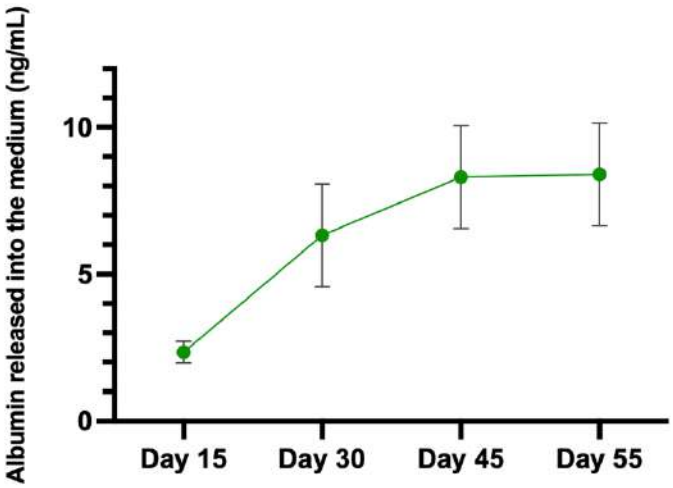

Figure 4.36. Albumin concentration (ng/mL) released into the culture medium by Hep - Orgs at different time points of *in vitro* growth. Data are presented as mean ± SD from at least three independent experiments.

Hepatic markers expression

To characterize Hep - Orgs, immunofluorescence staining was performed for Hepatocyte Nuclear Factor 4 alpha (HNF4α), a nuclear transcription factor essential for liver development, function, and metabolism. A subset of nuclei showed positive staining for HNF4α. Organoids were stained also for Phalloidin and DAPI (as shown in Figure 4.37).

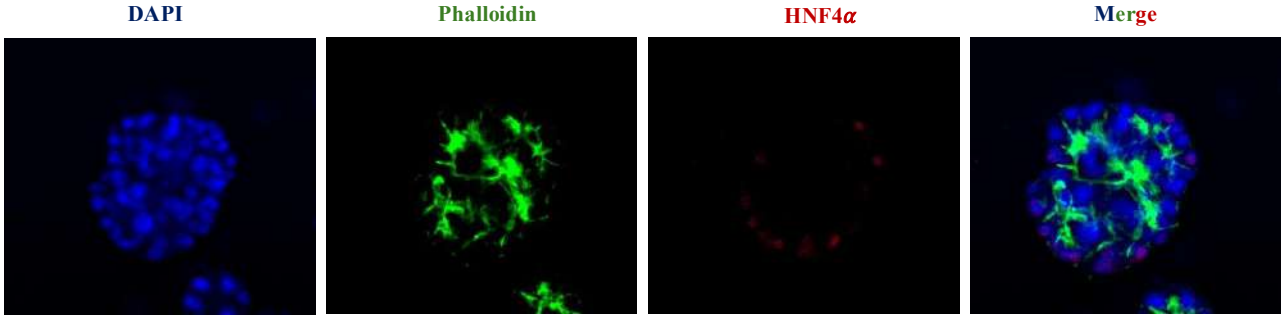

Figure 4.37. Staining for DAPI, Phalloidin, and HNF4α on the obtained Hep - Orgs. Magnification 40X. This experimental part of the project was carried out by Dr. Davide Selvestrel of the Advanced Disease Models Group, led by Professor Giovanni Sorrentino, at the International Centre for Genetic Engineering and Biotechnology (ICGEB) in Trieste, Italy. Images were acquired with a ZEISS - LSM - 880 Confocal microscope.

HNF4α is known as a regulator of the expression of multiple genes, including HNF41α, and plays a critical role in the development and function of the liver, kidney, and intestine. The expression of this hepatic marker was also assessed by RT - PCR and compared with its expression in primary hepatocytes (used as a positive control). A reduced expression level was observed in Hep - Orgs (Figure 4.38).

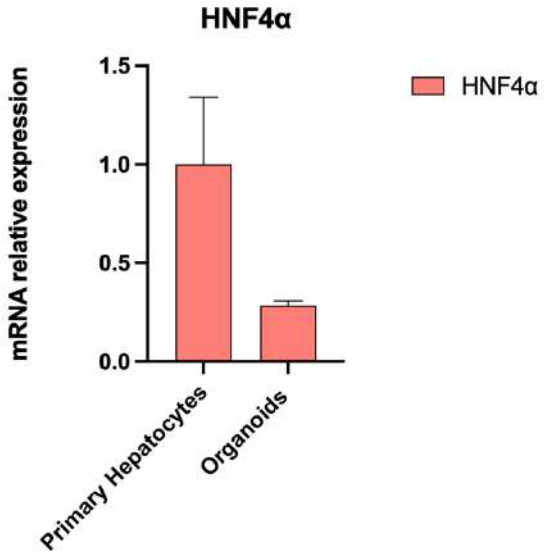

Figure 4.38. Analysis of HNF4α gene by RT - PCR in primary hepatocytes and Hep - Orgs. Data were normalized to β - actin and GAPDH (housekeeping genes). Primary hepatocytes are considered as positive control (expression = 1). Data are reported as average ± SD of at least 3 biological samples.

4.5.4. Hep - Orgs as a Model of Drug - induced Cholestasis

4.5.4.1. Effects on Biliary Function and Bile Canaliculi Structure

To assess whether this model was suitable for studying cholestasis, we induced the pathology using a specific pharmacological agent and subsequently investigated bile acid transport capacity by evaluating bile canaliculi morphology through the 5 (6) - carboxyfluorescein diacetate (CDFDA) assay. Intrahepatic cholestasis was induced in Hep - Orgs by treatment with Cyclosporine A (CsA) at 10 μM for 24 hours or 50 μM for 4 hours. Following CsA exposure, biliary excretion was assessed using CDFDA (0.5 μM for 2 hours), and CDFDA clearance was analyzed with a Nikon A1 MP microscope (Figure 4.39).

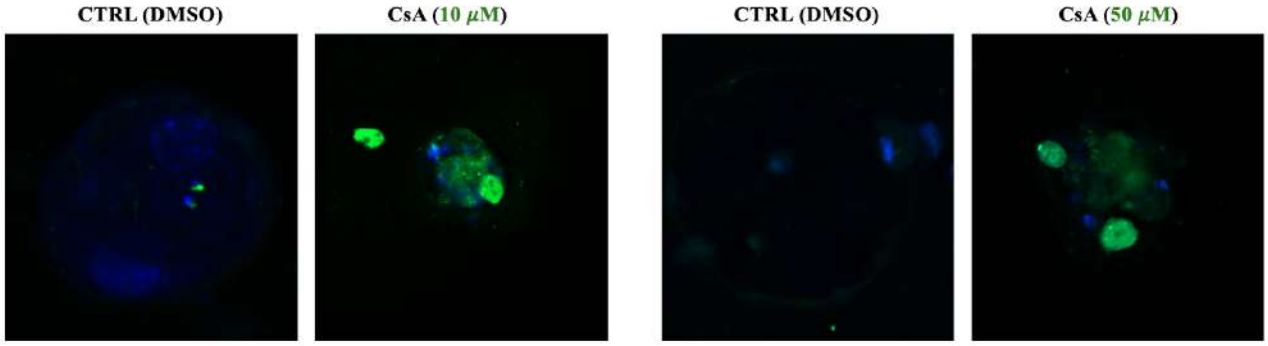

Figure 4.39. Comparison of CDFDA accumulation was performed between Csa - treated Hep - Orgs (10 μM and 50 μM) and DMSO controls. CDFDA clearance was subsequently assessed using a Nikon A1 MP microscope with the support of Prof. Gabriele Baj (Department of Life Sciences, University of Trieste, Italy).

The effect of CsA treatment was also assessed by examining morphological alterations in the bile canalicular structure and the cytoskeleton of Hep - Orgs. Specifically, staining of *zonula occludens* - 1 (ZO - 1), a tight junction protein that co - localizes with pericanalicular F - actin, was performed on samples treated with DMSO or 50 μM CsA for two hours (Figure 4.40).

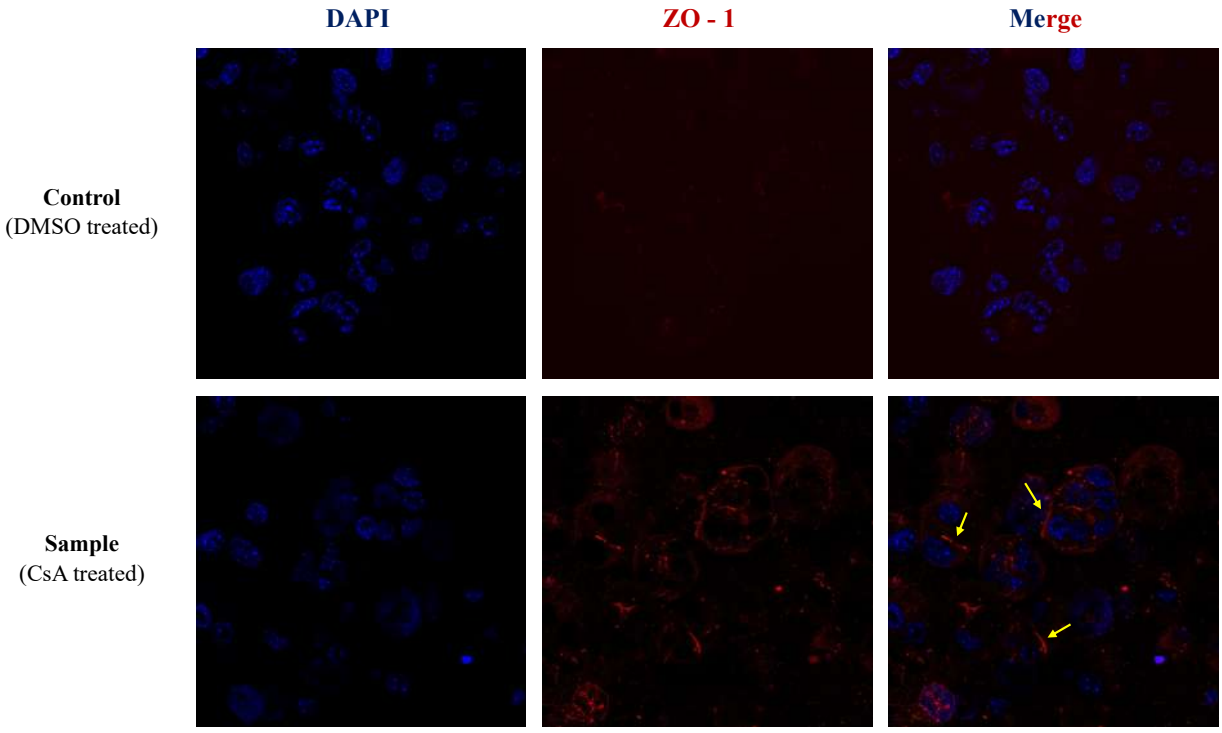

Figure 4.40. Comparison of ZO - 1 staining (in red) between CsA - treated Hep - Orgs (50 μM) and DMSO controls. The figure shows DAPI staining (in blue, first column), ZO - 1 staining (in red, second column), and the merged images (third column). Images were acquired with the support of Dr. Martina Conti from CNR - IOM laboratory (Trieste, Italy) using a Leica Stellaris 5 confocal microscope (magnification 20X).

Figure 4.40 illustrates the differences between the control samples, in which the ZO - 1 signal is virtually undetectable, and the CsA - treated Hep - Orgs. In the treated organoids, a clear canalicular

constriction is observed, highlighted by a pronounced ZO - 1 signal (indicated by yellow arrows) particularly evident at the junctions between adjacent cells within the organoids.

Subsequently, using Hep - Orgs treated under the same conditions, the effect of CsA treatment on the cytoskeleton was assessed, specifically through F - actin staining. In addition, a further characterization of the hepatic marker HNF4α was performed on the analyzed samples (Figure 4.41).

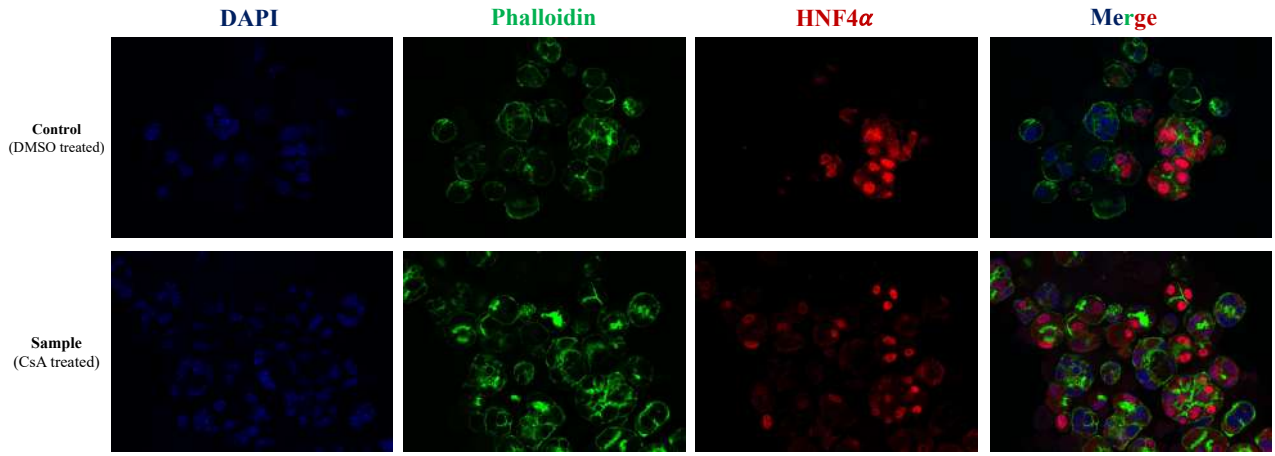

Figure 4.41. Comparison of F - actin staining was performed between CsA - treated Hep - Orgs (50 μM) and DMSO controls. The figure shows DAPI staining (in blue, first column), F - actin staining (in green, second column), HNF4α staining (in red, third column), and the merged images (fourth column). Images were acquired using a ZEISS Apotome 3 Microscope (magnification 20X) with the support of Dr. Davide Selvestrel from the Advanced Disease Models Group, led by Professor Giovanni Sorrentino, at the International Centre for Genetic Engineering and Biotechnology (ICGEB) in Trieste, Italy.

These results indicate that CsA treatment leads to a disrupted F - actin distribution, resulting in canalicular constriction. This effect is evident (Figure 4.41) from the increased green signal observed in treated samples, which is specifically localized at the cell junctions, compared to the controls. HNF4α staining facilitates the visualization of cell nuclei and, importantly, helps to distinguish which organoid samples are composed of multiple hepatocyte - like cells, as opposed to other structures present within the droplets (e.g. single hepatocytes) that do not exhibit the same level of hepatic maturation.

Taken together, these findings indicate that CsA treatment of Hep - Orgs induces bile canalicular constriction (as also demonstrated by the assay evaluating dichlorofluorescein efflux), accompanied by alterations in ZO - 1 localization and pericanalicular F - actin organization.

4.5.4.2. Effects on ER and Oxidative Stress

The effect of CsA on endoplasmic reticulum (ER) stress was further assessed by RT - PCR in Hep - Orgs treated with DMSO (control) and Hep - Orgs exposed to 50 μM CsA. The analysis focused on the expression of C/EBP Homologous Protein (CHOP) and Glucose - regulated Protein 78 (GRP78). The first protein works as a transcription factor and it is activated through the PERK - eIF2α - ATF4 pathway, being overexpressed under apoptotic conditions of chronic or unresolved ER stress. The second protein is a molecular chaperone that acts as a central regulator of the unfolded protein response (UPR), promoting usually cell survival upon accumulation of misfolded proteins.
This analysis revealed that gene expression levels of both markers were increased in Hep - Orgs treated with CsA compared to DMSO - treated controls, with CHOP expression elevated by approximately two - fold (Figure 4.42).

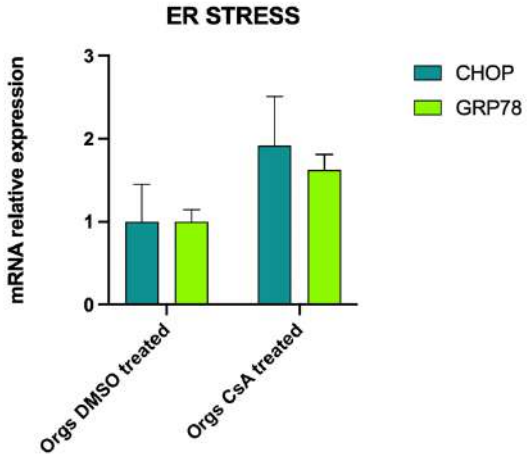

Figure 4.42. Analysis of CHOP (teal blue) and GRP78 (green) gene expression by RT - PCR in Hep - Orgs treated with DMSO (control) and Hep - Orgs treated with CsA. Data were normalized to β - actin and GAPDH (housekeeping genes). Data are reported as average ± SD of at least 3 biological samples.

In addition, also the effect of CsA on oxidative stress was assessed by RT - PCR in Hep - Orgs treated with DMSO (control) and Hep - Orgs exposed to 50 μM CsA. The analysis focused on the expression of Nuclear Factor Erythroid 2 - Related Factor (NRF2) gene, known as an important player in maintaining cellular redox balance and protecting against oxidative damage.
Figure 4.43 shows the result of the gene expression analysis, underlying an increase in the expression of this gene in the 50 μM CsA - treated Hep - Orgs.

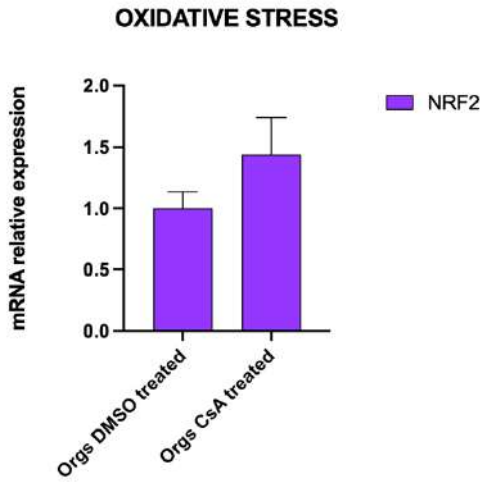

Figure 4.43. Analysis of NRF2 gene expression by RT - PCR in Hep - Orgs treated with DMSO (control) and Hep - Orgs treated with 50 μM CsA. Data were normalized to β - actin and GAPDH (housekeeping genes). Data are reported as average ± SD of at least 3 biological samples.

5. DISCUSSION

The aim of this thesis was to establish and characterize two complementary models for the investigation of liver diseases: a 2D human - derived system and a 3D murine - derived system. The rationale behind this dual approach is to provide, on one hand, a patient - specific platform (2D model) tailored to the genetic background of the original donor, and on the other hand, a standardized comparative tool (3D model) capable of elucidating the molecular mechanisms underlying different pathologies.

The discussion will follow the same thematic order as the results section, maintaining a correspondence between the respective subchapters.

5.1. PTEC Isolation and Culture from Urine: Protocol Improvements (Step 1)

With regard to the 2D model, the starting point was Step 1 of the protocol developed in this work. The primary objective was to achieve efficient isolation of urinary proximal tubular epithelial cells (PTEC) from samples obtained from healthy donors, followed by their successful plating.
During the development of this protocol, several challenges were encountered in the isolation of PTEC from both female and male donor samples, primarily attributable to gender - and donor - specificity as well as to the timing of sample processing after collection. As described in the Methods section and further illustrated in the Results, starting from the protocol established by Zhou (40) and introducing specific modifications, we achieved a final yield of 40% ± 20%.

The first major issue encountered during sample preservation and subsequent plating was the frequent occurrence of bacterial and fungal contamination. To address this problem, antibiotics (Penicillin - Streptomycin and Gentamicin) and antifungal (Amphotericin B) agents were added to the urine samples, thereby limiting microbial proliferation during the storage period.
Given the evidence from literature (77) that the use of antibiotics in cell culture can induce genomic alterations in gene expression and regulation, particular caution was exercised during the culture of PTEC. Since these cells were intended for experiments involving dedifferentiation into iPSC and

reprogramming into hepatocytes, we sought to minimize antibiotic exposure by either avoiding their use altogether or, when deemed indispensable, applying them only at low concentrations (P/S 1%, Gentamicin 0,5%).

The initial decision to preserve samples for 24 hours prior to plating was driven by practical constraints commonly associated with patient - derived specimens, which are typically collected in clinical settings and require transport over long distances. Conversely, for healthy donors located near the laboratory, as in the present study, such logistical barriers are absent, making processing within 4 hours of collection both feasible and preferable. Notably, prolonged (24 hours) preservation markedly reduces cell viability and adhesion efficiency, ultimately lowering culture yields.
Indeed, from the earliest attempts to establish this protocol, it became evident that plating within 4 hours of collection substantially improved yield compared to a 24 - hour preservation period. Specifically, 4 hours preservation followed by plating resulted in a total yield of 53%, compared with the 21% of the 24 hours preservation. Nonetheless, the relatively high standard deviation (48%) highlighted considerable variability across samples, suggesting that while shorter preservation improves overall efficiency, additional biological and technical factors likely contribute to the heterogeneity of outcomes. This observation underscored the need for further optimization of pre - analytical conditions to enhance reproducibility and robustness.
According to the EFLM European Urinalysis Guidelines (78), urine specimens can be categorized into random urine (a portion of single voided urine without specification of volume, time of day, or patient preparation), first morning urine (the specimen collected immediately after overnight bed rest and before breakfast or other activities), and second morning urine (a specimen collected 2 - 4 hours after the first morning void). Both the quantity and quality of urine samples are highly variable and strongly influence the success rate of PTEC culture establishment. Notably, urine specimens collected within the first 4 hours after waking up, thus corresponding to the third category described above, tended to yield the most successful PTEC establishment (79).

As previously outlined, two major issues emerged during this initial phase. The first was donor - specific variability, reflected in differences in the adhesion efficiency of PTEC across individuals. The second was related to gender - associated differences, with male - derived samples exhibiting higher adhesion efficiency compared to those obtained from female donors.

To investigate donor - related specificity, strip test analysis was performed on the samples at the time of collection. Among the parameters evaluated, we observed that samples with a pH ≥ 7 displayed a higher percentage of cell adhesion.
It was noticed that samples with a neutral to mildly basic pH were exhibiting greater urinary cell adhesion after sample storage at 4°C. However, this effect was observed in male samples but not in female ones, suggesting the involvement of additional variables for this gender.
To counteract the physiologically acidic nature of urine during 24 - hour storage, phosphate buffer was added immediately after collection, thereby reducing the detrimental effects of low pH on urinary cell survival.

Although the literature has not extensively highlighted substantial differences between female and male samples (40), in our experience the higher proportion of squamous cells in female urine, which compete with PTEC for adhesion, rendered the PTEC culture particularly challenging compared with male samples. The use of 20 μm strainers proved effective in isolating urinary cells, as these were able to pass through the filters while squamous cells and other impurities were retained. Most notably, the use of the strainer enabled the isolation of PTEC from samples that, without it, failed to show any cell adhesion or growth.

The combined use of these two approaches led to a modest improvement in the overall process yield, which increased from 21% to 25%. Notably, a pronounced effect was observed in female samples, where urinary cell adhesion rose from 6% to 26%. In contrast, male samples exhibited a reduction, with adhesion decreasing from 37% to 25%. These findings are supported by the lower standard deviation observed, indicating reduced variability and more heterogeneous data. Despite these gender - related differences, the final yield was comparable between groups.

After recognizing the importance of gender and donor - specific influences, the protocol modifications were applied to samples plated within 4 hours of collection.
Since the use of 20 μm filters were found to reduce yield in male samples, their application was restricted to female samples, whereas the use of buffer was extended to all samples.
These protocol modifications ultimately enabled the establishment of a standardized procedure, comprising 4 - hour preservation at 4°C in the presence of antibiotics and antifungals, buffer supplementation to stabilize sample pH during storage, and the selective use of 20 μm cell filters for female samples, which together resulted in an overall yield of 40% ± 20%. While this yield remains relatively modest, the most critical outcome is that PTEC were successfully obtained from all donors

included in the study. This finding indicates that, despite inherent variability and some limitations in efficiency, the finalized procedure achieved a sufficient level of robustness to ensure reproducibility across diverse donor backgrounds.

The rationale underlying our decision to analyse specific parameters using the strips, and consequently to employ phosphate buffer to achieve pH values that enhance cell adhesion, was to identify one or more factors that could be modulated in a non - invasive manner and rapidly controlled prior to cell plating. Indeed, additional elements – such as inter - donor variability in the expression of adhesion molecules (e.g. βig – h3 (80) and cadherins (81)) or differences in hormonal status (82) (83) between male and female patients – may substantially contribute to variability in PTEC isolation efficiency. However, in our opinion, these factors cannot be readily assessed or modified in a non - invasive way before plating. Therefore, our approach focused on experimentally controllable parameters that could partially mitigate inter - experimental variability despite the inherent limitations in biological replication.
The most relevant outcome was the successful isolation of PTEC from all healthy donors included in the study, which supports and underscores the validity of the modified isolation protocol employed.

Once PTEC colonies were obtained, they were characterized in terms of epithelial and renal marker expression. The results presented in this thesis are consistent with those reported by Zhou et al. (84), in which the epithelial markers Claudin - 1 and E - cadherin, the renal markers NR3C2 and L1CAM, and the fibroblast marker SLUG were assessed. Similarly to that study, multiple urine - derived cell samples were analyzed here to obtain a broader overview and an averaged expression profile of epithelial and renal markers. Although the levels of renal marker expression were lower than those reported by Zhou, particularly for L1CAM, the molecular analysis of PTECs confirmed their epithelial - renal identity.
In addition to the molecular characterization, the results of the immunofluorescence experiments provided a deeper understanding of the cellular architecture of PTEC. Specifically, F - actin staining highlighted the morphology of individual cells (Field 1, Figure 4.11) and colonies (Field 2, Figure 4.11), corroborating previously reported findings (84). In contrast, ZO - 1 staining in isolated PTEC exhibited a weaker signal compared to that described in the literature, a result most likely attributable to technical factors, particularly the specific antibody employed.

5.2. iPSC Generation from PTEC and Their Subsequent Culture (Step 2)

The literature indicates that induced - pluripotent stem cells have been generated from patient through the reprogramming of fibroblasts, peripheral blood mononuclear cells and other sources (79) (85).
It is well established that iPSC derived from distinct somatic sources exhibit variable differentiation propensities, largely attributable to the residual epigenetic memory retained from the donor cells (84) (86). Importantly, urine - derived cells constitute an attractive somatic source for iPSC generation owing a good reprogramming efficiency (39). In this context, urine sample collection provided a non - invasive source of somatic cells from both healthy controls and affected individuals. For this project, a lentiviral system was employed to generate iPSC from PTEC, following the protocol described by Zhou et al. and by Overeem et al. (40) (68) with the modification of using alternative plasmids.

The generation of iPSC colonies requires extensive genetic and epigenetic remodelling, a process that is both prolonged and variable. Such variability can markedly influence reprogramming efficiency and may explain, at least in part, the differences in the yields that can be observed across different experiments. In particular, based on our experience (data not shown), the ratio between urinary cell number and viral load represents a critical determinant of reprogramming success. A low number of plated PTEC used for transduction resulted in suboptimal outcomes, underscoring the importance of carefully optimizing cell density and viral dosage to maximize reprogramming efficiency and minimize cellular stress during iPSC generation. When evaluating the transduction efficiency obtained in this study (around 45%) and comparing it with the value reported by Zhou et al. (40) (100% GFP - positive cells 72 h post - transduction), it can be inferred that the efficiency of transduction is strongly influenced by the specific plasmids employed and by the procedural approach, as the present protocol utilized plasmids different from those used by Zhou. Moreover, differences in cell types as well as donor - dependent variability must be considered. The latter appeared particularly relevant in our experiments since iPSC were not obtained from all the donors (data not shown), indicating that intrinsic donor - dependent factors play a crucial role in determining reprogramming outcomes. The variability observed is unlikely to be explained by differences in viral membrane permeability, but rather by distinct reprogramming competence across donor cells. Several intrinsic barriers, such as the epigenetic configuration of the somatic cell, are known to restrict reprogramming efficiency and the generation of high - quality iPSC (87).

Moreover, technical variables, including the quality of plasmids used for the HEK293T transfection, may further contribute to inconsistencies in reprogramming efficiency (7).
It has also to be considered that PTEC can be cryopreserved in liquid nitrogen for extended periods; however, post - thaw variability is not always optimal, as a fraction of the recovered cells fail to maintain a fully healthy state. This condition appears to directly influence iPSC generation efficiency, since successfully reprogramming was observed only when morphologically healthy PTEC were employed. Comparable limitations were also detected with freshly established PTEC colonies, as not all colonies exhibited optimal viability.

After the appearance and subsequent expansion of iPSC clones, their validation was addressed through a molecular assessment of pluripotency markers by PCR. These markers were employed as a reference parameter for the comparison of the four protocols under evaluation and the results will be discussed in detail in subchapter 5.3.

Given the results obtained in this specific step of the protocol, in line with recent studies on iPSC derived from PTEC (79) and with the recommendations provided by STEMCELL Technologies (88), the need for a more comprehensive characterization of both the generated PTEC populations and the final hPSC clones became evident. Such extended characterization is expected to provide a more robust evaluation of the derived cell lines and will be pursued in the forthcoming stages of the study. Robust and standardized procedures, as recommended by International Stem Cell Banking Initiative (ISCBI) and International Society for Stem Cell Research (ISSCR) (89), are crucial to mitigate variability and quality concerns in hPSC research. Such practices enable rigorous quality control, reducing risks of contamination, genetic drift, and functional inconsistencies, thereby enhancing data reliability, experimental reproducibility, and translational potential of stem cell - based applications.

As a future step of this protocol, the project will establish a structured cell banking system to ensure the quality, consistency, and reproducibility of hPSC research. The creation of a cell bank represents a critical step in this process, as it provides a stable, quality – controlled source of cells that enhances experimental rigor and supports reproducibility across studies. Two distinct cell banks will be developed: one for PTEC and one for iPSC. An *Initial* PTEC cell bank will be created and progressively expanded to generate a *Reference* bank, which will undergo comprehensive characterization (including karyotyping, STR profiling, RNA sequencing, markers analysis, and mycoplasma testing). These characterized PTEC will serve as the source material for iPSC generation. Subsequently, a *Master* cell bank of iPSC will be established, thoroughly characterized

for genomic stability, pluripotency, and differentiation potential. From the Master cell bank, a *Working* cell bank will be derived to provide standardized, well - characterized cell stocks for future experimental applications.

In addition to the importance of PTEC and iPSC characterization, during validation of iPSC derived via lentiviral methods, particularly using a reprogramming plasmid that includes a tdTomato reporter, a significant concern has been observed: the persistence of Yamanaka - factors gene expression in these iPSC (See Results, subchapter 4.2.1.). This residual expression raises issues, because such factors, if not fully silenced or removed, may hamper the capacity of iPSC to commit to hepatic lineages with the fidelity and efficiency required for downstream differentiation.
A parallel can be drawn to the work of Kuehle et al. (90), who addressed a similar problem in murine iPSC systems. In their study, a lentiviral vector carrying the reprogramming cassette (including tdTomato linked to Yamanaka factors) was engineered with Flp recognition target (FRT) sites within the long terminal repeats (LTRs). After reprogramming, they used Flp recombinase to excise the reprogramming cassette, thereby generating “factor - free” iPSC. Importantly, these authors observed that following excision, the residual LTR element allowed for lineage tracing, while reduction of transgene copy number and decreased transgene expression improved the epigenetic and functional profile of the iPSC lines.
In line with the approach described by Kuehle et al. (90), a potential solution to the issue observed in the iPSC generated at this stage of the protocol could involve the use of Flp recombinase to target the FRT sites integrated within these cells. This strategy would allow the excision of both the tdTomato reporter and the Yamanaka factor, thereby reducing residual transgene expression and potentially enhancing the efficiency of hepatic differentiation. Furthermore, excision of the reprogramming cassette may facilitate restoration of normal epigenetic regulation, reducing the risk of aberrant gene silencing in differentiated progeny.
In summary, we think that residual expression of Yamanaka factors represents a significant limitation for hepatic differentiation of iPSC; however, the strategy involving FRT - mediated cassette excision via Flp recombinase offers a feasible route to generate factor - free iPSC with enhanced safety and differentiation potential.

This limitation associated with the use of lentiviral vectors simultaneously raises the broader question of adopting alternative reprogramming strategies. In particular, as highlighted in studies reporting the generation of iPSC from PTEC (79), one promising approach to consider is the use of Sendai virus - based systems.

The Sendai virus represents a powerful tool for iPSC generation, as it avoids genomic integration due to the absence of a DNA phase. It ensures efficient delivery of Yamanaka factors, with Fusaki et al. (91) reporting nearly 100% transduction efficiency in fibroblasts even at low Multiplicity of Infection (MOI). Its broad tropism, mediate by binding to sialic acid on cell - surface glycoproteins, and the sustained expression of reprogramming factors achieved through viral RNA polymerase following a single transduction, further underscore its advantages over integrative systems (92).

Looking ahead, alongside the through characterization of the generated iPSC and the establishment of a PTEC and iPSC biobank, the use of Sendai virus is proposed as an alternative strategy for reprogramming PTEC. While this method offers clear advantages in terms of safety and efficiency, its significantly higher cost compared to lentiviral approaches remains an important factor to weigh when considering its broader implementation.

5.3. iPSC Differentiation into Hepatocytes - Protocol Comparison (Step 3)

Over the last ten years, numerous strategies have been devised to promote the differentiation of human induced pluripotent stem cells into hepatocyte - like cells *in vitro*. These include the ectopic expression of key hepatic transcription factors via viral vectors (27), supplementation with growth factors (93), exposure to small molecules (94), as well as protocols that combine both approaches to mimic the major signalling cascades governing embryonic liver development (95). The establishment of *in vitro* liver disease models using human iPSC - derived HLCs has proven successful, enabling a deeper understanding of disease pathophysiology and facilitating the development of novel therapeutic strategies (13).

Despite these advances, generating fully functional hepatocytes through directed differentiation remains a substantial challenge (32). Although hepatocyte - like cells (HLCs) can be obtained with these methods, the overall efficiency, reproducibility, and robustness of differentiation remain suboptimal. Furthermore, the differentiated cell populations often display considerable heterogeneity, with cells representing varying maturation states and, at times, off - target phenotypes. This variability raises important concerns regarding their reliability and utility in downstream biomedical applications (13).

Thus, the establishment of a differentiation platform that yields hepatocytes with high efficiency, uniformity, reproducibility and mature hepatic features is of critical importance for the advancement of this field.

In this project, four approaches to hepatocytes differentiation, derived from established strategies, were developed, and the resulting hepatocytes - like cells (HLCs) were evaluated both phenotypically and functionally at four distinct stages of the differentiation process (iPSC, Definitive Endoderm, Hepatic Progenitors, and Hepatocyte - like cells). The HLCs were characterized in terms of cellular morphology, hepatic gene expression assessed at the molecular level and by immunofluorescence, as well as functional activity through measurement of albumin secretion. Of note, one of these protocols, provided by STEMCELL Technologies (72), is commercially available and, to date, has been validated exclusively through data reported in a poster presentation (https://cdn.stemcell.com/media/files/scientificposter/SP00283_Efficient_Generation_of_Functionally_Relevant_hPSC_Derived_Hepatocytes_and_Liver_Organoids_for_Hepatotoxicity_and_Liver_Biology_Modeling.pdf), an aspect that makes the comparative analysis carried out in this thesis particularly noteworthy.

As previously noted, it is important to consider that the persistent expression of Yamanaka factors in the iPSC used for differentiation may have compromised their ability to undergo efficient induction into hepatocytes, with potential consequences on cellular morphology, hepatic maturation, and functional performance.

When considering a general comparison among the protocols, based on protocol duration, the culture medium employed, the coating applied, and the initial number of cells, different observations can be made.

Coating constitutes a critical factor for iPSC culture, as it ensures proper cell adhesion and provides essential extracellular cues for the maintenance of pluripotency. In hepatocyte differentiation protocols, the choice of coating significantly affects the efficiency of the process by modulating both cell survival and functional maturation.

With regard to the first two protocols, both developed by the same research group, the Overeem protocol involves an initial coating with vitronectin, which does not present practical challenges (68). In contrast, the Matakovic, Mallanna, STEMCELL protocols, and the Overeem protocol in the second part, employ hESC - qualified Matrigel as a coating, which requires greater technical care. Specifically, based on our experience, it is crucial to adhere to the timing necessary for the coating stabilization, to carefully control the temperature at which the plates are maintained, and to perform visual inspection to ensure a homogeneous distribution.

An additional variable that proved decisive in differentiating the outcomes of the tested protocols was the initial cell seeding strategy. The Mallanna and STEMCELL protocols, which rely on initiating induction from a confluent monolayer, facilitated robust expansion but simultaneously introduced a confounding factor: the excessive proliferation resulted in a substantial proportion of cell death during subsequent differentiation stages. This dynamic raises the possibility that part of the reduced efficiency observed in these protocols may stem not only from intrinsic features of the induction steps but also from the stress associated with overconfluence and cell turnover.

Conversely, the Overeem and Matakovic protocols, which begin with single - cell iPSC plating, confronted the opposite challenge. The technical difficulty of achieving sufficient numbers to establish a stable monolayer likely compromised reproducibility and efficiency. In this respect, the requirement for single - cell seeding, while theoretically advantageous for uniform induction, appears to expose the system to greater variability and technical fragility, particularly when scaling up or attempting repeated trials.

Equally, significant was the role of the culture support. The markedly improved cell growth observed in larger well formats (e.g. 2 - well ibidi® chambers) compared to smaller - well supports suggests that physical parameter such as available surface area and meniscus effects are not merely practical considerations but may actively influence cell behaviour. This highlights how methodological details, often considered secondary, can critically shape experimental outcomes and potentially confound the interpretation of protocol efficiency.

Taken together, these observations suggest that differences in initial cell number, seeding strategy, and culture support may account for at least part of the variability between protocols. Thus, the relative success or failure of a given differentiation method cannot be attributed solely to the defined biochemical cues but must also be understood considering the underlying technical framework within which these cues are applied.

Based on the comparative analysis of the four protocols, the most evident differences concern both the duration of individual differentiation steps and the specific media formulations and supplementary factors employed. A closer comparison reveals that the majority of the key signalling molecules employed, such as Activin A, BMP4, FGF2, HGF, B27, and Oncostatin M, are largely conserved across methods. While the variations in timing and composition clearly shape the trajectory of differentiation, they also underscore a broader point: protocols that rely on investigator - prepared media (such as those of Overeem, Matakovic, and Mallanna) are inherently more susceptible to operator - dependent variability. Small inconsistencies in the preparation or handling of growth factors and supplements can have a measurable impact on reproducibility and final outcomes. By

contrast, the STEMCELL protocol, although less transparent in terms of composition, mitigates this limitation by relying entirely on standardized commercial media. This characteristic reduces the potential for technical variability between experiments and operators, thereby ensuring higher reproducibility at the expense of reduced flexibility, and mechanistic insight into the role of individual components.

Another important difference among the protocols concerns the approaches used to promote hepatocyte polarization. In the Overeem, Matakovic, and Mallanna protocols, Oncostatin M (OSM) is incorporated into the final maturation medium. OSM, a member of the interleukin - 6 family of cytokines, has been widely reported to play a key role in hepatocyte maturation, particularly in the induction of functional polarization, bile canalicular formation, and the establishment of apical - basolateral domains through gp130 - mediated signalling pathways (96). By contrast, the composition of the commercial STEMCELL medium remains undisclosed, making it impossible to ascertain whether OSM is present.

Beyond cytokine supplementation, further methodological differences are evident. Both the Overeem and Matakovic protocols include a Matrigel overlay during the final days of differentiation, a step intended to mimic extracellular matrix cues and thereby reinforce cytoskeletal organization and tight junction assembly. The combination of suitable factors such as OSM with structural support provided by Matrigel has been shown to synergistically enhance the acquisition of hepatocyte polarity and functional competence (30) (97).

Collectively, in our opinion, these observations suggest that protocol performance is governed less by “which factors” are used than by how and when they are applied, the degree of standardization in media formulation, and whether the culture system supplies the biophysical context required for stable hepatocyte polarity.

Indeed, despite the use of a matrix such as Matrigel for overlay formation and the supplementation of the culture media with Oncostatin M, the HLCs generated through the experimental protocols under analysis lack key *in vivo* characteristics, including cellular polarity, as further confirmed by z - stack analyses of HLCs performed with confocal microscopy by our collaborators (data not shown).

Protocol - dependent morphological differences emerged despite shared differentiation cues. The primary divergence arises at seeding: Overeem and Matakovic begin from single iPSC, whereas Mallanna and STEMCELL start from confluent monolayers, the latter showing more cell death during differentiation. At definitive endoderm, all protocols yield polygonal cells; Overeem shows adhesion differences consistent with vitronectin versus Matrigel coating. At the hepatic - progenitor stage,

Matakovic displays a more pronounced nuclear - to - cytoplasmic ratio, while monolayer - derived protocols show signs of over proliferation but otherwise comparable morphology. By the final stage, Mallanna and STEMCELL converge on a polygonal monolayer, Matakovic presents larger cytoplasm with binucleation (hepatocyte hallmark), and Overeem shows focal multilayering. Collectively, these features indicate that initial seeding strategy and substrate choice shape downstream morphological outcomes despite shared factor regimens.

Importantly, because cross - protocol comparison cannot rest only on cellular morphology, which offers an incomplete and potentially misleading readout, gene - expression profiling was undertaken to enable a more rigorous assessment.

The aim of analyzing the pluripotency - associated genes SOX2, OCT3/4, and NANOG was to confirm that, starting from the initial stage of differentiation and progressing toward the HLC stage, their expression would progressively decline and ultimately be absent at the terminal stages. The obtained results demonstrate that, with the exception of the persistent SOX2 expression observed in the Matakovic protocol, all three pluripotency markers exhibited a consistent downregulation pattern across the different differentiation strategies. In addition, the expression of OCT3/4 was further investigated through immunofluorescence assays, which confirmed its absence at the HLC stage.
The persistence of SOX2 for one specific protocol may therefore reflect a protocol - specific limitation, possibly related to suboptimal signalling cues or insufficient epigenetic remodelling required for full expression of the pluripotency network. At the same time, previous studies have shown that SOX2 can persist or be regulated differently compared to OCT3/4 and NANOG, which may account for its divergent expression pattern in this specific protocol relative to the others (98). Nevertheless, it is important to consider the broader issue of residual expression of Yamanaka factors in these iPSC, which may in turn influence their differentiation potential.

When examining the expression of hepatic genes, particularly ASGR2, SERPINA1, ALBUMIN, and APOF, marked differences emerged among the protocols. The absence of ASGR2, SERPINA1, and ALBUMIN expression in the Overeem and Matakovic protocols strongly suggests that these strategies do not support the acquisition of mature hepatic features, given the central role of these genes in hepatocyte identity and function. Interestingly, APOF expression was detectable in both protocols, at levels lower than HepG2 but higher than the UpCyte control, indicating that partial activation of lipid metabolism - related pathways can occur even in the absence of broader hepatic maturation. In contrast, the Mallanna and STEMCELL protocols generated HLCs with robust

expression of all four genes, underscoring their superior capacity to drive functional hepatocyte - like phenotypes. The divergence between protocols highlights how critical gene networks may remain silenced or insufficiently activated depending on the differentiation strategy employed. This not only points to protocol - specific limitations, but also raises concerns regarding the functional competence of HLCs lacking key markers such as albumin, which is widely regarded as a benchmark of hepatocyte maturity (99). Regarding the expression of APOF in qualitative PCR, the absence of detectable amplification across all analyzed protocols, despite its expression being observed in quantitative PCR, suggests a potential issue related to the primer used in the qualitative assay.
When assessing albumin secretion into the culture medium by HPs and HLCs, the overall data indicate a general concordance between transcriptional and functional readouts. Specifically, the Overeem and Matakovic protocols showed both low ALB transcript levels and reduced albumin secretion, whereas the Mallanna and STEMCEL protocols displayed higher expression levels accompanied by increased secretion. Among the protocols tested, Mallanna and STEMCELL demonstrated the most robust functionality in terms of albumin production, further supporting their superiority in promoting hepatocyte - like phenotypes.

When evaluating the expression of the second group of hepatic genes (TTR, HNF4α, and AFP), heterogeneous trends were again observed across protocols. In the case of the Overeem protocol, the final HLC exhibited low levels of TTR expression, although still higher than the positive control, together with an absence of HNF4α expression and progressively decreasing trend of AFP. Since TTR encodes one of the three pre - albumins, its reduced expression in HLC compared to the HP stage may reflect differential regulation of pre - albumin synthesis at distinct stages of hepatic differentiation. The lack of HNF4α expression is particularly critical, as this transcription factor is hepatocyte - specific and plays a central role in establishing and maintaining hepatic identity; its absence at the HLC stage therefore indicates incomplete maturation within this protocol (100). A more detailed consideration regarding AFP expression will be addressed later in this section.
A comparable gene expression trend was also observed for the Matakovic protocol.
In contrast, the Mallanna and STEMCELL protocols exhibited a distinct profile, characterized by markedly higher expression levels of both TTR and HNF4 relative to the other two protocols. This pattern strongly suggests that these protocols support a more advanced degree of hepatic maturation at the HLC stage. Of particular importance is the induction of HNF4, which was clearly detectable at both the HP and HLC stages and progressively increased compared to the preceding DE stage.
In our opinion, these divergent outcomes among protocols may be attributable to differences in the molecular cues and culture conditions employed. For instance, variations in growth factor

supplementation, signalling pathway modulation, or timing of differentiation steps could differentially influence the activation of hepatic transcriptional networks Such protocol - dependent disparities underscore the critical importance of optimizing differentiation strategies to achieve functionally competent HLC.

With respect to AFP expression, all the analyzed protocols exhibited detectable levels, particularly in the HP and HLC stages. This expression, which was especially pronounced in the Mallanna and STEMCELL protocols, was further examined in the context of existing literature to determine whether it should be interpreted as a negative indicator of hepatocyte immaturity or as a positive marker of active cellular regeneration. While AFP is typically expressed during early human fetal development, several studies have also highlighted its relevance in stem cell research and regenerative medicine. In fact, following birth, the regulatory mechanisms controlling AFP expression undergo a developmental shift, with AFP enhancers, active during fetal stage, becoming repressed and redirected toward sustaining albumin transcription throughout adulthood. Notably, AFP overexpression has been reported in models of partial hepatectomy, where it was transiently induced for several days in proliferating hepatocytes, as well as in hepatocytes undergoing mitosis following chemically induced liver injury (101) (102) (103). The observation that the Mallanna and STEMCELL protocols, which also proved superior in terms of global gene expression profiles, display high AFP levels could therefore be interpreted positively, reflecting the regenerative potential of this protein rather than merely an indication of incomplete maturation.

Overall, for this group of genes as well, the Mallanna and STEMCELL protocols appear to outperform the Overeem and Matakovic approaches, further supporting their superiority in promoting hepatic maturation.

5.3.1. Limitations and Future Perspectives of the iPSC - derived HLC Model

Our findings are consistent with recent studies focusing on HLC research. As highlighted in the literature, the identification of morphological, phenotypic, and functional characteristics is essential for the reliable generation of functionally mature HLCs from iPSC. Although numerous studies have investigated protocols for HLC differentiation, there is currently no standardized method for their evaluation (104). Despite the challenges associated with their culture, including technical complexity, limited maintenance over time, and the need for invasive isolation procedures, primary human

hepatocytes (PHHs) remain the reference standard. For this reason, commercially available cell lines such as UpCyte® cells may represent a valid alternative for use as controls.

Among the key parameters used to assess HLC validity, morphological features are particularly relevant. As previously discussed, differentiated HLCs typically display polygonal shapes and an increased nucleus - to - cytoplasm ratio, reflecting their progression toward a hepatocyte - like phenotype. In addition, the expression of hepatocyte - specific genes and proteins is routinely examined, as we did, through immunofluorescence staining and quantitative real - time PCR.

Notably, iPSC - derived HLCs currently resemble fetal hepatocytes, likely corresponding to a developmental stage between the late first trimester and adulthood. This developmental immaturity is reflected in their functional profile: HLC express fetal markers such as AFP (assessed in our protocols) and CYP3A7, whereas the expression levels of adult - specific CYP enzymes, including CYP3A4, remain significantly lower compared to primary hepatocytes (105). In addition, HLCs are currently insufficiently mature to be employed in transplantation contexts, either as an intermediate or permanent alternative to orthotopic liver transplantation, due to their limited functional capacity and lack of cellular homogeneity (104). These observations collectively highlight the current limitations in achieving fully mature and functional HLCs *in vitro*, as further confirmed by our protocol comparison, which did not identify HLCs displaying characteristics fully consistent with those of primary hepatocytes.

To date, most disease models have focused on either acquired metabolic disorders, such as MAFLD and MASH, or inherited metabolic diseases, including α1 - antitrypsin deficiency and Wilson's diseases. Some models have also been extended to infectious diseases, such as malaria and hepatitis. In general, inherited disorders that primarily affect a single cell type are easier to model, as HLCs alone are sufficient to reproduce key pathological features and to evaluate candidate drugs for their ability to reverse or mitigate the disease phenotype. Nevertheless, although they have demonstrated expected responses to known drugs and toxins, their current level of functional maturity and consistency is insufficient to support the reliable screening of novel compounds without additional independent validation (104).

Considering our work, future directions for this 2D differentiation approach will include repeating all protocols starting from the same urine - derived iPSC colonies treated with flippase to address the issues related to persistent Yamanaka factor and tdTomato expression; implementing additional functional assays, such as cytochrome activity and bile acid metabolism, to obtain a clearer assessment of which strategy most effectively yields mature induced hepatocytes; and further

optimizing the Mallanna and STEMCELL protocols, for instance by introducing a Matrigel overlay to enhance cellular polarization.

Starting from the premise that the primary objective of this study was not to establish a novel differentiation protocol for generating HLCs, but rather to compare existing protocols in order to identify the most effective one, it is evident that several refinements could be introduced based on recent advances in the field. In particular, the use of Laminin521 as a coating substrate should be considered in future protocols, given its demonstrated ability to better support the formation of biliary tubular structures. This approach is also incorporated in commercial differentiation kits, such as those from STEMCELL Technologies, alongside Matrigel. Similarly, the implementation of transwell systems could enhance both basal and apical molecular uptake and secretion, thereby enabling HLC metabolic activity to more closely mimic physiological conditions.
Another important aspect to consider is the establishment of co - culture systems with other relevant cell types, potentially in combination with 3D culture platforms. Such approaches may facilitate the development of more complex *in vitro* liver models capable of more accurately recapitulating the hepatic microenvironment, thereby improving their applicability for disease modelling and therapeutic testing (105) (104).
Furthermore, recent efforts by various research groups have led to the development of online tools. Such as HLCompR (106), which enable the comparison of specific pathways and provide a deeper understanding of different HLC models and differentiation protocols. HLCompR allows researchers to examine the expression of individual genes or entire gene sets of interest to select the most suitable HLC model.

Within the framework of personalized medicine, particularly for genetically defined forms of PFIC as well as for cases of unknown cholestasis (where pathogenic mechanisms require further elucidation), and drug - induced cholestasis, non - invasively derived HLC models from urine represent a promising and highly adaptable tool. Notably, this approach could be applied to PFIC6 to investigate the localization of the bile salt export pump (BSEP) and its relationship with MYO5B mutations. For PFIC6 specifically, five reported case studies have examined this link between MYO5B variants and BSEP trafficking: three describe disrupted apical BSEP localization associated with MYO5B defects (107) (108) (109), whereas two report preserved BSEP positioning despite pathogenic mutations (110) (111). These discrepancies highlight the need for reliable *in vitro* systems capable of recapitulating hepatocyte architecture, apical - basal polarity, and bile canalicular function, while remaining feasible for repeated derivation from patients. In this context, HLC generated from

PTEC offer a powerful platform for mechanistic studies and therapeutic testing. Their suitability for functional assays, including the assessment of bile acid transporter expression and activity, make them particularly advantageous. Overall, such non - invasive patient - specific models have the potential to advance precision diagnostics and unravel pathogenic pathways in both genetically characterized and yet - undefined cholestatic diseases.

Nevertheless, given the intrinsic limitations of conventional two - dimensional systems, the study of hepatic diseases requires reliable three - dimensional models that more accurately recapitulate liver architecture and function. Such organotypic models, including Hep - Orgs, represent a frontier for personalized medicine and enable long - term hepatocyte culture. The success of this technique relies on the availability of viable primary hepatocytes, which in turn depends on efficient liver perfusion and isolation procedures. Although technically demanding and prone to pitfalls such as contamination, suboptimal digestion, or reduced cell viability, when properly performed, these standardized protocols ensure high - quality hepatocytes with preserved integrity and functionality, which are essential for downstream applications (76).

5.4. 2D and 3D Cultures from Rat Primary Adult Hepatocytes

The present study focused on the generation of Hep - Orgs from adult hepatocytes, following the methodology described by Peng and colleagues (63).
For the development of Hep - Orgs cultures, primary hepatocytes (PHs) were obtained through the establishment of a liver perfusion procedure in rats. During the planning phase, the PREPARE guidelines (112) (Topic A1) checklist was carefully considered. Particular attention was devoted to reviewing relevant literature, comparing previous protocols, and establishing contact with some of the original authors. The use of Hep - Orgs itself represent a refinement strategy, as they can be kept in culture for up to seven months, thus contributing to the reduction of animal numbers (112) (Topic A3). An experienced technician was selected to perform the procedure, minimizing the use of surplus animals (112) (Topic B5).

Among the most recent publications describing rat liver perfusion are those of Ng (113) and Shen (73). However, the present protocol addresses aspects not covered in those works, particularly the use of commercial solutions and the optimization of precise cannulation to ensure efficient *in situ* liver perfusion and digestion. Unlike the mentioned protocols, which employed home - prepared solutions, the present protocol relies on commercial perfusion and digestion buffers, reducing the variability in

buffer preparation, increasing reproducibility, and avoiding the use of excessive digestive enzymes that can compromise hepatocyte viability and quality. Furthermore, whereas the protocol of Ng (113) requires removal of the liver prior to digestion, the current method performs perfusion and digestion with the liver *in situ*.

Complete drying of tubing after ethanol treatment, followed by washing with medium, was essential, since even minimal ethanol injection into the liver results in immediate hepatocyte death. The temperature of the perfusion and digestion solutions was also critical. The perfusion buffer was pre - warmed to 42°C prior to surgery, whereas the digestion buffer was placed in the warming bath only during the perfusion step, in order to preserve collagenase activity. The addition of a bubble trap upstream of the catheter prevented air bubbles from entering the liver during perfusion (113).

Appropriate buffer composition, perfusion pressure, and flow rate are essential (113).
Since hepatocyte adhesion is calcium - dependent (73), the perfusion buffer consisted of a calcium - free solution containing EDTA to disrupt calcium bridges between cells, thereby facilitating blood clearance. Perfusion for 8 - 15 minutes at 10 mL/min was necessary to achieve effective EDTA penetration; inadequate perfusion resulted in incomplete digestion.

The digestion buffer contained calcium, as collagenase activity is calcium - dependent. For the commercial digestion buffer employed, perfusion was maintained for 15 minutes at a minimum flow rate of 20 mL/min, corresponding to 300 mL in total. Incomplete digestion resulted in persistent cell - cell junctions, causing mechanical stress and reduced viability during subsequent dissociation. Gradual increase of the flow rate minimized cellular stress. Transient clamping of the inferior vena cava, which induced liver swelling, significantly enhanced digestion efficiency and cell yield. At the end of the process, the liver acquired a soft, light - brown appearance. Subsequent washing of the isolated liver in PBS supplemented with 3% penicillin/streptomycin reduced microbial load and minimized the risk of contamination during downstream procedures.

During hepatocyte isolation under sterile conditions, the use of 25 mL serological pipettes preserved cell viability compared to smaller pipettes. An additional step was introduced to increase primary hepatocytes yield: after the release of cells from the digested liver and subsequent filtration, William's complete medium was poured over the remaining tissue to repeat the scraping step under the hood. This facilitated further recovery of cells from the liver capsule. However, the application of excessive pressure during filtration was found to negatively affect cell viability (114).

This surgical and liver perfusion procedure was initially established in the rat model rather than in the mouse, as the larger size of the animal facilitated the technical steps. The protocol enabled the isolation of primary hepatocytes, which were subsequently plated into two - dimensional culture; however, these cells exhibited a progressive loss of morphology, function, and expression of hepatic markers (Results subchapter 4.4.2.). For this reason, the culture of Hep - Orgs was pursued. Hep - Orgs were maintained in culture for nearly 15 days, although no evident growth was observed beyond day 5, as confirmed also by the EdU assay performed on day 15 (Results subchapter 4.4.3.).

For these reasons, the study was extended to the mouse model, which appears to exhibit a greater potential for Hep - Orgs formation compared with the rat.

5.5. 3D Culture from Mouse Primary Adult Hepatocytes

The surgical procedure in mice proved technically challenging due to the small size of the animals. Following methodological refinements, we achieved a high yield of viable primary hepatocytes, which enabled the establishment of three - dimensional Hep - Orgs cultures. *In vitro* culture of Hep - Orgs was successfully developed, displaying robust proliferation from the earliest stages and adopting a grape - like morphology, consistent with the observations reported by Peng et al. (63).
The Hep - Orgs demonstrated sustained growth and long - term expansion, remaining viable in culture for over two months. At 14 days of culture, RT - qPCR analysis confirmed the expression of hepatic marker genes. Hep - Orgs maintained their morphological integrity and exhibited a high proliferative capacity for more than one month, as evidenced by EdU incorporation assay. Luce et al. confirm that one of the key functional features to be assessed in order to establish the validity of the organoid model is the ability of the organoids themselves to produce albumin (49). The Hep - Orgs under investigation secreted high levels of albumin into the culture medium, indicating preserved functional activity. Albumin release increased progressively between day 14 and day 30, and remained stable thereafter, correlating with Hep - Orgs growth dynamics.

According to Luce et al. (49), HNF4α represents one of the most relevant hepatic transcription factors being essential for the establishment of hepatocyte identity and functional maturation. In this study, immunofluorescence analysis revealed that HNF4α expression in Hep - Orgs was mainly restricted to the nuclei of peripheral cells within the organoid (Figure 4.37). This spatially confined pattern, also described in literature, suggests that only a subset of cells acquires a more defined hepatic

identity, while the inner cell populations may remain in a less differentiated state. In addition, it is well known that cells located in the inner region of non - vascularized hepatic organoids undergo necrotic degeneration once a critical size threshold is exceeded, primarily due to limited access to oxygen and essential nutrients (115). At the molecular level, although HNF4α gene expression was found to be more than twofold lower compared to primary hepatocytes, it is important to note that primary hepatocytes, while representing the gold standard for modelling liver physiology and disease, can typically be maintained in culture for no longer than approximately five days. This limited viability constitutes a major constraint when compared with the long - term stability and functional persistence exhibited by Hep - Orgs. Importantly, the Hep - Orgs generated in this study exhibited a robust secretion of albumin into the culture medium, which represents a key functional feature of hepatocytes.

Taken together, these findings underscore the need for further optimization of differentiation protocols, potentially through the incorporation of supportive cell types (e.g., stellate cells, Kupffer cells, endothelial cells), microfluidic systems, or biochemical cues that better mimic the native liver niche. Addressing these limitations will be essential to enhance the physiological relevance of hepatic organoids for disease modelling, drug testing, and regenerative applications (53).

5.5.1. Hep - Orgs as a Model of Drug - induced Cholestasis

To assess whether this model could be suitable for the study of cholestatic liver diseases, the previously described 3D system was complemented with functional assays, specifically focusing on the study of biliary function. Cyclosporine A (CsA) has been reported to act as a competitive inhibitor of substrate transport mediated by the bile salt export pump (BSEP), multidrug resistance protein 2 (MRP2), and P - glycoprotein (P - gp) at the canalicular membrane (116) (117). Dichlorofluorescein (CDFDA) is commonly employed to visualize biliary canaliculi, taking advantage of the fact that, once internalized by the cells, intracellular esterases deacetylate the compound, leading to the formation of the oxidized product DCF, which exhibits strong fluorescence (118).
Regarding this part of the project, a dichlorofluorescein assay was employed, combined with the administration of CsA to evaluate potential differences between control organoids (treated with DMSO), and drug - treated organoids. For this specific assay, previously described established protocols for hepatic organoid models (118), which employed other compounds (most notably, troglitazone), were taken in consideration to induce bile flow impairment. The accumulation of fluorescent marker reported in these literature models, in particular in the biliary cysts, was likewise

observed in the Hep - Orgs under investigation, thereby supporting the potential of this model for the study of diseases characterized by alteration in bile flow (subchapter 4.5.3.1).

In Hep - Orgs treated with 50 μM CsA, we observed clear structural alterations of the bile canaliculi, characterized predominantly by canalicular constriction and accompanied by marked changes in cytoskeletal organization. These effects were particularly evident from the redistribution of ZO - 1 and the remodelling of pericanalicular F - actin, as revealed by phalloidin staining. HNF4α staining was used exclusively as an indicator of hepatic identity, and positive expression was confirmed in the Hep - Orgs. These findings are consistent with the results previously reported by Sharanek and colleagues (119) (120), who investigated the effects of various cholestatic drugs on bile canaliculi. In their studies, CsA induced a progressive constriction of the canalicular lumen, whereas other compounds such as Fasudil, α - Naphthylisothiocyanate (ANIT), deoxycholic acid (DCA), and Bosetan caused a pronounced dilation of bile canaliculi. Sharanek et al. further demonstrated that these structural modifications correlated with pericanalicular F - actin remodelling and junctional disorganization, highlighting cytoskeletal and junctional perturbations as early events in drug - induced cholestatic injury.

In addition to visualizing the accumulation of the fluorescent probe within the biliary cysts and to observe the modifications correlated with F - actin and ZO - 1, the perturbations induced by drug administration were further confirmed by assessing the expression levels of the ER stress markers CHOP and GRP78, as well as the oxidative stress marker NRF2 (Results subchapter 4.5.4.2.). These findings are consistent with those reported by Sharanek, further supporting a mechanistic link between CsA treatment and the induction of both oxidative and ER stress. In particular, while Sharanek observed a rapid upregulation of ROS - related markers, including NRF2, and ER - stress genes, including CHOP and GRP78, following CsA exposure, our data similarly demonstrate the overexpression of NRF2 alongside CHOP and GRP78. These results, obtained in a 3D model rather than in the 2D systems previously reported in the literature, reinforce the notion that CsA promotes hepatocellular injury through converging oxidative and ER stress pathways (119).

It should be noted that, considering the treatment with CsA, the use of 3D hepatic organoids introduces differences in the visualization of markers such as ZO - 1 and in the assessment of morphological changes in F - actin, when compared to the studies by Sharanek et al., which employed 2D models (HepaRG cell line). However, the Hep - Orgs model developed in this study enables the visualization of clear differences between treated and control samples, which will require further

investigation through additional assays. From a practical perspective, isolating exclusively multicellular Hep - Orgs proved challenging, as single hepatocytes and cellular debris frequently remained present even after the washing steps included in the immunofluorescence protocol. At the same time, the use of hepatic markers such as HNF4α enabled the specific identification of cell aggregates that effectively corresponded to Hep - Orgs. Overall, the use of immunofluorescence in suspension proved to be much more effective than conventional 2D immunofluorescence. In the future, this approach will also enable the evaluation of hepatic markers and cytoskeletal components through the analysis of organoid sections obtained by resin embedding, after appropriate protocol optimization.

Perspectives and Applications of the Hep - Orgs Model

Peng and colleagues (63) underlined that the majority of hepatocytes exhibit limited proliferative activity in the healthy liver, which likely contributes to the difficulty of establishing long - term cultures from hepatocytes and other primary cell types that are inherently challenging to expand. Their data show that the inflammatory cytokine TNFα, in combination with specific growth factor and small molecules, enables the long - term culture of primary hepatocytes, cells that have historically been difficult to maintain and expand *in vitro*, while preserving their functional properties.

Importantly, the findings reported by literature (63) (121) strongly support the potential of this model to recapitulate key aspects of hepatic physiology and regeneration. Indeed, *in vitro* expanded Hep - Orgs maintained a broad range of liver - specific functions after long - term expansion and subsequent induction. Notably, in our work we investigated hepatic markers expression, hepatocytes proliferation, albumin secretion and dye excretion into bile canaliculi. Collectively, the results presented by Peng and validated also in our Hep - Orgs model underscore the suitability of this approach for faithfully reproducing liver - specific functional and regenerative processes *in vitro*, which is crucial for the validation and application of the model in hepatic research. Notably, Kim et al. (121) provide a further validation of this organoid model derived from primary mouse hepatocytes as a platform for investigating diverse metabolic pathways. Primary mouse hepatocytes were isolated by two - step collagenase and embedded in Matrigel to generate Hep - Orgs, which maintained or increased the expression of different hepatic markers, supporting stability and maturation of hepatic functions in 3D. In particular, they confirmed that Hep - Orgs exhibit long - term culture stability, maintenance of hepatocyte identity, and stimulus - responsive metabolic gene expression across

glucose, cholesterol, and ethanol conditions, supporting their validity as an *in vitro* surrogate for mouse hepatocyte function, thereby paving the way for additional applications of this model.

An important aspect to highlight is that only a limited number of protocols successfully generate Hep - Orgs from primary hepatocytes, particularly from human sources. While organoid culture systems enable the propagation of functional adult mouse hepatocytes and human fetal hepatoblasts, their applicability to human adult hepatocytes remains restricted. Consequently, there is a lack of strategies that can simultaneously support the long - term expansion and preservation of adult primary hepatocytes (PHH) functionalities. This limitation represents a significant barrier to the advancement of human hepatocyte - based applications in regenerative medicine, drug discovery, and toxicology.
However, recent work by Igarashi et al. has led to significant improvements in the culture of hepatic organoids (Hep - Orgs) derived from human hepatocytes. The authors optimized organoid culture conditions that enable both the long – term expansion and the proper differentiation of primary human hepatocytes (PHHs). The resulting hepatocyte organoids exhibit metabolic functions closely resembling those of native PHHs. This accurate *in vitro* recapitulation of hepatocyte metabolism marks a pivotal advancement in the field of functional organoid medicine. Notably, the researchers developed a novel culture medium that promotes the efficient formation of small cystic organoids characterized by a thick monolayer expressing hepatocyte markers such as albumin and HNF4α. Their findings also highlight the crucial role of Oncostatin M, previously discussed in this thesis in relation to Step 3 (2D model), in enhancing hepatocyte maturation (122). These advances not only facilitate more human - relevant models for studying liver diseases and exploring therapeutic strategies but also provide valuable insights and methodological cues that may be applied to Hep - Orgs derived from mouse hepatocytes, as investigated in the present work.
From the perspective of developing donor - specific models to enable personalized studies of liver pathologies, the use of human - derived hepatocytes to generate human hepatic organoids remains an attractive possibility. Such an approach would allow the establishment of individualized *in vitro* systems that faithfully recapitulate patient - specific liver physiology and disease mechanism. However, the inherently invasive nature of obtaining primary human hepatocytes, typically through liver biopsy, renders this strategy less feasible in the near term and limits its broader applicability. In contrast, the use of animal - derived models currently represents a more practical and accessible alternative for refining hepatic organoid systems and for preclinical translational research.

Ramli et al. (118) established human iPSC - derived hepatic organoids that preserve 3D tissue architecture and, critically, a contiguous bile - canaliculi network, addressing the current scarcity of

in vitro models capable of capturing multicellular liver organization and disease development. Beyond this conceptual advance, their work provides a practical framework of validation assays for hepatocyte - centric pathology, particularly cholestasis. Specifically, they implemented a dichlorofluorescein canalicular transport assay to quantify bile flow and demonstrated troglitazone - induced acute disruption of canalicular function. This assay is directly transferable to our platform and informs our evaluation of whether Cyclosporine A can recapitulate canalicular dysfunction consistent with cholestasis. In this context, the model also serves as a robust platform for determining which pharmacologic agents most faithfully recapitulate drug - induced cholestasis within the organoid setting. To achieve a more comprehensive validation, the assay repertoire should be expanded to include analyses of cellular composition and structural remodelling, quantitative measurements of cytochromes activities, and deeper molecular profiling (e.g. transcriptomic and proteomic characterization).

The liver comprises two broad cellular compartments: parenchymal and non - parenchymal. Parenchymal cells consist predominantly of hepatocytes (~80%) and biliary epithelial cells (bile duct epithelial cells; BECs/cholangiocytes, (~20%), whereas the non - parenchymal compartment includes Kupffer cells (resident macrophages), hepatic stellate cells, and liver sinusoidal endothelial cells (LSECs). BECs mediate the collection and transport of bile acids through the biliary tree, while hepatocytes execute nutrient and energy metabolism, xenobiotic biotransformation and detoxification, and the synthesis of circulating proteins. In line with this, our Hep – Orgs are optimally suited for investigating hepatocyte - centric pathologies; conversely, the interrogation of complex multicellular disease processes is more appropriately undertaken using multicellular liver organoid models that incorporate also non - parenchymal lineages (121).

Given the need for multiple interacting hepatic lineages to dissect molecular mechanisms and intercellular communication in complex disorders such as fibrosis, researchers increasingly employ iPSC - based systems. The reprogramming and directed differentiation capacity of iPSC enables the generation of multicellular liver organoids that capture key epithelial and non - epithelial components and their crosstalk. For example, Ramli and colleagues established hepatobiliary organoids composed of hepatocyte - and cholangiocyte - like cells, showing preservation of physiological features, including functional, contiguous bile ducts that were acutely disrupted by troglitazone, and documented functional readouts (albumin, apolipoprotein B, γ - glutamyl transferase, alkaline phosphatase) alongside modelling of free - fatty - acid - induced steatosis; while lacking hepatic stellate cells and thus not fully recapitulating fibrogenesis, this platform is well suited to interrogate lipid accumulation and MASLD as upstream drivers of fibrosis (118).

Ouchi et al generated multicellular human liver organoids that, following stepwise specification from iPSC, reproduce steatosis and its downstream inflammatory and fibrotic sequences; organoids exhibited dose - dependent lipid deposition and ballooning, Kupffer - like cell activation with TNFα and IL - 8 upregulation, and fibrosis marked by increased α - SMA, vimentin, P3NP, collagen deposition, and tissue stiffening (123).

Takebe and colleagues further recapitulated zonal liver architecture *in vitro* by modulating culture conditions, mapping hepatoblast trajectories by RNA - seq and demonstrating functional benefit after transplantation into rats (124).

Guan et al. used CRISPR - engineered iPSC - derived hepatic organoids to model ARPKD - associated cholangiopathy and congenital hepatic fibrosis, revealing a multicellular composition (hepatocyte - like cells, ductal - like cells, and bi-potential progenitor cells, as well as endothelial and stellate - like cells) by scRNA - seq (125).

Collectively, iPSC - based multicellular organoids offer a versatile, mechanistically informative platform to study intercellular signalling, disease initiation, and progression beyond the reach of hepatocyte - based systems (126).

6. CONCLUSIONS

In this study, a comprehensive workflow was developed and optimized for the generation of donor - specific hepatocyte - like cells (HLCs) from urinary - derived proximal tubular epithelial cells (PTEC) through induced - pluripotent stem cells (iPSC). In addition to this 2D - model, a 3D model was developed obtaining Hep - Orgs from mouse primary hepatocytes. The main conclusions and future research perspectives are summarized below.

Overall, regarding the 2D - model, the following conclusions can be drawn:

- Optimization of PTEC isolation:
  - A standardized protocol for PTEC isolation was successfully established, achieving an overall yield of 40%
  - The main determinants of variability were identified as gender - specific and donor - specific effects
  - The introduction of phosphate buffer (0.05 M) for pH stabilization, together with 20 μm strainers (applied selectively to female samples) markedly improved sample quality and cell adhesion while reducing microbial contamination
  - Short - term processing (within 4 hours of collection) significantly enhanced viability compared to 24 - hour storage, confirming the critical influence of pre - analytical conditions
  - These optimizations enabled the isolation of PTEC from all donors, demonstrating the robustness and reproducibility of the final workflow.
- Generation of induced - pluripotent stem cells (iPSC):
  - PTEC were successfully reprogrammed into iPSC using a lentiviral vector system, yielding colonies expressing pluripotency markers
  - Reprogramming efficiency was influenced by cell confluence, viral load, and donor variability, underscoring the importance of balanced cell density and viral dosage
  - The persistence of Yamanaka - factor expression represents a critical limitation, potentially affecting downstream hepatic differentiation; future work will address this through FRT - mediated excision or Sendai virus - based non - integrative reprogramming

- The establishment of dual cell banks (PTEC and iPSC), in accordance with ISSCR and ISCBI standards, will ensure quality control, traceability, and reproducibility in subsequent applications.

- Differentiation into Hepatocyte - Like Cells (HLCs)
  - Four differentiation protocols (Overeem, Matakovic, Mallanna and STEMCELL) were systematically compared in terms of duration, culture medium, coating, and initial cell seeding strategy
  - Mallanna's and STEMCELL protocols showed the most consistent outcomes, with up - regulation of hepatic genes (ALB, ASGR2, SERPINA1, APOF, TTR, HNF4α) and higher albumin secretion, indicating superior hepatic maturation
  - In contrast, Overeem's and Matakovic's protocols yielded less mature phenotypes with incomplete expression of key hepatic markers
  - Persistent SOX2 expression and lack of cellular polarity (as confirmed by confocal analyses) highlight ongoing challenges in achieving full hepatocyte functionality
  - Morphological and molecular data together emphasize that protocol performance depends not only on biochemical cues, but also on technical parameters such as seeding density, substrate, and well format.
- Overall implications, future perspectives, and limitations
  - The study established a non - invasive, donor - derived cell source of iPSC generation, offering translational potential for personalized liver disease modelling
  - Remaining limitations, such as incomplete hepatic polarization and residual pluripotency, will be addressed through enhanced reprogramming fidelity, matrix optimization, and extended maturation strategies
  - Collectively, the results provide a validated and scalable 2D human cell platform, forming the basis for future 3D - modelling and patient - specific therapeutic studies.

In parallel with the establishment of the 2D human cell - based platform, a 3D murine organoid model was developed and characterized to investigate the molecular and functional mechanisms underlying hepatic disorders within a controlled, reproducible system. The integration of both models was designed to enable translational comparison between individual genetic backgrounds and conserved pathophysiological pathways. The following conclusions can be drawn:

- Establishment and optimization of the 3D culture system
  - The murine 3D liver organoid system was successfully generated from primary hepatocytes
  - Morphologically, organoids displayed the expected cystic and budded architecture.
  - Albumin secretion assay revealed functional maturation
  - These optimized conditions provided a robust foundation for subsequent studies.
- Assessment of the model's suitability for studying drug - induced cholestasis
  - The results after CsA treatment demonstrate that the established 3D model is capable of reproducing drug - induced hepatotoxic phenotypes, supporting its suitability for mechanistic toxicology and preclinical drug testing.
  - The 3D organoid model exhibited enhanced tissue organization, polarization, and metabolic functionality, reflecting a physiologically faithful microenvironment
  - However, due to its murine origin, the model is primarily suited for mechanistic and proof - of - concept studies, serving as a complementary tool to validate and refine hypotheses generated in the human platform.

Given the overall validity of our Hep - Orgs platform, extending its applicability to multifactorial diseases and to conditions involving additional hepatic lineages will require the development and optimization of multicellular organoid systems. A practical and broadly implementable approach is the derivation of patient - specific iPSC from urine - derived cells, a non-invasive source that facilitates repeated sampling and longitudinal study designs. Used alongside our Hep - Orgs as a functional reference, these multicellular organoids would allow systematic study of physiological and pathological mechanisms in both 2D hepatocyte monolayers and 3D organoids, improving mechanistic insight and translational relevance.

7. BIBLIOGRAPHY

1. Asrani SK, Devarbhavi H, Eaton J, Kamath PS. Burden of liver diseases in the world. J Hepatol. 2019 Jan 1;70(1):151–71.

2. Xiao J, Wang F, Yuan Y, Gao J, Xiao L, Yan C, et al. Epidemiology of liver diseases: global disease burden and forecasted research trends. Sci China Life Sci. 2025 Feb;68(2):541–57.

3. Fabris L, Strazzabosco M. Rare and undiagnosed liver diseases: challenges and opportunities. Transl Gastroenterol Hepatol. 2021 Apr 5;6:18.

4. Feldman AG, Sokol RJ. Neonatal cholestasis: emerging molecular diagnostics and potential novel therapeutics. Nat Rev Gastroenterol Hepatol. 2019 June;16(6):346–60.

5. Fargo MV, Grogan SP, Saguil A. Evaluation of Jaundice in Adults. Am Fam Physician. 2017 Feb 1;95(3):164–8.

6. De Bruyne R, Van Biervliet S, Vande Velde S, Van Winckel M. Clinical practice: neonatal cholestasis. Eur J Pediatr. 2011 Mar;170(3):279–84.

7. Overeem AW, Li Q, Qiu YL, Cartón-García F, Leng C, Klappe K, et al. A Molecular Mechanism Underlying Genotype-Specific Intrahepatic Cholestasis Resulting From MYO5B Mutations. Hepatol Baltim Md. 2020 July;72(1):213–29.

8. Esteve C, Francescatto L, Tan PL, Bourchany A, De Leusse C, Marinier E, et al. Loss-of-Function Mutations in UNC45A Cause a Syndrome Associating Cholestasis, Diarrhea, Impaired Hearing, and Bone Fragility. Am J Hum Genet. 2018 Mar 1;102(3):364–74.

9. Bashir A, Hoilat GJ, Sarwal P, Mehta D. Liver Toxicity. In: StatPearls [Internet]. Treasure Island (FL): StatPearls Publishing; 2024 [cited 2024 Aug 23]. Available from: http://www.ncbi.nlm.nih.gov/books/NBK526106/

10. Bjornsson ES, Devarbhavi HC. Drug induced cholestatic liver diseases. Hepatology. :10.1097/HEP.0000000000001052.

11. Felzen A, Verkade HJ. The spectrum of Progressive Familial Intrahepatic Cholestasis diseases: Update on pathophysiology and emerging treatments. Eur J Med Genet. 2021 Nov;64(11):104317.

12. Roy-Chowdhury N, Wang X, Guha C, Roy-Chowdhury J. Hepatocyte-like cells derived from induced pluripotent stem cells. Hepatol Int. 2017 Jan;11(1):54–69.

13. Corbett JL, Duncan SA. iPSC-Derived Hepatocytes as a Platform for Disease Modeling and Drug Discovery. Front Med. 2019;6:265.

14. S D, R K. A Review of the Regulatory Challenges of Personalized Medicine. Cureus. 16(8):e67891.

15. Goldberg A, Mack CL. Inherited Cholestatic Diseases in the Era of Personalized Medicine. Clin Liver Dis. 2020 Apr 4;15(3):105–9.

16. Carbone M, Sharp SJ, Flack S, Paximadas D, Spiess K, Adgey C, et al. The UK-PBC risk scores: Derivation and validation of a scoring system for long-term prediction of end-stage liver disease in primary biliary cholangitis. Hepatol Baltim Md. 2016 Mar;63(3):930–50.

17. Du B, Mu K, Sun M, Yu Z, Li L, Hou L, et al. Biliary atresia and cholestasis plasma non-targeted metabolomics unravels perturbed metabolic pathways and unveils a diagnostic model for biliary atresia. Sci Rep. 2024 July 9;14(1):15796.

18. Flattmann FE, Mohiuddin FS, Singh A, Tandon A, Lockett SJ, Hirsch JD, et al. Odevixibat: A Novel Bile Salt Inhibitor Treatment for Pruritus in Progressive Familial Intrahepatic Cholestasis. Cureus. 16(3):e56886.

19. Nittono H, Suzuki M, Suzuki H, Sugimoto S, Mori J, Sakamoto R, et al. Navigating cholestasis: identifying inborn errors of bile acid metabolism for precision diagnosis. Front Pediatr. 2024;12:1385970.

20. Lammers WJ, Hirschfield GM, Corpechot C, Nevens F, Lindor KD, Janssen HLA, et al. Development and Validation of a Scoring System to Predict Outcomes of Patients With Primary Biliary Cirrhosis Receiving Ursodeoxycholic Acid Therapy. Gastroenterology. 2015 Dec;149(7):1804-1812.e4.

21. Zöllner J, Williamson C, Dixon PH. Genetic issues in ICP. Obstet Med. 2024 Sept;17(3):157–61.

22. Seladelpar. In: LiverTox: Clinical and Research Information on Drug-Induced Liver Injury [Internet]. Bethesda (MD): National Institute of Diabetes and Digestive and Kidney Diseases; 2012 [cited 2025 Oct 25]. Available from: http://www.ncbi.nlm.nih.gov/books/NBK608065/

23. Yi S, Kim I, Hager R, Strazzeri MM, Garrard L, Matsubayashi T, et al. Food and Drug Administration Approval Summary: Odevixibat (Bylvay) for the Treatment of Pruritus With Progressive Familial Intrahepatic Cholestasis. Gastro Hep Adv. 2025;4(4):100596.

24. Amirneni S, Haep N, Gad MA, Soto-Gutierrez A, Squires JE, Florentino RM. Molecular overview of progressive familial intrahepatic cholestasis. World J Gastroenterol. 2020 Dec 21;26(47):7470–84.

25. Nuciforo S, Heim MH. Organoids to model liver disease. JHEP Rep Innov Hepatol. 2021 Feb;3(1):100198.

26. Grandy R, Tomaz RA, Vallier L. Modeling Disease with Human Inducible Pluripotent Stem Cells. Annu Rev Pathol Mech Dis. 2019 Jan 24;14(Volume 14, 2019):449–68.

27. Hannoun Z, Steichen C, Dianat N, Weber A, Dubart-Kupperschmitt A. The potential of induced pluripotent stem cell derived hepatocytes. J Hepatol. 2016 July 1;65(1):182–99.

28. Rombaut M, Boeckmans J, Rodrigues RM, van Grunsven LA, Vanhaecke T, De Kock J. Direct reprogramming of somatic cells into induced hepatocytes: Cracking the Enigma code. J Hepatol. 2021 Sept 1;75(3):690–705.

29. Vasconcellos R, Alvarenga ÉC, Parreira RC, Lima SS, Resende RR. Exploring the cell signalling in hepatocyte differentiation. Cell Signal. 2016 Nov;28(11):1773–88.

30. Xie Y, Yao J, Jin W, Ren L, Li X. Induction and Maturation of Hepatocyte-Like Cells In Vitro: Focus on Technological Advances and Challenges. Front Cell Dev Biol [Internet]. 2021 Nov 26 [cited 2025 Aug 9];9. Available from: https://www.frontiersin.org/journals/cell-and-developmental-biology/articles/10.3389/fcell.2021.765980/full

31. Zeilinger K, Freyer N, Damm G, Seehofer D, Knöspel F. Cell sources for in vitro human liver cell culture models. Exp Biol Med Maywood NJ. 2016 Sept;241(15):1684–98.

32. Baxter M, Withey S, Harrison S, Segeritz CP, Zhang F, Atkinson-Dell R, et al. Phenotypic and functional analyses show stem cell-derived hepatocyte-like cells better mimic fetal rather than adult hepatocytes. J Hepatol. 2015 Mar;62(3):581–9.

33. Tricot T, Verfaillie CM, Kumar M. Current Status and Challenges of Human Induced Pluripotent Stem Cell-Derived Liver Models in Drug Discovery. Cells. 2022 Jan 27;11(3):442.

34. Oliveira Arcolino F, Tort Piella A, Papadimitriou E, Bussolati B, Antonie DJ, Murray P, et al. Human Urine as a Noninvasive Source of Kidney Cells. Stem Cells Int. 2015;2015:362562.

35. Cerneckis J, Cai H, Shi Y. Induced pluripotent stem cells (iPSCs): molecular mechanisms of induction and applications. Signal Transduct Target Ther. 2024 Apr 26;9(1):112.

36. Liu G, David BT, Trawczynski M, Fessler RG. Advances in Pluripotent Stem Cells: History, Mechanisms, Technologies, and Applications. Stem Cell Rev Rep. 2020 Feb 1;16(1):3–32.

37. Matiukhova M, Ryapolova A, Andriianov V, Reshetnikov V, Zhuravleva S, Ivanov R, et al. A comprehensive analysis of induced pluripotent stem cell (iPSC) production and applications. Front Cell Dev Biol [Internet]. 2025 May 8 [cited 2025 Aug 7];13. Available from: https://www.frontiersin.org/journals/cell-and-developmental-biology/articles/10.3389/fcell.2025.1593207/full

38. Poetsch MS, Strano A, Guan K. Human Induced Pluripotent Stem Cells: From Cell Origin, Genomic Stability, and Epigenetic Memory to Translational Medicine. Stem Cells Dayt Ohio. 2022 June 22;40(6):546–55.

39. Raab S, Klingenstein M, Liebau S, Linta L. A Comparative View on Human Somatic Cell Sources for iPSC Generation. Stem Cells Int. 2014;2014:768391.

40. Zhou T, Benda C, Dunzinger S, Huang Y, Ho JC, Yang J, et al. Generation of human induced pluripotent stem cells from urine samples. Nat Protoc. 2012 Dec;7(12):2080–9.

41. Zhuo JL, Li XC. Proximal nephron. Compr Physiol. 2013 July;3(3):1079–123.

42. Benda C, Zhou T, Wang X, Tian W, Grillari J, Tse HF, et al. Urine as a source of stem cells. Adv Biochem Eng Biotechnol. 2013;129:19–32.

43. Rahmoune H, Thompson PW, Ward JM, Smith CD, Hong G, Brown J. Glucose transporters in human renal proximal tubular cells isolated from the urine of patients with non-insulin-dependent diabetes. Diabetes. 2005 Dec;54(12):3427–34.

44. Ray A, Joshi JM, Sundaravadivelu PK, Raina K, Lenka N, Kaveeshwar V, et al. An Overview on Promising Somatic Cell Sources Utilized for the Efficient Generation of Induced Pluripotent Stem Cells. Stem Cell Rev Rep. 2021 Dec;17(6):1954–74.

45. Bondue T, Arcolino FO, Veys KRP, Adebayo OC, Levtchenko E, van den Heuvel LP, et al. Urine-Derived Epithelial Cells as Models for Genetic Kidney Diseases. Cells. 2021 June 6;10(6):1413.

46. Jansen J, Schophuizen CMS, Wilmer MJ, Lahham SHM, Mutsaers H a. M, Wetzels JFM, et al. A morphological and functional comparison of proximal tubule cell lines established from human urine and kidney tissue. Exp Cell Res. 2014 Apr 15;323(1):87–99.

47. Mihevc M, Petreski T, Maver U, Bevc S. Renal proximal tubular epithelial cells: review of isolation, characterization, and culturing techniques. Mol Biol Rep. 2020 Dec;47(12):9865–82.

48. Osonoi S, Takebe T. Organoid-guided precision hepatology for metabolic liver disease. J Hepatol. 2024 May;80(5):805–21.

49. Luce E, Messina A, Duclos-Vallée JC. Hepatic organoids as a platform for liver disease modeling and the development of novel therapies. Clin Res Hepatol Gastroenterol. 2025 July 1;49(7):102647.

50. Prior N, Inacio P, Huch M. Liver organoids: from basic research to therapeutic applications. Gut. 2019 Dec;68(12):2228–37.

51. Huch M, Gehart H, van Boxtel R, Hamer K, Blokzijl F, Verstegen MMA, et al. Long-Term Culture of Genome-Stable Bipotent Stem Cells from Adult Human Liver. Cell. 2015 Jan 15;160(1–2):299–312.

52. Jalan-Sakrikar N, Brevini T, Huebert RC, Sampaziotis F. Organoids and regenerative hepatology. Hepatol Baltim Md. 2023 Jan 1;77(1):305–22.

53. Afonso MB, Marques V, van Mil SWC, Rodrigues CMP. Human liver organoids: From generation to applications. Hepatol Baltim Md. 2024 June;79(6):1432–51.

54. Huch M, Dorrell C, Boj SF, van Es JH, Li VSW, van de Wetering M, et al. In vitro expansion of single Lgr5+ liver stem cells induced by Wnt-driven regeneration. Nature. 2013 Feb;494(7436):247–50.

55. Harrison SP, Baumgarten SF, Verma R, Lunov O, Dejneka A, Sullivan GJ. Liver Organoids: Recent Developments, Limitations and Potential. Front Med. 2021;8:574047.

56. Cheng L, Hansen NF, Zhao L, Du Y, Zou C, Donovan FX, et al. Low incidence of DNA sequence variation in human induced pluripotent stem cells generated by non-integrating plasmid expression. Cell Stem Cell. 2012 Mar 2;10(3):337–44.

57. Wu F, Wu D, Ren Y, Huang Y, Feng B, Zhao N, et al. Generation of hepatobiliary organoids from human induced pluripotent stem cells. J Hepatol. 2019 June;70(6):1145–58.

58. Zacharis ED, Morell CM, Tomaz RA, Shahsavari A, Grey-Wilson C, Pesic M, et al. Wnt signalling maintains self-renewal of human hepatoblasts without blocking their differentiation. Dev Camb Engl. 2025 Nov 15;152(22):dev205026.

59. Italy · country details · hPSCreg [Internet]. [cited 2025 Dec 15]. Available from: https://hpscreg.eu/browse/country/it?utm_

60. Caiazza C, Parisi S, Caiazzo M. Liver Organoids: Updates on Disease Modeling and Biomedical Applications. Biology. 2021 Aug 27;10(9):835.

61. Zhu X, Zhang B, He Y, Bao J. Liver Organoids: Formation Strategies and Biomedical Applications. Tissue Eng Regen Med. 2021 Aug;18(4):573–85.

62. Hu H, Gehart H, Artegiani B, LÖpez-Iglesias C, Dekkers F, Basak O, et al. Long-Term Expansion of Functional Mouse and Human Hepatocytes as 3D Organoids. Cell. 2018 Nov 29;175(6):1591-1606.e19.

63. Peng WC, Logan CY, Fish M, Anbarchian T, Aguisanda F, Álvarez-Varela A, et al. Inflammatory Cytokine TNFα Promotes the Long-Term Expansion of Primary Hepatocytes in 3D Culture. Cell. 2018 Nov 29;175(6):1607-1619.e15.

64. Peng WC, Kraaier LJ, Kluiver TA. Hepatocyte organoids and cell transplantation: What the future holds. Exp Mol Med. 2021 Oct;53(10):1512–28.

65. Lei Z, Yang Y, Xiang Y. The utilisation of biliary organoids for biomedical applications. Front Bioeng Biotechnol [Internet]. 2025 Jan 7 [cited 2025 Dec 13];12. Available from: https://www.frontiersin.org/journals/bioengineering-and-biotechnology/articles/10.3389/fbioe.2024.1501829/full

66. Marsee A, Roos FJM, Verstegen MMA, Marsee A, Roos F, Verstegen M, et al. Building consensus on definition and nomenclature of hepatic, pancreatic, and biliary organoids. Cell Stem Cell. 2021 May 6;28(5):816–32.

67. Guan Y, Xu D, Garfin PM, Ehmer U, Hurwitz M, Enns G, et al. Human hepatic organoids for the analysis of human genetic diseases. JCI Insight. 2017 Sept 7;2(17):e94954, 94954.

68. Overeem AW, Klappe K, Parisi S, Klöters-Planchy P, Mataković L, du Teil Espina M, et al. Pluripotent stem cell-derived bile canaliculi-forming hepatocytes to study genetic liver diseases involving hepatocyte polarity. J Hepatol. 2019 Aug;71(2):344–56.

69. Takahashi K, Yamanaka S. Induction of pluripotent stem cells from mouse embryonic and adult fibroblast cultures by defined factors. Cell. 2006 Aug 25;126(4):663–76.

70. Matakovic L, Overeem AW, Klappe K, van IJzendoorn SCD. Induction of Bile Canaliculi-Forming Hepatocytes from Human Pluripotent Stem Cells. Methods Mol Biol Clifton NJ. 2022;2544:71–82.

71. Mallanna SK, Duncan SA. Differentiation of hepatocytes from pluripotent stem cells. Curr Protoc Stem Cell Biol. 2013 Sept 20;26:1G.4.1-1G.4.13.

72. STEMdiff™ Hepatocyte Kit | STEMCELL Technologies [Internet]. [cited 2025 Oct 28]. Available from: https://www.stemcell.com/products/stemdiff-hepatocyte-kit.html

73. Shen L, Hillebrand A, Wang DQH, Liu M. Isolation and primary culture of rat hepatic cells. J Vis Exp JoVE. 2012 June 29;(64):3917.

74. Kluiver TA, Kraaier LJ, Peng WC. Long-Term Expansion of Murine Primary Hepatocyte Organoids. Methods Mol Biol Clifton NJ. 2022;2544:1–13.

75. Charni-Natan M, Goldstein I. Protocol for Primary Mouse Hepatocyte Isolation. STAR Protoc. 2020 Sept 18;1(2):100086.

76. Tiriticco V, Codotto G, Blarasin B, Salvoza N, Stebel M, Tiribelli C, et al. Rat Liver Perfusion and Primary Hepatocytes Isolation: An Old Procedure Crucial for Cutting-Edge 3D Organoids Culture. JoVE J Vis Exp. 2024 Nov 22;(213):e66857.

77. Ryu AH, Eckalbar WL, Kreimer A, Yosef N, Ahituv N. Use antibiotics in cell culture with caution: genome-wide identification of antibiotic-induced changes in gene expression and regulation. Sci Rep. 2017 Aug 8;7(1):7533.

78. Kouri TT, Hofmann W, Falbo R, Oyaert M, Schubert S, Gertsen JB, et al. The EFLM European Urinalysis Guideline 2023. Clin Chem Lab Med CCLM. 2024 Aug 1;62(9):1653–786.

79. Dionne O, Sabatié S, Fortin F, Corbin F, Laurent B. Efficient generation of human induced pluripotent stem cells from urine samples of patients with Fragile X syndrome. Front Cell Dev Biol. 2024;12:1489190.

80. Park SW, Bae JS, Kim KS, Park SH, Lee BH, Choi JY, et al. Beta ig-h3 promotes renal proximal tubular epithelial cell adhesion, migration and proliferation through the interaction with α3β1 integrin. Exp Mol Med. 2004 June 1;36(3):211–9.

81. Hills CE, Jin T, Siamantouras E, Liu IKK, Jefferson KP, Squires PE. “Special K” and a Loss of Cell-To-Cell Adhesion in Proximal Tubule-Derived Epithelial Cells: Modulation of the Adherens Junction Complex by Ketamine. PLoS ONE. 2013 Aug 29;8(8):e71819.

82. Leung JC, Chan LY, Tang SC, Lam MF, Chow CW, Lim AI, et al. Oxidative damages in tubular epithelial cells in IgA nephropathy: role of crosstalk between angiotensin II and aldosterone. J Transl Med. 2011 Oct 6;9:169.

83. Muff R, Fischer JA, Biber J, Murer H. Parathyroid hormone receptors in control of proximal tubule function. Annu Rev Physiol. 1992;54:67–79.

84. Zhou T, Benda C, Duzinger S, Huang Y, Li X, Li Y, et al. Generation of Induced Pluripotent Stem Cells from Urine. J Am Soc Nephrol. 2011 July;22(7):1221.

85. Bhattacharyya A, Zhao X. Human pluripotent stem cell models of Fragile X syndrome. Mol Cell Neurosci. 2016 June 1;73:43–51.

86. Kim K, Doi A, Wen B, Ng K, Zhao R, Cahan P, et al. Epigenetic memory in induced pluripotent stem cells. Nature. 2010 Sept 16;467(7313):285–90.

87. Haridhasapavalan KK, Raina K, Dey C, Adhikari P, Thummer RP. An Insight into Reprogramming Barriers to iPSC Generation. Stem Cell Rev Rep. 2020 Feb;16(1):56–81.

88. Human Pluripotent Stem Cell Banking [Internet]. [cited 2025 Oct 28]. Available from: https://www.stemcell.com/psc-cell-quality/cell-banking

89. Ludwig TE, Andrews PW, Barbaric I, Benvenisty N, Bhattacharyya A, Crook JM, et al. ISSCR standards for the use of human stem cells in basic research. Stem Cell Rep. 2023 Sept 12;18(9):1744–52.

90. Kuehle J, Turan S, Cantz T, Hoffmann D, Suerth JD, Maetzig T, et al. Modified lentiviral LTRs allow Flp recombinase-mediated cassette exchange and in vivo tracing of “factor-free” induced pluripotent stem cells. Mol Ther J Am Soc Gene Ther. 2014 May;22(5):919–28.

91. Fusaki N, Ban H, Nishiyama A, Saeki K, Hasegawa M. Efficient induction of transgene-free human pluripotent stem cells using a vector based on Sendai virus, an RNA virus that does not integrate into the host genome. Proc Jpn Acad Ser B Phys Biol Sci. 2009;85(8):348–62.

92. Sendai Virus - an overview | ScienceDirect Topics [Internet]. [cited 2025 Sept 17]. Available from: https://www.sciencedirect.com/topics/neuroscience/sendai-virus

93. Song Z, Cai J, Liu Y, Zhao D, Yong J, Duo S, et al. Efficient generation of hepatocyte-like cells from human induced pluripotent stem cells. Cell Res. 2009 Nov;19(11):1233–42.

94. Siller R, Greenhough S, Naumovska E, Sullivan GJ. Small-molecule-driven hepatocyte differentiation of human pluripotent stem cells. Stem Cell Rep. 2015 May 12;4(5):939–52.

95. Carpentier A, Nimgaonkar I, Chu V, Xia Y, Hu Z, Liang TJ. Hepatic differentiation of human pluripotent stem cells in miniaturized format suitable for high-throughput screen. Stem Cell Res. 2016 May;16(3):640–50.

96. van der Wouden JM, van IJzendoorn SCD, Hoekstra D. Oncostatin M regulates membrane traffic and stimulates bile canalicular membrane biogenesis in HepG2 cells. EMBO J. 2002 Dec 2;21(23):6409–18.

97. Swift B, Pfeifer ND, Brouwer KLR. Sandwich-cultured hepatocytes: an in vitro model to evaluate hepatobiliary transporter-based drug interactions and hepatotoxicity. Drug Metab Rev. 2010 Aug;42(3):446–71.

98. Kallas A, Pook M, Trei A, Maimets T. SOX2 Is Regulated Differently from NANOG and OCT4 in Human Embryonic Stem Cells during Early Differentiation Initiated with Sodium Butyrate. Stem Cells Int. 2014;2014(1):298163.

99. Zabulica M, Srinivasan RC, Vosough M, Hammarstedt C, Wu T, Gramignoli R, et al. Guide to the Assessment of Mature Liver Gene Expression in Stem Cell-Derived Hepatocytes. Stem Cells Dev. 2019 July 15;28(14):907–19.

100. Li J, Ning G, Duncan SA. Mammalian hepatocyte differentiation requires the transcription factor HNF-4alpha. Genes Dev. 2000 Feb 15;14(4):464–74.

101. Yeo YH, Lee YT, Tseng HR, Zhu Y, You S, Agopian VG, et al. Alpha-fetoprotein: Past, present, and future. Hepatol Commun. 2024 Apr 12;8(5):e0422.

102. Camper SA, Tilghman SM. Postnatal repression of the alpha-fetoprotein gene is enhancer independent. Genes Dev. 1989 Apr;3(4):537–46.

103. Sell S. Heterogeneity of alpha-fetoprotein(AFP) and albumin containing cells in normal and pathological permissive states for AFP production: AFP containing cells induced in adult rats recapitulate the appearance of AFP containing hepatocytes in fetal rats. Oncodevelopmental Biol Med J Int Soc Oncodevelopmental Biol Med. 1980;1(2):93–105.

104. Graffmann N, Scherer B, Adjaye J. In vitro differentiation of pluripotent stem cells into hepatocyte like cells - Basic principles and current progress. Stem Cell Res. 2022 May;61:102763.

105. Luo Q, Wang N, Que H, Mai E, Hu Y, Tan R, et al. Pluripotent Stem Cell-Derived Hepatocyte-like Cells: Induction Methods and Applications. Int J Mol Sci. 2023 Jan;24(14):11592.

106. Ardisasmita AI, Schene IF, Joore IP, Kok G, Hendriks D, Artegiani B, et al. A comprehensive transcriptomic comparison of hepatocyte model systems improves selection of models for experimental use. Commun Biol. 2022 Oct 14;5(1):1094.

107. Gonzales E, Taylor SA, Davit-Spraul A, Thébaut A, Thomassin N, Guettier C, et al. MYO5B mutations cause cholestasis with normal serum gamma-glutamyl transferase activity in children without microvillous inclusion disease. Hepatol Baltim Md. 2017 Jan;65(1):164–73.

108. Qiu YL, Gong JY, Feng JY, Wang RX, Han J, Liu T, et al. Defects in myosin VB are associated with a spectrum of previously undiagnosed low γ-glutamyltransferase cholestasis. Hepatol Baltim Md. 2017 May;65(5):1655–69.

109. Girard M, Lacaille F, Verkarre V, Mategot R, Feldmann G, Grodet A, et al. MYO5B and bile salt export pump contribute to cholestatic liver disorder in microvillous inclusion disease. Hepatol Baltim Md. 2014 July;60(1):301–10.

110. Matarazzo L, Bianco AM, Athanasakis E, Serveres M, Francalanci P, Cenacchi G, et al. MYO5B Gene Mutations: A Not Negligible Cause of Intrahepatic Cholestasis of Infancy With Normal Gamma-Glutamyl Transferase Phenotype. J Pediatr Gastroenterol Nutr. 2022 May 1;74(5):e115–21.

111. Cockar I, Foskett P, Strautnieks S, Clinch Y, Fustok J, Rahman O, et al. Mutations in Myosin 5B in Children With Early-onset Cholestasis. J Pediatr Gastroenterol Nutr. 2020 Aug;71(2):184–8.

112. Smith AJ, Clutton RE, Lilley E, Hansen KEA, Brattelid T. PREPARE: guidelines for planning animal research and testing. Lab Anim. 2018 Apr;52(2):135–41.

113. Ng IC, Zhang L, Shen NNYY, Soong YT, Ng CW, Koh PKS, et al. Isolation of Primary Rat Hepatocytes with Multiparameter Perfusion Control. J Vis Exp JoVE. 2021 Apr 5;(170).

114. Cabral F, Miller CM, Kudrna KM, Hass BE, Daubendiek JG, Kellar BM, et al. Purification of Hepatocytes and Sinusoidal Endothelial Cells from Mouse Liver Perfusion. J Vis Exp JoVE. 2018 Feb 12;(132):56993.

115. Guan Y, Peltz G. Hepatic organoids move from adolescence to maturity. Liver Int. 2024;44(6):1290–7.

116. Akashi M, Tanaka A, Takikawa H. Effect of cyclosporin A on the biliary excretion of cholephilic compounds in rats. Hepatol Res. 2006 Mar 1;34(3):193–8.

117. Sharanek A, Azzi PBE, Al-Attrache H, Savary CC, Humbert L, Rainteau D, et al. Different Dose-Dependent Mechanisms Are Involved in Early Cyclosporine A-Induced Cholestatic Effects in HepaRG Cells. Toxicol Sci. 2014 Sept 1;141(1):244–53.

118. Ramli MNB, Lim YS, Koe CT, Demircioglu D, Tng W, Gonzales KAU, et al. Human Pluripotent Stem Cell-Derived Organoids as Models of Liver Disease. Gastroenterology. 2020 Oct;159(4):1471-1486.e12.

119. Sharanek A, Azzi PBE, Al-Attrache H, Savary CC, Humbert L, Rainteau D, et al. Different dose-dependent mechanisms are involved in early cyclosporine a-induced cholestatic effects in hepaRG cells. Toxicol Sci Off J Soc Toxicol. 2014 Sept;141(1):244–53.

120. Sharanek A, Burban A, Burbank M, Le Guevel R, Li R, Guillouzo A, et al. Rho-kinase/myosin light chain kinase pathway plays a key role in the impairment of bile canaliculi dynamics induced by cholestatic drugs. Sci Rep. 2016 May 12;6:24709.

121. Kim HM, Kim Y, Kim Y, Kim YJ, Ko KS. Organoid Establishment of Long-Term Culture Using Primary Mouse Hepatocytes and Evaluation of Liver Function. Prev Nutr Food Sci. 2023 Sept 30;28(3):360–9.

122. Igarashi R, Oda M, Okada R, Yano T, Takahashi S, Pastuhov S, et al. Generation of human adult hepatocyte organoids with metabolic functions. Nature. 2025 May;641(8065):1248–57.

123. Ouchi R, Togo S, Kimura M, Shinozawa T, Koido M, Koike H, et al. Modeling Steatohepatitis in Humans with Pluripotent Stem Cell-Derived Organoids. Cell Metab. 2019 Aug 6;30(2):374-384.e6.

124. Takebe T, Wells JM. Organoids by design. Science. 2019 June 7;364(6444):956–9.

125. Guan Y, Xu D, Garfin PM, Ehmer U, Hurwitz M, Enns G, et al. Human hepatic organoids for the analysis of human genetic diseases. JCI Insight. 2017 Sept 7;2(17):e94954, 94954.

126. Codotto G, Blarasin B, Tiribelli C, Bellarosa C, Licastro D. Decoding Liver Fibrosis: How Omics Technologies and Innovative Modeling Can Guide Precision Medicine. Int J Mol Sci. 2025 Jan;26(6):2658.

8. ACKNOWLEDGEMENTS

I would like to express my sincere appreciation to all those who contributed to this work.

Special thanks are extended to the members of the Medical Genetics Laboratory, led by Professor Adamo Pio d'Adamo, at the IRCCS Materno Infantile "Burlo Garofolo" Hospital (Trieste, Italy), for the multicentric project we conducted together on hiHeps differentiation from hiPSC. In particular, I want to thank Dr. Mariateresa Di Stazio, Cecilia Del Vecchio, Francesco Giambuzzi, and Ilaria Ziccardi.

I would like to thank Dr. Martina Conti and Dr. Laura Andolfi from the CNR - IOM laboratory (Trieste, Italy) for their technical assistance and helpful discussions regarding the immunofluorescence experiments.

Gratitude is further extended to Prof. Giovanni Sorrentino, Dr. Davide Selvestrel, and Dr. Beatrice Anfuso from the Advanced Disease Models Group (International Centre for Genetic Engineering and Biotechnology (ICGEB) in Trieste, Italy) for their valuable collaboration and support throughout the development of the Hep - Orgs model.

Sincere thanks are also due to Prof. Gabriele Baj from the Department of Life Sciences for his precious help with the Hep - Orgs immunofluorescence experiments, and Prof. Lucio Torelli from the Department of the Medical and Surgical Sciences for the statistical analysis regarding the 2D model.